INVESTIGATIONS INTO THE ROLE OF α-AMINO ACIDS AS CHIRAL MODIFIERS FOR NI-BASED ENANTIOSELECTIVE HETEROGENEOUS HYDROGENATION CATALYSTS

Karen E. Wilson

A Thesis Submitted for the Degree of PhD
at the
University of St Andrews

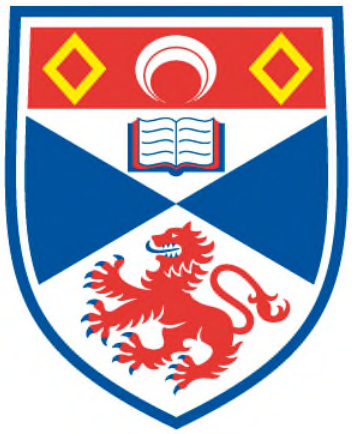

2011

Investigations into the Role of α-Amino Acids as Chiral Modifiers for Ni-based Enantioselective Heterogeneous Hydrogenation Catalysts

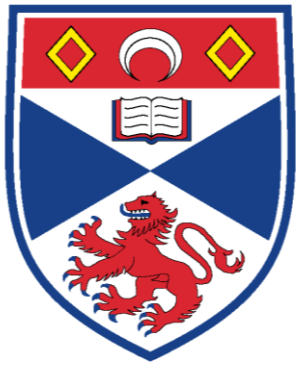

University
of
St Andrews

A thesis submitted in accordance with the requirements of the University of St. Andrews for the degree of Doctor of Philosophy.

Karen E. Wilson

Under the supervision of Dr. Christopher J. Baddeley

March 2011

Declaration

I, Karen Wilson, hereby certify that this thesis, which is approximately 66,000 words in length, has been written by me, that it is the record of work carried out by me and that it has not been submitted in any previous application for a higher degree.

I was admitted as a research student in October 2007 as a candidate for the degree of Ph.D; the higher study for which this is a record was carried out in the University of St Andrews between 2007 and 2011.

Date: Signature of candidate:

I, Dr. C. J. Baddeley, hereby certify that the candidate has fulfilled the conditions of the Resolution and Regulations appropriate for the degree of Ph. D. in the University of St Andrews and that the candidate is qualified to submit this thesis in application for that degree.

Date: Signature of supervisor:

In submitting this thesis to the University of St Andrews we understand that we are giving permission for it to be made available for use in accordance with the regulations of the University Library for the time being in force, subject to any copyright vested in the work not being affected thereby. We also understand that the title and the abstract will be published, and that a copy of the work may be made and supplied to any bona fide library or research worker, that my thesis will be electronically accessible for personal or research use unless exempt by award of an embargo as requested below, and that the library has the right to migrate my thesis into new electronic forms as required to ensure continued access to the thesis. We have obtained any third-party copyright permissions that may be required in order to allow such access and migration, or have requested the appropriate embargo below.

The following is an agreed request by candidate and supervisor regarding the electronic publication of this thesis:

Embargo on all or part of printed copy and electronic copy for the same fixed period of 1 year on the grounds that publication would preclude future publications.

Date: Signature of candidate:

Signature of supervisor:

Abstract

The hydrogenation of *β*-ketoesters over chirally modified Ni catalysts is a celebrated and thoroughly researched example of an enantioselective heterogeneous catalytic reaction. Enantioselective heterogeneous processes, although extremely attractive in terms of fewer complications in the separation of products from the catalyst, are hindered in their viability as industrial applications due to the lack of detailed knowledge on how chirality is conferred to the metal surface. Surface science techniques have afforded substantial progress into determining mechanisms between modifier, reactant and catalyst to explain the source of enantioselectivity of the system. In this study, a combination of solution and ultra-high vacuum (UHV)-based experiments allow a more realistic interpretation of the surface chemistry underpinning the catalytic reaction as the key step in achieving enantioselective performance is the adsorption of chiral modifiers from solution.

The behaviour of *(S)*-aspartic acid and *(S)*-lysine on Ni{111} and their interaction with the prochiral *β*-ketoester methylacetoacetate is investigated in this study to understand their potential as chiral modifiers for the system. In UHV, scanning tunnelling microscopy (STM), reflection absorption infrared spectroscopy (RAIRS), and temperature programmed desorption (TPD) are used to analyse the conformation and order of the amino acids on the metal, and their thermal stability. Additionally, liquid-solid interface RAIRS and X-ray photoelectron spectroscopy (XPS) are used to examine the modified Ni surface, prepared under aqueous conditions, to give an accurate representation of the catalytic studies. It has been found highly likely that, for *(S)*-aspartic acid modified Ni{111}, enantioselective sites exist at step or step/kink defects, formed by corrosive leaching of the Ni substrate. Conversely, lysine appears to bind with a high sticking probability to Ni, in the form of lysine islands, and does not appear to etch the Ni chirally.

Finally, similar experiments have been carried out on Au{111}, where lysine was found to chiral restructure the surface and form nanofingers, and 2D Ni clusters grown on Au{111} in order to investigate the formation of possible metal-organic frameworks.

Keywords: Heterogeneous catalysis, enantioselective, chirality, nickel, amino acid, ultra-high vacuum, liquid-solid interface.

Acknowledgements

I would first like to thank my supervisor, Dr. Chris Baddeley, for introducing me to the world of surface science. His fascination and enthusiasm for the subject influenced me greatly, and our fruitful discussions constantly kept me optimistic throughout my studies. No matter how busy, Chris has been available to offer help and advice, and I will always be grateful for that.

I would also like to thank my postdoc, Dr. Aoife Trant, for the generous time afforded in helping me get to grips with UHV equipment as well as useful discussions. Thanks must also go to Drs. Steve Francis and Federico Grillo for their considerable help in all things surface science – from suggestions for experiments to advising solutions to problems encountered. My thanks go also to Prof. Neville Richardson for use of the UHV-STM and RAIRS chambers, Dr. Ron Brown at the University of Edinburgh for XPS time, and Dr. Herbert Früchtl for computational modelling assistance. I am grateful to the discussions with many academics, both at St Andrews and beyond, from whom I have gained so much.

The warmth and friendliness of the St Andrews Surface Science department is something which made my arrival at St Andrews all the more easier and which I appreciate greatly. I must thank those past and present; Andrew Haire, Sean Jensen, Lanxia Cheung, Alex Murdoch, Nicola Toma, John Greenwood, Tim Jones and Riho Green; who have each, in their own way, contributed to my time at St Andrews.

On a personal level, my gratitude to friends for all the support and laughs during my PhD; especially Val, Fed, Alistair, Stuart, Kirsty and Lesley-Ann; our nights out and holidays have kept me sane throughout! Huge thanks to Tom, whose amazing ability to put up with me makes me all the more proud to have him in my life.

Most importantly, a huge thanks to my family, especially to my parents, Ian and Linda, and brother Scott, for their unwavering support and love throughout my studies; if it wasn't for the words of encouragement over all these years I doubt I would find myself here now.

List of Publications

1. Understanding the Surface Chemistry of Enantioselective Heterogeneous Reactions: Influence of Modification Variables on the Interaction of Methylacetoacetate with (*S*)-Aspartic Acid Modified Ni{111}

K.E. Wilson & C.J. Baddeley, *Journal of Physical Chemistry C.,* **113** (2009), 10706.

2. XPS Studies of the Effects of Modification pH on the Interaction of Methylacetoacetate with *(S)*-Aspartic Acid-Modified Ni Surfaces.

K.E. Wilson & C.J. Baddeley, *Journal of Catalysis,* **278** (2011), 41.

3. Fundamental Investigations of Enantioselective Heterogeneous Catalysis.

C.J. Baddeley, T.E. Jones, A.G. Trant & K.E. Wilson, *submitted to Topics in Catalysis, February 2011.*

4. (S)-Lysine Adsorption induces the Formation of Gold Nanofingers on Au{111}.

K.E. Wilson, H. A. Früchtl F. Grillo, & C.J. Baddeley, *accepted by RSC Chemical Communications, June 2011.*

5. *(S)*-Lysine Adsorption on Au{111} Surfaces: A RAIRS and HREELS Study.

K.E. Wilson, F. Grillo & C.J. Baddeley (in preparation).

Postgraduate Modules Undertaken

1. Computational Chemistry - 2 credits.
2. Electron Microscopy - 2 credits.

List of Acronyms and Units

Acronyms

Auger Electron Spectroscopy	AES
Concentric Hemispherical Energy Analyser	CHA
Density Functional Theory	DFT
Enantiomeric excess	e.e.
Face centred cubic	fcc
Fourier Transform Infrared	FTIR
Full Width Half Maximum	FWHM
High Resolution Electron Energy Loss Spectroscopy	HREELS
Inelastic Mean Free Path	IMFP
Local Density of States	LDOS
Low Energy Electron Diffraction	LEED
Mercury Cadmium Telluride	MCT
Methyl acetoacetate	MAA
Methyl-2-hydroxybutyrate	MHB
Polarisation-Modulation Reflection Absorption Infrared Spectroscopy	PM-RAIRS
Polysuccinimide	PSI
Raney Nickel	RNi
Reflection Absorption Infrared Spectroscopy	RAIRS
Retarding Field Analyser	RFA
Scanning Tunnelling Microscopy	STM
Temperature Programmed Desorption	TPD
Ultra-High Vacuum	UHV
X-Ray Photoelectron Spectroscopy	XPS

Symbols

Ångstrom	Å	Degrees Celsius	°C
Electron volt	eV	Kelvin	K
Kilovolt	kV	Langmuir (1 L = 10^{-6} $Torrs^{-1}$)	L
Millimolar	mM	Monolayer	ML
Nanoampere	nA	Nanometre	nm
Second	s	Volt	V

Table of Contents

Chapter 5 Characterisation Studies of Ni{111} modified with *(S)*-lysine in UHV and liquid phase conditions

Chapter 1

Introduction

Louis Pasteur, the inventor of the concept of molecular chirality, once said "*life, as it is known to us, is a direct result of the asymmetry of the universe*" [1] and, increasingly, it can be found that chirality is wholly connected to the world in which we live, and its importance can be observed in many different fields. Catalysis is one such field. Chiral catalysis has developed substantially in recent years as the demand for enantiomerically pure compounds in the chemical and pharmaceutical industry grows. Originally, it was the high product selectivity capability of a catalyst which was of utmost importance, whereas nowadays optimum catalytic conditions for certain reactions are well established and the aim is to examine the workings of the systems at the molecular level. The ability to tailor surfaces to exact specifications to enable successful and reproducible chiral catalysis allows advancement in the field as well as development of future applications.

The work presented in this thesis is part of ongoing research into chiral heterogeneous catalysis and examines the importance of chiral modification of metal substrates and the understanding of how changes of various modification parameters such as pH and temperature cause effect. The work endeavours to examine how these factors could be incorporated into the design of a heterogeneous catalyst suitable for chiral catalysis.

1.1 SIGNIFICANCE OF CHIRALITY

Many naturally occurring compounds have an inherent chirality which describes the geometry of the molecules. A molecule with chirality refers to the property by which the mirror image of the molecule will not be superimposable upon itself. The two mirror image forms are known as enantiomers and, despite having identical chemical compositions, can often have different physical and biological properties. Chiral

molecules are named using Cahn-Ingold-Prelog rules which give priority to the groups or atoms surrounding the stereocentre in terms of increasing atomic number. The letters *R* (*rectus* – right) and *S* (*sinister* - left) are used after the assignment of priority has been determined [2]. Figure 1.1 illustrates the Cahn-Ingold-Prelog convention for the naming of chiral molecules, with the molecule viewed along the bond between central atom and lowest priority substituent (atom 4).

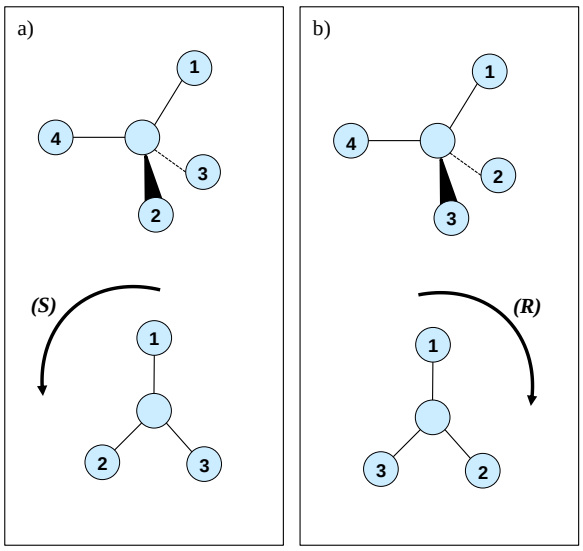

Fig. 1.1 Schematic diagram for the assignment of the a) *(S)*-enantiomer and b) *(R)*-enantiomer.

A pair of enantiomers can be distinguished by their ability to rotate the plane of polarisation of a beam of plane-polarised light in a clockwise or anticlockwise fashion, due to the difference in refractive indices. From this, it is possible to determine enantiomeric excess (e.e.) from values of the pure enantiomer and of a mixture in which one enantiomer is present in greater quantities than the other (Equation 1.1).

$$\%ee = \frac{[(R)\text{-}enantiomer] - [(S)\text{-}enantiomer]}{[(R)\text{-}enantiomer] + [(S)\text{-}enantiomer]} \times 100$$

Equation 1.1

Enantiomeric excess measurements were first carried out in 1815 by Biot [3] and have become a standard in industry due to numerous instances where enantiomers of the same compound have caused varied effects within the body. As most drugs consist of chiral molecules a “lock-and-key” mechanism occurs within cells, which are themselves made of enzymes and other receptors which possess chirality, resulting in only one enantiomer of the drug binding preferentially. The binding of

the opposite enantiomer can cause a completely different effect to the cells. One such example, which unfortunately resulted in detrimental consequences, was the prescription of thalidomide to pregnant women. Although the drug was prescribed as a pure enantiomer, *in vivo* interconversion occurred to racemise the drug within the body. While one enantiomer treated nausea effectively, the other was found to cause foetal damage [4]. Nowadays, large scale pharmaceuticals, fine chemicals and agrochemicals are increasingly produced as enantiomerically pure compounds. This can be because of superior performance from an enantiomerically purer form, and because, from a safety point of view, regulatory boards demand stringent evaluation of a biologically active racemate before rendering the product safe.

1.2 ENANTIOSELECTIVE CATALYSIS

A catalyst is classed as a substance which accelerates the rate of a chemical reaction without undergoing permanent chemical change itself. One of the first significant uses in the 20^{th} century of a catalyst in a reaction can be attributed to Wilhelm Ostwald who received the Nobel Prize in Chemistry in 1909 for his work on the conversion of ammonia to nitric acid, using Pt as a catalyst [5]. Since the pioneering work of Ostwald, catalyst use in all types of industry has increased dramatically, with the majority of all chemical products going through at least one catalytic process. Catalysis continues to grow in importance, flanking the need for increasingly efficient chemical processes in industry and academia, and as a result different types of catalysis have been studied, as well as cross disciplinary research into improving catalysts by examination at a molecular level.

Enantioselective catalysis deals with the production of an excess of one enantiomeric form over the other. The current industrial route to enantioselective control of a reaction pathway is to use either homogeneous or enzyme catalysis. However, the advantages connected with the use of a heterogeneous process, such as the ease of catalyst separation and regeneration has encouraged the growth of enantioselective heterogeneous catalysis.

A number of triumphs have occurred in enantioselective homogeneous catalysis in recent years. The Nobel Prize in Chemistry in 2001 was awarded to Knowles, Noyori and Sharpless for their pioneering work in the use of organometallic complex catalysts containing carefully designed chiral ligands in industry. Enantioselectivity is bestowed by forcing prochiral reagents into certain geometries by use of bulky ligands attached to the organometallic catalyst, allowing an enantioselective reaction to occur [6].

A comparable development of enantioselective heterogeneous catalysis with homogeneous catalysis has not yet occurred due to difficulties in creating well-defined, reproducible and stable chiral sites on a solid support. Heterogeneous processes are procedures hampered by the fact that several variables must be taken into account, and appropriate catalysts have to be employed in the reaction. Metal catalysts do not possess an inherent chirality and so enantioselectivity is only manifested if the overall reaction takes place in a chiral environment. Chirality can be imparted in several ways: - by depositing a metal onto solid chiral supports, by forming chiral surfaces on achiral metal crystals, or by absorbing chiral organic modifier molecules onto the surface of a metal. Another concept is the "heterogenising" of homogeneous catalysts, which involves tethering a homogeneous system to a heterogeneous support [7]. These strategies have been developed over time to varying degrees of success and important results have emerged. The use of chiral organic modifier molecules has been the most promising route to date, shown in the successful implementation in the Pt and Ni catalysed hydrogenation reactions of α- and β- ketoesters respectively [8, 9].

A chiral surface can be formed from any crystal that lacks a centre of symmetry. One such crystal is quartz, which was used as one of the first chiral supports for the attachment of Cu, Ni, Pd and Pt catalysts, to use in the dehydrogenation of racemic butan-2-ol [10]. A measurable e.e. of 10%, although low by today's expectations, gave evidence that enantioselectivity occurred due to the chiral arrangement of the

crystal. Subsequent researchers began to use natural fibres for chiral supports, such as the successful use of silk-Pd catalysts by Izumi in 1956, and the use of cellulose by Harada in 1970 [11]. In later years, a SiO_2 support was tested with the Ni catalyst used in the enantioselective hydrogenation of methylacetoacetate (MAA) to methyl-3-hydroxybutyrate (MHB) and higher enantioselectivities were achieved compared to unsupported Ni [12]. However, with the exception of the silk-Pd catalyst, the enantioselectivities were found to be poor, and the results of the silk-Pd catalyst were later found to be difficult to reproduce [9]. Consequently, a far more comprehensive study into the mechanism of conveying chirality from the support to the metal surface is needed to optimise the enantioselectivity of the system.

A crucial difference between inorganic crystals such as the intrinsically chiral quartz described previously and catalytic metals is that, in their bulk form, metals have an achiral structure. Metal particles however are very rarely perfectly achiral and usually contain kink defects which can be chiral under appropriate conditions. A face-centred cubic (fcc) metal single crystal can be made intrinsically chiral under appropriate conditions by cutting to expose a high Miller index plane with the majority of kink sites of a certain symmetry. The bulk lattice of the metal will remain achiral, but the surface of the material will be chiral. This was demonstrated by McFadden *et al.* on a silver single crystal, cut to expose the $Ag(643)^R$ and $Ag(643)^S$ surfaces [13]. Low energy electron diffraction (LEED) experiments were carried out to prove that the surfaces were enantiomers of one another; however the group could not identify enantiospecificity in the desorption of the chiral alcohol 2-butanol. Some time later, Attard and co-workers provided the first experimental observations of an adsorption energy difference for each enantiomer of D- and L-glucose when adsorbed on a chiral $Pt(643)^S$ electrode [14]. Sholl *et al.* investigated this system further by developing a molecular simulation to show that adsorption energies varied substantially for different enantiomers [15]. Numerous other studies, such as the study by Gellman *et al.* on (*R*)-3-methyl-cyclohexanone adsorbed enantioselectively on $Cu(643)^R$ and $Cu(643)^S$, add to the observation of enantiospecificity at a metal surface in the absence of any chiral modifier [16].

However, there are limitations to this strategy which renders the chiral metal surfaces challenging for use in real catalyst systems. There are concerns about the stability of the chiral sites under various reaction conditions, the low proportion of chiral sites on the surface, and the possible bias caused by differences in size between the reactant molecules and the surface.

An alternative route to achieving a chiral metal surface is to adsorb a suitably chiral organic molecule onto the active phase of the catalyst. Ideally, the molecule should contain a functional group which allows adsorption to the substrate, as well as a functional group which interacts with reactant molecules. There is a wealth of literature documented following the use of chirally modified surfaces to catalyse enantioselective reactions, specifically the nickel catalysed hydrogenation of β-ketoesters and the platinum catalysed hydrogenation of α-ketoesters. It is especially desirable to have the ability to catalyse hydrogenation reactions as it is the starting point of many different reactions to yield various functional groups [11].

The addition of a chiral modifier onto a metal surface was first reported in 1939 by Lipkin and Stewart who reported on the reduction of methylcinnamate using Raney Ni modified by D-glucose, and a Pt catalyst modified by hydrocinchonine [17]. Following these initial promising studies, several other groups chose to modify Pt and Ni catalysts with chiral acids, gaining substantial enantiomeric excesses [9,18,19]. Subsequent research has mainly focused on the Ni and Pt catalyst systems, systematically changing many different variables in an attempt to optimise the catalytic conditions.

1.3 Ni-CATALYSED HYDROGENATION OF β-KETOESTERS

The enantioselective hydrogenation of β-ketoesters over a hydroxyl or amino acid – modified Raney Ni (herein denoted RNi) surface was the first successful chiral heterogeneous catalytic reaction and has been researched in great detail in Japan since the late 1950s [19,20]. Akabori and co-workers originally discovered that all

of the amino acids they tested caused some enantioselective hydrogenation activity of ethyl methyl ketone and allyl alcohol reagents [21]. The next paper in the series [22] found that MAA gave an excellent e.e. result when hydrogenated over RNi treated with several modifiers, and so this reagent has continued to be studied by research groups up to the present day. Catalysed hydrogenation of MAA with *(R)*-hydroxy or *(S)*-amino acid modifiers yields *(R)*-MHB in excess, whereas *(S)*-hydroxy or *(R)*-amino acids yields *(S)*-MHB (Figure 1.2). MHB is an important intermediate in the synthesis of MK-0507, used in the treatment of glaucoma [23].

Preliminary experiments in 1958 by Isoda *et al.* achieved enantioselectivities of 2.5–36% for modified RNi catalysts [19]. Although low, the enantioselectivity values showed potential for further work into the system. Research from the work has been continued by Izumi [9], and Tai and Harada [20] in Japan whilst, in Europe, catalysis groups led by Webb [8], Keane [24] and Sachtler [25] have also made notable contributions. Numerous transition metals were considered, including Ru, Co and Cu, with Ni giving the highest enantiomeric excess when modified with tartaric acid (denoted TA herein). At present, e.e.'s of over 95% have been achieved using an *(R,R)*-TA modified RNi catalyst with NaBr as a co-modifier [9]. To date, there is an extensive amount of work published on the modified Ni system, with groups documenting the most successful combinations of modification and reaction variables needed for high enantiomeric excesses.

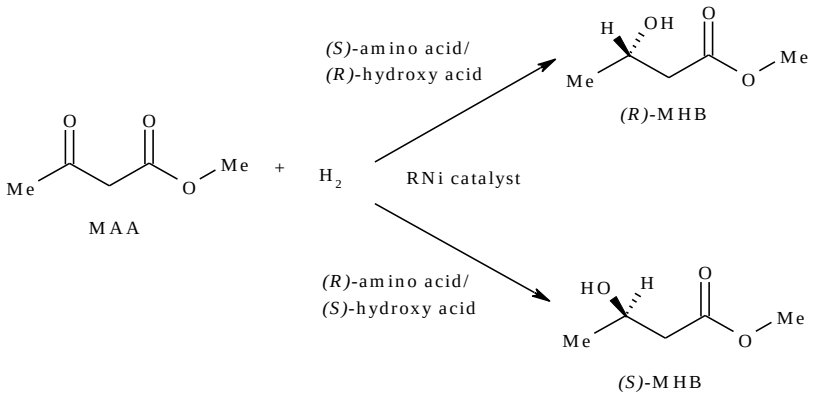

Fig. 1.2 Enantioselective hydrogenation of the β-ketoester methylacetoacetate over modified RNi catalyst.

In Figure 1.3, the procedure of hydrogenation of MAA to MHB over a RNi catalyst is summarised. The degree of enantioselectivity depends greatly on the modification conditions. Modifier concentration, temperature, pH and modifying time are all crucial variables which alter the performance of the catalyst [9].

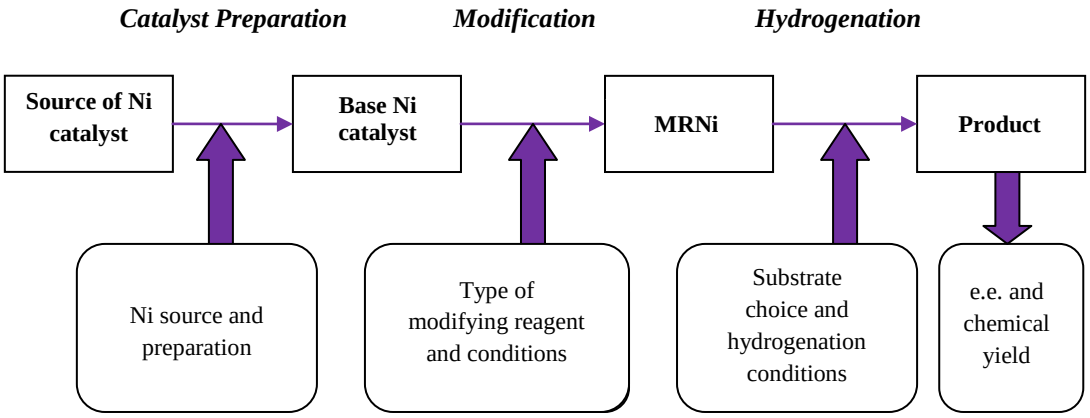

Fig. 1.3 Procedure for the enantioselective hydrogenation with modified RNi catalysts. Adapted from [20].

1.3.1. MODIFIER CONCENTRATION

The extent of adsorption of TA on the RNi surface depends strongly on the modifier concentration. Webb and co-workers presented results that showed, at low concentrations of tartaric acid, only a small fraction of adsorbed MAA was influenced by the modifier, resulting in an overall racemic hydrogenation [26]. Similarly, at high concentrations, the adsorbed MAA could be trapped by modifier molecules causing stereochemical interference, also resulting in a racemic product. An optimum concentration would allow the MHB enantioselective conversion to be at its highest level, whilst keeping loss of activity due to leaching of Ni from the catalyst surface to a minimum. It was found that a TA surface coverage of approximately 0.2 ML gave the highest e.e, where in this case 1 ML corresponds to a surface saturated by tartaric acid.

1.3.2. METAL LEACHING

Leaching of Ni from the RNi surface has been found to occur extensively. The effect of crystal size of the Ni catalyst on the enantioselectivity was studied by Nitta *et al.*

[27]. It was found that the greater the crystallite size the higher the enantioselectivity, suggesting large ensembles of regularly arranged Ni atoms were desirable for sufficient modifier adsorption. Webb and co-workers, whilst studying TA-modified Ni, found a progressive leaching of Ni into the solution (accompanied by a colour change from clear to light green) at the end of the modification process, resulting in a complex which, without any pre-treatment, was catalytically active and enantioselective [26]. Hoek and Sachtler had earlier proposed a model based on the possibility of a nickel tartrate complex forming upon modification and either remaining on the silica support or desorbing into the modifier solution [25], which gave credence to the experimental results found by Webb and co-workers.

1.3.3. MODIFICATION TEMPERATURE

Modification temperature has also been found to affect enantioselectivity of the product, as in the case of *(S)*-glutamic acid (herein *(S)*-Glu) modified RNi [21]. When modified with *(S)*-Glu below 353 K, MAA hydrogenates to the *(R)*-MHB product whereas, as temperatures were elevated, the enantioselectivity decreased markedly, until temperatures above 353 K yielded the antipode product (Figure 1.4).

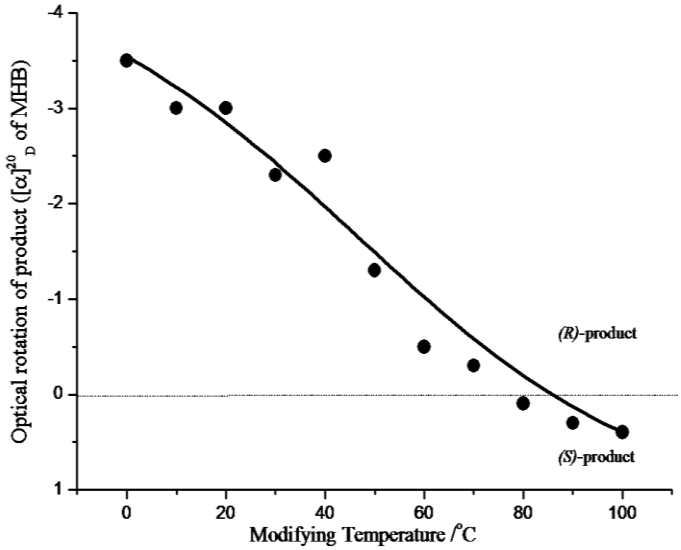

Fig. 1.4 Effect of modification temperature on the (S)-Glu modified RNi catalysed hydrogenation of MAA. Adapted from [22].

This result infers two different enantioselective sites on the surface of the catalyst, whose ratio varies corresponding to the different modifying temperature. This temperature-dependent switch in enantioselectivity has also been found for several

other α-amino acid modifiers such as *(S)*-alanine, *(S)*-phenylalanine and *(S)*-proline [28].

1.3.4. MODIFICATION pH

The pH of the modifying solution was found to strongly alter the enantioselectivity of the MAA hydrogenation. It had been reported for TA that an optimum enantioselectivity was achieved at pH 5.1 (for RNi). It also appeared that surface coverage was linked to modification pH, and so control of the pH of the modifier ensured the TA molecules bound to the catalyst surface in a geometrically more appropriate form for enantioselectivity [26]. To adjust pH values of the selected modifier solution, alkali hydroxides were used. It was found NaOH gave a much higher enantioselectivity than other alkali hydroxides tested as potential pH adjusters, suggesting that the cation radius may critically affect adsorption [9].

1.3.5. USE OF CO-MODIFIERS

Another important parameter in the modification conditions is the use of a sodium salt as a co-modifier to enhance the selectivity of the *(R,R)*-TA modified hydrogenation of MAA. The idea of a co-modifier was discovered unexpectedly when increases in the e.e. of the modified catalyst occurred in the presence of chloride and sulfate contaminants in the water [20]. Amongst those studied, NaBr caused the strongest improvement to the enantioselectivity, even though it possesses no enantioselectivity itself. There are several ongoing arguments on the actual mode of the co-modifier, with the idea of the NaBr blocking unmodified (bare) metal sites and thus lowering their racemic hydrogenation activity combined with the enhanced stabilisation of the active NiTA complexes the most popular theory [8].

1.3.6. REACTION VARIABLES

Reaction variables can also strongly affect the enantiomeric excess of the product in RNi catalysed MAA hydrogenation. The hydrogenation is preferably carried out in liquid phase and so emphasis has been placed on research into the most appropriate

choice of solvent. Orito *et al.* showed high enantioselectivities for the hydrogenation of MAA over a Ni/Pd/kieselguhr catalyst using aprotic semipolar solvents such as tetrahydrofuran (herein THF) and ethyl acetate [20]. Temperatures between 333 – 373 K, H_2 pressures between 80 – 120 bar and constant agitation of the reaction suspension have been found to reproducibly achieve high enantioselectivity values [22].

1.4 Pt CATALYSED HYDROGENATION OF α-KETOESTERS

The Pt-catalysed hydrogenation of α-ketoesters has also received particular attention since the system was first studied by Orito and co-workers in the late 1970s [8]. The enantioselective hydrogenation of methyl pyruvate over a cinchona-modified Pt catalyst yielded the formation of *(R)-(+)-* or *(S)-(-)*-methyl lactate, depending on the cinchona alkaloid modifier employed (Figure 1.5).

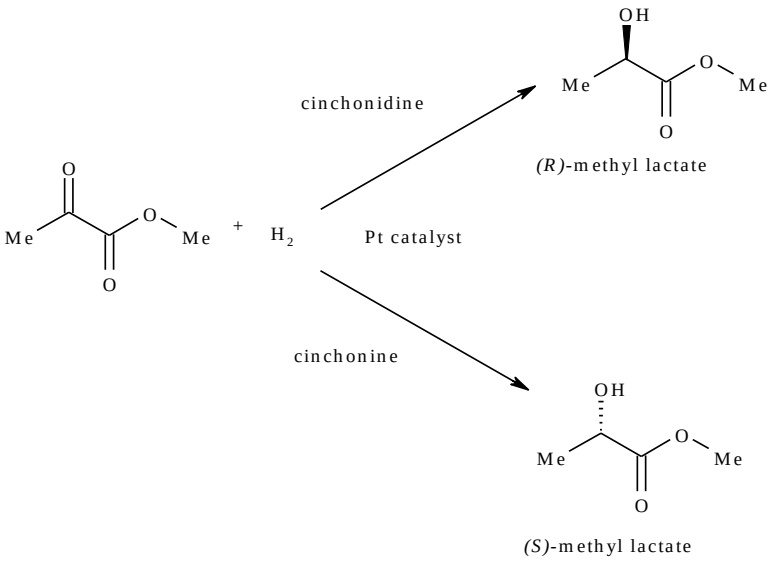

Fig. 1.5 Enantioselective hydrogenation of the α-ketoester methyl pyruvate over a cinchona-modified Pt catalyst.

In the absence of the modifier, both enantiomers of the reactant molecule are chemisorbed on the Pt surface with the same adsorption energy, yielding a racemic mixture of methyl lactate product. Upon adsorption of a cinchona modifier

molecule, hydrogenation of methyl pyruvate preferred one enantiomeric product over the other. Cinchona alkaloids, derived from the bark of cinchona trees, were chosen as suitable modifiers after previous successful applications in homogeneous enantioselective reactions [20]. Methyl lactate is an important precursor in the flavouring and fragrance industries.

As for the Ni-catalysed system, enantiomeric excess was found to be sensitive to a host of different variables – from pre-treatment procedures, to modification and reaction variables (for example, a choice of solvent, temperature and concentration of modifier) [8]. At optimum conditions, Pt catalysts modified with the cinchona alkaloid cinchonidine achieved yields of up to 95% e.e. when used in the hydrogenation of ethyl pyruvate to *(R)-(+)*-ethyl lactate.

1.5 PROPOSED CATALYST MODELS

For the two previously mentioned systems, a model of the catalytic process is obviously desirable, especially in terms of determining the mode of action promoting enantioselectivity. Numerous theories have been proposed to account for the enantioselective behaviour.

1.5.1. TEMPLATE MODEL

For the case of the Pt-catalysed system, the "template model" was initially put forward as a possible explanation of the enantioselective methyl pyruvate hydrogenation to *(R)-(+)*-methyl lactate [8]. Briefly, garnered from experimental studies on reaction and modification variables by the groups of Blaser [11], Baiker [29] and Wells [8], a set of observations were made which resulted in the proposal of a model in which the L-shaped cinchonidine modifier molecules adopt a porous ordered arrangement on the Pt surface, leaving a remaining chiral ensemble of "bare" Pt atoms in such an arrangement that only one enantioface of the reactant molecule accessed the pores. Formation of the other enantiomer would be disfavoured due to steric hindrance by the modifier, introducing enantioselectivity to the surface as a

result (Figure 1.6). Site A in Figure 1.6 indicates the enantioselective hydrogenation site which favours methyl pyruvate adsorption reacting with H_2 from below to give the *(R)-(+)*-methyl lactate product. It should be noted that, in the template model, no bonding interaction is required between the prochiral reagent and the modifier molecule array.

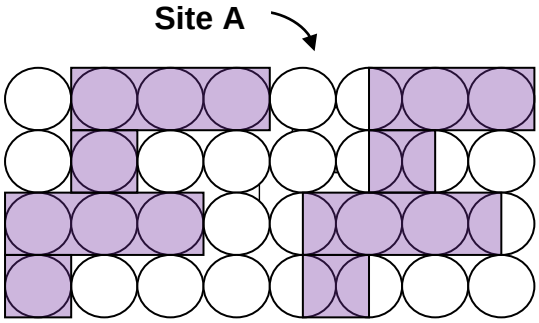

Fig. 1.6 Proposed template model by Wells and co-workers to show modification of Pt(100) surfaces by chiral modifier cinchonidine (L-shaped modifier). Adapted from [8].

The template model was later discredited when strong evidence was shown in STM studies of docking interactions between the reagent molecule and modifier in the Pt/cinchona/α-ketoester system [30]. Independently, McBreen and co-workers used RAIRS to obtain information on the orientation of the methyl pyruvate molecule adsorption on clean and NEA-modified Pt{111} surfaces [31]. It was established that a 1:1 interaction occurred between both molecules, identified as hydrogen-bonding between the reactant carbonyl group and the modifier amine group. These results added to mounting evidence against the template model and led to the development of an alternative known as the "active chiral site" model, or 1:1 interaction model.

1.5.2. ACTIVE CHIRAL SITE MODEL

The "active chiral site model" suggests that a 1:1 bonding mechanism occurs between the modifier and reactant molecules, and an ordered arrangement of modifiers is not important to the enantioselectivity of the system. The model is thought to equally apply to the adsorption of MAA on the modified Ni catalyst surface. Ordered arrangements of chiral modifiers such as hydroxy- and amino acids

have only been observed at very high coverages (e.g. for *(R,R)*-TA [32] and *(S)*-Glu [33]), and such a dense coverage prohibits the co-adsorption of the MAA reactant molecules. In the case of an *(R,R)*-TA modified system, Tai and Sugimura discussed the possibility of the formation of two hydrogen bonds between the adsorbed bitartrate modifier and the β-ketoester ketone groups [34]. This transpired from numerous hydrogenation studies of a variety of methyl esters of α-, β-, γ-, and δ-keto acids which showed MAA to give the highest enantioselectivity results, suggesting the distance between the two carbonyl groups in the diketo form to be critical in allow the formation of a stabilising hydrogen bonding effect. This type of anchoring of the molecules would explain the observations made by Webb and co-workers [26, 35], that an intermediate concentration of TA would effectively give an optimum enantioselective coverage as it would allow the distance between the adsorbed TA molecules to be sufficient enough to accommodate an adsorbed MAA molecule in a 1:1 ratio between modifier and reactant, but also small enough to minimise the number of racemic sites. This model would appear suited to the Ni catalytic series as the small, mobile hydroxy- and amino acid modifiers are likely to interact with neighbouring modifiers by H-bonding interactions.

1.5.3. ALTERNATIVE MODELS

Various other proposals have been suggested for the Ni system. The adsorbed organometallic complex model, proposed originally by Klabunovskii and co-workers in the late 1960s [36], and revised by Hoek and Sachtler in later years [25], may have some relevance in the catalytic process. It is well known that Ni can leach from the catalyst surface and so it is a strong possibility that an adsorbate-induced restructuring procedure may take place. It was suggested that a catalytically active intermediate of a Ni ion, having been leached due to modification and reaction conditions, may exist on the metal surface surrounded by the reactant and modifier molecules, with remaining coordination sites involved in the docking of the reactant as well as the dissociative hydrogenation. In brief, it appears that the concept of chiral modifier adsorbates interacting with the prochiral reagent through hydrogen bonding, and also the possibility of leaching, are two important parameters in the

optimisation of the level of enantioselectivity in the catalytic systems studied. Knowledge of the modified interface would allow justified predictions to be made as to how the most successful systems operated, and conversely why other pairings failed to give high enantioselectivities.

1.6 SURFACE SCIENCE STUDIES OF CATALYST SYSTEMS

The nature of the modified surface complex formed when a chiral modifier is adsorbed onto a metal catalyst surface is important in that it provides a model which is potentially significant for examining the geometry and interaction of the incoming reactant species. A simplistic view of the modifier and substrate is to think of the model as static and the modifier molecules only adopting one particular orientation. The ways in which chiral modifiers are adsorbed and structured on a surface are ideally analysed by surface science techniques. In the past twenty years, there has been a considerable expansion of knowledge on how chirality may be imparted to a metal surface by modifier molecules for the Pt and Ni catalytic systems [37], using surface science techniques. The first foray into using surface science as an approach to examine the adsorption of α-hydroxy and α-amino acids involved a study by Baddeley and Raval into the adsorption of *(R,R)*-TA on Cu{110} [38]. Much work has continued on similar substrate/modifier systems, veering towards their behaviour under ambient conditions using *in-situ* techniques. The benefit of using *in-situ* techniques is that catalytic conditions can be mimicked more accurately, depositing modifiers and prochiral reagents directly from solution and allowing parameters such as modification temperature and solution pH, which can significantly alter the operation of the catalyst, to be easily altered.

1.6.1. HYDROXYL ACID MODIFIERS

1.6.1.1. TARTARIC ACID MODIFIER

Tartaric acid is a chiral hydroxyl acid which can exist in at least three different forms (depending on temperature and coverage), each of which have been identified on a Cu{110} single crystal surface by means of RAIRS [38]. At low coverages, and

after an adsorption temperature increase to 405 K, *(R,R)*-TA is in its bitartrate form, which was found by a combination of RAIRS, LEED and scanning tunnelling microscopy (STM) to bestow long-range ordered chiral structures on the Cu{110} surface. The low coverage phase was thought to be relevant in the enantioselective hydrogenation of *β*-ketoesters as it had space to accommodate the reactant molecule. The empty nanosized chiral channels, as shown in Figure 1.7, were suggested to offer docking sites for the MAA reactant molecules in a preferred orientation only, thereby creating an enantioselective site for hydrogenation, and bringing renewed relevance to the template model as proposed previously for the Pt catalytic system by Wells and co-workers [8]. Further work on the system by Barbosa and Sautet used density functional theory (DFT) modelling to demonstrate stabilising intramolecular hydrogen bonding between the *α*-hydroxy groups and carboxylate groups of the TA molecules, however this was not thought to influence the long range order since adjacent molecular species were too far apart to allow significant H-bonding interactions [39]. Instead, a combination of pairwise attractive interactions and adsorbate-induced stress (caused by the adsorption of more than three carboxylate groups adjacent to each other) created the formation of long range order of bitartrate species, with empty troughs [40].

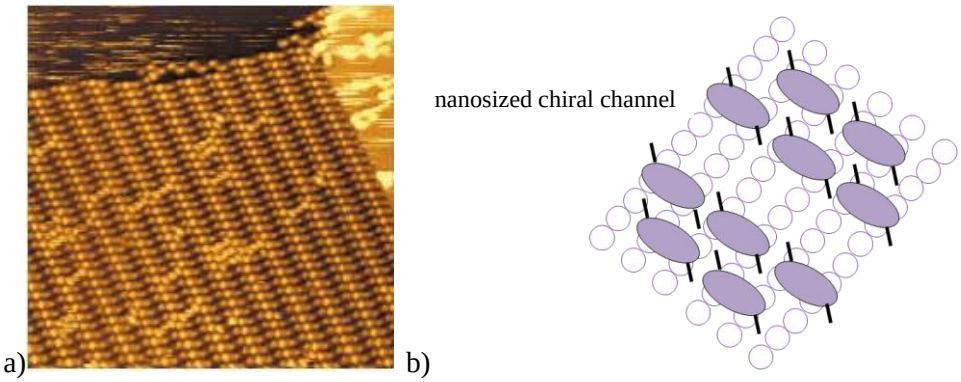

Fig. 1.7 Extended (9 0, 1 2) chiral phase of *(R,R)*-TA on Cu{110} a) 150 x 200 Å STM image showing chiral channels and b) a model of empty chiral channels deducted from STM, RAIRS and LEED analysis. Adapted from [41].

STM investigations were carried out on the behaviour of both enantiomers of TA on the Cu{110} surface which showed the chirality of the surface to be switched, presenting the first STM evidence of a chiral domain across an entire surface [41]. Although the work was carried out on a Cu surface, and not on the catalytically

relevant Ni surface, it was extremely valuable in demonstrating the considerable effect changing typical catalytic parameters such as concentration and temperature has on the nature of the adsorbed species and the extent of ordering on the surface, giving rise to enantioselectivity in the hydrogenation reaction. The study also gave first-hand evidence of the reasoning behind why tartaric acid gave the most successful enantiomeric excesses (e.e.) in the catalytic work.

Following from the seminal work of Baddeley and Raval, studies progressed onto the more applicable Ni{110}-tartaric acid system [42]. Humblot *et al.* used a combination of STM, LEED and RAIRS to determine the ordering of *(R,R)*-tartaric acid on the metal surface. As for Cu{110}, the adsorbed TA molecules adopted various forms on the Ni{110} surface depending on temperature and coverage, with the bitartrate forming at 300 K, a much lower temperature (orientation verified by RAIRS). However, it was found that, contrary to TA on the Cu{110} surface, no long range ordered structures were observed on the Ni{110} surface, due to the more localised bond of the adsorbate molecules to Ni atoms which reduced the lateral mobility of the tartaric acid. It was thought the chirality of the molecule was imparted to the metal surface by the adsorbate adsorption causing a local chiral restructuring of the metal surface, as opposed to the Cu{110} case in which the adlayer itself bestowed chirality. Local chirality has the predicament that the mirror reconstruction is equally allowed on the surface, but in the Ni{110}/TA case spin-polarised calculations were carried out which showed a difference in the adsorption energy between the two different footprint geometries large enough to ensure over 90% of the adsorbed bitartrates adopted one chiral footprint [43].

Jones and Baddeley also chose to study the TA-modified Ni system, but selected the more thermodynamically stable {111} crystal face, expected to be the dominant face on the Ni nanoparticles used in catalysis, as found on a truncated octahedral particle, a common nanoparticle shape [32]. The monotartrate and bitartrate species were detected on the surface; their presence dependent on temperature and coverage as in

the case of Cu{110} and Ni{110}. Due to the greater reactivity of the Ni{111} surface, it was found through RAIRS and TPD data that CO(ads) coexisted with the tartrate species on the surface, only being displaced by higher coverages of *(R,R)*-TA. The tartrate adlayers were found to order over a smaller area than on the previously studied metals, also attributed to the greater surface reactivity. The nature of the adsorbed species at modification temperatures of 300 K and 350 K appeared to differ, with ordered monotartrate structures at 300 K hydrogen bonded intermolecularly between the α-hydroxy groups of neighbouring molecules, and the carboxylate functionality binding to the Ni{111} surface, while a bitartrate species at 350 K was proposed to intermolecularly H-bond around a central bitartate species on the surface, stabilising the adlayer at higher temperatures.

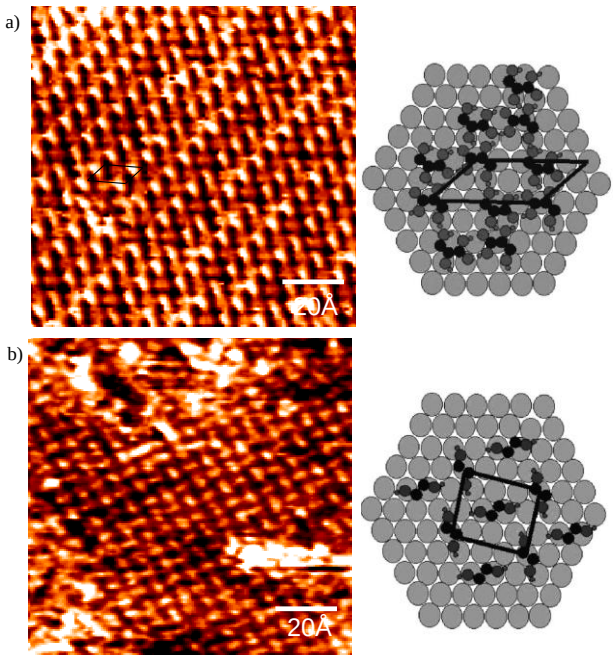

Fig. 1.8 STM images and corresponding models for a) extended (5 0, 1 2) chiral phase of *(R,R)*-TA on Ni{111} at 300 K and b) (4 -1, -1 3) phase at 350 K. Adapted from [32].

1.6.2 AMINO ACID MODIFIERS

Amino acids have two functional groups – the carboxylic acid group and the amino group – either or both of which have the potential to bind to a metal surface, (depending on its nature) and some have active side groups which allow further interaction with the surface. From a potentially vast array of possible compounds, only 20 α-amino acids are commonly found to form part of proteins, all with

chirality, except glycine. Previous extensive work by Izumi and co-workers pinpointed several α-amino acids which give reasonable e.e. values for the Ni catalysed *β*-ketoester hydrogenation. Amino acids *(S)*-Val, *(S)*-Glu, *(S)*-Ala, *(S)*-Asp and *(S)*-Lys showed moderate e.e. values of 0-15% in preliminary catalytic studies (Figure 1.9 and Table 1.1), and so all displayed the potential to be studied more extensively in a systematic fashion [9]. Indeed, several of these molecules have been studied in a series of papers from the findings of Izumi and co-workers – focusing on modifying temperature [22], modifier pH [45], modification concentration [27] – similar to the methodical work carried out in the first catalytic studies of *(R,R)*-TA. Primary amino residues of amino acids were found to be necessary for the hydrogenation to proceed enantioselectively, after studies on N-substituted amino acids and derivatives of *(S)*-Glu and *(S)*-Asp produced racemic products [22]. This in itself gave a wealth of useful data to help in choosing amino acid modifier candidates for surface science studies on the catalytic system. Where enantiomeric excess values are not directly accessed from literature, Equation 1.2 is used, where $[\alpha]_D^{20}$ for optically pure MHB has a value of -22.95 [44].

$$e.e. = \frac{[\alpha]_D^{20}\ hydrogenation\ product}{[\alpha]_D^{20}\ optically\ pure\ MHB} \times 100$$

Equation 1.2

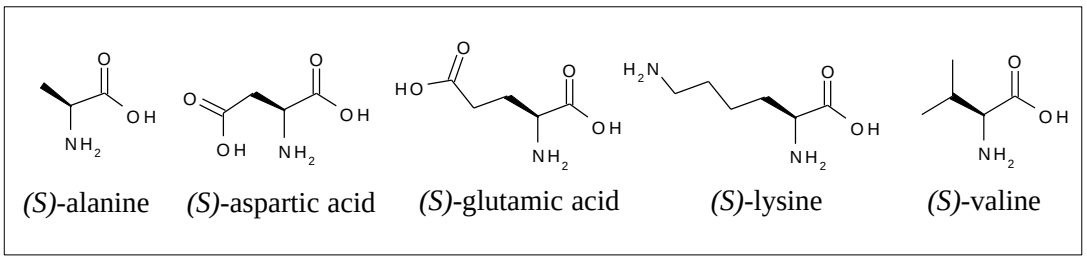

(S)-alanine *(S)*-aspartic acid *(S)*-glutamic acid *(S)*-lysine *(S)*-valine

Fig. 1.9 Molecular structures of studied amino acids.

Modifying reagent	**e.e. (%)**
(R,R)-Tartaric acid	25.6
(S)-Alanine	1.1
(S)-Aspartic acid	8.2
(S)-Glutamic acid	8.9
(S)-Lysine	6.3
(S)-Valine	13.2

Table 1.1 Correlation between optical yield and amino acid modifier for MAA hydrogenation over modified RNi catalyst (modifying conditions: isoelectric point, 0°C, reaction conditions: MAA (neat), 70°C, atmospheric P).

1.6.2.1 ALANINE

Alanine was the first chiral amino acid to be studied on the Cu{110} surface at a molecular level. As the nature of an adsorbed molecule in terms of its chemical form and orientation is the directing factor in its likelihood to order on a metal surface, RAIRS has been used extensively in studies. Williams *et al.* discovered by RAIRS that the adsorption geometry of the molecules on the surface changed depending on coverage [46]. This is an observation that has repeatedly been found for many other amino acids on metal surfaces. By STM data, it was established that adsorbed alanine produced local chirality as long as its chiral centre was not altered on adsorption on the metal surface. Alanine could also form a chiral supramolecular assembly on the Cu{110} surface; well-ordered adlayer arrays, driven by H-bonding, to give a homochiral 2D phase across the surface [47]. Alanine is a logical molecule to study due to it being the simplest chiral α-amino acid but, likely because of its low enantioselectivity (see Table 1.1), surface science studies have not progressed regarding its potential as a modifier for the Ni-catalysed β-ketoester hydrogenation.

1.6.2.2 GLUTAMIC ACID

In contrast, glutamic acid, studied more extensively as a modifier in the catalytic experiments by Izumi and co-workers [22,28] showed, in addition to a reasonably moderate e.e. value (8.9 %), an interesting change in enantioselectivity of the product depending on modification temperature (Figure 1.4). *(S)*-Glu was originally studied by UHV-STM and RAIRS on the Ag{110} substrate in an attempt to determine intermolecular interactions rather than the influence of the bond between the molecule and substrate (adlayers on Ag{110} have a weaker molecule-surface interaction compared to adlayers on Cu{110}) [48]. It was found that *(S)*-Glu adsorbed predominantly in its anionic form, and caused adsorbate induced faceting to the Ag surface. After the initial Ag substrate study, STM and RAIRS experiments were carried out on the adsorption of *(S)*-Glu on Ni{111} as a function of temperature by Baddeley and co-workers [33]. Two different mechanisms were proposed at the temperatures of 300 K and 350 K due to the occurrence of significant

corrosion at step edges by the adsorbate at higher temperatures. The lack of corrosion at 300 K and the presence of *(S)*-Glu in its zwitterionic form suggested a 1:1 interaction, with the NH_3^+ group available to H-bond with a *β*-ketoester reagent, which could favour the formation of the *(R)*-enantiomeric product. Conversely, the corrosion present at 350 K may hint at the production of chiral step-kink sites, which could favour the *(S)*-enantiomer.

Although UHV results on the *(S)*-Glu modified Ni system provided interesting data on the root of enantioselectivity, UHV techniques are far removed from the liquid-solid interface environment employed in both the modification step and in the catalytic reaction. To address this, Baddeley and co-workers carried out work on *(S)*-Glu in the liquid-solid interface environment to emulate the modification conditions where the catalyst operates most effectively [49]. The chemical form of an amino acid can vary depending on the conditions of the surrounding environment, so consequently Baddeley and co-workers carried out RAIRS studies under non-UHV conditions to characterise the effect of pH on the adsorption from solution of *(S)*-Glu on Ni{111}. These conditions were also applied to a study on the influence of modification temperature change, as a progression of the UHV work [49].

1.6.2.3 OTHER AMINO ACIDS

A vast amount of studies have been carried out on most of the remaining essential amino acids although with a more fundamental focus on understanding the manner in which biologically active molecules bind to a range of metal surfaces, rather than from a catalytic aspect. Understanding the adsorption mechanism is important in the development of biocompatible materials [50], biosensors [51] and biocatalysts [52]. Chiral amino acids such as *(S)*-phenylalanine [53], *(S)*-aspartic acid [54], and *(S)*-lysine [55 – 59] have been studied on various Cu crystal faces, as well as *(S)*-alanine [60], *(S)*-glycine [61] and *(S)*-proline [62] on palladium, whilst other transition metals such as Ag have been used less extensively. The utilisation of the knowledge

found in these extensive studies has great potential when examining those amino acids suitable for use as chiral modifiers in the Ni system.

1.6.3 ENANTIOSELECTIVE HYDROGENATION OF METHYLACETOACETATE

The simplest *β*-ketoester, methylacetoacetate, is the prochiral reagent hydrogenated enantioselectively over a modified Ni catalyst to MHB. It has two tautomeric forms and can exist in either its diketone or enol form in the gas phase (Figure 1.10).

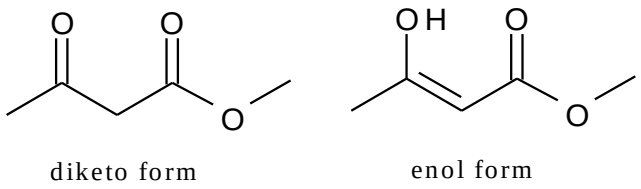

Fig. 1.10 Methylacetoacetate in its diketo and enol tautomeric forms.

Jones and Baddeley carried out UHV-STM, RAIRS and TPD studies on the adsorption of MAA onto an *(R,R)*-tartaric acid modified Ni{111} surface and found evidence discounting the template model between MAA and *(R,R)*-tartaric acid [63]. MAA could not adsorb under UHV conditions onto an *(R,R)*-tartaric acid-saturated Ni{111} surface, suggesting the tartrate adlayer used all available functional groups to form lateral interactions between the neighbouring molecules. The 1:1 interaction model appears to be more likely for the system as MAA adsorption rearranged nearby tartrate species and produce local ordering (Figure 1.11). A low coverage regime of tartaric acid and MAA appeared to suggest a structure of one MAA and one tartrate per unit cell, which would result in an enantioselective formation of the MHB product.

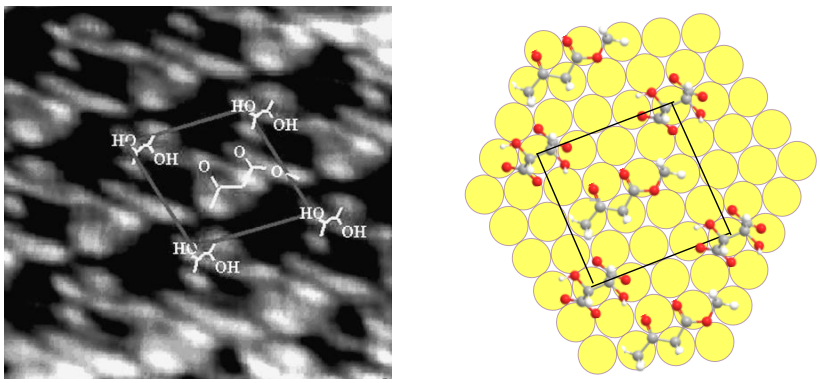

Fig. 1.11 STM image of a low MAA dose onto a Ni{111} surface modified with a low coverage of *(R,R)*-TA. From [63].

Analogous studies of the interaction of MAA with *(S)*-Glu-modified Ni{111} mirrored the aforementioned *(R,R)*-tartaric acid work by proposing a similar model, with the MAA adsorbing in its diketo tautomeric form parallel to the surface at modification temperatures of 300 K, H-bonded to the NH_3^+ and aliphatic COOH groups of zwitterionic *(S)*-Glu [33]. At a modification temperature of 350 K, the point at which the hydrogenation would experience a change in enantioselectivity, MAA adsorbs in the enol form. The liquid-solid interface study of the same system showed that, the more protonated the glutamate modifier, the greater the tendency towards diketone formation, as well as the change in tautomeric form as a function of modification temperature [49].

1.7 BIMETALLIC CATALYSTS

There has been much use of catalysts containing two or more metals in heterogeneous catalysis [64]. A wealth of academic research has focused on combinations of metals from Groups 8-10 and one from Group 11. Fundamental studies investigated the influence a bimetallic system has on the activity of a catalyst. The reasoning behind the enhanced performance of a bimetallic catalyst is thought to be down to two causes: ensemble and ligand effects. Ensemble effects are structural in nature, with the dilution of an active metal by an inert second metal to deplete the number of active sites which may be more favourable for an undesirable competing reaction. Ligand, or electronic, effects suggest the electronic properties of one element are modified by the presence of a second element, and thus changing the chemisorption properties of the surface. The two different metal atoms retain their

identity in terms of chemical and reaction properties and the local density of states (LDOS) parameter is altered for each atom type [65, 66].

The use of Au, predetermined as chemically inert, has been found to display high catalytic activity when combined with a second metallic element, superior to that of either metallic component when assessed separately. For example, the selectivity of Au-Pd alloys in acetic acid, anhydride and acetaldehyde production (all partial oxidation products) is at a maximum at a composition of 80% Au and 20% Pd [67]. It is thought selectivity enhancement in the case of these reactions is due to Au decreasing the number of adjacent Pd sites available for full oxidation, and so enhancing the number of single Pd sites and thus favouring partial oxidation. Enhancement of rate has also been acknowledged for bimetallic systems, for the water formation reaction from H_2 and O_2 over a silica-supported Au-Pd catalyst, the number of H_2 molecules reacted per surface Pd atom per second (turnover frequency) reached a maximum at an intermediate Au coverage, attributed to the ligand effect [68]. Regarding the use of Au and Ni in bimetallic catalytic systems, small quantities of Au on Ni in the steam reforming reaction initiates a promotion effect. Gold, which has no activity on its own for the aforementioned reaction, is thought to reduce unwanted carbon deposition on the active Ni sites, therefore enhancing the selectivity of the reaction [69].

1.8 THESIS OVERVIEW

When designing the geometry of a modifier overlayer for a catalyst surface, the coverage, orientation and robustness of the modifier are all important factors to take into account. The key step in achieving enantioselective performance is the adsorption of chiral modifiers from solution, and therefore there is a view to use a combination of both solution and ultra-high vacuum experiments to allow a more realistic interpretation of the surface chemistry underpinning the catalytic reaction. The behaviour of the Ni/glutamic acid modifier system has been analysed in ambient conditions [49] to allow an understanding of the nature of the modified surface, as well as the interaction with the prochiral reagent MAA. Towards this end, two

amino acids closely related to glutamic acid – aspartic acid and lysine – are presented within this thesis as possible modifiers in the Ni-catalysed enantioselective hydrogenation of MAA, and probed using a combination of UHV (STM, RAIRS, TPD, HREELS) and liquid-solid interface (RAIRS, XPS) techniques. Additionally, similar experiments carried out on 2D Ni clusters grown onto Au{111} are discussed in order to investigate the corrosion of small Ni particles by amino acids – thought to be an important phenomenon in the catalytic reaction [70].

1.9 REFERENCES

[1] J.P. Riehl, *Mirror-Image Asymmetry: An Introduction to the Origin and Consequences of Chirality,* J. Wiley & Sons (ed): New Jersey, 2010.

[2] R.S. Cahn, C. Ingold & V. Prelog, *Angewandte Chemie International Edition,* **5** (1966) 385.

[3] R. Raval, *Current Opinion in Solid State and Materials Science,* **7** (2003) 67.

[4] R. Raval, *Cattech,* **5** (2001) 12.

[5] G. Ertl & H-J Freund, *Physics Today,* **52** (1999) 32.

[6] W.S. Knowles, *Angewandte Chemie International Edition,* **41** (2002) 1999.

[7] Z. Ma & F. Zaera, *Design of Heterogeneous Catalysis: New Approaches Based on Synthesis, Characterisation and Modelling,Chapter 5,* U.S. Ozkan (ed): Wiley-VCH (Weinheim), 2007, 113.

[8] G. Webb & P. B. Wells. *Catalysis Today,* **12** (1992) 319.

[9] Y. Izumi. *Advanced Catalysis,* **32** (1983) 215.

[10] G. M. Schwab & L. Rudolph, *Naturwiss,* **20** (1932) 362.

[11] H. U.Blaser; *Tetrahedron: Asymmetry*, **2** (9) (1991) 843.

[12] Y. Nitta, O. Yamanishi, F. Sekine, T. Imanaki & S. Teranishi, *Journal of Catalysis,* **79** (1983) 475.

[13] C.F. McFadden, P. Cremer & A. Gellman, *Langmuir,* **12** (1996) 2483.

[14] G.A. Attard , A. Ahmadi, J. Feliu, A. Rodes, E. Herrero, S. Blais & G. Jerkiewicz, *Journal of Physical Chemistry B,***103** (1999) 1381.

[15] D.S. Sholl, A. Asthagiri & T. Power, *Journal of Physical Chemistry B,* **105** (2001) 4771.

[16] A.J. Gellman, J.D. Horvath & M.T. Buelow, *Journal of Molecular Catalysis A,* **167** (2001) 3.

[17] D. Lipkin & T.D. Stewart, *Journal of the American Chemistry Society,* **61** (1939) 3295-3297.

[18] Y. Nakamura, *Bulletin of the Chemical Society Japan,* **16** (1941) 367.

[19] T. Isoda, A. Ichikawa & T. Shimamoto, *Rikagaku Kenkyusho Hokuku,* **34** (1958) 134.

[20] A. Tai & T. Harada; *Tailored Metal Catalysts,* Y. Isawawa (Ed.), D Reidel, (1986) 265.

[21] H. Fukawa, Y. Izumi, S. Komatsu & S. Akabori, *Bulletin of the Chemical Society Japan,* **35** (1962) 1703.

[22] Y. Izumi, M. Imaida, H. Fukawa & S. Akabori, *Bulletin of the Chemical Society Japan,* **36** (1963) 21.

[23] A.J. Blacker & R.A. Holt, *Chirality in Industry II,* J. Wiley & Sons (ed): New Jersey, 1997.

[24] M. A. Keane. *Langmuir,* **13** (1997) 41.

[25] A. Hoek & W. M. H. Sachtler. *Journal of Catalysis,* **58** (1979) 276.

[26] A. Bennett, S. Christie, M.A. Keane, R.D. Peacock & G. Webb, *Catalysis Today,* **10** (1991) 363.

[27] Y. Nitta, F. Sekine, T. Imanaka & S. Teranishi, *Bulletin of the Chemical Society Japan,* **54** (1981) 980.

[28]Y. Izumi, M. Imaida, H. Fukawa & S. Akabori *Bulletin of the Chemical Society Japan,* **36** (1963) 155.

[29] A. Baiker, *Catalysis Today*, **100** (2005) 159.
[30] J.M. Bonello, F.J. Williams & R.M. Lambert, *Journal of the American Chemistry Society*, **125** (2003) 2723.
[31] S. Lavoie, M.A. Laliberté & P.H. McBreen, *Journal of the American Chemistry Society*, **125** (2003) 15756.
[32] T.E. Jones & C.J. Baddeley, *Surface Science*, **513** (2002) 453.
[33] T.E. Jones, M.E.Urquhart & C.J. Baddeley, *Surface Science*, **587** (2005) 69.
[34] A. Tai and T. Sugimura, *Chiral Catalyst Immobilisation & Recycling*. D.E De Vos (ed.) Wiley-VCH (2000) 173.
[35] M. A. Keane & G. Webb, *Journal of Molecular Catalysis*, **73** (1992) 91.
[36] Y.I. Petrov & E.I. Klabunovskii, *Kinetic Catalysis*, **8** (1967) 814.
[37] C.J. Baddeley, *Topics in Catalysis*, **25** (2003) 17.
[38] M. Ortega Lorenzo, S Haq, T. Bertrams, P.W. Murray, R. Raval & C.J. Baddeley, *Journal of Physical Chemistry B*, **103** (1999) 10661.
[39] L.A.M.M. Barbosa & P. Sautet, *Journal of the American Chemistry Society*, **123** (2001) 6639.
[40] C.G.M. Hermse, A.P. van Bavel, A.P.J. Jansen, L.A.M.M. Barbosa, P. Sautet & R.A. van Santen, *Journal of Physical Chemistry B*, **108** (2004) 11035.
[41] M. Ortega Lorenzo, C.J. Baddeley, C. Muryn & R. Raval, *Nature*, **404** (2000), 376.
[42] V. Humblot, S. Haq, C. Muryn, W. Hofer & R. Raval, , *Journal of the American Chemistry Society*, **124** (2002) 503.
[43] W.A. Hofer, V. Humblot, R.Raval, *Surface Science*, **554** (2004) 141.
[44] T. Osawa, A. Ozawa, T. Harada & O. Takayasu, *Journal of Molecular Catalysis A:Chemical*, **154** (2000) 271.
[45] Y. Izumi, S. Tatsumi & M. Imaida, *Bulletin of the Chemical Society Japan*, **42** (1969) 2373.
[46] J. Williams, S. Haq & R. Raval, *Surface Science*, **368** (1996) 303.
[47] S.M. Barlow, S. Louafi, D.Le Roux, J. Williams, C. Muryn, S. Haq & R. Raval, *Surface Science*, **590** (2005), 243.
[48] T.E. Jones & C.J. Baddeley, *Langmuir*, **21** (2005) 9468.
[49] T.E. Jones, A.E.Rekatas & C.J. Baddeley, *Journal of Physical Chemistry C*, **111**(2007) 5500.
[50] T. Hanawa, *Journal of the Royal Society Interface*, **6** (2009) S361.
[51] M.U. Ahmed, M.M. Hossain & E. Tamiya, *Electroanalysis*, **20** (2007), 616.
[52] R.N. Patel, *Coordination Chemical Review*,**252** (2008) 659.
[53] H. Wang, X. Y. Zhao, R.G. Zhao & W.S. Wang, *Chinese Physics Letters*, **18** (2001) 445.
[54] H. Wang, X.Y. Zhao & W.S. Yang, *Acta Physica Sinica*, **49** (2000), 1316.
[55] X.Y. Zhao, *Journal of the American Chemistry Society*, **122** (2000) 12584.
[56] X.Y. Zhao, R.G. Zhao & W.S. Wang, *Langmuir*, **16** (2000) 9812.
[57] V. Humblot, C. Methivier, R. Raval & C-M Pradier, *Surface Science*, **601** (2007) 4189.
[58] V. Humblot, C. Methivier & C-M Pradier, *Langmuir*, **22** (2006) 3089.
[59] T. Eralp, A. Shavorskiy & G. Held, *Surface Science*, **605** (2011) 468.
[60] F. Gao, Z. Li, Y. Wang, L. Burkholder & W.T. Tysoe, *Surface Science*, **601** (2007) 3276.

[61] F. Gao, Z. Li, Y. Wang, L. Burkholder & W.T. Tysoe, *Journal of Physical Chemistry C,* **111** (2007) 9981.
[62] F. Gao, Y. Wang, L. Burkholder & W.T. Tysoe, *Surface Science,* **601** (2007) 3579.
[63] T.E. Jones & C.J. Baddeley, *Surface Science,* **519** (2002) 237.
[64] J.H. Sinfelt, *Surface Science,* **500** (2002) 923.
[65] C.J. Baddeley, *The Chemical Physics of Solid Surfaces,* **10** (2002) 495.
[66] V. Ponec, *Applied Catalysis A: General,* **222** (2001) 31.
[67] J. Schwank, *Gold Bulletin,* **18 (1)** (1985), 2.
[68] Y.L. Lam, J. Criado & M. Boudart, *Nouvelle Journal de Chimie,* **1** (1977) 461.
[69] F. Besenbacher, I. Chorkendorff, B.S. Clausen, B. Hammer, A.M. Molenbroek, J.K. Nørskov & I. Stensgaard, *Science*, **279** (1998) 1913.
[70] A.G. Trant, T.E. Jones & C.J. Baddeley, *Journal of Physical Chemistry C,* **111** (2007) 10534.

Chapter 2

Introduction

The primary aim in the development of surface science techniques is to provide a tool which allows insight into the nature of surface structure, adsorbate reactivity and geometry at the molecular level. In heterogeneous catalysis terms it has been of great interest to try to identify the intermediate steps of the reaction, to visualise the active sites of a catalyst, and to understand how the products are formed using an array of surface science methods. With the advancement of a range of surface spectroscopies, scanning probe microscopies and ultra-high vacuum (UHV) equipment, many of these systems have successfully been characterised in great detail.

Heterogeneous catalysts are intrinsically difficult systems to classify. For catalytic phenomena to be observed at the nanoscale, several difficulties need to be overcome, such as the high typical operating temperature and pressure of the catalyst (typically > 200°C and in the range of 1 – 100 bar [1]) and the difficulty in identifying the active phase structure on the various types of surfaces. The approach of surface science is to use highly simplified models as far as possible. Usually the catalyst of interest is prepared as a single crystal (intrinsically a well-defined material) onto which the adsorption of simple atomic or molecular adsorbates is carried out in a precise UHV environment. The surface science approach creates "pressure" and "material" gaps, which must be acknowledged when assessing results, but is still a very powerful means to investigate elementary catalytic processes [2]. A variety of surface science analytical tools are employed to characterise catalysts under these conditions, of which the theoretical principles are detailed in this chapter.

2.1 THE UHV SYSTEM

An ultra-high vacuum is essential for many surface science studies as it preserves an atomically clean and well-defined surface, virtually free from contaminants, for the

duration of the experiment. Systems held at a base pressure of $<10^{-9}$ Torr are typically considered to be in a UHV environment. Although studies under UHV may be far removed from the actual operating conditions of the system being modelled, they offer accurate predictions of adsorbate interactions with surfaces, isolated from any interfering gas phase species. From consideration of the kinetic theory of gases, Equation 2.1 demonstrates that the rate of surface bombardment by gaseous molecules (*Z)* is directly proportional to the pressure (*p)*. To achieve a small *Z* value, which is desirable, it is noted that the pressure needs to be as low as possible, if all other parameters are kept constant [3A].

$$Z = \frac{p}{(2\pi mkT)^{1/2}} \qquad \textbf{Equation 2.1}$$

UHV conditions are achieved by a combination of rotary, turbomolecular and ion pumps (although frequently diffusion pumps in place of turbomolecular), to create a high pumping speed. A simplified diagram of the UHV chamber used for typical temperature programmed desorption (TPD) studies, but equally applicable for other UHV-based work, is shown in Figure 2.1. After the sample is mounted in the chamber, the system is baked for several hours at elevated temperatures to facilitate desorption of traces of hydrocarbons, water and other gaseous species adsorbed onto the walls of the stainless steel chamber as well as on components. Components such as filaments are also degassed after bake-out to reduce the pressure further and to remove any remaining contaminants.

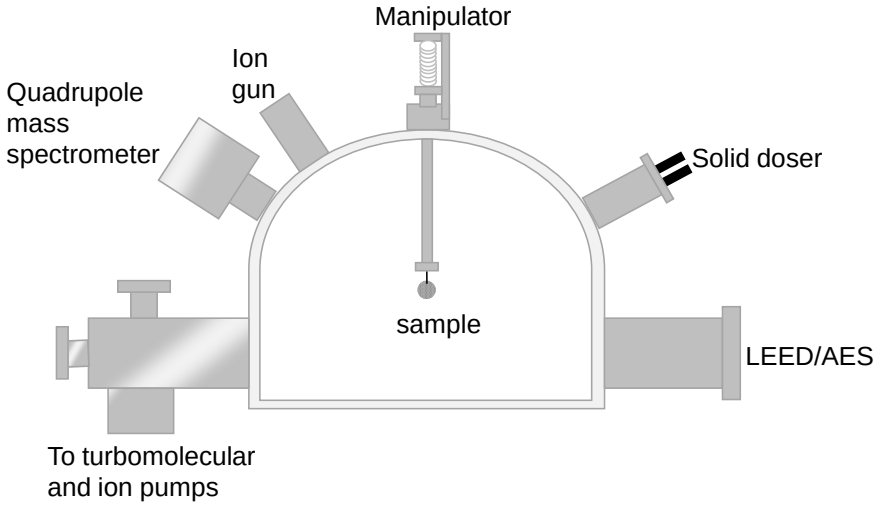

Fig. 2.1 Schematic diagram of the TPD chamber showing major components.

The most common method of surface cleaning within the UHV system is to use argon ion bombardment [3A]. This method consists of bombarding the surface with Ar^+ ions which transfer energy to the substrate and cause the surface atoms to break their bonds and desorb into the vacuum. Sputtering, as this technique is also known, is then followed by annealing of the crystal to produce an atomically flat surface essentially devoid of defects. Repeated sputter-anneal cycles may need to be carried out to achieve a suitably clean substrate to work on. The cleanliness of the sample is verified by Auger electron spectroscopy (AES) and low energy electron diffraction (LEED), described in detail in Sections 2.3.1.1 and 2.4.1.

Species are dosed onto the substrate in a variety of ways depending on their physical state. If the compound is solid at room temperature, it is dosed via sublimation by means of a heated glass capillary tube doser. The vapour pressure of the compound is controlled within the chamber by a leak valve. If, however, the compound is in liquid form, its vapour may be dosed directly into the chamber.

2.2 ANALYTICAL TECHNIQUES

The analytical techniques which are used in surface science are varied and must be suitable for investigating many detailed properties of surfaces. As a generalisation, the techniques can be used to probe the structure and composition of surfaces, as well as adsorbed overlayers. This chapter details the principles, operations and applications of several of the most common techniques in surface science, which are used within the experimental chapters of this thesis. Auger electron spectroscopy (AES) and low energy electron diffraction (LEED) are generally used as support techniques at the onset of an investigation to determine the cleanliness of a surface and chemical composition. Structural studies of the surface and adsorbates are then carried out using a technique such as scanning tunnelling microscopy (STM), which allows direct visualisation of the surface. Further studies can be done on adsorbates using spectroscopic techniques such as reflection-absorption infrared spectroscopy (RAIRS), electron energy loss spectroscopy (EELS) and X-ray photoelectron spectroscopy (XPS), and

temperature-programmed desorption (TPD) is also employed to determine the stability relationship of the adsorbates with the substrate.

2.3 SPECTROSCOPIES

Spectroscopic techniques can be categorised by the type of species used as a probe, and the nature of the analysed species (Figure 2.2). AES and EELS broadly fall under the "electron in-electron out" category (although AES can also be a "photon in-electron out" technique), whilst RAIRS can be classified as a "photon in-photon out" experiment. Finally, XPS is a "photon in-electron out" technique.

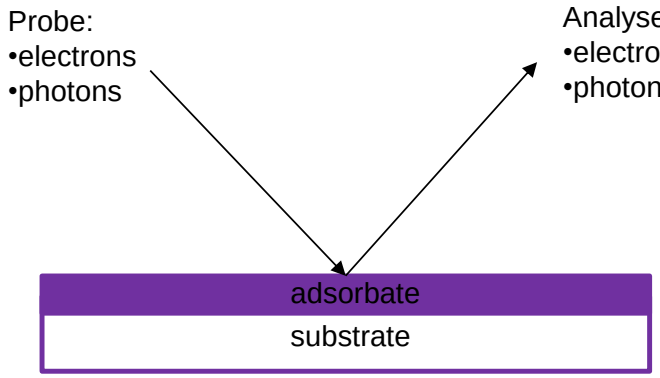

Fig. 2.2 Schematic diagram of types of spectroscopic techniques.

2.3.1 ELECTRON-IN, ELECTRON-OUT SPECTROSCOPIES

If a monoenergetic beam of electrons is incident on a surface, the majority of the incident electrons will lose energy due to interaction with the surface atoms. The intensities of the primary electrons will vary as a function of the distance travelled into the solid, which is characterised by the inelastic mean free path (IMFP). The IMFP (λ) is a measure of the distance an electron beam can travel before its intensity decays to 1/e of its initial value. Electrons with a small IMFP are highly surface sensitive as they can only travel a small distance into the material before undergoing inelastic processes. The IMFP is only weakly dependent on the material it passes through but highly dependent on kinetic energy. This phenomenon is shown in Figure 2.3 in the form of a universal curve [3B].

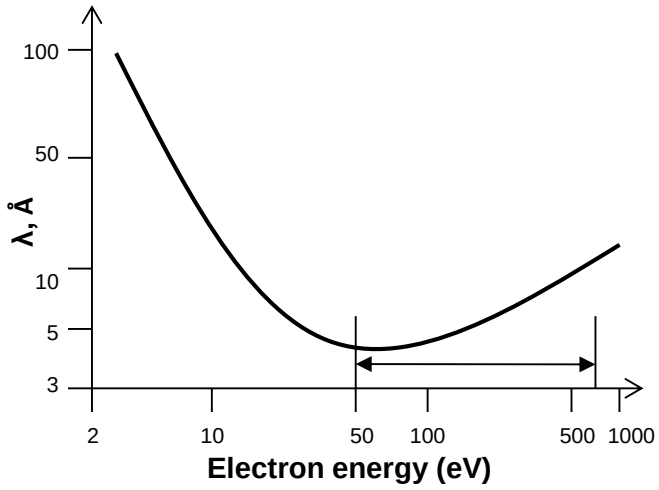

Fig. 2.3 Universal curve showing variation of IMFP of an electron in a solid with its kinetic energy. The double arrow indicates the range where surface sensitivity is greatest. From [3B].

The secondary electrons which are emitted from the sample lose different amounts of energy depending on the energy loss event. In electron spectroscopy we are mainly interested in low-energy electrons in the range 50 – 1000 eV which, as illustrated by Figure 2.3, have the smallest IMFP and so provide a highly surface-sensitive probe for chemical composition [4]. The electrons may be liberated from the specimen as a result of a radiationless relaxation of an ionised atom (in AES) or a photoemission process (in XPS).

2.3.1.1 AUGER ELECTRON SPECTROSCOPY

Auger electron spectroscopy is a surface-sensitive spectroscopic technique which has widespread applicability in the field of surface analysis. It is used, in conjunction with other techniques, to collect information on the composition of a crystal surface and takes advantage of the detectable emission of low energy electrons in the Auger process. In this study, the cleanliness of the Ni{111} and Au{111} surfaces were determined using AES to ensure that impurities such as carbon or sulfur had been sufficiently removed by sputtering and annealing cleaning procedures.

Auger electrons were first predicted theoretically by Lise Meitner in 1923, and experimentally by Pierre Auger in 1925, after whom electrons of this type were named [5]. Although the scientific foundations were laid in the 1920s, it was not until the 1950s and 1960s, when UHV instrumentation advanced, that AES was made commercially feasible. Since the 1960s, there have been widespread applications of AES for elemental analysis and imaging of surfaces, aided by the finding by Harris in 1967 that Auger transitions could be accurately identified by differentiating the spectra to enhance the Auger peaks with respect to the more abundant secondary electron peaks [6]. Studies have since been carried out in producing characteristic Auger spectra for many elements with three or more electrons [7].

AES is a three-level process which arises from the relaxation of a photoemission ion by an Auger transition. Figure 2.4 shows the whole process; from the excitation of the original sample with a beam of primary electrons (energy, *E*) to create core holes (Figure 2.4a), followed by the relaxation of the excited atom by filling the core hole with an electron from a higher electron shell to rearrange the charge distribution of the atom, to the release of the energy as an Auger electron (Figure 2.4b). The Auger electron is the dominant decay form for light elements. In fact, for atomic numbers less than 20, 90% of all atom relaxation is by Auger emission [5].

The kinetic energy of the $KL_1L_{2,3}$ transition (E_{KLL}) in Figure 2.4 can be calculated using Equation 2.2, where ϕ is the work function of the spectrometer and takes into account the energy required to remove an electron from the Fermi level of a solid to the vacuum level, as well as the electrostatic environment of the electron and several instrumental correction factors [8].

$$E_{KLL} = E_K - E_{L1} - E_{L2,3} - \varphi \qquad \textbf{Equation 2.2}$$

It can be noted from the equation that the kinetic energy is independent of the incident electron energy. The kinetic energy is solely characteristic of the binding energy of the electrons within the atoms, and so is a useful measure of elemental identification [3B]. Auger peaks are small in size, equating to only a small fraction of the total number of detected secondary peaks, and so can be very difficult to accurately identify. A modulation technique of differentiating the kinetic energy against the number of electrons enables the Auger peaks to be enhanced as well as removing the more intense but unwanted peaks.

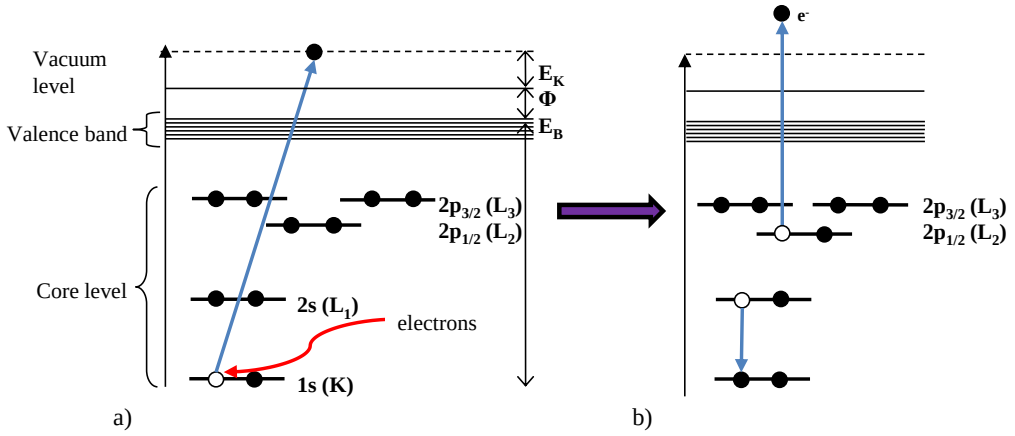

Fig. 2.4 Schematic diagrams of: a) the ejection of an electron induced by an electron beam and, b) the relaxation of the excited atom and release of Auger electron. Adapted from [3].

In the simplest terms, the three essential components of an electron spectrometer are the sample of interest, a source of primary radiation, and an energy analyser. In our AES studies, the source of the primary radiation is an electron beam produced by thermionic emission from a LaB_6 filament. The secondary electrons are detected by an Omicron retarding field analyser (RFA), which is used in conjunction with LEED optics. Briefly, the signal leaving the LEED screen is filtered and amplified by a pre-amplifier and sent into a lock-in amplifier. The lock-in also receives the original AC voltage from the signal generator ($V_0\sin(\omega t)$, where V_0 is the modulation voltage), and "locks-in" to the second harmonic (i.e. the signal 2ω). The output is then sent to a computer where it appears on the screen as voltage is scanned over a defined range. A more indepth discussion of the LEED set-up is given in Section 2.4.1.

2.3.1.2 ELECTRON ENERGY LOSS SPECTROSCOPY

In EELS, a monoenergetic electron beam, generally sourced from thermoionic emission from a hot filament, of approximately 2 – 10 eV is scattered off a surface, and the energy losses are determined. High-resolution EELS (HREELS), which is used in our studies, gives information on the vibrational excitation of the surface and the adsorbates. The main advantage of HREELS is that it can be used to analyse the low frequency region below 800 cm^{-1}, which is the limit for most detectors used in infrared spectroscopy, and so can be used to investigate substrate-adsorbate bonds [9].

The absolute energy of the elastically scattered electrons is unimportant as the centre of the elastic peak, the largest peak in the spectrum, is fixed as zero energy. The spectral resolution is then measured from the width of the elastic peak (full width at half maximum FWHM) [9]. The inelastic electron peaks can then be interpreted in a similar fashion to infrared spectroscopy.

There are two different types of electron scattering operating, in terms of changes in momentum of the scattered electron. An elastic (dipole) scattering mechanism operates in the specular direction ($\theta_i = \theta_f = 45°$) for low impact energies at small deflection angles via a virtually identical metal-surface selection rule to RAIRS. The long-range interaction between the electric field generated by the electron and the oscillating dipole of the adsorbate, as well as the response of the metallic valence electrons, determines whether the dynamic dipole component can contribute to the signal or not (only vibrational modes associated with a dipole moment orientated along the normal of the metal surface will contribute). Dipole scattering involves little momentum transfer parallel to the surface and so the scattered electrons emerge along the specular angle (Figure 2.5).

In inelastic (impact) scattering, the electron interacts with the electron shell of the surface atoms on an extremely short length scale, creating a broad angular distribution, and losing energy to the vibrational mode of the adsorbate on the surface. Due to this momentum exchange off-specular scattering occurs. Overtone excitations are favoured and features lying far from the elastic peak can be easily identified. The specular direction has no enhanced importance in impact scattering, and so this characteristic helps to distinguish between non-dipole and dipole modes [10].

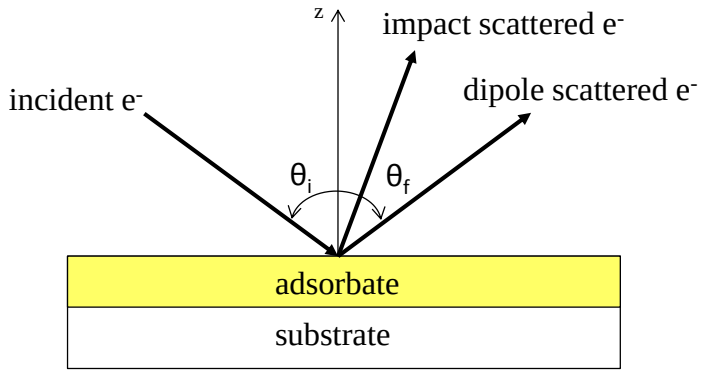

Fig. 2.5 EELS process. Adapted from [10].

EELS instrumentation (Figure 2.6) consists of an electron gun, monochromator, series of focusing lenses, and an analyser and detector [11]. Potentials are applied to the lens systems to focus and decelerate the electron beam. The monochromator selects electrons within a narrow energy window by electrostatic deflection, and a second lens system focuses the monochromatic electrons onto the sample surface. The monochromator works in such a way that only electrons with certain energies are allowed to pass, when different potentials are applied to the set of plates and focusing lenses. The back scattered electrons reach the analyser, which consists of different plates kept at different potentials to avoid dispersion of the beam, and are then converted by the electron multiplier at the detector to a pulse.

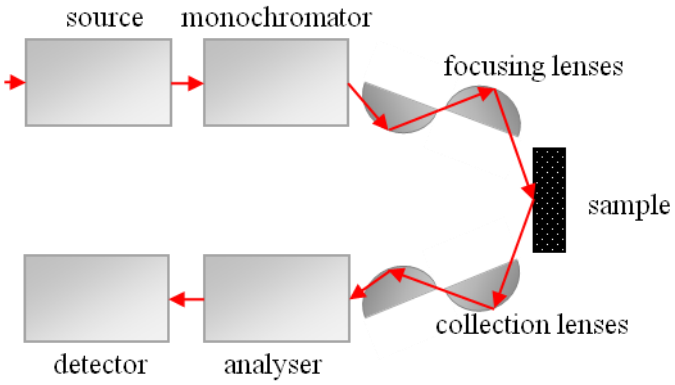

Fig. 2.6 EELS Instrumentation. Adapted from [10].

2.3.2 PHOTON-IN, PHOTON-OUT SPECTROSCOPY

Vibrational spectroscopy utilising a photon beam as a probe offers an important and useful tool for identifying species which are adsorbed onto a surface, and can also predict the geometry of the adsorbed species. In this research project RAIRS features heavily which has the great advantage, being a photon-based technique, of being applicable in both UHV and high pressure, liquid-solid interface studies, and so allows studies to be carried out under realistic conditions.

In the same way that gas and bulk systems must have a change in dipole moment (to be infrared active) or change in molecular polarizability (to be Raman active) with vibrational motion, the molecules of a liquid or gas adsorbed on the surfaces of metal single crystals must also experience a change.

2.3.2.1 REFLECTION-ABSORPTION INFRARED SPECTROSCOPY

For studies on low surface area samples, such as single crystals, with surfaces opaque to IR radiation, the reflection-absorption mode is used. The presence of infrared bands for adsorbates on a metal substrate depends upon a strict metal-surface selection rule. A dipole moment on top of a metal surface will create an image-dipole moment in the metal surface valence electrons. If a molecule lies flat on the surface with a dipole moment in one direction, this will create the opposite dipole moment in the surface (valence electrons in the metal respond to the vibrations of the

molecules) and therefore cancel out. Conversely, if the dipole moment change is perpendicular to the surface, there will be an enhancement of the dipole [12]. A simple schematic diagram is shown in Figure 2.7a to demonstrate this. For any adsorbate vibrations at angles between the parallel and perpendicular extremes, the signal can be divided into both components. In a RAIRS experiment, the incident IR beam is reflected from the surface of a metal single crystal at grazing incidence of 85° (i.e. almost parallel to the surface), where the IR frequency matches the vibrational frequency of an adsorbate present on the surface. The IR photons interact with the surface in a way to change the amplitude and phase of the radiation upon reflection [3C]. The perpendicular component of the incoming polarised infrared photon (E_p) has a phase shift related to the angle of incidence and, as described above, if this interacts with the vibrational modes which have a dipole moment perpendicular to the surface it will give an enhanced IR active signal. Equally, the electric field vector of the parallel component of the IR radiation (E_s) will be surface inactive as it cannot interact with the surface dipoles, and as shown in Figure 2.7, E_s^i and E_s^r have a 180° phase shift and so cancel each other out.

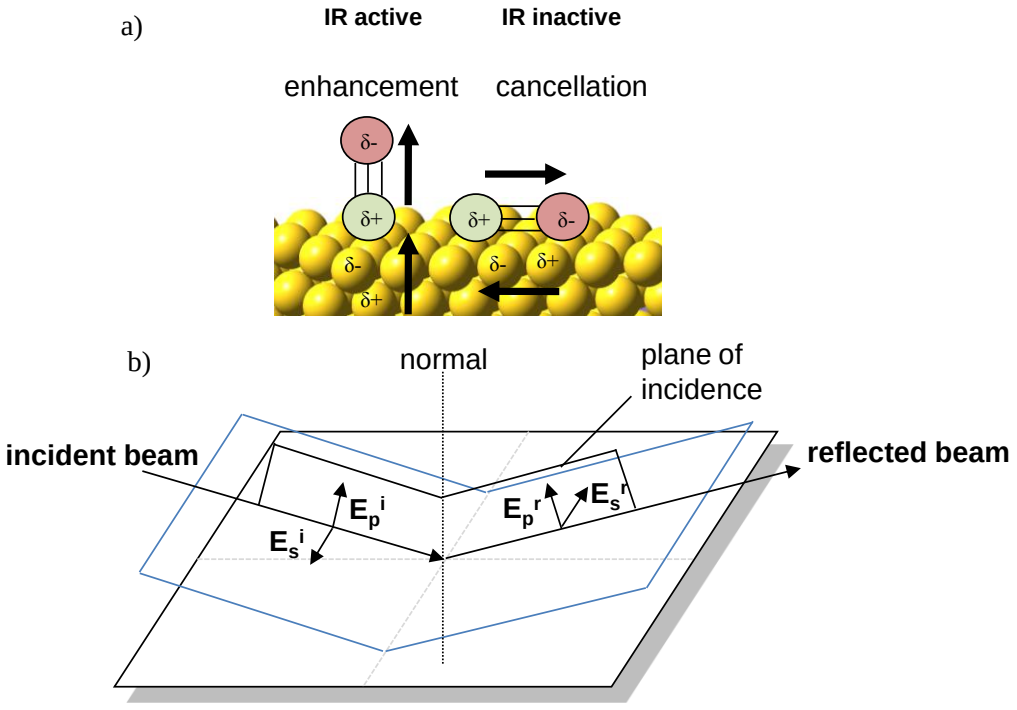

Fig.2.7 a) Enhanced and cancelled vibration modes of a molecule adsorbed on a surface and b) interaction of IR photon beam radiation with vibrational modes present on surface. Adapted from [12].

Figure 2.8 shows a schematic diagram of the RAIRS apparatus. The infrared radiation is polarised before focusing onto the sample surface at grazing incidence. The reflected beam is then focused by a lens onto a photoconductive semiconductor detector (typically mercury cadmium telluride MCT) [3C]. The signal for reflection absorption mode is very weak compared with transmission IR for example, firstly due to the smaller numbers of molecules at the surface compared to the bulk (10^{14} molecules cm^{-2} as opposed to 10^{21} molecules cm^{-3}), and secondly because of the small amount of adsorbed molecules compared to the number of surface atoms (a typical concentration of adsorbed molecules on a surface is 1nM per cm^2) [3D]. A Fourier-Transform Infrared (FTIR) spectrometer is employed to overcome these limitations as it has the advantage of obtaining all vibrational information in the spectra, in conjunction with a Michelson interferometer [13].

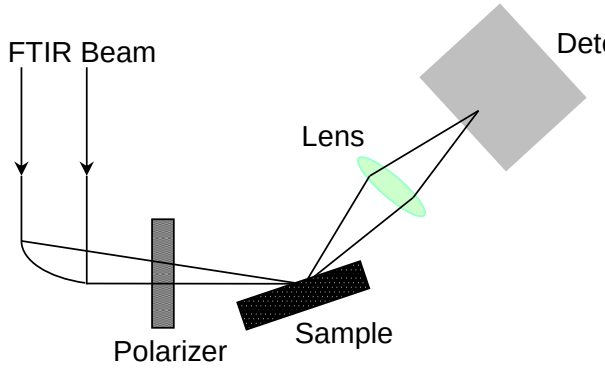

Fig. 2.8 Schematic birds eye view diagram of RAIRS apparatus.

RAIRS enables spectra to be collected with very high spectral resolution (< 0.01 cm^{-1}) but has the disadvantage of a limited wavenumber range ($\bar{\nu} \geq 800$ cm^{-1}), with the majority of detectors being rather insensitive at the lower wavenumbers [9]. It is therefore invaluable in its interrogation of medium frequency vibrations such as carbonyl, methyl and amine stretches, however cannot examine substrate-adsorbate bonding (the use of HREELS is needed, as described in Section 2.3.1.2.).

2.3.3 PHOTON-IN, ELECTRON-OUT SPECTROSCOPY

As described previously in Section 2.3.1, the secondary electrons emitted from a sample may be freed by a bombardment of electrons on the surface (in AES), or by a photoemission process providing the photon energy *hv* is greater than the work function of the solid.

2.3.3.1 X-RAY PHOTOELECTRON SPECTROSCOPY

X-ray photoelectron spectroscopy is an extremely versatile technique whose inherent specificity allows the determination of elements present on a surface, as well as their chemical environment. The technique is based on the photoelectric effect which was discovered in 1887 by Hertz [14] and justified by mathematical means by Einstein in 1905 [15]. The binding energy of the electron (E_B) is a quantity which identifies the electron in terms of its element and atomic energy level and is independent of the X-ray photon energy ($h\nu$). In gas phase spectroscopy, the binding energy E_B represented in Equation 2.3 is equal to the ionisation energy of the atom, whereas in solid-phase spectroscopy it is more convenient to refer to the Fermi level of the metal and alter the equation to Equation 2.4, including the work function, φ.

$$h\nu = E_B + E_K \qquad \textbf{Equation 2.3}$$

$$h\nu = E_K + E_B + \varphi \qquad \textbf{Equation 2.4}$$

In XPS, the photon source is a monochromatic beam of X-rays which has a sufficiently high energy to cause photoemission from the core levels of the surface atoms into the vacuum, as shown in Figure 2.9. Photoemission of electrons from a well-defined core level will produce electrons with fixed binding energies depending on the element. The chemical state of an atom will influence the exact binding energy, with a higher oxidation state giving a higher E_B due to the greater difficulty to extract an electron from an atom which is already electron deficient. Also, electrons with different angular momentum will exhibit different binding energies due to spin-orbit coupling. For example, a *p*-electron has a total angular momentum (J) of 3/2 or 1/2 resulting in a double peak in the XPS spectrum, and the intensity of spin orbit coupled peaks is proportional to ($2J + 1$).

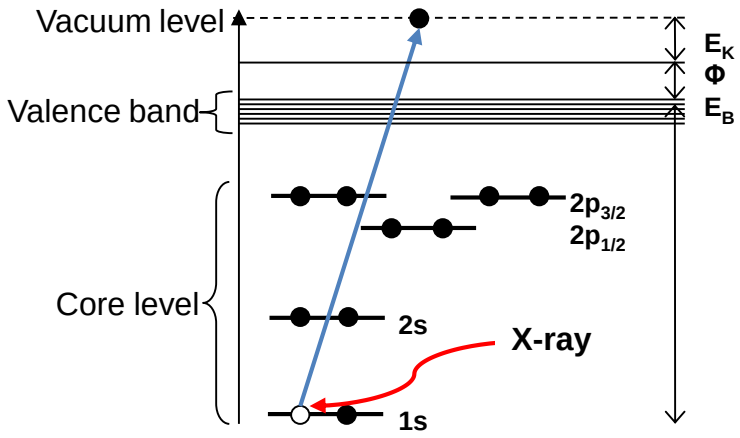

Fig. 2.9 X-ray photoemission process.

The XPS apparatus is shown schematically in Figure 2.10. The photon source is a water cooled AlKα anode where monochromatic X-rays are produced by bombardment with high energy electrons emitted from a thermal source. X-rays are then diffracted in a quartz crystal lattice to reduce the X-ray line width and remove satellite peaks, which occur due to inelastic scattering, and the X-ray is focused onto the sample. The majority of electron energy analysers are the hemispherical sector type (Figure 2.10). This consists of a pair of concentric hemispherical electrodes between which the collected electrons can pass. If the electrons have energies equal to the pass energy of the analyser then they can pass through to the detector. Any electrons with either greater or less energy will follow paths whose radii are larger or smaller than the mean radius and so will not reach the detector [4]. The detector operates by counting the number of electrons arriving and multiplying; therefore resulting in 10^8 electrons for every electron arriving at the detector [4].

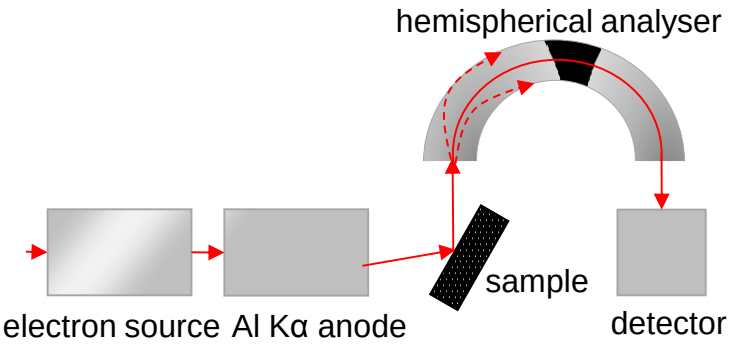

Fig. 2.10 X-ray apparatus.

2.4 DIFFRACTION

2.4.1 LOW ENERGY ELECTRON DIFFRACTION

Low energy electron diffraction is a spectroscopic technique which can be thought of as a surface sensitive analogue of X-ray diffraction, only applicable to single crystal surfaces. It is often classed as the oldest of modern surface techniques as primary LEED studies were carried out in 1927 by Davisson and Germer who showed electron diffraction from the surface of a Ni single crystal [16]. This phenomenon could only happen if the electrons has de Broglie wavelength-like properties.

The de Broglie wavelength originates from the wave-particle duality proposal in the thesis of de Broglie in 1924 that all matter has wave properties and the wavelength can be related to the momentum of the particles [17]. Equation 2.5 illustrates this relationship.

$$\lambda = \frac{h}{mv}$$ **Equation 2.5**

Davisson and Germer used the de Broglie relationship to calculate the interatomic spacing within the Ni crystal, and verified their measurements with results found by X-ray diffraction. This was an important fundamental discovery as it was the first experimental demonstration of the wave property of electrons.

Following an interim period of inactivity, the late 1950s and early 1960s heralded a new era for surface science, motivated mainly by advances in UHV technology, as well as development of LEED probes. UHV allowed the creation of reliably clean surfaces for LEED analysis which had previously been hampered by surface contamination difficulties. The benefit of LEED is that it is an ideal probe of geometric structure of a metal or semiconductor surface. It is routinely used to determine unit shapes and sizes, verify the structure and quality of single crystals, as well as investigating the thermodynamics and kinetics of ordering in overlayers and reconstructions [18]. There are alternative techniques which provide similar surface

crystallographic information, but none are as well established as LEED and so the system remains extremely popular with surface science research groups worldwide.

The LEED apparatus (Figure 2.11**)** is used in conjunction with AES setup as the electrons are produced by heating the same LaB_6 filament. A beam of electrons of 0 – 1000 eV kinetic energy are fired at the earthed sample and then scattering elastically from the surface. A voltage is supplied to one of the LEED grids which enables all electrons below said voltage to be rejected before reaching the LEED screen. The elastically scattered electrons are then accelerated towards a fluorescent phosphor-coated screen and are converted to an optical signal to produce a fluorescent spot [3B].

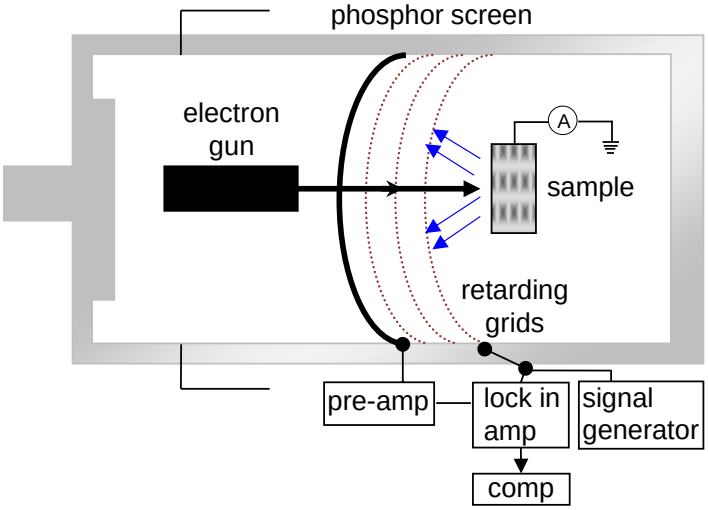

Fig. 2.11 LEED apparatus.

As the de Broglie wavelengths of the electrons have the same order of magnitude as the interatomic spacing between the atoms/molecules of the sample, a diffraction pattern is formed. Equation 2.6 shows the inverse relationship between the interatomic spacing, a, and the scattering angle, θ_a. This results in an observed diffraction pattern in which the reciprocal lattice of the real space structure is viewed. Therefore, when a is large, the angle θ_a will be small [12].

$$n\lambda = a \sin \theta_a \qquad \textbf{Equation 2.6}$$

One of the most common tasks is to observe a diffraction pattern for a clean surface and the difference when controlled adsorption in the gas or liquid phase is carried

out. In this research project, LEED is used primarily for assessing the cleanliness of a surface in conjunction with AES. A clean, well-ordered surface is necessary to allow fair comparison of results therefore, after sufficient sputter-anneal cycles, a pattern consisting of sharp spots on the LEED screen indicates a well ordered surface ready for experiments.

2.5 MICROSCOPY

2.5.1 SCANNING TUNNELLING MICROSCOPY

A breakthrough in surface science occurred in the early 1980s when the Scanning Tunnelling Microscope was developed. This non-optical microscopy technique allowed atomic scale imaging of surfaces for the first time, in contrast to the more traditional spatially averaged surface science techniques [19].

Optical microscopy has been a well-used technique since the 15th century. Although it has long been an invaluable technique to examine small objects, there is a fundamental limit of resolution of approximately 150 nm [20]. For objects such as bacteria and cells, an optical microscope is entirely feasible but, in order to be able to probe structure at the atomic level, an alternative microscope is needed, with a shorter wavelength. The solution was to use bound electrons which already exist within the solid, thus bypassing the need for electron sources, or even light of a specific wavelength, in an operation known as electron tunnelling [20]. Classically, the average kinetic energy available to electrons is one thousandth of the work function, ensuring the electrons are tightly held by the sample orbitals, with a non-zero probability of tunnelling. However, a violation of classical laws can occur when the tip of an atomically sharp needle is brought to within a few Ångstroms of the surface as, at these distances, the electron wavefunctions are not entirely confined to the surface atoms, but penetrate the potential energy barrier a few nanometres into the vacuum between the surface and the tip. This “leakage of electrons through classically forbidden zones” is known as quantum tunnelling [21]. Quantum tunnelling, which forms the basis of an STM signal, is shown in Figure 2.12.

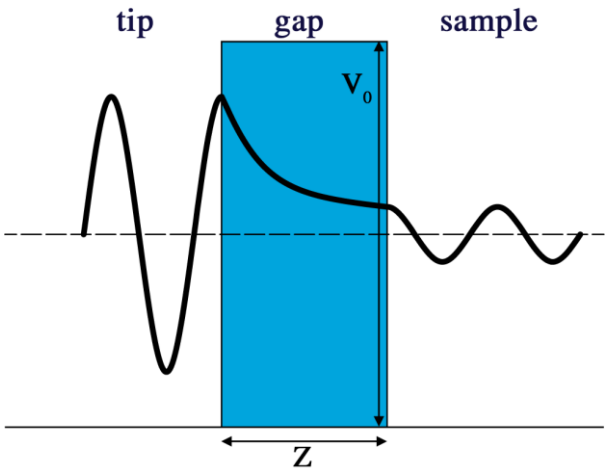

Fig. 2.12 Schematic diagram of quantum tunnelling through a potential energy barrier of magnitude V_0. The energy of the tunnelled particle is the same, only the probability of the process is decreased.

Equation 2.7 shows the transmission probability (T) as calculated by quantum mechanics, where Z is the width of the barrier and $k_1 = \sqrt{2m(V_0 - E)}/\hbar$ (m is the mass of the electron and h is Planck's constant). Note that $\lambda_{electron} = \frac{2\pi}{k_1}$, i.e. k is the wavenumber.

$$T = \frac{1}{1 + \frac{V_0^{\ 2} \sinh^{\ 2}(k_1 Z)}{4E(V_0 - E)}}$$ **Equation 2.7**

When the electron wavelength is smaller than the width of the barrier, Equation 2.7 can be rewritten as Equation 2.8, where c is a constant [22].

$$T \approx c.e^{-2k_1 Z}$$ **Equation 2.8**

Equation 2.8 illustrates the exponential dependence of the tunnelling probability of the electron as a function of the width of the barrier and highlights that tunnelling is an extremely localised phenomenon, confined only to the apex atom of the etched tip and the surface immediately below. A small potential (V_{bias}), lower than the work function of the surface φ_s, is applied to the tip and the electrons close the Fermi level (E_{Fermi}) tunnel to unoccupied states (Figure 2.13). When the tip is biased in a negative sense, electrons will tunnel from the tip to the sample whereas, if the tip is positively biased, the electrons tunnel in the opposite direction [20]. On conductive surfaces (e.g. a metal single crystal), tunnelling parameters are usually in the range of 0.01 – 1.0 V and 0.01 – 10 nA, giving a tip-sample distance of approximately 5 Å (Z).

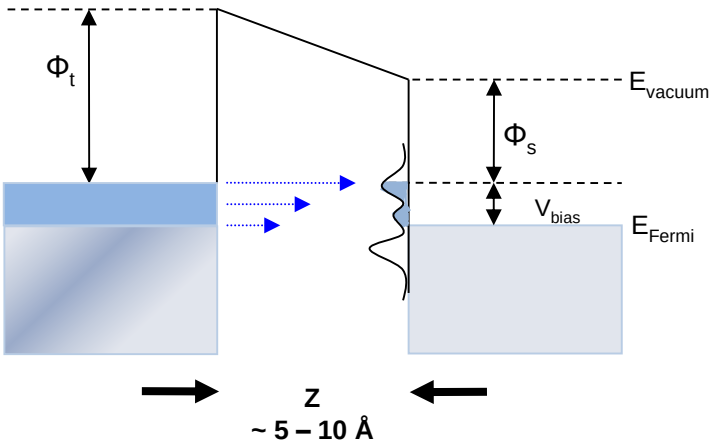

Fig. 2.13 Potential energy tunnelling diagram for a positively biased sample. Adapted from [3].

The STM tip is usually scanned over the surface of the sample to measure the variation of the tunnelling current with distance. This procedure, the so-called constant current mode, is favoured for imaging rough surfaces and provides better spatial resolution and stability than the alternative constant height mode. A diagram of the two types of scanning modes is shown in Figure 2.14, as well as the basic set-up of an STM instrument [23].

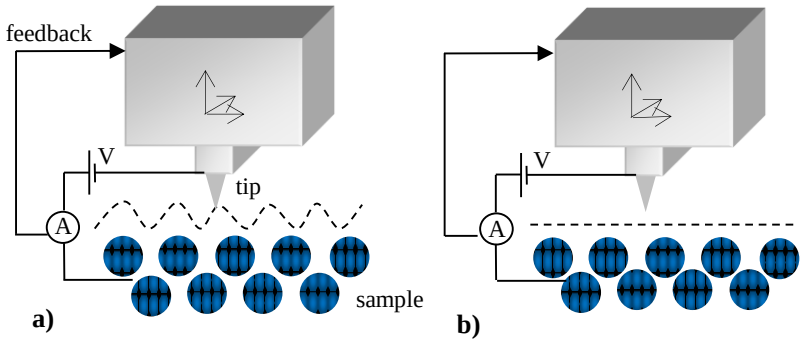

Fig. 2.14 Schematic diagram of STM tip used in: a) constant current, and b) constant height modes. Adapted from [23].

The basic set-up consists of a metal tip, a piezoelectric drive, a voltage supply and a set of electronic equipment for data output. The equipment is isolated by means of creating as rigid an STM system as possible to dampen the vibrations as strongly as possible. Piezoelectric translators are used in the x-, y- and z- directions and are designed to be extremely sensitive to voltage change and so voltages from 1 mV to 1000 mV cause a displacement of ~1 Å to 1 μm, allowing exact manipulation of the

tip. A feedback circuit is essential to control the tip-sample distance by comparing the current signal with a pre-defined current set point. The tip itself can influence the resolution and shape of the scan, depending on its size and shape. The tip must be as atomically sharp as possible and is typically constructed from tungsten, platinum-iridium or gold. Preparation of tips can be carried out in a variety of different ways, with the most common procedures being mechanical shearing, electrochemical etching by dissolution of the tip, and controlled crashing of the tip on the metal surface [20].

Although atomic information is gathered from the resulting topography data, STM does not directly image atoms, but measures electron density near the Fermi level, and so images differing local bonding environments and thus gives a representation of the electronic structure of the surface. Careful analysis is required to distinguish features due to a topography change or a change in the local density of states. Therefore, extreme care is taken in converting STM images into mechanistic models of the surfaces; by acknowledging anticipated behaviour of the surface with the adsorbates, as well as combining results with computer modelling and other surface science techniques.

2.6 DESORPTION STUDIES

2.6.1 TEMPERATURE-PROGRAMMED DESORPTION

Temperature-programmed desorption is a surface technique which purposefully desorbs an adsorbed species from the surface to provide information relating to the strength of interactions between both [12].

In a TPD experiment, a metal substrate surface is dosed with the desired molecular species at a particular temperature to obtain a certain surface coverage. The sample is then heated in a linear fashion to desorb species from the surface, and the desorbed gas phase molecules are detected at a quadrupole mass spectrometer. The

temperature dependence of the amount of adsorbates desorbed into the gas phase can then give important information on the binding energy of the bound species. TPD experiments were carried out in a vacuum chamber with base pressure of 1×10^{-10} mbar. The chamber is fitted with a quadrupole mass spectrometer, facilities for LEED and AES and sample cleaning via argon ion sputtering, as shown in Figure 2.1.

The data from a TPD experiment can provide several pieces of information. The position of the peak relates to the enthalpy of desorption whilst the area under the peak is proportional to the surface coverage (providing other variables of the experiment, i.e. the distance between sample and mass spectrometer, the pumping speed of the vacuum, and the rate of heating, are kept constant).

For the simplest case, TPD data can be used to estimate desorption activation energy, E_d, of a compound from a substrate [2]. The rate constant, k_d, may be expressed through Arrenhius-type kinetics and so increases exponentially with temperature T. Equation 2.9 shows this relationship, where A is the pre-exponential factor and R is the gas constant.

$$k_d = A \exp\left(\frac{-E_d}{RT}\right) \qquad \textbf{Equation 2.9}$$

The rate of desorption of the molecule as the temperature ramp is applied is expressed in Equation 2.10, where N is the number of adsorbed molecules and m is the order of the reaction:

$$\frac{-dN}{dt} = k_d N^m \qquad \textbf{Equation 2.10}$$

Equation 2.10 can be rewritten if a substitution is first carried out where β is the heating rate:

$$\frac{dN}{dt} = \frac{dN}{dT} \times \frac{dT}{dt} = \frac{dN}{dT}\beta$$ **Equation 2.11**

Therefore, substituting into Equation 2.9 gives Equation 2.12**,** and a further differentiation with respect to T and equating to zero gives Equation 2.13:

$$\frac{-dN}{dt} = N^{m}\frac{A}{\beta}\exp(-E_d / RT)$$ **Equation 2.12**

$$\frac{E_d}{RT^2} = \frac{A}{\beta} mN^{m-1}\exp(-E_d / RT)$$ **Equation 2.13**

If the desorption process is zero order (i.e. m = 0), common for multilayer systems, then the process is independent of coverage (N) and rises with increasing temperature ($\frac{-dN}{dt} = \frac{A}{\beta}\exp(-E_d / RT)$). Desorption peaks in the TPD spectra would have a tendency to have a leading edge increasing to the desorption maximum (T_d) before decreasing sharply.

For a first order process, which is likely for molecules at submonolayer coverages, the rate depends on the number of adsorbed molecules on the surface ($\frac{-dN}{dt} = \frac{A}{\beta} N\exp(-E_d / RT)$). Redhead showed that the relationship between maximum temperature T_{max} and E_d is linear between a certain range and the rearrangement of the first order process equation is shown in Equation 2.14. It must be noted however that, to determine E_d, there must be a reliable known value for A [7].

$$E_d = RT_{\max}\left[\ln\left(\frac{AT_{\max}}{\beta}\right) - 3.46\right]$$ **Equation 2.14**

First order desorption peaks are typically asymmetric in shape with a longer leading edge. Second order kinetics are also expected for submonolayer coverages, arising from a recombination of two species before desorption. This type of process would give broader and more symmetric peaks around T_d.

As described, peak shapes can provide a large amount of information on the type of desorption process occurring. However, if lateral interactions also exist between the adsorbate molecules these may change peak shape or position. In the case of attractive interactions E_d may be significantly increased whilst, for repulsive interactions, a lower E_d may be recorded for increasing coverages and desorption peaks may be split [24]. There may also be a variety of bonding sites on the surface with differing desorption energies which produce multiple or overlapping peaks.

2.7 DESCRIPTION OF UHV CHAMBERS USED WITHIN RESULTS CHAPTERS

UHV experiments within this thesis were carried out in a variety of UHV chambers. UHV-STM and RAIRS experiments were carried out in an Omicron UHV system with a base pressure of 1×10^{-10} mbar (referred to herein as Chamber 1). The system consists of three linked chambers: a central chamber with crystal preparation facilities for argon ion sputtering, AES and LEED, a second chamber housing the RAIRS instrument with a Nicolet Nexus 860 FTIR spectrometer and MCT detector used to acquire RAIRS data and appropriate valves for dosing solid and liquid species, and a third for STM.

Chamber 2 is set up to perform TPD experiments and consists of a PSP Vacuum Technologies UHV chamber with a base pressure of 1×10^{-10} mbar. The chamber consists of argon ion sputter facilities for cleaning, in addition to LEED and AES to analyse the cleanliness of the metal surface.

Chamber 3 houses an HREELS set-up with a VSW HIB1000 double pass spectrometer with a primary energy of 4 eV and a typical resolution of the elastic peak of 80 cm^{-1}. HREELS measurements are carried out in the specular direction, and maximum likelihood-based resolution enhancement methods were used to

recover the spectrum from broadening by the instrument, leading to an improved resolution of ca. 60 cm^{-1}.

2.8 SUMMARY

Experimental techniques for surface science are well developed and detailed work can be carried out on the interface of two phases where heterogeneous catalysis occurs. Surface science is by design an instrumentally intensive experimental science and so the progress made in the construction and improvement of experimental probes has enabled the field to become as large and diverse as it is today. Experimentation requires an intervention of multiple techniques and so all of the instrumentation explained in this chapter, alongside many others, has to be well understood and employed by the typical surface scientist.

2.9 REFERENCES

[1] M. Bowker, *The Basis and Applications of Heterogeneous Catalysis,* OUP, Oxford, 1998.

[2] G. Ertl & H-J. Freund, *Physics Today,* **52** (1999) 32.

[3] G. Attard & C. Barnes, *Surfaces,* OUP, Oxford, 1998 A) 23-27 B) 43-60 C) 78-80 D) 71-75

[4] J. F. Watts & J. Wolstenholme, *An Introduction to Surface Analysis by XPS and AES,* J. Wiley & Sons, Chichester, 1988.

[5] G.B. Hoflund, *Handbook of Surface and Interface Analysis,* J.C. Riviere (Ed.); CRC Press LLC, 1998

[6] N.H. Turner, *Handbook of Surface Imaging and Visualisation,* A.T. Hubbard (Ed.); CRC Press LLC, 1995

[7] J. W. Nienmantsverdriet, *Spectroscopy in Catalysis – An Introduction,* VCH, Weinheim, 1993.

[8] J.F Moulder, W.F. Stickle, P.E. Sobol & K.D. Bomben, *Handbook of XPS,* Perkin-Elmer Corp (Ed.); Eden Prairie, USA, 1992.

[9] K.W. Kolasinski, *Surface Science 2nd Edition,* Wiley & Sons, 2008.

[10] M. Pemble, *Surface Analysis: The Principal Techniques,* J.C. Vickerman (Ed.); Wiley & Sons, Chichester, 1997.

[11] N. V. Richardson, *Current Opinion in Solid State and Materials Science,* **2** (1997) 517.

[12] D. Woodruff & T. Delchar, *Modern Techniques of Surface Science*, Cambridge University Press, Cambridge, 1986.

[13] B. J. Barner, M.J. Green, E.I. Saez & R.M. Corn, *Analytical Chemistry,* **63** (1991) 55

[14] H. Hertz, *Annalen der Physik,* 31 (1887) 983

[15] A. Einstein, *Annalen der Physik,* **17** (1905) 132

[16] D.O. Hayward, *Quantum Mechanics for Chemists,* E.W. Abel (Ed.); RSC, Cambridge, 2002. 12-16.

[17] *Nobel Lectures, Physics 1922-1941,* Elsevier (Ed.); Amsterdam, 1965.

[18] M.G. Lagally & J.A. Martin, *Review of Scientific Instruments,* **54** (1983) 1273

[19] G. Binning, H. Rohrer, Ch. Geber, & E. Weibel, *Physical Review Letters*, **49** (1982), 57

[20] C. Bai, *Scanning Tunnelling Microscopy and Its Applications,* Springer (Ed.); Shanghai, 1995.

[21] P.W. Atkins, *Physical Chemistry 7th Edition,* OUP, Oxford, 2002.

[22] D.J. Griffiths, *Introduction to Quantum Mechanics*, Prentice-Hall, 2004.

[23] P.A. Christensen, *Chemical Society Review,* (1992) 197

[24] J.L. Sales & G. Zgrablich, *Physical Review B,* **35** (1987) 9520

Chapter 3

Characterisation Studies of Ni{111} modified with (S)-aspartic acid and MAA under UHV conditions

3.1 INTRODUCTION

The ways in which chiral modifiers are adsorbed and structured on a surface are ideally analysed by surface science techniques under UHV conditions. It is an interesting study to deduce the form an amino acid may adopt upon adsorption at a metal surface, not least for their importance in chiral modification. Surface science methods under UHV control allow characterisation at the fundamental molecular level by creating an easily controlled environment, and are the most common techniques for studying the adsorption of a host of modifiers on metals. In recent years there has been a growing interest in biologically active molecules bound to metals in fields ranging from biomaterials to biocatalysis, which has resulted in increased surface science studies in these areas.

3.1.1 THE USE OF AMINO ACIDS

Amino acids often exhibit complex behaviour due to several active functional groups, which can afford investigations into possible different intermolecular interactions. The capability of amino acids to form ordered structures on metal surfaces was first discovered by Somorjai and co-workers in 1978 using LEED, where tryptophan enantiomers were shown to form structures on Cu related by a mirror inversion [1]. The advent of STM several years later enabled amino acid/metal systems to be thoroughly studied to gain an insight into molecular organisation on the surface, and bonding modes the amino acid can adopt.

The adsorption of the simplest amino acid, glycine, onto Cu{110} [2,3] was the first to be studied using RAIRS, STM, TPD and LEED and allowed certain adsorption characteristics to be deduced, which were later to be recognised in the more complex, chiral amino acids [4,5]. A comprehensive study by Yang and co-workers reviews STM and LEED studies of amino acids on Cu. It was found, for the most part, amino acids changed phase as a function of coverage [5].

Catalytic studies by Izumi *et al.* found that RNi modification with α-amino or α-hydroxy dicarboxylic acids gave a higher enantioselectivity than α-amino or α-hydroxy monocarboxylic acids [6]. Therefore amino acids such as aspartic acid and glutamic acid were more favourable as modifiers and showed the potential to be studied further. The only study of aspartic acid adsorption on single crystal surfaces to date is that carried out by Yang and co-workers on Cu{001}, chosen as the reactivity of the surface would not be strong enough to break up the molecule upon adsorption [7]. It was found that two adsorption phases existed at low coverage, and no ordered overlayer structure was present at high coverages. It was postulated that the second carbonyl group on the side chain accounted for the difference in adsorption behaviour compared to other amino acids.

3.1.2. MAA ADSORPTION ONTO CHIRALLY MODIFIED METAL SURFACES

The first known enantioselective heterogeneous hydrogenation of MAA was carried out within a comprehensive study by Izumi and co-workers, where it was discovered that MAA was one of the best β-ketoester substrates, originally hydrogenated to *(R)*-MHB to give an e.e. of 15%, which was improved over the years to greater than 98% [8]. The obvious desire for more intensive investigations led to systematic catalytic studies being carried out to optimise numerous reaction and modification conditions. Hypothetical models were simulated to predict the catalytic behaviour, taking into account the number of different parameters and different possible states of the

molecules. As discussed in detail in Section 1.6.3, surface science techniques have afforded great progress in determining the mechanism between modifier, reactant and catalyst at a molecular level.

The first surface science report, to our knowledge, of MAA adsorption was on the Cu{110} surface in the PhD thesis of Lorenzo [9]. MAA was first adsorbed onto unmodified Cu{110} on which it was found to adsorb in its enol form, interacting through its carbonyl group normal to the surface. On a *(R,R)*-tartaric acid modified surface a low coverage of modifier, in its bitartrate form, is required to facilitate MAA adsorption (suggesting bare metal sites are needed for co-adsorption), and the molecule binds in its enol tautomer form (Figure 3.1), with the ester carbonyl interacting with the surface and the enolate interacting with OH groups on the tartaric acid molecules. Further work on MAA adsorption on modified Ni{111} surfaces has been carried out and are described in detail in Section 1.6.3.

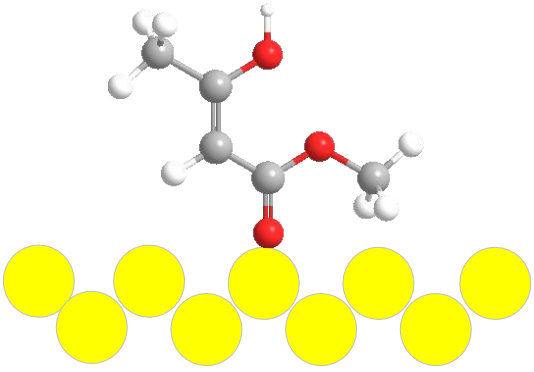

Fig 3.1 MAA adsorption on bitartrate *(R,R)*-TA-modified Cu{110}; MAA in enol form on surface.

3.1.3. AIM OF RESEARCH

The object of this chapter is to characterise the adsorption of *(S)*-aspartic acid on a Ni{111} surface. Ni is preferred due to its catalytic relevance in the *β*-ketoester hydrogenation reaction. Klabunovskii and co-workers discovered early on that Ni catalysts yielded the highest enantioselectivity and activity in the hydrogenation [10] and so the interaction of amino acids on this surface is highly relevant. *(S)*-aspartic acid has shown moderate enantioselectivity when used as a modifier in the reaction and so it is desirable to add to previous vacuum studies of amino and hydroxyl acids

on Ni{111} [11-14] to aid in the understanding of the interaction of chiral modifiers with metal surfaces and thus how they impart chirality to the system, as well as to add to the fundamental adsorption studies of biologically active molecules in metal complexes.

Thermal desorption techniques and surface vibrational spectroscopy are employed in this research to characterise the adsorption properties of *(S)*-aspartic acid on the model catalyst Ni{111} surface. These techniques are also utilised in determining the form and interaction of MAA with the modified surface.

The morphology of the Ni{111} surface after adsorption of *(S)*-aspartic acid as a function of coverage is studied using UHV-STM. STM is also used to investigate the effect on the architecture of the modifier after annealing the modified surface, as well as the adsorption of MAA onto the modified Ni{111}.

3.2 EXPERIMENTAL

3.2.1. UHV STM AND RAIRS EXPERIMENTAL CONDITIONS

(S)-aspartic acid was dosed under UHV conditions by means of a sublimation doser, shown in Figure 3.2. An electrical feedthrough flange with two copper electrodes and two thermocouple electrodes surrounds a small glass tube containing the sample, around which is wound tungsten filament which is itself connected to the copper rods to complete the electrical circuit. The glass tube is resistively heated and the temperature monitored through the thermocouple wire from the sample attached to the electrodes. The aspartic acid source is isolated from the chamber by a gate valve and the dosing line is baked overnight at an elevated temperature before use. The aspartic acid source is then outgassed at 410 K for approximately one hour before dosing. Dosing of aspartic acid, or any other solid, in such a way makes it difficult to assign coverage in terms of number of Langmuirs (1 Langmuir = 1×10^{-6} $Torrs^{-1}$) as the amount of Asp sublimed into the chamber will differ for apparently identical

temperatures, due to a temperature gradient across the source. Therefore, in these studies, dosage is measured in terms of seconds of exposure as this is felt most accurate, and allows comparisons between different UHV chambers.

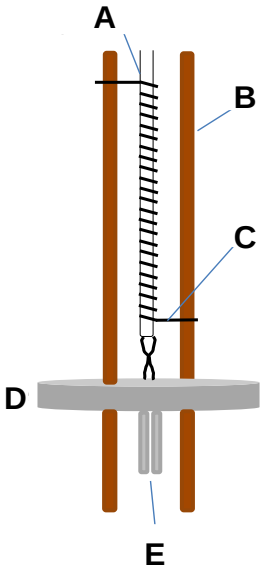

Fig. 3.2 Schematic diagram of sublimation doser. A: glass tube; B: power electrodes; C: heating wire; D: feedthrough flange and E: thermocouple electrodes.

Cleaning of the Ni{111} single crystal is carried out in the preparation chamber of Chamber 1 (see Section 2.8) by cycles of argon ion bombardment (2 kV) and annealing to 893 K until a sharp (1×1) LEED pattern is observed. The sample is then transferred to the RAIRS chamber and a background RAIR spectrum is taken of the clean Ni{111}, followed by sublimation of *(S)*-Asp (Fluka Biochemika 97%), heated to ~430 K, onto the substrate (held at 300 K). The sample is transferred to the STM chamber where images are acquired in constant current mode using an electrochemically etched W tip. All STM images are recorded at 300 K. Subsequent STM imaging following MAA adsorption is carried out by exposing the surface to MAA, purified by repeated freeze-pump-thaw cycles, dosed directly into the STM chamber from the RAIRS chamber by the opening of a succession of gate valves to achieve the desired vapour pressure.

3.2.2. UHV TPD EXPERIMENTAL CONDITIONS

Chamber 2 is employed in the TPD experiments. Clean samples are left to cool to room temperature before exposure to *(S)*-Asp and MAA. *(S)*-Asp is sublimed into the chamber via the opening of a gate valve after thoroughly outgassing and heating to

approximately 430 K. MAA is purified by freeze-pump-thaw cycles and dosed via a leak valve into the main chamber. After exposure, the pressure in the main chamber is allowed to return to base level before starting the TPD experiment. If the sample is annealed prior to dosing, the sample is allowed to cool to room temperature before positioning in close proximity to the quadrupole mass spectrometer within the main chamber, and a temperature ramp is applied, heating through the wires used to mount the sample onto the manipulator. The mass spectrometer records the species which desorb from the Ni{111} surface as the temperature ramp of an approximately linear rate of 4 Ks^{-1} was applied. In the preliminary TPD experiments, all masses in the range 0–150 amu were monitored to note which peaks increased as a function of sample temperature. With this knowledge in hand, it was decided to monitor *m/z* values of *2, 17, 18, 28* and *44*, representing H_2, NH_3, H_2O, CO and CO_2 respectively. This would allow establishment of whether the molecular desorption occurs on the substrate or if dissociation occurs before desorption.

3.3 RESULTS AND DISCUSSION

3.3.1 UHV RAIRS

3.3.1.1 ADSORPTION OF *(S)*-ASPARTIC ACID ON Ni{111} AS A FUNCTION OF COVERAGE AT 300 K

RAIRS data was acquired as a function of *(S)*-aspartic acid exposure on a Ni{111} surface at a modification temperature of 300 K. As the RAIRS chamber is attached to the STM chamber (Chamber 1), this allows a direct comparison of the molecular form and orientation suggested by RAIRS with the obtained STM images. In several instances a mixture of species may be present on the surface, as well as extensive intermixing of group modes, making it difficult to unambiguously assign adsorption characteristics, and therefore well-informed suggestions are made for the most likely conformation. It is also important to take into account that, when a monolayer of amino acids is adsorbed onto a solid substrate, intermolecular interactions are different from those in the gas, solid or aqueous phases. This is due to substrate-adsorbate interactions, as well as restricted intermolecular interactions between

adsorbates in two dimensions. Figure 3.3 shows RAIRS spectra during increasing coverage of *(S)*-Asp on the Ni{111} surface at 300 K, with assignments shown in Table 3.1. Previous infrared studies of aspartic acid are used to assign band positions [15-18].

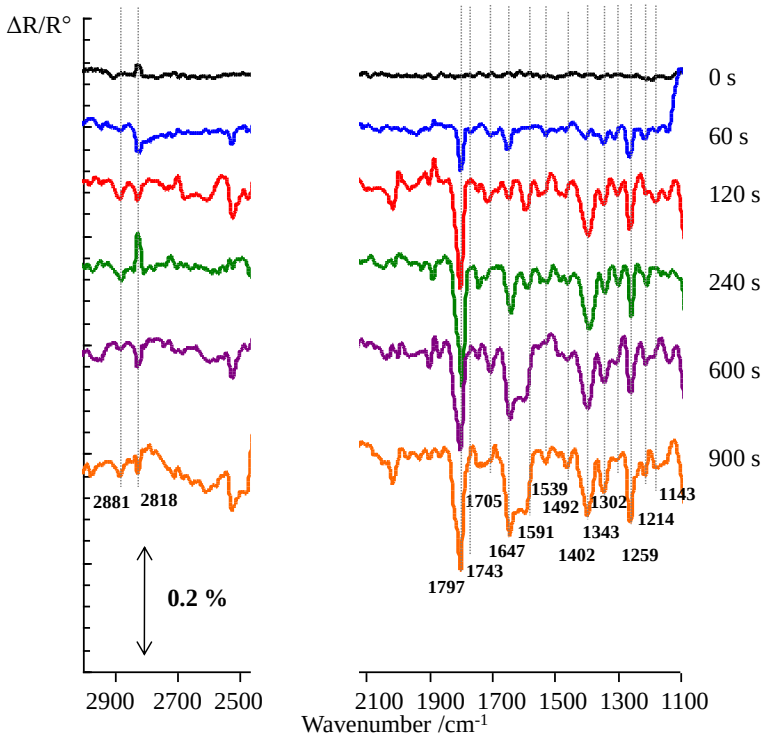

Fig. 3.3 UHV RAIRS of increasing coverage of *(S)*-aspartic acid on Ni{111} at a single crystal temperature of 300 K.

300 K /wavenumbers in cm^{-1}		**Assignment**
Low coverage	**High coverage**	
2881	2881	ν_{as} (CH_2)
2818	2818	ν_s (CH_2)
1797	1797	ν_s (C=O) imide
1743	-	ν_{as} (C=O) imide
-	1705	ν(C=O) γ-carboxylic acid
1647	1647	δ_{as} (NH_3^+)
-	1591	ν_{as} (COO^-) α-carboxylate
1529	1539	ν_{as} (COO^-) γ-carboxylate
-	1492	δ_s (NH_3^+)
1402	1402	ν_s (COO^-) α- and γ-carboxylate
1343	1343	CH_2 wag
1302	-	$\delta(CH_2)$ + ν(CC)+ ν(CN)
1259	1259	ν(C-O) + δ(O-H)
1214, 1192, 1143	-	C-N in (C=O)-NH, C-N in (C=O)-NR-(C=O)

Table 3.1 Assignments of UHV RAIRS bands of *(S)*-aspartic acid on Ni{111} at 300 K adsorption temperature. Assignments from Refs. 15-18.

Peaks at 2881 and 2818 cm^{-1} are present at all coverages and are assigned to the asymmetric and symmetric stretching vibrations of the CH_2 groups respectively. Their relatively weak intensity may indicate the geometry of the molecular backbone as less than perpendicular on the surface [19]. At low coverage, the spectrum is dominated by bands at 1797, 1743, 1302, 1214 and 1143 cm^{-1} which saturate after ~240 s, followed by the growth of new bands. The 1797 cm^{-1} peak is rather difficult to assign explicitly, certainly depending on the RAIRS data alone. One possibility is that it is due to the presence of CO on the surface, presumed to adsorb from the background atmosphere in the chamber (seen previously in *(R,R)*-tartaric acid studies on Ni{111} [11]) or via decomposition of aspartic acid. Peaks representing the CO stretch are found to increase in wavenumber as CO coverage is increased, suggesting a change in adsorption position. Fig 3.4 shows three different adsorption models for CO on Ni{111}: three-fold hollow site (~ 1816 cm^{-1}), bridge site (~1919 cm^{-1}) and on-top site (~2052 cm^{-1}) [20-23].

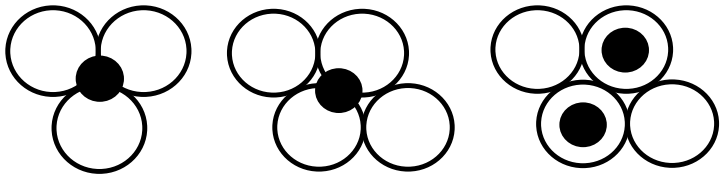

Fig. 3.4 CO adsorption modes on Ni{111}

In the present study there is no change in the CO position with increasing coverage, which would suggest that the CO does not change adsorption site on the Ni{111} surface, even with an increasing coverage of *(S)*-aspartic acid. This appears contradictory to that observed previously where the CO molecules ultimately adopt the on-top site position as adsorption sites become more scarce [23]. Another peculiarity is that the intensity of the peak at 1797 cm^{-1} continues to grow in size alongside increasing aspartate coverage. This is in contrast to previous studies of *(R,R)*-TA on Ni{111} where the CO is displaced by increased *(R,R)*-TA adsorption to leave a Ni{111} surface essentially free from CO, with only tartrate molecules present in the RAIR spectrum [11]. The fact that the peak in Figure 3.3 does not shift in position nor decrease in intensity implies that either the CO molecules remain co-adsorbed with the aspartic acid on the surface, aiding the bonding of the amino acid molecules, or the peak may be assigned to another vibrational mode.

A distinct possibility, which stems from the fact that the peak value is slightly lower than those previously noted for a CO stretch on a Ni{111} surface, is that polysuccinimide (PSI) oligomers may be present on the substrate. PSI is a polymer formed upon thermal polycondensation of aspartic acid [24, 25]. This reaction is shown in Figure 3.5.

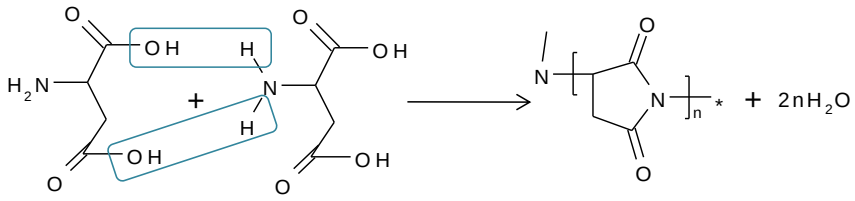

Fig. 3.5 Thermal polycondensation of aspartic acid to polysuccinimide.

Normally occurring at 180°C, it has been found that the process can occur at lower temperatures using a catalyst [26]. In the present case, the Ni surface could catalyse the condensation reaction, and so remove the need for heating. In contrast to previous work on *(S)*-Glu on Au{111}/Ni [27] where it was proposed that the C-backbone of the amino acid underwent an internal cyclisation process to produce pyroglutamate, it is understood that, due to the energetically unfavourable formation of a 4-membered ring if aspartic acid was to intramolecularly cyclise, it would be highly unlikely that the formation of such a large ring strain would compete over intermolecular coupling and so is much more probable that polycondensation takes place. We assume PSI formation would occur on the surface and not in the doser; this assumption is made due to observing aspartic acid IR peaks in tandem with PSI peaks, suggesting a possible co-adsorption of the two species on the surface depending on coverage. From the low coverage RAIR spectra in this study, the aforementioned intense peak at 1797 cm^{-1} could feasibly be assigned as the symmetric succinimide carbonyl stretch and the peak at 1743 cm^{-1} the asymmetric stretch [28,29]. Further indications that polysuccinimide may be present on the surface is the presence of a band at 1302 cm^{-1}, representing $\delta(CH_2)$ + ν(CC)+ ν(CN), and small bands at 1214 and 1143 cm^{-1}, which can be assigned to the imide C-N-C stretch [30]. However, very closely related bands in wavenumber at 1210 and 1141 cm^{-1} have been assigned from experimental FTIR as ν(CC)+ ν(CN) and ν_s(C-

$OH)_{COOH}$ respectively [16], and so the assignments of these lower wavenumber peaks are not conclusive.

Examining the intensities of the apparent polysuccinimide peaks at low coverages allows some deduction of the molecular geometry of the adsorbed species. The presence of the symmetric imide carbonyl stretch suggests the molecule is not parallel to the surface. The two peaks representing the C-N-C imide stretch are low in intensity which suggests the backbone of the ring may be lying near-to-parallel on the Ni{111} surface. This is illustrated in Figure 3.6.

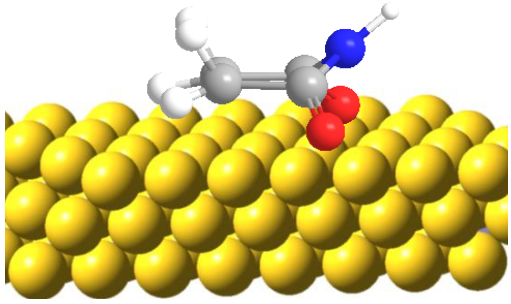

Fig. 3.6 Schematic illustration of the proposed orientation of a succinimide monomer on the Ni{111} surface.

With increasing coverages of *(S)*-Asp several new peaks appear alongside succinimide-related peaks. The dominant peak at 1797 cm^{-1} remains at higher coverages, suggesting the continuing presence of either succinimide or CO on the surface. The band at 1705 cm^{-1} can be attributed to $\nu\ (C{=}O)_{COOH}$ of the γ-carboxylic acid group, whilst the bands at 1647 and 1492 cm^{-1} are the asymmetric and symmetric NH_3^+ deformations. The bands at ~1540 cm^{-1} and ~1400 cm^{-1} are weak in intensity and so indicate the lack of asymmetric and symmetric $\nu(COO^-)$ of the γ-carboxylate group. At higher coverages, the succinimide peaks appear to retain their intensity but become overwhelmed by the growth of features more typical of an aspartate species. The analysis is indicative of the presence of the zwitterionic form of *(S)*-aspartic acid, whereby the amine group is protonated and the α-carboxylic acid group is deprotonated, while the aliphatic side chain consists of a carboxylic acid at the γ-position. There is some indication that the anionic form is present at the highest coverage due to the presence of the $\delta(NH_2)$ band at 1537 cm^{-1} (downshifted

substantially from the gas phase molecule vibration mode due to the fact that the N atom interacts with the Ni surface [31]. There are very few RAIRS investigations of amino acids on Ni surfaces, however a number of spectroscopic studies of amino acids of Cu surfaces allow comparison with the current study. On Cu, each amino acid studied was found to have an adsorption geometry dependent on surface coverage, with the anionic form of the amino acid being most dominant [2,32-34]. However, in studies of *(S)*-Glu on Ni{111} [35] and *(S)*-Ala on Pd{111} [36], the molecules adsorbed in their zwitterionic form at lower coverages, and their anionic form at high coverages.

More typical aspartate species appear at intermediate coverages alongside the initial succinimide species – in the first instance in the zwitterionic form, and ultimately as a mixture of zwitterions and anions at high coverage when multilayers are present. In its zwitterionic form, aspartic acid would not bond to the surface through the NH_3^+ group or side chain COOH group and so would be relatively flexible on the Ni{111}, insinuating a variety of possible bonding geometries. The strength of the asymmetric NH_3^+ deformation and weakness of the symmetric deformation suggests the C-N backbone is relatively perpendicular to the substrate surface. At its highest coverages, aspartic acid also exists in its anionic form, with the COO^- and NH_2 groups of the amino moiety binding to the Ni surface, leaving the bulky $–CH_2$-COOH chain free to approach adjacent aspartate NH_2 groups to allow a C=O···H-N hydrogen bonding interaction. Models of the aspartate molecules at intermediate and high coverages are illustrated in Figure 3.7.

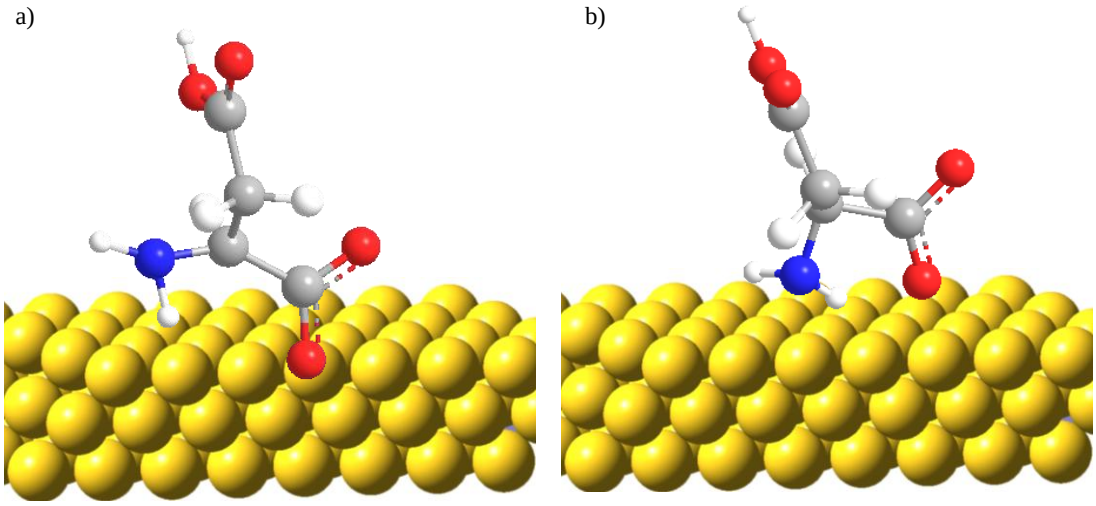

Fig. 3.7 Possible molecular orientation of (S)-Asp on Ni{111} surface at a) intermediate coverages and b) high coverages, based exclusively on RAIRS data.

3.3.1.2 INCREASING MAA COVERAGE ON *(S)*-ASP MODIFIED Ni{111} AT 300 K

Studying the adsorption of MAA onto modified Ni{111} by RAIRS is important in that it provides evidence of how the reactant interacts with the modified surface. As described in Section 1.5.2., an active chiral site model was previously postulated as the most popular mechanism for *(R,R)*-tartaric acid [12] and *(S)*-glutamic acid [35] systems on Ni{111}, with the likelihood of two hydrogen bonds between the modifier functional groups and the β-ketoester ketone and ester groups [37]. It was suggested an intermediate coverage of modifier molecules would be ideal to produce distances between adsorbed modifier molecules large enough to fit MAA molecules in a one-to-one interaction, but low enough to minimise any racemic interactions on terraces.

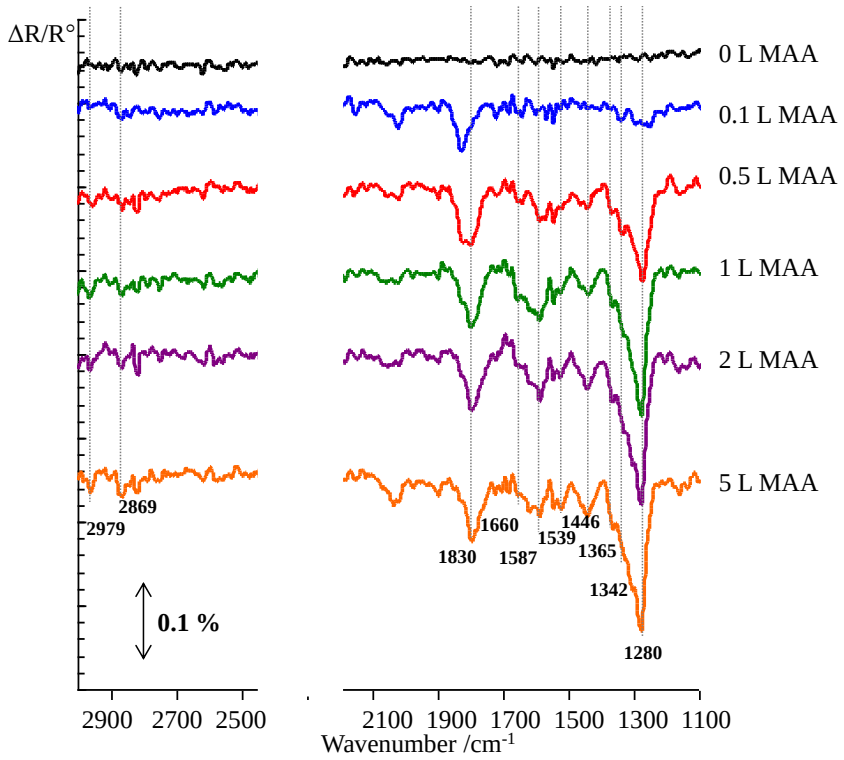

Fig. 3.8 Increasing MAA adsorption on low (10 s) coverage *(S)*-aspartic acid modified Ni{111}.

In this study, adsorption of MAA on low (10 s) coverage *(S)*-Asp modified Ni{111} at 300 K as a function of increasing MAA dose has been studied by UHV-RAIRS and is illustrated in Figure 3.8. It is to be noted that the MAA single beam spectra are ratioed against the spectra of the modified and washed surface, which allows identification of the bands corresponding to MAA only. Upon initial exposure to MAA, a peak at 1830 cm^{-1} dominates the spectrum, which is assigned as CO adsorption in 3-fold hollow sites [20-23]. This would suggest that MAA is unable to displace the CO from the modified surface. With increasing exposure to MAA, this peak remains present, although alongside a rise in bands at 1660, 1587, 1446 and 1280 cm^{-1}. These are assigned (see Table 3.2) as peaks corresponding to the presence of the enol tautomer of MAA [38]. This would suggest that, even at low coverages of *(S)*-Asp, the modifier has a discernable influence on the geometry of the MAA molecules. The presence and strength of certain peaks may also help to elucidate the geometry of the MAA molecule on the surface. The two strongest bands in each of the spectra are the CO adsorption and the $\nu(C\text{-}OH)_{enol}$. The presence of CO throughout all the stages of the experiment suggests that MAA is

likely to be unable to displace it from the surface, especially as the CO is bound at the 3-fold hollow sites, effectively the most attractive position for the molecules. The relative strength of the $\nu(C\text{-}OH)_{enol}$ band and presence of the combination bands at 1550 – 1700 cm^{-1} suggest that, by application of the surface selection rule, the molecule may be twisted with the alcohol group tilted with respect to the Ni surface.

The presence of the enol form of MAA on low coverage *(S)*-Asp modified Ni{111} is at odds with the result found for the same coverage of *(S)*-Glu where the bands were very similar to those for MAA on clean Ni{111} [13]. In that study, it was assumed that the majority of MAA was adsorbing on the terrace regions and no strong interaction was occurring with adsorbed glutamate on the step edges. In the present case, discovering that the enol form of MAA is dominant is encouraging for the suggestion that succinimide may be present at low coverages which would more likely favour bonding to the enol form. Chiral step-kink sites may also be present and they may contribute significantly to the enantioselectivity of the hydrogenation of MAA by forcing the reactant molecules into specific orientations.

MAA + *(S)*-Asp/Ni{111} 300 K /wavenumbers in cm^{-1}	**Assignment**
2979	ν_{as} (CH_3)
2869	ν_{s} (CH_3)
1830	ν $(CO)_{3\text{-}fold}$
1660	ν $(C{=}C)_{enol}$ + ν $(C{=}O)_{enol}$
1587	β-keto, H-bonded to ester group (enol)
1539	ν $(C{=}C)_{enol}$
1446	δ_{as} (CH_3)
1365	δ_{s} (CH_3)
1342	γ $(C\text{-}H)_{enol}$
1280	ν $(C\text{-}OH)_{enol}$

Table 3.2 Assignments of IR peaks observed in the adsorption of MAA on (S)-Asp modified Ni{111} at 300 K. Assignments from Ref. 38.

Considering that succinimide may be present on the Ni{111} surfaces at low coverages and from the observations in the RAIRS experiments for MAA on the modified surface a model of the likely hydrogen bonding which would occur

between the enol form of MAA and a succinimide molecule can be built, as shown in Figure 3.9.

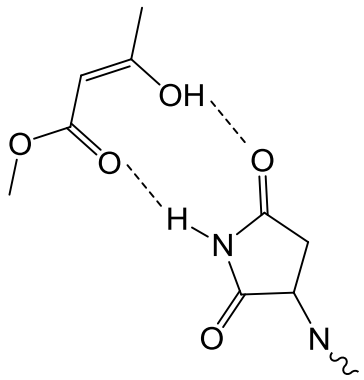

Fig. 3.9 Proposed hydrogen bonding structure between the enol tautomer of MAA and succinimide.

Focusing on the alternative suggestion that chiral faceting may be in play on the surface, it is impossible to ascertain whether chiral step-kink sites are present by RAIRS results alone. It is important to state however that, if a 1:1 interaction model between the MAA and the altered kink site is valid, then there needs to be a difference in adsorption energy of the two faces of MAA to allow enantiospecific adsorption.

To correlate the behaviour of MAA on an *(S)*-Asp -modified Ni{111} surface to that found for *(S)*-Glu and *(R,R)*-TA at room temperature, MAA was dosed on a saturation coverage of aspartic acid (Figure 3.10). It can be clearly seen that MAA does not appear to bind to an *(S)*-Asp saturated Ni surface as no new features are observed. This confirms that the sticking probability of MAA is close to zero on *(S)*-Asp saturated Ni{111} and therefore must need the space between modifier molecules to access free metal sites. The present results mimic those of MAA adsorbed on saturation coverages of *(R,R)*-TA and *(S)*-Glu on Ni{111} [12,13].

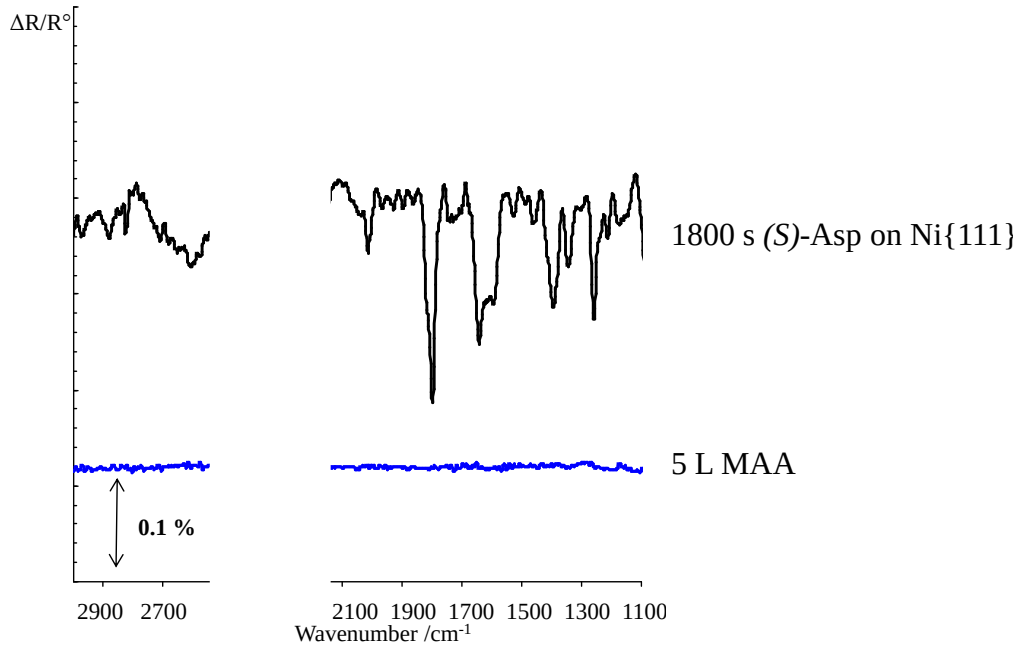

Figure 3.10 RAIRS spectra following MAA adsorption on a saturation *(S)*-aspartic acid modified Ni{111} surface at 300 K (MAA spectra ratioed against the spectra recorded following the washing of the modified catalyst surface).

3.3.2 UHV TPD

3.3.2.1 TPD STUDIES OF INCREASING *(S)*-ASPARTIC ACID COVERAGE ON Ni{111} AT A SUBSTRATE TEMPERATURE OF 300 K

Figures 3.11a-c shows the TPD data acquired following the adsorption of *(S)*-aspartic acid on Ni{111} as a function of coverage at 300 K. The primary desorption products observed occurred at *m/z* values 2 (H_2), 28 (CO) and 44 (CO_2). Analysis of the surface after the TPD experiments by AES confirmed that the resulting Ni{111} surface was free from adsorbates. A low temperature peak is observed at approximately 310 K for several of the desorption spectra. This can be assigned to an artefact created by desorption from the sample mounting, due to its irreproducibility in shape and position [22]. The molecular mass fragments at *m/z* 133 as well as *m/z* 99 were also analysed by the mass spectrometer, due to the RAIRS data suggesting possible succinimide formation at low coverages, but inspection of the thermal evolution products showed no desorption of the molecular

ion (*m/z* 133) or succinimide ion (*m/z* 99) from the surface at any coverage, suggesting a reaction limited desorption process. This would imply that intermolecular bonds break prior to molecule-metal bonds, with H_2, CO and CO_2 primary products released.

The shapes of the TPD peaks are influenced by factors such as intermolecular interactions between adsorbates, as well as pumping speed. If a range of different intermolecular geometries exist, the TPD spectra will show several peaks at different T_d values. Conversely, a single broadened peak will suggest molecular fragments desorbing with only slightly different T_d values. A range of T_{max} values is observed in the present study over the range 330 – 850 K. The first is a low temperature desorption with T_{max} values ranging from 365 – 385 K, a second weak desorption occurs for CO at *ca.* 430 K, as well as higher T_{max} peaks at 530 – 610 K at increased coverages. For CO_2, no desorption peak is observed at low coverages, until a sharp peak at ~380 K appears at higher coverages.

a) *m/z* 2

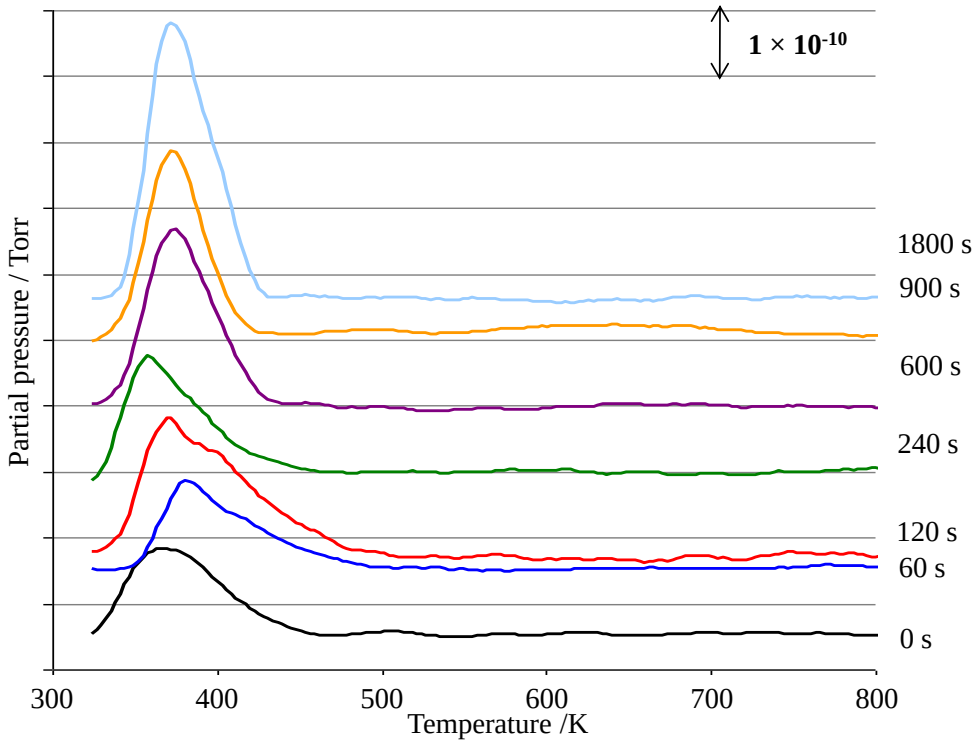
1 × 10-10
Partial pressure / Torr
1800 s
900 s
600 s
240 s
120 s
60 s
0 s
300
400
500
600
700
800
Temperature /K

b) *m/z* 28

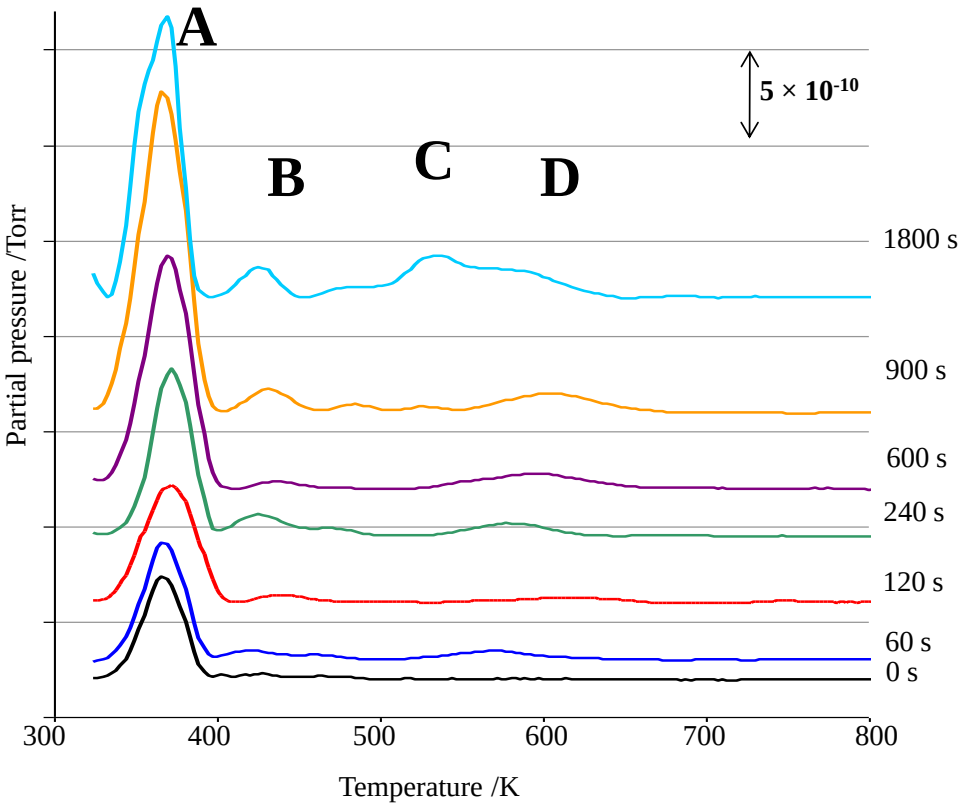
A
B
C
D
5 × 10-10
Partial pressure /Torr
1800 s
900 s
600 s
240 s
120 s
60 s
0 s
300
400
500
600
700
800
Temperature /K

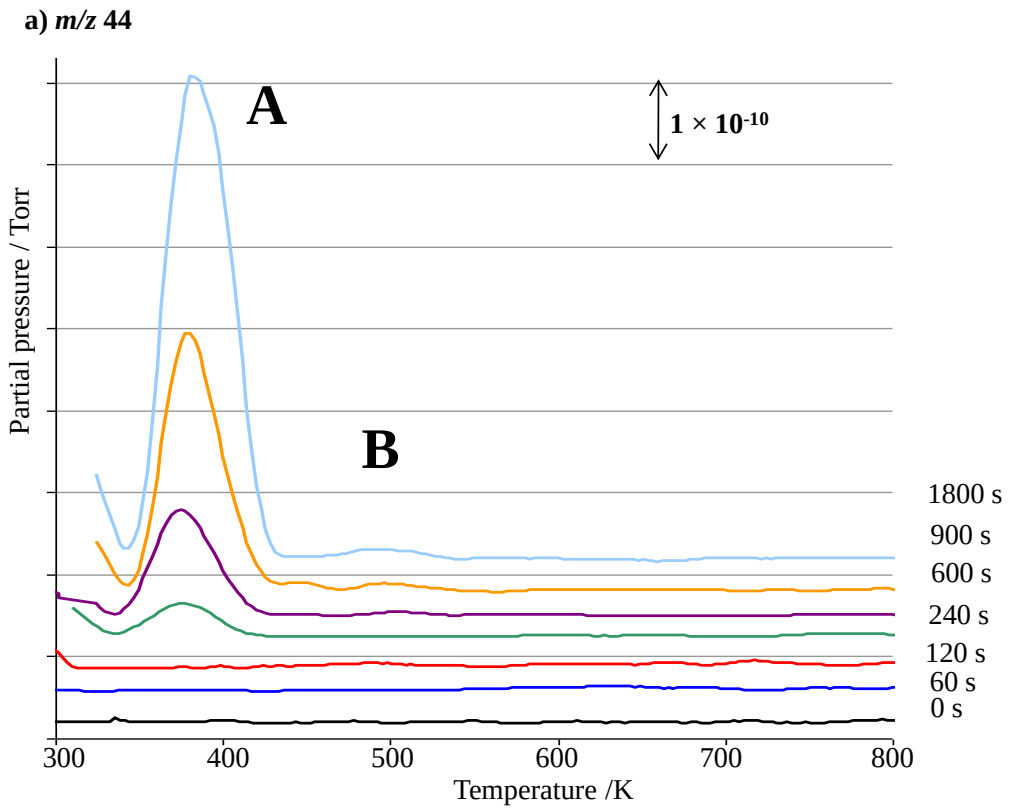

Fig. 3.11 UHV TPD spectra following *(S)*-aspartic acid adsorption on Ni{111} at 300 K with increasing coverages monitoring masses a) 2 (H_2); b) 28 (CO) and c) 44 (CO_2).

H_2 TPD spectra are notoriously complex due to the recombination and desorption of atomic H on the surface by background accumulation, as well as the presence of hydrocarbons from the adsorbate. The amounts of co-adsorbed CO on the surface may also markedly influence the hydrogen adsorption properties, and hence change the desorption characteristics [39]. The most likely sources of atomic hydrogen are from the background, the conversion of aspartic acid to aspartate (deprotonation of the carboxylic acid group to desorb H_2 as the product), and further decomposition of surface nitrogen-containing species. Previous literature has shown that atomic H desorbs from Ni{111} with two desorption maxima: the lower at ~330 K formed only after the adsorption sites for hydrogen at ~370 K are filled [39]. In Figure 3.11a, a hydrogen desorption peak appears at 374 K on the non-dosed Ni{111} surface. This can be assigned to the presence of background H_2 which dissociates on the Ni{111} surface. At 60 s and 120 s doses of *(S)*-aspartic acid, the peak is observed to have a trailing higher T_d tail, making the peak more asymmetric. This asymmetry begins to decrease as coverage is increased, ultimately resulting in a

sharp desorption peak at 373 K for 1800 s *(S)*-Asp dose, with only a small hint of a higher temperature shoulder peak at 400 K. The broadness of the peak is due to a series of decomposition processes occurring around a similar temperature, a result most likely of aspartic acid decomposition at higher coverages.

CO is present on a nominally "clean" Ni{111} surface, shown in the TPD spectra in Figure 3.11b as an asymmetric peak with T_{max} of 370 K (labelled **A**). This suggests that, as expected, the Ni surface has interacted with a residual background level of CO whilst cooling after cleaning. In previous studies by Netzer and Madey [20], it was found that CO desorbed initially at *ca.* 450 K, before shifting to *ca.* 425 K at higher CO coverages. The lower value recorded in our experiments may be justified by work carried out by Held *et al.* [22], in which features at lower T_d values were attributed to structural changes of the CO layer, with CO possibly being displaced from 3-fold hollow sites to atop sites (more energetically unfavourable thus lower desorption temperatures). However, compared to previous studies on *(R,R)*-TA on Ni{111} [40], the CO TPD peak in the present spectrum does not shift to this lower value with increasing adsorbate coverage as expected, but is at the 370 K position from the onset. This most likely suggests a relatively large coverage of CO on the surface from the beginning of the TPD experiments, with the presence of the adsorbate shifting the CO TPD peak marginally to a lower temperature by the presence of a shoulder at highest coverages at 355 K. This verifies that CO desorption is desorption-rate limited, with the change of position of the TPD peak due to repulsive interactions between adsorbates as the number of adsorption sites on Ni{111} become more limited. Interestingly, as the coverage of adsorbate increases, the full-width at half maximum (FWHM) of the 370 K peak initially increases, up to coverages of 240 s, and then decreases to approximately the value found on the "clean" Ni surface. At the highest coverage, fitting (carried out in the Microcal Origin Peak Fitting add-on program) identified that the peak consisted of two Gaussian fits with narrower FWHMs (Table 3.3).

exposure time /s	T_d /K	FWHM /K
0	369.5	28.2
60	371	28.6
120	374.9	35.5
240	376.9	26.8
600	374	28.6
900	372	27.0
1800	376, 360 (shoulder)	15.8, 18

Table 3.3 FWHMs for CO TPD peak in the adsorption of *(S)*-aspartic acid on Ni{111} at 300 K.

Alongside this change in the peak behaviour at 240 s dose and above, several features grow or appear in the TPD spectra at all doses. A peak at 438 K (labelled **B**), becoming sharper and shifting to 428 K at higher temperatures, with a shoulder at 485 K, indicates that the adsorbate has decomposed and bonded partially as a CO species to the Ni{111} surface. A broad peak at 586 K at 240 s dose, a shoulder of a higher T_d peak at 558 K for 600 s and a separate peak at 530 K (with shoulder at 490 K) for the 900 s and 1800 s spectra is assigned to another, more stable species desorbing from the surface (**C**). The likely reason for the shift in temperature is because the increase in coverage on the surface leaves less room for the species to stabilise. Finally, a high T_d peak in the region of 600 K (**D**) is assigned as $C_{(ads)}$ and $O_{(ads)}$ recombination of the decomposed material.

CO_2 desorption peaks in a TPD spectra are diagnostic of the presence of amino acid on the surface, as any residual CO_2 will readily undergo dissociative chemisorption to CO + O on Ni [41]. The CO_2 TPD spectra for increasing coverages are shown in Figure 3.11c. Following a 240 s dose of *(S)*-aspartic acid, a symmetrical broad peak appears at 381 K (**A**), which becomes sharper at the highest coverages. At coverages lower than 240 s, no CO_2 desorption is observed, inferring that either no aspartic acid is present at such coverages, or a different conformation. A very small peak at 513 – 493 K (**B**) is also present at the higher coverages. The areas of the desorption signal versus exposure time is plotted for similar CO and CO_2 TPD peaks and shown in

Figure 3.12. It can be observed that, with the mentioned residual CO presence and lack of initial CO_2 taken into consideration, the areas increase in a likewise fashion to the point at 900 s, where CO appears to reach a saturation point and decreases in area compared to CO_2 which continues to increase. This observation allows us to postulate that aspartic acid has successfully displaced some of the CO species from the surface, and also suggests that the CO and CO_2 desorption features at this region may not originate from the same process. This postulation is also supported by the fact that the desorption peak intensities of CO at all coverages are greater than CO_2, whereas one may expect the ratio to be close to unity if both originated from the scission of the C-C bonds in the aspartate molecules to release the two carboxylate groups. Peaks in region **B** in the CO_2 TPD spectra are coincident with the peak at 490 K in the CO TPD higher coverage spectra.

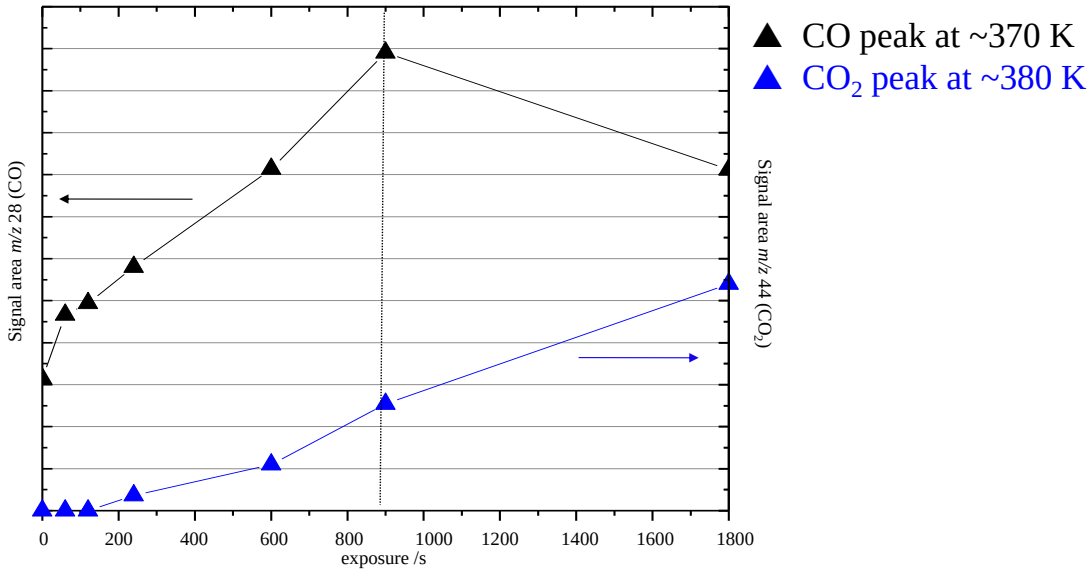

Fig. 3.12 Desorption signal areas of CO (black triangles) and CO_2 (blue triangles) versus exposure time.

It was found in previous studies of glycine and alanine on Pd{111} that the zwitterionic form of the amino acid decomposed almost exclusively at the C-C bond to desorb CO_2, CO, methyl(ethyl)amine and HCN and/or at the C-N bond which would yield COO^- and NH_3 from the surface [36,42]. In the case of aspartic acid, which is one of the amino acids with an acidic side chain, it would be more probable that a scission would take place at both C-C bonds, with the decomposition pathways shown in Figure 3.13; proposed from the RAIRS results that the aspartic acid adsorbs

at intermediate (≥ 240 s) coverages on the surface in its zwitterionic form. Clearly there will be several alternative pathways, with complete decomposition of the aspartic acid being likely due to the considerable amount of H_2 shown in the desorption spectra.

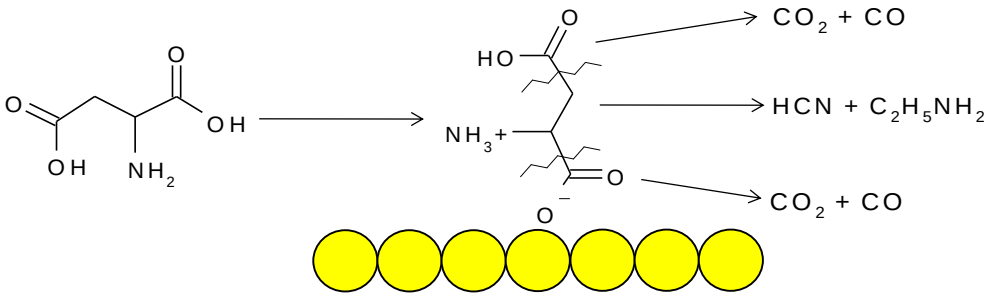

Fig. 3.13 Likely thermal decomposition pathway for aspartic acid on Ni{111}.

The reaction pathway in Figure 3.13 is valid only if aspartate is present on the metal surface. TPD experiments were also carried out for *m/z* values of 17 and 27 (not shown), which would be expected to show some desorption as the two species NH_3 and HCN are likely products of the pathway in Figure 3.13. Surprisingly, it was discovered that neither of the nitrogen-containing fragments were present in the desorption spectra. The other possible species present on the surface, after strong suggestions from the RAIRS data in Section 3.3.1, is succinimide. If succinimide was present on the surface at low doses, a likely desorption product would be CO, but not CO_2 (see Figure 3.5). This would appear to fit into the analyses of the TPD spectra at low coverages (below 240 s dose), where it is obvious that a decomposition pathway occurs for the species on the surface which liberates CO at 370 K, but no CO_2. It would be expected that H_2O would be formed as a by-product from the polycondensation; and indeed the mass spectra run before the TPD experiments do show an increase in *m/z* H_2O; however the TPD spectra do not show a desorption peak for H_2O. This may be justified however by the likelihood that, if the aspartic acid does polymerise on the surface, the water is quickly desorbed into the chamber atmosphere before TPD experiments take place.

An alternative theory is that the sticking probability of the Ni{111} surface for aspartate species is initially low at low coverages, until increasing coverages form

nucleation points for aspartate islands to grow in size and desorb as CO and CO_2 in the TPD spectra. Whilst it has not been possible to confirm or refute this claim due to lack of literature on the topic, it can be expected that, due to the high reactivity of Ni, it is highly unlikely that amino acids would find it impossible to stick at low coverages, and this has been confirmed several times over in previous work of amino and hydroxy acids on Ni [11,14]. Thus, from the TPD results, which are relatively unusual compared to those seen previously for similar systems [36,42,43], it is postulated that succinimide is formed at low coverages. In the CO spectra, it can be assumed that the lowest T_d peak at ~ 370 K is due to background CO co-adsorbed on the surface, most likely on the atop positions due to the large amount seemingly present, and is there at all coverages. Its increase in peak width up to 240 s (see Table 3.3) would suggest that the succinimide species on the surface increases in coverage, with a desorption temperature close enough to 370 K to affect the T_d peak shape. The peak at 428 K in the CO TPD spectra is suggested as the desorption of succinimide, due to its continued presence at all coverages, plus the lack of a coincident peak in the CO_2 spectra. The presence of a CO_2 desorption peak at 380 K at coverages at and above 240 s highlights the presence of aspartic acid. At the higher coverages, the CO TPD results show a peak at 490 K, which is also apparent in the CO_2 TPD at identical coverages, assigned to the decomposition of a slightly more stable species of aspartic acid. This second species is thought to form after the first decomposition/desorption process at 380 K, which creates more space on the surface for neighbouring aspartate molecules to adopt a more stable configuration. Finally, features at approximately 600 K in the CO TPD spectra correspond to the $C_{(ads)} + O_{(ads)}$ recombination of the decomposed material [44], which is confirmed by a lack of any further CO_2 desorption features.

3.3.2.2. TPD STUDIES OF MAA ADSORPTION WITH INCREASING (S)-ASPARTIC ACID COVERAGE ON Ni{111} AT A SUBSTRATE TEMPERATURE OF 300 K

In an attempt to elucidate the influence of aspartic acid on the desorption kinetics of MAA, TPD spectra were carried out on a 5 L MAA dose (1×10^{-8} Torr for 500 s) on

varying coverages of *(S)*-Asp modified Ni{111}. An early study by Yasumori carried out desorption experiments of MAA on unmodified and modified Ni catalyst powder [45]. On the unmodified surface, MAA desorption was found to be a 1st order process (the adsorbed species was in its molecular form), desorbing at 349 K. On the tartaric acid-modified Ni surface, MAA desorption was found to be stabilised to some extent, and a T_d value of 364 K was recorded. In previous desorption studies by Jones and Baddeley [12], no molecular desorption of MAA was found to occur, and so any desorption pathway was assumed to be via a decomposition mechanism. The thermal decomposition pathway is known for the closely related ester methyl acetate, and results in $CO_{(ads)}$ and $H_{(ads)}$ as the major decomposition products [46]. By extension of these and other previous results [12], the molecular desorption of MAA is shown in Figure 3.14, with desorption products consisting entirely of CO and H_2.

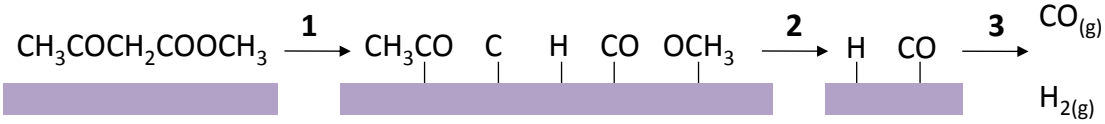

Fig. 3.14 Thermal decomposition pathway for MAA. Adapted from [45].

Figure 3.15 shows the TPD spectra for *m/z* values of 2, 28 and 44 for the desorption of MAA on *(S)*-Asp modified Ni{111} and unmodified Ni{111}. Figure 3.15a shows the H_2 desorption spectra for the experiment. At a 5 L MAA dose onto clean Ni{111}, a broad feature at 362 K with a trailing high temperature tail signals the desorption of H_2. The broad shoulder is likely to be due to the desorption of recombined $H_{(ads)}$ on the surface as temperature increases, possibly originating from H adsorbed at step edges or defect sites, as well as from CH_x species which further decompose to give H_2. As coverage of the modifier is increased to submonolayer levels, the desorption peak becomes sharper and more dominant, with the peak centred at 371 K. At saturation coverages of *(S)*-Asp (900 s), the main desorption peak shifts to a slightly higher temperature, and the beginnings of a peak at 435 K emerge within the higher temperature tail.

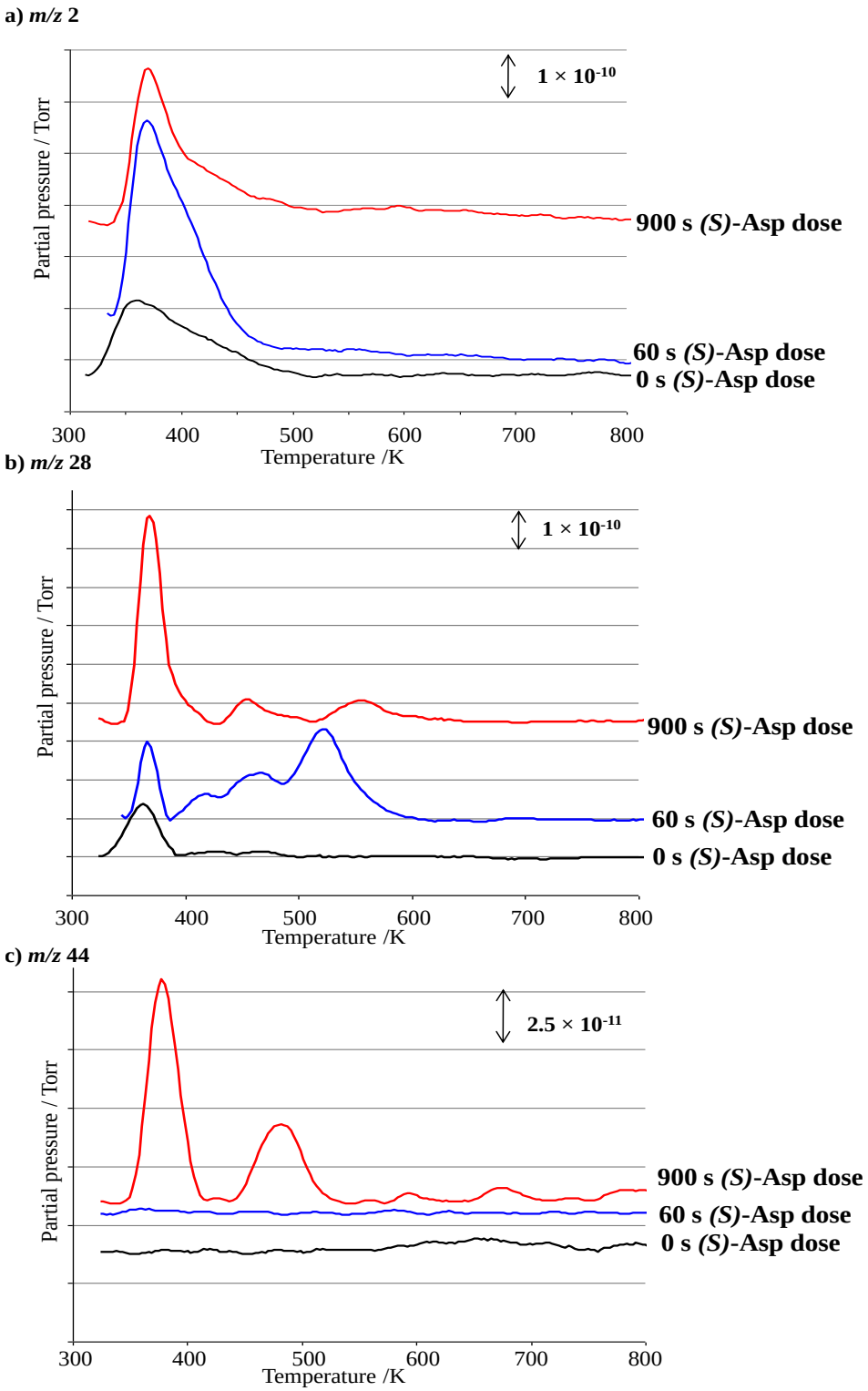

Fig. 3.15 UHV TPD spectra following 5 L MAA adsorption onto modified Ni{111} at increasing *(S)*-aspartic acid coverages at 300 K with increasing coverages monitoring masses a) 2 (H_2); b) 28 (CO) and c) 44 (CO_2).

The CO TPD spectrum for a 5 L coverage of MAA onto unmodified Ni{111}, shown in Figure 3.15b, presents a small peak at 366 K. This is due to MAA molecules forcing $CO_{(ads)}$ into atop sites, similar to that observed for high coverages of *(S)*-aspartic acid on the surface in Figure 3.11b. As no higher temperature peaks are noted for MAA on the unmodified surface, it can be assumed that MAA decomposes with all oxygen atoms removed in the single CO feature. Once co-adsorption takes place with a low coverage of modifier, presumed to be in a succinimide form due to previous TPD and RAIRS results, a marked difference in the CO TPD spectrum occurs, with peaks at 417 K, 465 K and 524 K emerging, alongside the desorption feature at 366 K. The presence of extra features is substantial evidence that there must be interactions between the MAA molecules and either the modifier molecules or step-kink sites produced by the modifier, thus reinforcing the idea of a 1:1 interaction between MAA and the modified substrate surface. Furthermore, the TPD data suggests that, with aspartate molecules on the surface, the methylacetoacetate molecules are stabilised as a higher desorption temperature is noted compared with the CO TPD data in Figure 3.11, and thus it could be suggested that the blockage of the Ni step sites with aspartate decreases the decomposition of MAA.

At saturation coverages of *(S)*-aspartic acid, 5 L MAA dosed onto the surface gives CO desorption peaks at 372 K, 451 K (with a shoulder at 493 K) and 550 K. Comparing these peak positions to those found for a saturation coverage of *(S)*-Asp in Figure 3.11c, the overall peak envelope is found to be similar, but peaks shift slightly, from 435 K in Figure 3.11c, to 448 K in the present TPD spectrum; and from 606 K to 550 K. This would suggest that the adsorbate is marginally more stabilised on the surface, possibly due to the time dependence of the stability of the aspartate molecules, i.e. the extra time taken for the chamber pressure to recover before dosing MAA may aid in the growth of different desorption kinetics at the slightly higher temperature of 448 K [40]. The peak at 550 K is within the expected desorption temperature of $C_{(ads)} + O_{(ads)}$ recombination [44].

Finally, the CO_2 TPD spectra is shown in Figure 3.15c, which indicate the presence of modifier on the surface as MAA itself does not decompose to give CO_2 as a decomposition product (see Figure 3.14). At a 5 L MAA dose onto the unmodified Ni{111} surface, no CO_2 desorption peak is noted. After a 60 s dose of *(S)*-Asp and 5 L MAA dose, CO_2 is still not observed as desorbing from the surface. This finding gives credence to the possibility of succinimide being present and binding to the MAA, as neither molecule would decompose to give a CO_2 desorption feature. Otherwise, step-kink sites could be instrumental in binding the MAA to the surface. At saturation coverages of *(S)*-aspartic acid, a 5 L dose of MAA gives a CO_2 desorption spectrum with a large peak at 380 K, a small peak at 428 K, and a separate peak at 487 K. Compared to the analogous TPD spectrum for the same coverage of *(S)*-Asp without the MAA dose, the peak at 487 K is quite different in its intensity. This would suggest that, if the Ni surface is assumed to be saturated by aspartate, the desorption kinetics of the surface aspartate species is time-dependent (as noted previously for tartaric acid [11]).

3.3.3 UHV STM

The morphology of *(S)*-aspartic acid on a Ni{111} surface at varying coverages at room temperature was topographically imaged using STM. We chose not to use LEED in our experiments as previous attempts led to substantial beam damage to the aspartate overlayer on the Ni{111} surface. This was similar to work carried out in our group on tartaric acid and glutamic acid on Ni{111} [11,14]. It was proposed that the electrons stimulate decomposition of the overlayer as the Ni has a high density of electrons states near to the Fermi level. Therefore, although LEED is used in the experiments to ascertain the cleanliness of the Ni surface, it is not used to examine ordered adlayer structures.

3.3.3.1 LOW COVERAGE (S)-ASPARTIC ACID ON Ni{111} AT A TEMPERATURE OF 300 K

Figure 3.16 shows an STM image of a low (60 s) coverage of *(S)*-Asp on Ni{111}, with molecular features adsorbing predominantly in the vicinity of step edges on the upper terraces. It is to be noted that these features are not present on a clean Ni surface. It is clear that the diffusion of the aspartate molecules is limited by the substrate-adsorbate interaction as opposed to any lateral interactions between the molecules. Adsorbates are known to typically interact more strongly with substrate atoms at step edges due to the lower coordination number of the metal atoms, which results in there being more localised *d*-states to interact with the adsorbate orbitals. A low coverage of molecules will generally traverse the atomically flat terraces until they reach the more stable step edges and nucleate, in this case as oligomers of four or five features in length.

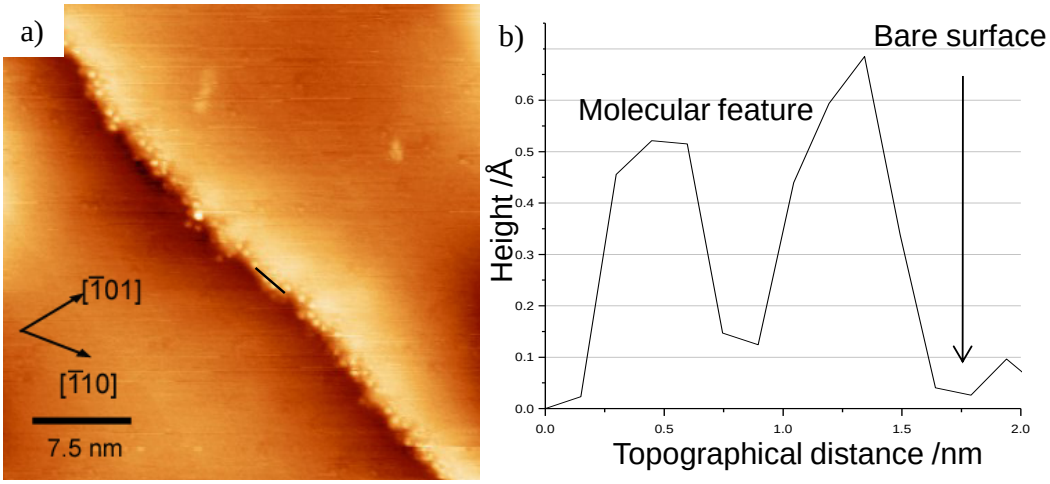

Fig. 3.16 a) STM image of a 60 s coverage of *(S)*-aspartic acid on Ni{111} (37.5 × 37.5 nm^2, -1.5 V, 0.5 nA) and b) the height profile across the line as indicated in the STM image.

Figure 3.16 shows clear STM evidence of the preference of aspartate adsorbates to bind to the slightly charge deficient upper step edges. Isolated molecules of similar shape and size (approximately 6 Å in diameter) are observed along the edges in Figure 3.16a, as well as adsorbate clusters four to five features in size. The preference of the aspartic acid molecules to bind to the upper terrace of a step can be neatly explained by the Smoluchowski effect [47]. At a step, electrons find it

difficult to immediately change state to mimic the sharp discontinuity of atomic structure as this would cause an unfavourably large electron kinetic energy. Smoluchowski suggested that the electron density smoothes out or redistributes its charge across local densities of states at surface protrusions to reduce kinetic energy, and hence the total energy of the surface. This would result in a charge transfer from the upper-terrace to the lower terrace, with enhanced empty states above the step and full states below [47] as shown in Figure 3.17. The zigzag line corresponds to the corrugation of a {110} surface and the wavy line represents the charge distribution. This smoothing mechanism on a close-packed surface such as fcc{111} has the least effect on the work function of the stepped surface, compared to more open surfaces, but may still be found to affect chemisorption at steps, and can lead to selective adsorption to the bottom or top terrace, depending on the nucleophilicity of the adsorbant species. Previous observations of the Smoluchowski effect on {111} surfaces include benzene on Cu{111} [48] and styrene on Au{111} [49]. It was found in both cases that the adsorbate molecules acted like nucleophiles and thus adsorbed on the above step edges, where electron depleted areas were present due to the Smoluchowski effect.

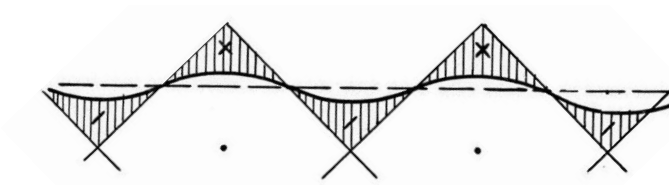

Fig. 3.17 Equilibrium charge distribution due to smoothing effect. From [47].

In Figure 3.18, the adsorbate molecules appear to have found it favourable to self assemble into ring structures, consisting of tetramers of the molecular features. The line profile shows that the individual protrusions forming the ring shape have an apparent diameter of approximately 6 Å, with an apparent STM height of 0.5 – 0.6 Å. Topographical measurements in STM are subject to some discrepancy as STM does not record atomic nuclei locations, but rather the local variation in electronic structure of the surface at the adsorbed molecules. The individual molecules could not be imaged in any greater resolution, presumably due to their mobility on the reactive Ni surface. Clusters on the whole appear isolated from adjacent clusters, despite distances between each being typically 2 – 3 nm (i.e. 4 – 5 molecular lengths

apart), suggesting no long range interactions. The appearance of the clusters suggests oligomer formation of the molecules (inset in Figure 3.18a), likely to be succinimide as suggested from the RAIRS and TPD results. In the centre of the cluster of four adsorbate molecules, a smaller protrusion ~5 Å in width is recorded. This protrusion can be tentatively assigned as a Ni adatom which could coordinate to the succinimide through either the carbonyl O or the imide N. As is clear from the RAIRS data in Section 3.3.1.1, it is likely the succinimide species is bound to the Ni via the carbonyl groups, which would leave the molecule free to tilt from the surface. The low temperature single peak in the TPD spectra at identical coverages points to a low desorption energy of the succinimide molecules and suggests a weakly bound geometry on the surface. Figure 3.18, with oligomers in close proximity to one another, would suggest significant supramolecular interactions which would account for the broadness of the low temperature TPD peak in the CO and H_2 spectra, as the molecules must break supramolecular bonds before desorbing from the substrate.

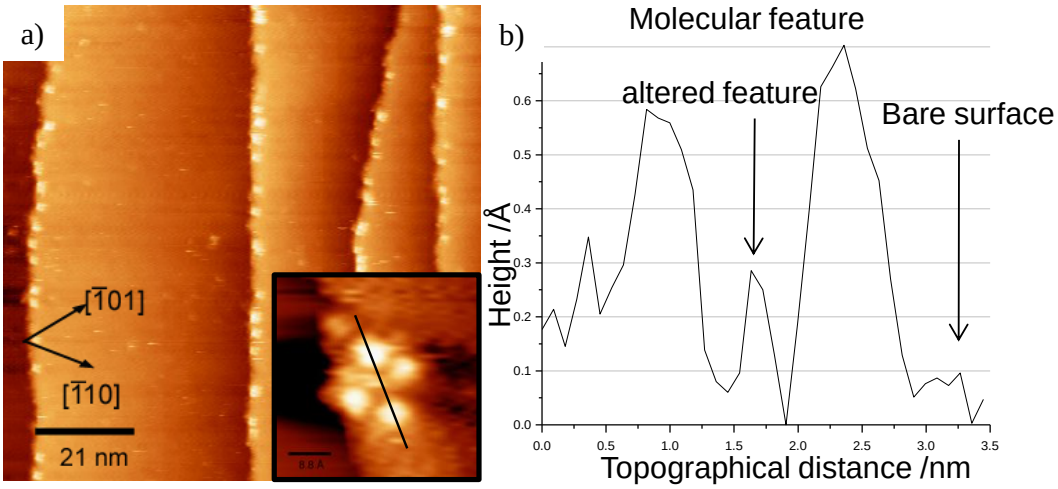

Fig. 3.18 a) STM image of clusters of succinimide molecules at low coverage on Ni{111} at room temperature (105 × 105 nm^2, -0.9 V, 0.84 nA) and b) the height profile across the line as indicated in the STM image.

The origin of the tetrameric clusters in the case of aspartic acid is intriguing and not previously observed for similar systems on Ni{111} [11,13,14]. STM work by Wang *et al.* of aspartic acid on Cu{001} [7] found a co-existence of two adsorption states at low coverages, explained by the fact that both carboxyl groups on Asp could be deprotonated which would give rise to two different states upon interacting with

the Cu surface. Indeed, aspartic acid had previously been shown in Cu complexes to react with the Cu^{2+} through both carboxyl groups. [50]. The study also found that the aspartate molecules were unable to form any ordered superstructures at high coverages on the Cu{001} surface, which was explained by the lack of intermolecular hydrogen bonding due to restrictions in the flexibility of the molecules bound by both carboxyl groups. It should be noted that, for the STM images in this section, the possibility that the tetrameric clusters are a result of STM tip artefacts has been discounted by carrying out extensive imaging of the clusters at a variety of different frame angles which showed the geometry of the features to be real.

Examining the tetramers in this study in greater detail, the recognition from TPD and RAIRS of the existence of succinimide at these coverages allows a possible model to be postulated. A model is shown in Figure 3.19 which accounts for ring formation, as well as matching the periodicity observed in STM. For this model to hold, dehydrogenation of the imide functionality would have to occur to form an oligomer of succinimide with a lone pair on the imide nitrogen, which could then complex with Ni^{2+}. Examining the crystallography of tetraaquobis(succinimidato)nickel(II) dehydrate from studies by Cumming and Hall [51], a very similar structure is shown to that proposed in Figure 3.19, with Ni-O and Ni-N distances *ca.* 2.1 Å. This arrangement also allows stabilisation via four intermolecular bonds between one carbonyl O atom and the imide H atom of the adjacent molecule, and so creates a desirable oligomer ring structure. Tysoe and co-workers [52] have recently reported tetramer structures for the closely related alanine and 2-aminobutanoic acid on Pd, with the driving force presumed to originate from the NH_3^+ and COO^- groups, whereas in the present case the Ni^{2+} adatom drives the isolated succinimide oligomers to form a more energetically favourable ring structure. The isolated position of the tetramers on the step edges only serve to indicate that the nearby steps of the substrate play an important role in the formation of the islands, the adsorbate interactions and the resulting island stability [48].

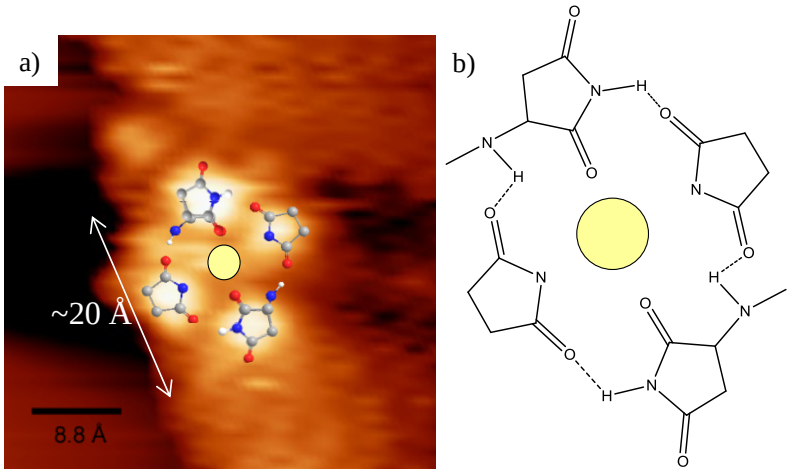

Fig. 3.19 Schematic model illustrating the shape of the tetramer rings of succinimide, interacting with a central Ni adatom.

3.3.3.2 INTERACTION OF MAA WITH LOW COVERAGE *(S)*-ASPARTIC ACID ON Ni{111} AT A TEMPERATURE OF 300 K

Figure 3.20 illustrates the interaction of 0.5 L MAA with a low coverage of aspartic acid on the Ni{111} surface. New molecular features are apparent at the edge of the steps, bound to existing species. From measurements, the features are approximately 7.5 Å in length which represents the length of an MAA molecule, and is too large to be deemed a succinimide molecule. With aspartic acid polymerising into its succinimide form RAIRS data confirmed that, at such low coverages, the MAA species appear predominantly in their enol form (Figure 3.9). The clusters on the step edges, although slightly streaked in the STM images, appear to have the same dimensions as the tautomer rings observed in section 3.3.3.1, and so it is reasonable to assume that the succinimide molecules are bound as in Figure 3.19.

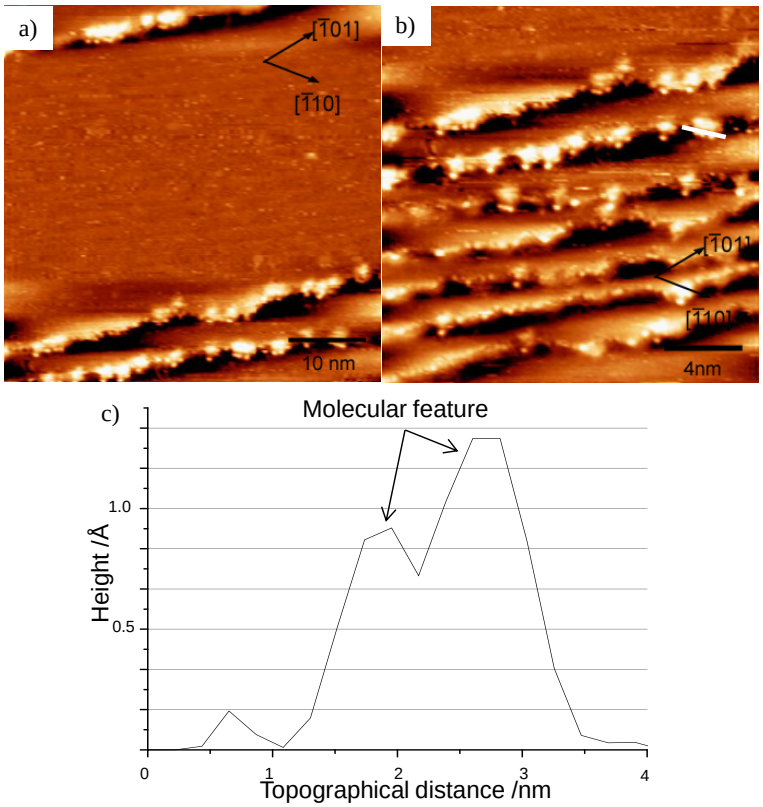

Fig. 3.20 STM images of the interaction of 0.5 L MAA with succinimide at low coverages on Ni{111} a) 50 × 50 nm^2, -0.92 V, 1.09 nA b) 8 × 8 nm^2, -0.92 V, 1.09 nA. The height profile across the line as indicated in the STM image is shown in c).

A likely model is shown in Figure 3.21. In this model, the imide and one carbonyl group of the succinimide molecule interact via hydrogen bonding with the enol –OH and ester C=O groups of the MAA molecule, with the enol form of MAA parallel to the surface as suggested by RAIRS. The MAA molecule could feasibly interact with the succinimide molecules at the step edge side, or at the other side of the ring. From the STM images, the MAA molecules appear to favour the step edge side, which could speculatively be due to an interaction involving the reactant and metal atoms at step edges. This would suggest that, although MAA can bind in either conformation, one enantiotopic face would be more favourable, as shown in Figure 3.21, due to the alignment of favourable hydrogen bonds (thus disfavouring a 180° rotation of the MAA molecules). Hydrogenation of the MAA molecules in this conformation would ultimately give the *(R)*-MHB product, as shown in Figure 1.1.

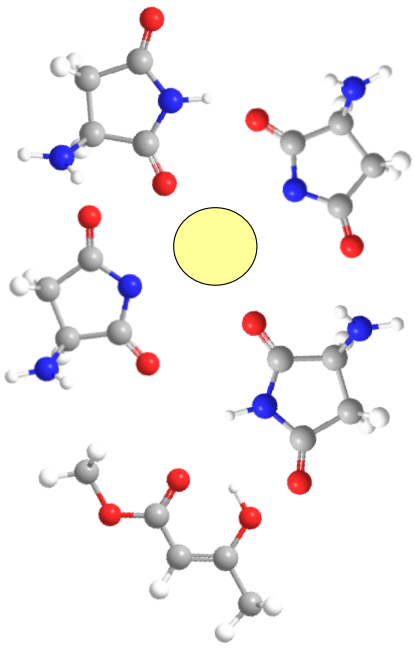

Fig. 3.21 Schematic possible model for the observed STM images in 3.20a) and b).

Substantial corrosion of the steps also occurred, observed in Figure 3.20, with the steps initially aligned along the close packed $[\bar{1}01]$ direction of the {111} surface, and reoriented to give a sawtooth type arrangement whereby the steps are aligned along the $[11\bar{2}]$ direction.

3.3.3.3 INTERMEDIATE COVERAGE *(S)*-ASPARTIC ACID ON Ni{111} AT A SUBSTRATE TEMPERATURE OF 300 K

As coverage is increased, the molecular features spread to the terraces. Isolated molecules of aspartate continue to exist along step edges, apparently causing considerable etching to the steps, as previously found in numerous amino acid on metal studies [14,53]. In Figure 3.22, steps are in the $[2\bar{1}1]$ direction with facets +20° to the steps. Step heights are approximately 2 Å (comparable to bare Ni{111} step heights of 2.04 Å).

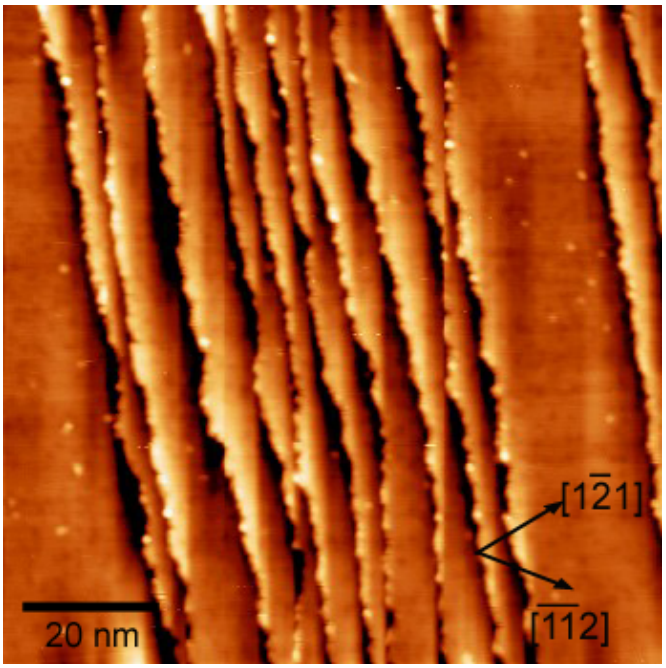

Fig. 3.22 STM image of clusters of succinimide oligomers at medium coverage on Ni{111} (105 × 105 nm^2, -0.9 V, 0.84 nA).

The tetrameric clusters which were present at low coverages at the step edges spread out onto the terraces. Figure 3.23a-d shows isolated clusters mainly consisting of a tetramer ring within which a fifth feature lies. This is shown clearly in the zoomed in image of Figure 3.23c, and the line profile in 3.23d. The presence of the tetramer feature at these coverages can again be assigned to rings of succinimide molecules hydrogen-bonded to one another, with a Ni adatom in the centre.

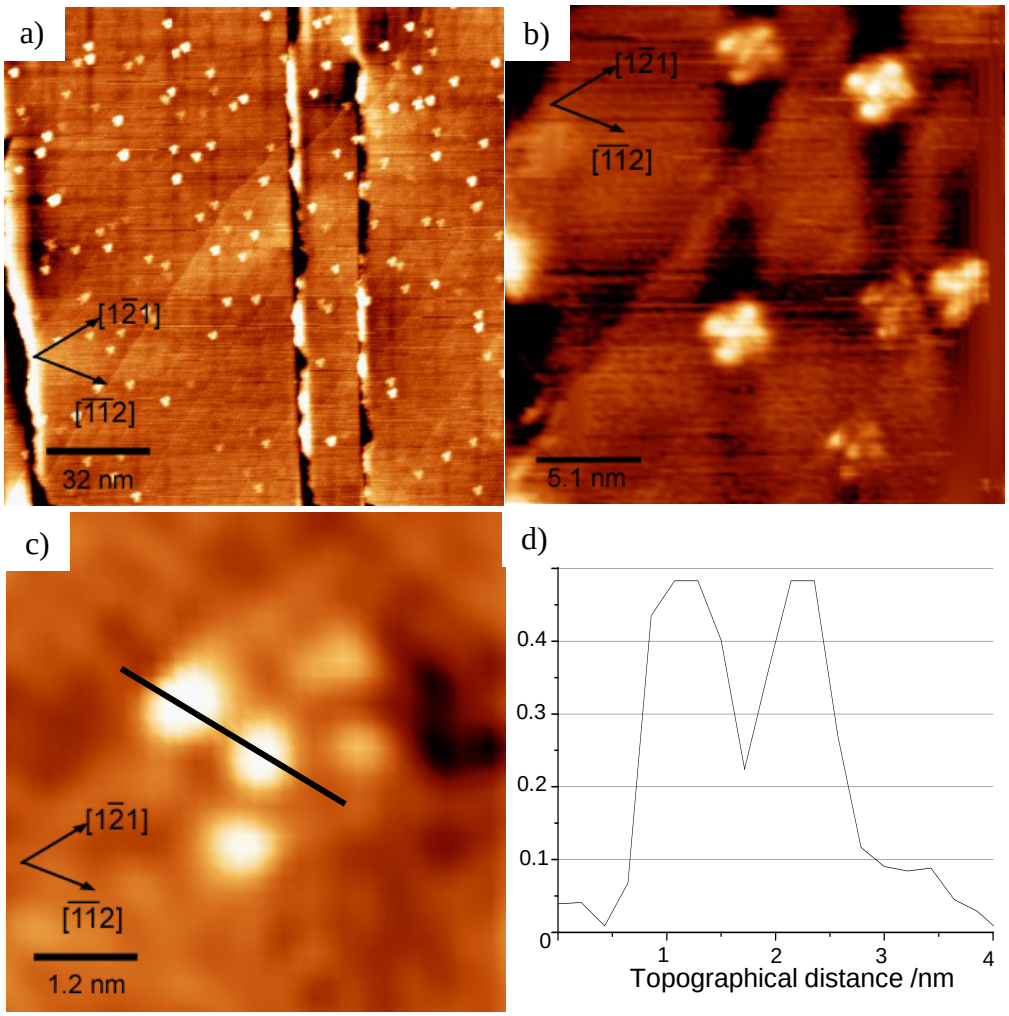

Fig. 3.23 b) STM images of tetramers of succinimide at intermediate coverage on Ni{111} a) 160 × 160 nm^2; b) 25.5 × 25.5 nm^2; c) 6 × 6 nm^2, all at -1.5 V, 0.5 nA, d) profile across the line as indicated in the STM image c).

3.3.3.4 HIGH COVERAGE *(S)*-ASPARTIC ACID ON Ni{111} AT A SUBSTRATE TEMPERATURE OF 300 K

At high coverages (900 s) of *(S)*-aspartic acid deposited on the Ni single crystal at 300 K a poorly defined coverage of aspartate species is observed on the surface (Figure 3.24). Features are typically 6.6 – 7.3 Å centre to centre, corresponding to individual aspartate molecules. A height of 1 Å suggests multilayer growth, as does the presence of several brighter features on the surface.

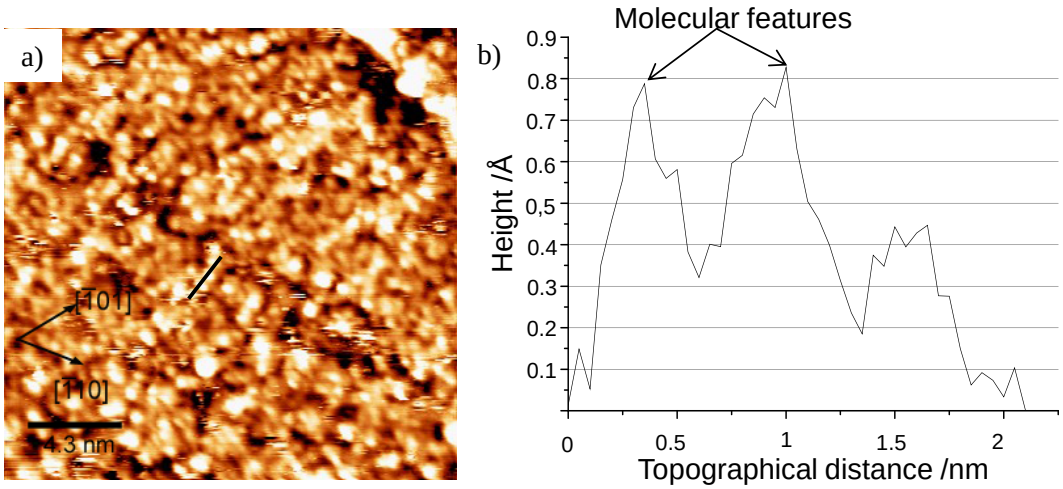

Fig. 3.24 STM image of *(S)*-aspartate molecules at high coverage on Ni{111} a) 21.5 × 21.5 nm^2, -1.5 V, 0.6 nA, b) height profile of line indicated in STM image in a).

Annealing the surface to 373 K before deposition of aspartic acid shows molecular features ~6.6 Å in diameter centre-to-centre and with a height of 0.5 Å, suggesting removal of the second layer due to the anneal. Short chains of aspartate dimers are present on the surface, presumably as a mixture of zwitterionic and anionic forms from the RAIRS results. This is shown in Figure 3.25.

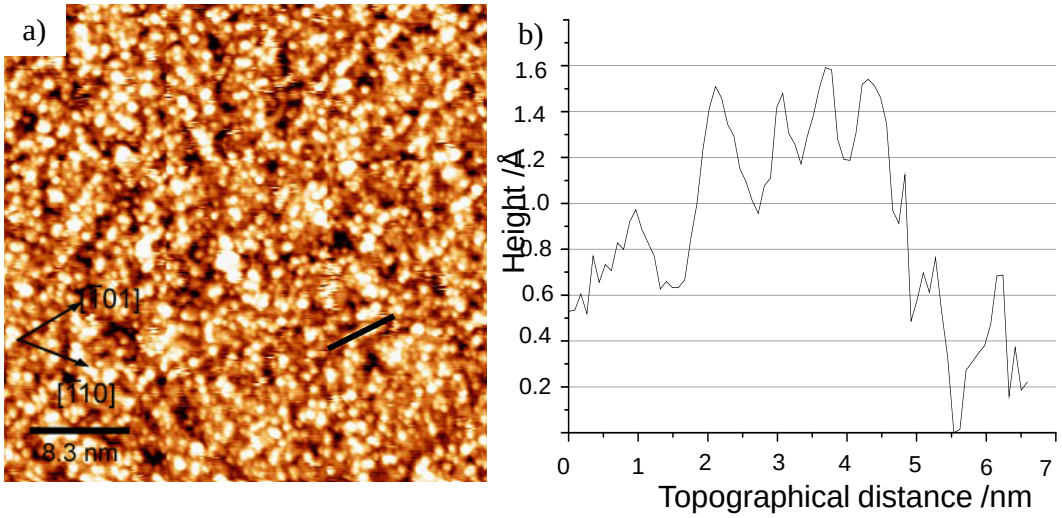

Fig. 3.25 STM image of *(S)*-aspartate molecules at high coverage on Ni{111} annealed to 373 K a) 41.5 × 41.5 nm^2, -1.3 V, 0.98 nA, b) height profile of line indicated in STM image in a).

STM was employed in studying the surface after MAA adsorption but images obtained did not show any differences in surface structure. As observed by RAIRS, and verified by the STM images, MAA will not bind to a saturated coverage of *(S)*-aspartic acid.

3.4 IMPLICATIONS FOR ENANTIOSELECTIVE CATALYSIS

In heterogeneous catalysis, the adsorption of *(S)*-Asp on Ni nanoparticles is known to create an enantioselective catalyst for the hydrogenation of the β-ketoester methylacetoacetate. Enantioselectivity has been measured to be approximately 8.2 % e.e [54]. It has been found in catalytic studies that, although aspartic acid closely resembles malic acid and glutamic acid in structure, the enantioselectivity of a nickel catalyst treated with aspartic acid is considerably smaller than one treated with either of the others [55]. Another interesting find was that an *(S)*-aspartic acid-modified Ni catalyst would produce the *(R)*-enantiomeric product of MHB, whilst *(S)*-malic acid would produce the *(S)*-product. In these early studies, it was postulated that the configuration and size of the modifier in question was very important to the activity and selectivity of the catalyst.

The use of UHV-based studies, although not as relevant as liquid phase studies into catalysts, does offer an important insight into the possible mechanism of the modifier interaction with the reactant at the surface. In the results presented in this chapter, the combination of RAIRS, TPD and STM has allowed a detailed examination into the importance of how the form adopted by aspartic acid at the surface relates to the levels of enantioselectivity observed in the catalytic work. It has been shown within this chapter that, at the low coverage regime, where the highest enantioselectivity takes place, the modifier is polymerised at the Ni surface to form polysuccinimide, which preferentially binds in tetramer structures at the top step edges. It should be noted that the polymerisation of the aspartate molecules is most likely entropically favoured by UHV conditions, and may not be applicable in liquid-solid interface studies (Chapter 4). The Ni{111} steps are observed to be facetted by the presence of the modifier. It has previously been proposed that organic molecules could

modify the surface by either templating with the reactant molecules, or reconstructing the substrate [56]. In the present case, it appears that a possible combination of both effects may contribute to the enantioselectivity of the system. The presence of a polymerised form of aspartic acid on the surface has not been hypothesised before this study. The presence of polysuccinimide, and their resulting ring-like formation, is expected to limit the enantioselectivity of the system as the tetramers are very localised and do not offer possibilities for long range order. Indeed, when MAA is adsorbed onto such a surface, MAA molecules appear to anchor to specific sides of the tetramers, as well as preferring the near step edge side of the tetramer. It has been deduced that MAA will successfully bind at these positions in an enantioselective fashion, due to a combination of being "pinned down" by the tetramers, as well as some interaction with the more reactive Ni at the step edges. It is therefore likely that these modified and facetted steps catalyse the reaction enantioselectively, as no other ordered structure of co-adsorbed aspartic acid and MAA is observed, while the remainder of MAA is hydrogenated racemically. This may account for the relatively low enantioselectivity in the *(S)*-aspartic acid-modified Ni{111} catalyst system, and also the difference in behaviour compared to seemingly closely related amino and hydroxy acids.

3.5 CONCLUSIONS

The adsorption of *(S)*-aspartic acid onto Ni{111} results in three distinct species depending on coverage. At low coverages, RAIRS has shown the presence of a succinimide species adsorbed onto the Ni surface. TPD supports the conclusion that succinimide molecules are present at low coverages, due to the lack of CO_2 desorption and presence of H_2 and CO. By analogy with previous studies of amino acids on metals, STM concluded that aspartic acid did not behave conventionally at low coverages but formed ring-like features at step edges consisting of polysuccinimide, and resulted in binding a small percentage of MAA in an enantioselective fashion to result in *(R)*-MHB formation after hydrogenation.

At intermediate coverages, in contrast to that observed previously for *(R,R)*-TA and *(S)*-Glu, there was no evidence of large supramolecular assemblies on the surface. Tetramer features were still present, although spread out onto the terraces as well as present at the step edges.

At higher coverages, RAIRS suggested aspartic acid was present in its zwitterionic and anionic forms, presumably due to the lack of free surface sites to catalyse the polymerisation of the aspartate molecules. TPD showed the emergence of desorption peaks more typical to aspartic acid desorption, with a desorption temperature of approximately 380 K. STM showed multilayer coverage of features assigned as aspartate molecules, which were desorbed to a single molecular layer once annealed. MAA was found to be unable to bind, which reiterates the need for space on the catalyst and the likelihood that MAA needs some interaction with Ni as well as the modifier molecules.

In summary, it is thought that, due to the amount of available space at low coverages and the facetted step kink catalytic sites on the substrate, aspartic acid can polymerise on the surface of the Ni{111} to form a polysuccinimide species, co-adsorbed with CO and H_2 from residual background gases. As progressively larger amounts of aspartic acid are dosed onto the surface, the polysuccinimide has less room to form and aspartic acid begins to competitively bind to the surface.

3.6 REFERENCES

[1] L.L. Atanasoska, J.C. Buchholz & G.A. Somorjai, *Surface Science,* **72** (1978) 189.
[2] S.M. Barlow, K.J. Kitching, S. Haq & N.V. Richardson, *Surface Science*, **401** (1998) 322.
[3] Q. Chen, D.J. Frankel & N.V. Richardson, *Surface Science,* **497**(2002) 37.
[4] S.M. Barlow & R. Raval, *Surface Science Reports,* **298**(2003) 1.
[5] X. Zhao, H. Wang, R.G. Zhao, W.S. Yang, *Materials Science & Engineering,* **16** (2001) 41.
[6] Y. Izumi, S. Yajima, K. Okubo & K.K. Babievsky, *Bulletin of the Chemical Society Japan,* **44** (1971) 1416.
[7] H. Wang, X.Y. Zhao & W.S. Yang, *Acta Physica Sinica,* **49** (2000), 1316.
[8] Y. Izumi. *Advanced Catalysis,* **32** (1983) 215.
[9] M.O. Lorenzo, PhD Thesis- *Complexities and Dynamics of the Enantioselective Site in Heterogeneous Catalysis,* University of Liverpool, 1999.
[10] A. Tai & T. Harada, *Tailored Metal Catalysts,* Y. Isawawa (Ed.); D Reidel, (1986) 265.
[11] T.E. Jones, C.J. Baddeley, *Surface Science,* **513** (2002) 453
[12] T. E. Jones and C. J. Baddeley. *Surface Science*, **519** (2002) 237
[13] T. E. Jones and C. J. Baddeley. *Langmuir*. **22** (2006) 148.
[14] A.G. Trant & C.J. Baddeley, *Journal of Physical Chemistry C,* **115** (2011) 1025.
[15] A.D. Roddick-Lanzilotta, A.J. McQuillan, *Journal of Colloid and Interface Science,* **227** (2000) 48.
[16] O.V. Cabral, C.A Téllez S., T. Giannerini & J. Felcman, *Spectrochimica Acta A,* **61** (2005) 337.
[17] J.L. Castro, M.A. Montanez, J.C. Otero & J.I. Marcos, *Journal of Molecular Structure,* **349** (1995) 113.
[18] J.F. Pearson & M.A. Slifkin, *Spectrochimica Acta A,* **28** (1972) 2403.
[19] C.E.D. Chidsey & D.N. Loiacono, *Langmuir,* **6** (1990) 682.
[20] F.P. Netzer & T.E. Madey, *Journal of Physical Chemistry,* **76** (1982) 710.
[21] K.S. Smirnov & G. Raseev, *Surface Science,* **384** (1997) L875.
[22] G. Held, J. Shuler, W Slarek & H-P. Steinruck, *Surface Science,* **398** (1998) 154.
[23] N. Ikemiya, T. Suzuki & M. Ito, *Surface Science,* **466** (2000) 119.
[24] J.Mosig, C.H. Gooding & A.P. Wheeler, *Industrial and Engineering Chemistry Research,* **36** (1997) 2163.
[25] S.W. Fox, *Geochimica & Cosmochimica Acta,* **59** (1995) 1213
[26] T. Yohozawa & A. Yokoyama, *Progress in Polymer Science,* **32** (2007) 147.
[27] A.G. Trant, T.E. Jones & C.J. Baddeley, *Journal of Physical Chemistry C,* **111** (2007) 10534.
[28] B. A. Stamboliyska, Y. I. Binev, V. B. Radomirska, J. A. Tsenov & I. N. Juchnovski, *Journal of Molecular Structure*, **516** (2000) 237.
[29] L. E. Niţă, A. P. Chiriac, C. M. Popescu, I. Neamţu & L. Alecu, *Journal of Optoelectronics & Advanced Materials,* **8(2)** (2006) 663.
[30] Q. Yuan, M. Wei, D. G. Evans, & X. Duan, *Journal of Physical Chemistry B,* **108** (2004) 12381.
[31] S.M. Barlow, K. J. Kitching, S. Haq, & N. V. Richardson *Surface Science*, **401** (1998) 322.

[32] J. Williams, S. Haq & R. Raval, *Surface Science,* **368** (1996) 303.
[33] S.M. Barlow, S. Haq & R. Raval, *Langmuir,* **17** (2001) 3292.
[34] E.M. Marti, C. Methivier, P. Dubot & C.M. Pradier, *Journal of Physical Chemistry B,* **107** (2003) 10785.
[35] T.E. Jones, M.E. Urquhart & C.J. Baddeley, *Surface Science,* **587** (2005) 69.
[36] F. Gao, Z. Li, Y. Wang, L. Burkholder & W.T. Tysoe, *Surface Science,* **601** (2007) 3276.
[37] C.J. Baddeley, *Topics in Catalysis,* **25** (2003) 17.
[38] N. V. Belova, H. Oberhammer & G.V. Girichev, *Journal of Physical Chemistry A,* **108** (2004) 3593.
[39] K. Christmann, O. Schober, G. Ertl & M. Neumann, *Journal of Chemical Physics,* **60** (1974) 4528.
[40] T.E. Jones, PhD Thesis *Investigations of a Model Enantioselective Heterogeneous Catalyst",* University of St Andrews, 2002.
[41] H-J. Freund & M.W. Roberts, *Surface Science Reports,* **25** (1996) 225.
[42] F. Gao, Z.Li, Y. Wang, L. Burkholder & W.T. Tysoe, *Journal of Physical Chemistry C,* **111** (2007) 9981.
[43] F.Gao, Y. Wang, L. Burkholder & W.T. Tysoe, *Surface Science,* **601** (2007) 3579.
[44] R.P. Holroyd & M. Bowker, *Surface Science,* 377-379 (1997) 786.
[45] I. Yasumori, *Pure and Applied Chemistry,* **50** (1978) 971.
[46] E. Zahidi, M. Castonguay & P.H. McBreen, *Journal of Physical Chemistry,* **99** (1995) 17906.
[47] R. Smoluchowski, *Physical Review,* **60** (1941) 661
[48] S.J.Stranick, M.M. Kamna & P.S. Weiss, *Surface Science,* **338** (1995) 41
[49] A.E. Baber, S.C. Jensen, E.V. Iski & E.C.H. Sykes, *Journal of the American Chemical Society,* **128** (2006) 15384
[50] Y-C. Liang & A. Olin, *Acta Chemica Scandinavica A,* **38** (1984) 247.
[51] H.J. Cumming & D. Hall, *Acta Crystallographica,* **B32** (1976) 1281.
[52] W.T. Tysoe, *Chiral Templates and Chiral Modifiers,* Oral Presentation ACS Boston, MA, 23rd August 2010.
[53] X.Y. Zhao, *Journal of the American Chemical Society,* **122** (2000) 12584
[54] Y. Izumi, S. Tatsumi & M. Imaida, *Bulletin of the Chemical Society of Japan,* **42** (1969) 2373.
[55] Y. Izumi, M. Imaida, H. Fukawa & S. Akabori, *Bulletin of the Chemical Society of Japan,* **36** (1963) 155.
[56] Q. Chen, D.J. Frankel & N.V. Richardson, *Langmuir,* **17** (2001) 8276.

Chapter 4

Influence of modification conditions on (S)-aspartic acid-modified Ni{111} and the interaction of MAA in liquid-solid interface conditions

4.1 INTRODUCTION

To date, there are two types of study on the Ni catalysed enantioselective hydrogenation of MAA, with an abundance of studies carried out on the characterisation of real catalysts [1,2] as well as on model catalysts under UHV conditions using nickel single crystals [3 – 6]. The issue with real catalyst studies is that it is very difficult to pin down the active site since the number and type of sites vary. Under low pressure control, modifier coverage can be accurately monitored, and secondary influences can be removed. Whilst this strictly controlled environment is undoubtedly attractive, the correlation between results obtained under these conditions to features found in catalytic work is uncertain. Hence, this chapter takes the "middle-ground" approach: using a well-defined single crystal surface but under more realistic conditions, in order to enhance the relevance of model studies in Chapter 3.

4.1.1. CATALYTIC IMPORTANCE

From the first modified Ni catalyst produced by Izumi and co-workers using an aqueous solution of monosodium glutamate in 1963 [7], as discussed in Section 1.6.2.2., extended catalytic studies have been carried out on various amino acids which have shown in experiments to be potential modifiers in the Ni catalysed hydrogenation reaction of β-ketoesters (Table 1.1) [1]. This chapter focuses on the use of aspartic acid as a chiral modifier. At room temperature and atmospheric pressure, aspartic acid is a white solid which, together with glutamic acid, is

classified as one of the two naturally occurring acidic amino acids. Aspartic acid differs from glutamic acid by having only one fewer methylene units in the side chain but is less effective as a chiral modifier, and exhibits rather different correlations between catalytic behaviour and modification conditions. The effect of varying the modification temperature and pH on the catalytic behaviour of the *(S)*-aspartic acid-modified Ni system is clearly shown in Figures 4.1a and b respectively [8]. Up to modification temperatures of 348 K, although there is a decrease in enantioselectivity, there is no evidence of an enantiomeric switch as a function of temperature, as previously exhibited by *(S)*-glutamic acid-modified Ni catalysts [7]. When *(S)*-aspartic acid was used as a modifier, *(R)*-MHB was produced in excess, with a sharp maximum in enantioselectivity following modification at pH 5.0 (Figure 4.1b).

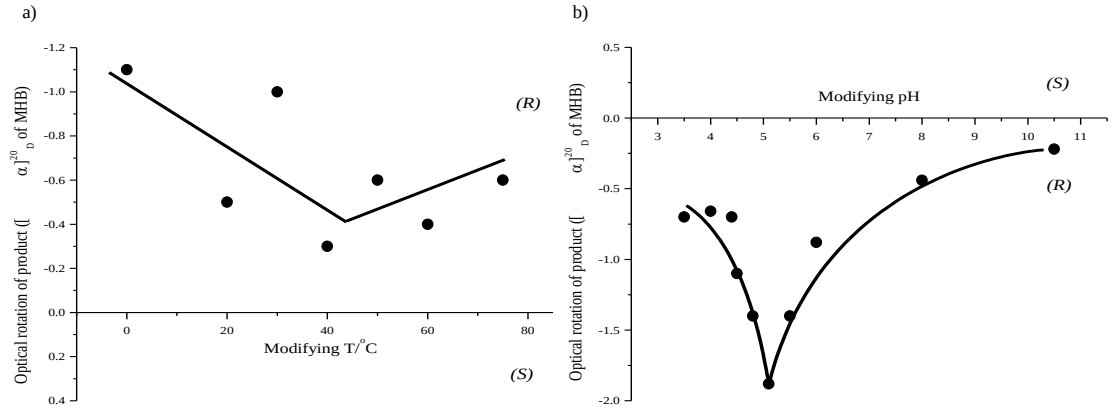

Fig. 4.1 Effect of varying a) the modification temperature, and b) the modification pH, on enantioselectivity of Raney Ni using *(S)*-aspartic acid as a modifier. From [8].

4.1.2. LIQUID-SOLID INTERFACE SURFACE SCIENCE STUDIES

Liquid-solid interface studies of functional modifiers on catalysts provide a new and more relevant strategy for examining the consequences of changing modification parameters. These types of studies allow conclusions to be made that incorporate modifier-substrate interactions as well as the influence of solvent effects, chemical forms induced by pH, and environmental factors.

In solution, aspartic acid has an isoelectric point of 2.77 and pK_a values of 2.1, 3.9 and 9.8, corresponding to the removal of protons from the carboxylic acid functionality of the amino acid, the aliphatic carboxylic acid and the NH_3^+ group respectively [9]. Four molecular ion aspartate species can exist, depending on pH values. Figure 3.2 shows the predominant *(S)*-aspartic acid species at varying pH: from cationic through to dianionic.

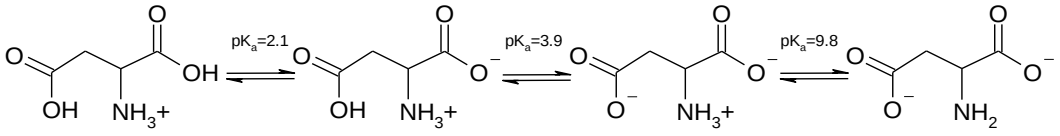

Fig. 4.2 Speciation of *(S)*-aspartic acid. From [9].

The out-of-vacuum approach has led to techniques such as RAIRS being used to great success to identify chemical species on a surface at a given pH and temperature [10-12]. This has allowed direct comparison with catalytic studies and, in turn, shown the dependence of the modification on such parameters, as well as determine the tautomeric form of MAA in existence when enantiomeric excess tends either towards the *(R)*- or *(S)*- product.

4.1.3. AIM OF RESEARCH

The crucial objective of the current research is to use liquid-solid interface approaches to ascertain: 1) the chemical form of aspartate species present at a range of modifying pH values, 2) the influence of a post modification water wash on the nature of the modified surface, 3) the interaction of MAA with *(S)*-Asp at different modifying pH, and 4) the influence of modification temperature on the system. The routine procedure for the Ni-catalysed MAA hydrogenation involves treating the prepared Ni catalyst in an aqueous solution of chiral modifier, and then filtering and washing the modified catalyst in water to remove any excess modifier from the surface of the nickel nanoparticles to leave submonolayer quantities of the adsorbate on the surface, before introduction of the MAA reagent.

In this chapter, two surface science techniques are used to investigate each step in the catalytic process. RAIRS was used to investigate the conformation of *(S)*-Asp on Ni at the different stages, as well as the co-adsorption of MAA, whilst XPS was used to assess the aspartate adlayers in a qualitative and quantitative manner. Both techniques, used in a manner to allow a close comparison to catalytic studies at each stage of the catalytic cycle, afford a much greater understanding of the mechanism of the Ni-catalysed β-ketoester hydrogenation.

4.2 EXPERIMENTAL

4.2.1 LIQUID-SOLID INTERFACE EXPERIMENTAL CONDITIONS

RAIRS experiments were recorded with a liquid-N_2-cooled mercury-cadmium-telluride detector set up in an external box, interfaced with a Digilab FTS7000 FTIR spectrometer. A mechanically polished Ni{111} single crystal was prepared by annealing at 1273 K for 8 hours in a tube furnace under a 5% H_2/Ar stream and cooling in the same atmosphere to room temperature before exposure to any solutions. PM-RAIRS was used to check the presence of surface molecular contaminants. The sample was immersed in a 10 mM *(S)*-Asp (Fluka Biochemika 97%) aqueous solution, diluted to concentration using Millipore water (18.2 MΩ), for 900 s under constant agitation. The pH was altered accordingly by addition of 1 M NaOH or concentrated HCl, while the temperature of the modification was controlled by use of a hot plate. The experimental pH values selected for this study were chosen to be lower or higher than each of the pK_a values in order to control the chemical form of the dominant species in solution (see Figure 4.2). For RAIRS experiments carried out in the absence of the *(S)*-Asp modifier, the pH of the aqueous solution was adjusted by the addition of concentrated HCl or 1 M NaOH. After modification, a RAIR spectrum (256 scans, 4 cm^{-1} resolution) was recorded and ratioed against a background spectrum of the unmodified surface. Additionally, the rovibrational bands associated with small changes in gas-phase water levels in the beam path were subtracted from the spectra. The modified surface was subsequently rinsed for several seconds in a water flow and another RAIR spectrum was taken. The sample was then immersed at 300 K for 900 s under constant agitation in a 1:1

mixture of MAA (Fluka ≥99%) in THF and a further RAIR spectrum obtained. All the measurements reported were recorded at room temperature.

For XPS experiments, A VG Sigma Probe spectrometer using Al Kα radiation (an angle between surface normal and analyser direction of 53°) with a 400 μm diameter spot (100 W) was used for the analysis, with a base pressure of 1×10^{-10} mbar. The concentric hemispherical energy analyser (CHA) with 80 eV pass energy (for full scan; 20 eV pass energy for component scans) was used, and a step size of 0.5 eV was used for the survey scan whilst 0.1 eV was used for individual component scans, each with a dwell time of 40 ms. To correct the shifts in binding energies of core levels due to the charging effect caused by the insulating properties of amino acids, the graphitic C 1s peak at 284.5 eV has been used as an internal reference. The cleaned Ni polycrystalline foil substrates were treated as for the RAIRS experiments in aqueous solutions of *(S)*-aspartic acid as a function of pH. A clean Ni foil sample was used as a control experiment. Prior to loading into UHV chamber, the samples were dried under a light $N_{2\,(g)}$ flow.

4.3 RESULTS AND DISCUSSION

4.3.1 LIQUID-SOLID INTERFACE RAIRS

4.3.1.1 ADSORPTION OF (S)-ASPARTIC ACID ON Ni{111} AS A FUNCTION OF MODIFICATION pH AT 300 K

Characteristic vibrations associated with the COOH groups of fully protonated aspartic acid are those of ν (C=O) distal and α-carboxylic acid groups, ν(C-O) and δ(O-H) at ~1740, 1400 and 1270 cm^{-1} respectively [9]. The protonated amino group NH_3^+ has characteristic symmetric and antisymmetric deformation bands at ~1520 cm^{-1} and 1660 cm^{-1} respectively. At higher pH values, deprotonation of the carboxylic acid proton generates a carboxylate group, which has a characteristic IR vibration of $\nu_{as}(COO^-)$ at ~1630 cm^{-1}, and the NH_2 group has an asymmetric stretch at ~1560 cm^{-1} (Figure 4.3).

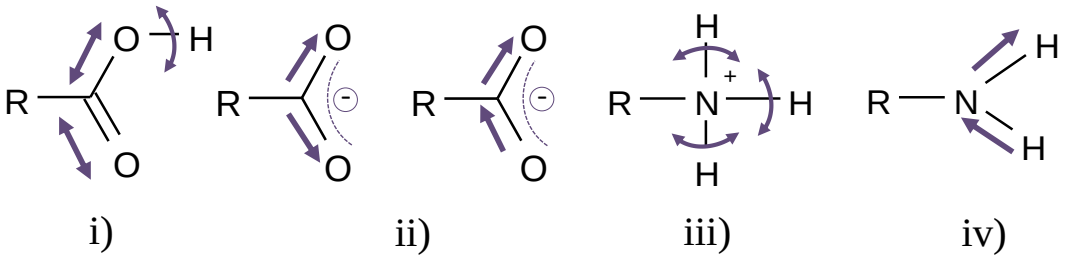

Fig. 4.3 IR vibrations for i) COOH group stretches, ii) symmetric and asymmetric COO^- stretches, iii) NH_3^+ deformations and iv) antisymmetric NH_2 stretch.

The adsorption of *(S)*-Glu as a function of modification pH and temperature has previously been investigated by Baddeley and co-workers [11]. It was found that the protonation of *(S)*-Glu on Ni{111} decreased with increasing pH, mimicking the behaviour in solution. Adsorption at 300 K at low pH showed evidence for the presence of the cationic glutamate species, which deprotonated with increasing pH ultimately to the dianionic species. Similarly, in the case of *(S)*-lysine on a Cu surface, the adsorbate retained the same chemical form as the molecules in solution [13].

Figure 4.4 shows the RAIRS spectra of the *(S)*-Asp modified Ni{111} single crystal modified at 300 K as a function of solution pH. Roddick-Lanzilotta and McQuillan reported *in-situ* IR studies of 100 mM aqueous *(S)*-aspartic acid solutions on a bare ZnSe prism as a function of pH, and assignments in this study will be supported from this work as well as others [9,14 –16]. Assignments of bands are shown in Table 4.1.

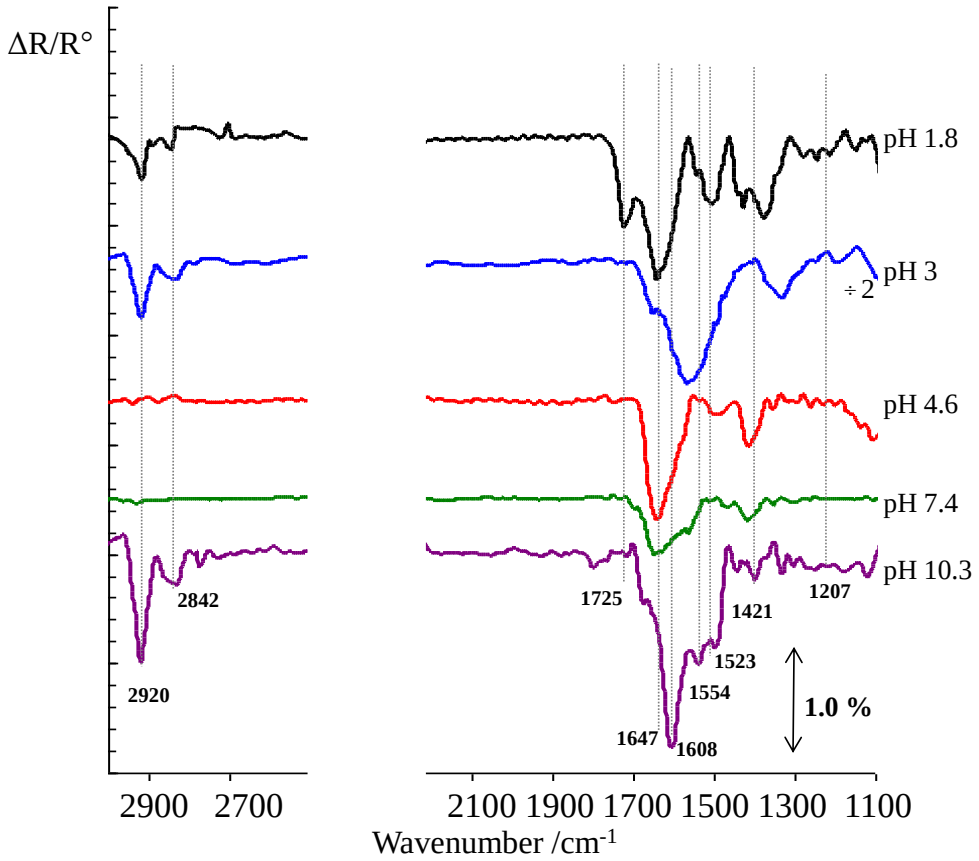

Fig. 4.4 RAIR spectra following adsorption of 10 mM *(S)*-aspartic acid on Ni{111} at 300 K as a function of pH.

Following modification at pH 1.8, peaks at 2926 and 2851 cm^{-1} represent $\nu(CH_2)_{as}$ and $\nu(CH_2)_s$ respectively, and are present at all pH values. Each band is well resolved, with the most intense band appearing at 1647 cm^{-1}. The peak at 1725 cm^{-1} is assigned as the symmetric stretch $\nu_s(C=O)$ of the α- and γ-carboxylic acid groups, whilst the peaks at 1644 cm^{-1} and 1523 cm^{-1} are designated as asymmetric and symmetric δ (NH_3^+) respectively. The band at 1384 cm^{-1} is the CH_2 wag. Finally, the band at 1242 cm^{-1} represents ν(C-O)+δ(O-H) of the carboxylic acid groups, supporting the assignment of aspartic acid in its cationic form.

Following modification at pH 3, the band at 1570 cm^{-1} appears, corresponding to $\nu_{as}(COO^-)$ of the α-carboxylate group. The asymmetric NH_3^+ deformation at 1654 cm^{-1} is weak, and the symmetric deformation at 1523 cm^{-1} is no longer present due to its weakness in intensity compared to the strong absorption of COO^-. Bands

corresponding to the coupled C-O stretch and O-H bend are still present, and so indicate that the *(S)*-Asp adsorbate is in its zwitterionic state.

The RAIR spectra following modification at pH 4.6 and 7.4 exhibit similar bands to those at pH 3, with the exception of the addition of bands at ~1508 cm^{-1} ($\nu_{as}(COO^-)$ γ-carboxylate) and ~1421 cm^{-1} ($\nu_s(COO^-)$ of both carboxylate groups), suggesting that the aspartic acid is in its anionic form.

Finally, following modification at pH 10.3, the defined peaks within the broad absorption band centred at 1608 cm^{-1} can be assigned as follows. The peak at 1608 cm^{-1} is likely to represent the $\nu_{as}(COO^-)$ α-carboxylate group as well as $\delta(NH_2)$, whereas the peaks at 1554 cm^{-1} and 1412 cm^{-1} are assigned, as at pH 4.6 and 7.4, as $\nu_{as}(COO^-)$ and $\nu_s(COO^-)$ respectively. The presence of the $\delta(NH_2)$ band teamed with only very weak NH_3^+ deformation bands suggests that *(S)*-aspartic acid is in its dianionic form.

Ni{111}/*(S)*-Asp 300 K /wavenumbers in cm^{-1}					Assignment
pH 1.8	pH 3	pH 4.6	pH 7.4	pH 10.3	
2926	2920	2953	2950	2922	$\nu_{as}(CH_2)$
2851	2842	2839	2843	2852	$\nu_s(CH_2)$
1725	-	-	-	-	$\nu_s(C=O)$
1644	1654	1647	1656	-	$\delta_{as}(NH_3^+)$
-	1570	1587	1581	1608	$\nu_{as}(COO^-)$ α-carboxylate
-	-	1508	1479	1554	$\nu_{as}(COO^-)$ γ-carboxylate
1523	-	-	-	-	$\delta_s(NH_3^+)$
-	-	1421	1425	1412	$\nu_s(COO^-)$ α and γ-carboxylate groups
1384	1338	-	-	-	CH_2 wag
1242	1207	-	-	-	ν (C-O) + δ(O-H)

Table 4.1 Assignments of RAIRS bands of *(S)*-aspartic acid on Ni{111} at 300 K adsorption temperature as a function of pH.

4.3.1.2 WATER WASH OF (S)-ASPARTIC ACID-MODIFIED Ni{111} AS A FUNCTION OF MODIFICATION pH AT 300 K

Figure 4.5 illustrates the RAIR spectra obtained after washing the *(S)*-Asp modified Ni sample prepared at 300 K. Examining the intensity of the peaks, the effect on the nature of the *(S)*-Asp modified Ni{111} after washing the modified surface is very dependent on the pH of the modifier. Across the pH range there is a decrease in band intensity of at least a factor of three. The relative abundance of the aspartate species decreases in particular at the intermediate pH values, and appears undetectable to the RAIRS technique i.e. only a very small fraction of monolayer coverage of adsorbate present, if at all.

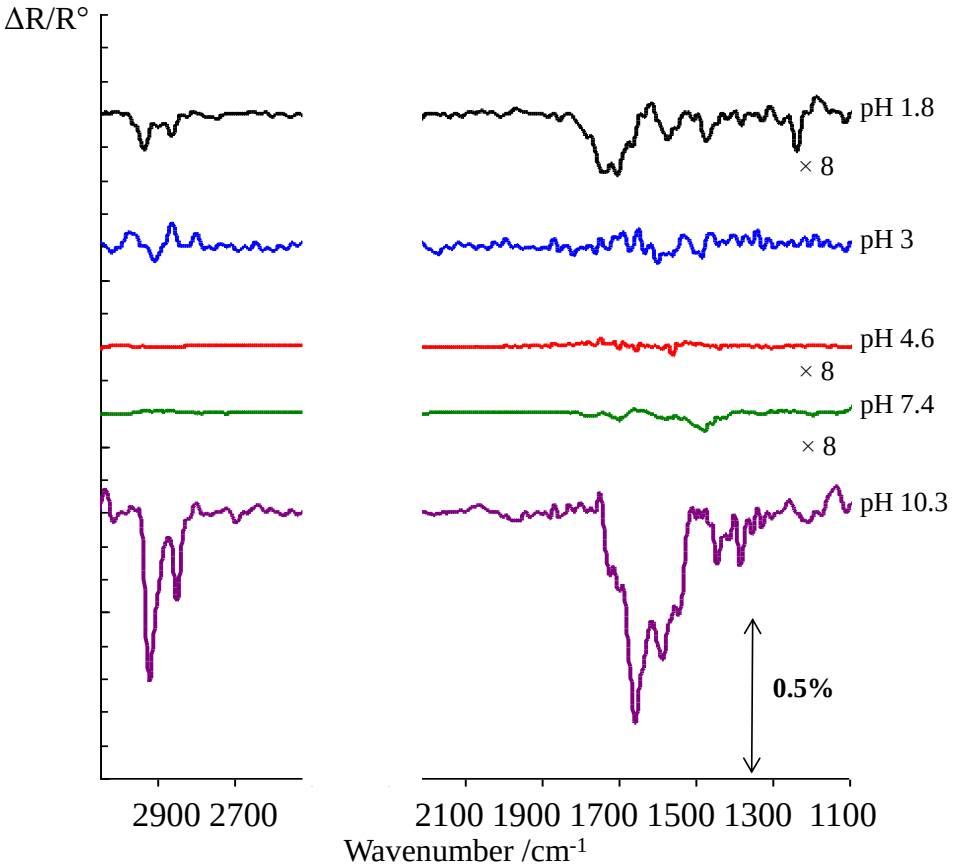

Fig. 4.5 RAIR spectra following a water wash of *(S)*-Asp modified Ni{111} at 300 K.

Interestingly, the intermediate pH range is the region in which the catalytic studies have shown the *(S)*-Asp modifier to be most enantioselective (Figure 4.1b). In the catalytic preparation, washing is expected to remove excess aspartic acid weakly

physisorbed to the surface, in order to leave submonolayer quantities behind on the surface. The wash is also likely to result in the leaching of nickel aspartate into the aqueous solution. It has previously been shown by Keane and Webb that leached Ni from a surface can itself be extracted and used as the effective hydrogenation catalyst [17]. If it is assumed that the present reaction is heterogeneously catalysed, as the original catalytic work indicates, two plausible explanations for this behaviour can be proposed based exclusively on the RAIRS evidence. It is important to note that *(S)*-Asp modified Ni catalysts give a relatively moderate enantiomeric excess when used in the hydrogenation of MAA to *(R)*-MHB (8.2% [1]), and so possible mechanisms take this into account, being based on the premise that enantioselectivity may not be widespread on the catalyst surface.

Firstly, if the Ni surface is vital in the catalytic steps, leaching of the Ni atoms from the surface by the chiral aspartate molecules is likely to leave behind a chiral surface arrangement of metal atoms. A high density of these chiral step-kink defects could themselves act as highly enantioselective catalytic sites for the reaction. Adsorbate-induced faceting is a well-established phenomenon following the adsorption of carboxylic acids at high molecular coverages in the submonolayer regime [18-21]. Previous STM work was carried out by Zhao and co-workers who demonstrated that the adsorption of *(S)*-lysine led to the formation of chiral Cu facets on a Cu{001} surface, indicating that the lysine adsorbate itself caused the surface Cu atoms to adopt an intrinsically chiral arrangement [22]. Gellman and co-workers pioneered studies on high Miller index step-kink surfaces which can exist in non-superimposable mirror forms [23]. They subsequently demonstrated that the interaction of the two enantiomers of propylene oxide with the two mirror equivalent surfaces was measurably different [24]. In addition, Attard and co-workers demonstrated that two enantiomers of glucose undergo very different electro-oxidation behaviour at a chiral Pt surface [25], whilst Sholl and co-workers have carried out several theoretical studies of hydrocarbons on chiral pure Pt surfaces and found differences in binding energies of chiral kink sites [26]. Chiral step-kink sites have also been shown, in work by Attard and co-workers, to contribute to the

enantioselectivity of Pt catalysts for ethyl pyruvate hydrogenation. The use of Bi to preferentially block step sites over Pt terrace {111} sites showed an increase in rate but decrease in enantiomeric excess which illustrated that sites at, or near to, steps were more enantioselective than sites on terraces [27]. It is clear that, in principle, surfaces with chiral arrangements of metal atoms could operate as enantioselective catalysts. It is also plausible that, as no aspartate molecules are detectable by RAIRS succeeding the water wash in the present case, the redistribution of the metal atoms due to the modification could preserve their chirality with very little or no aspartate coverage remaining.

An alternative explanation is to consider the influence the modifier has on the enantioface adsorption of MAA: it is possible it may spread further than just a nearest neighbour interaction. A typical Ni catalyst surface, on which one type of catalytically active site is "bare Ni", which will catalyse the reaction racemically, and the other type of site is, or has been, under the influence of chiral modifiers and has the potential to catalyse enantioselectively, allowing the MAA to interact directly with the modifier molecules via only one enantiotopic face. If chiral amplification is in play, a small but finite amount of modifier at the enantioselective sites, perhaps the step-kinks, could produce docking interactions which may favour one prochiral molecular geometry, and this interaction could be amplified to influence the geometry of molecules further out into the terrace regions and promote the chiral reaction. This has previously been suggested by Gellman and co-workers who studied the enantiospecific desorption of propylene oxide from chiral Cu{643} surfaces and showed that enantiospecificity was detected from terrace sites as well as from kinked steps [28]. Similar such effects have also been suggested by the Ernst group following co-adsorption of (chiral) tartaric acid and (achiral) succinic acid on Cu{110} [29,30].

RAIRS is not an accurate technique to use in a quantitative manner thus, from this work, it is impossible to differentiate between the two possible origins of the

enantioselectivity of the system. In Section 4.2.3.3.2. XPS is used to generate absolute values of aspartate molecules remaining on the surface after water washing to allow a more precise evaluation of how the catalyst behaves.

4.3.2.2 MAA ADSORPTION ON (S)-ASPARTIC ACID-MODIFIED Ni{111} AS A FUNCTION OF MODIFICATION pH AT 300 K

Figure 4.6 displays the RAIR spectra obtained after adsorbing the prochiral reagent MAA onto the modified and washed Ni{111} substrate. For processing, due to the complicity of the MAA RAIR spectra, each single beam spectrum of the MAA exposed surface is ratioed against the single beam spectrum of the modified and washed surface. This allows easier identification of the bands associated solely with MAA.

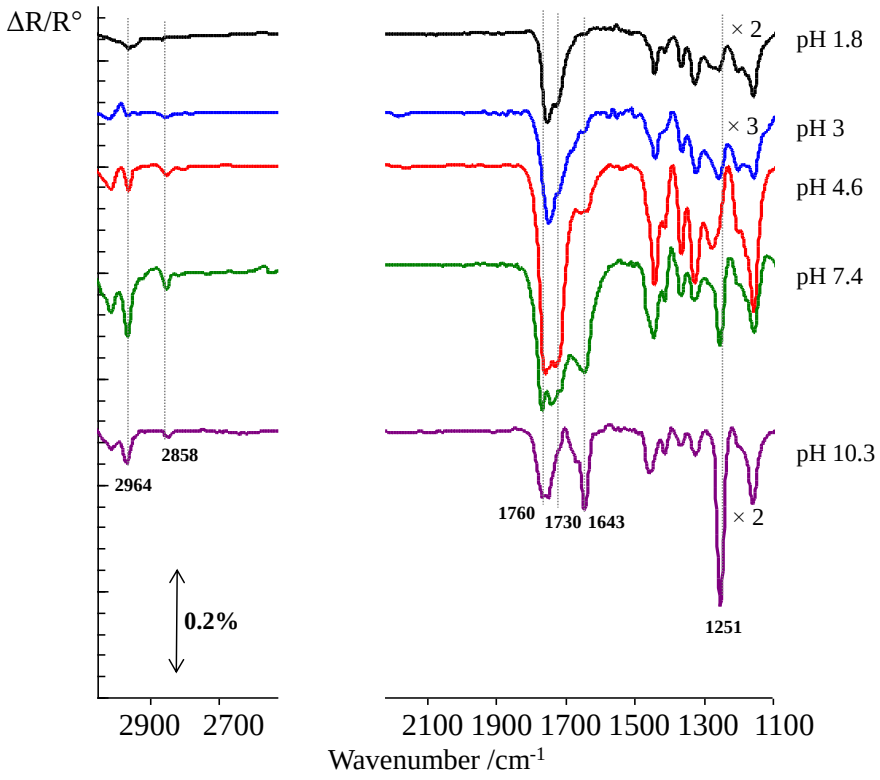

Fig. 4.6 RAIR spectra following immersion of *(S)*-aspartic acid modified and washed Ni{111} at 300 K in an MAA:THF solution at 300 K as a function of pH (MAA spectra ratioed against the spectra recorded following the washing of the modified catalyst surface).

MAA adsorption is identified by a series of negative bands. Peaks at 2964 and 2858 cm^{-1} are present, which represent various CH_2 stretches. The two dominant bands which represent the enol form at 1643 cm^{-1} (ν(C=O) + ν(C=C)) and 1251 cm^{-1} (ν(C-OH)). A strong peak at 1760 cm^{-1} (with a shoulder at 1730 cm^{-1}) is identified, which can be assigned to the diketo tautomer of MAA as the characteristic RAIR spectrum exhibits a strong negative absorption band at this wavenumber, representing $\nu(C=O)_{keto}$. At low pH, the diketo tautomer form of MAA is dominant, with no evidence corresponding to the enol form. As the pH increases, the enol contribution grows, culminating in a majority enol species present at pH 10.3. Assignments are shown in Table 4.2.

MAA + *(S)*-Asp/Ni{111} 300 K /wavenumbers in cm^{-1}	**Assignment**
2964	ν_{as} (CH_3)
2858	ν_s (CH_3)
1760, 1730	ν $(C=O)_{keto}$
1643	ν $(C=C)_{enol}$ + ν $(C=O)_{enol}$
1251	ν $(C-OH)_{enol}$

Table 4.2 Assignments of IR peaks observed in the adsorption of MAA on *(S)*-aspartic acid modified Ni{111}.

The adsorption form of MAA on the modified and washed surface appears to be influenced by the pH of the modifier. Figure 1.10 shows the MAA molecule existing in its two tautomeric forms. MAA is a β-carbonyl and has substituents from two different groups – the CH_3 group which is an electron donor and so stabilises the enol form, and the electron withdrawing group OCH_3 which favours the diketo form. In the gas phase MAA is found to exist in a tautomeric mixture [31]. When bonded to a chirally modified surface, the tautomeric form of MAA is found to be very sensitive to the nature of the surface [11, 12]. To understand the results in the present study, it is necessary to consider the form of the modifier and its bonding to MAA. At low pH, the protonated cationic aspartic acid species forms a hydrogen bond with the diketo form of MAA acting as a proton acceptor. At the higher pH values, the enol form of MAA is stabilised by acting as a hydrogen bond donor to the deprotonated species. A further experiment was carried out on MAA adsorption onto Ni{111} unmodified by *(S)*-Asp, the results of which are shown in Figure 4.7. The

experiment was carried out as previously, however with the aqueous solution pH altered only by the addition of HCl and 1 M NaOH to water. Peaks at 2934, 2854, 1753 and 1720 cm^{-1} appear at each pH value and do not change in intensity. These results verify that the switch from diketo to enol tautomer is solely associated with the presence of aspartate on the surface, since modification in merely water shows no dependence of the tautomeric form on the modification pH. The change of MAA form present on the surface is also much more dramatic on the washed and modified surface (Figure 4.6) compared to the unwashed surface (Figure 4.8). This suggests that the washing procedure carried out on the modified catalyst is also important and can influence the form the *β*-ketoester takes on the catalyst surface. This ultimately will have implications for the hydrogenation product formed as it was previously established for tartaric acid and glutamic acid that, under modification conditions where the catalyst operates most effectively for the production of *(R)*-MHB, the dominant form of MAA was found to be diketo in character [11,12].

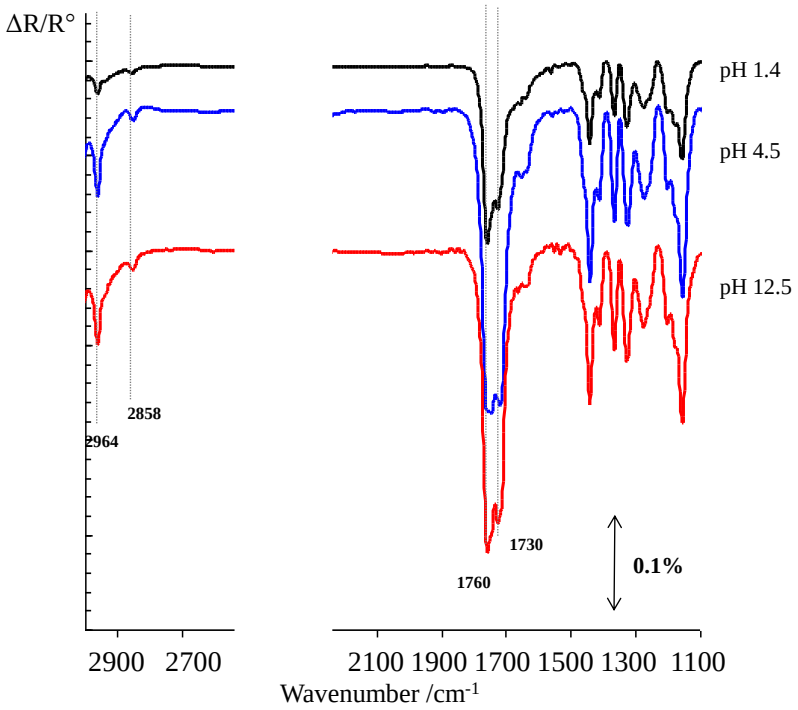

Fig. 4.7 RAIR spectra following immersion of unmodified Ni{111} at 300 K in an MAA:THF solution at 300 K as a function of pH.

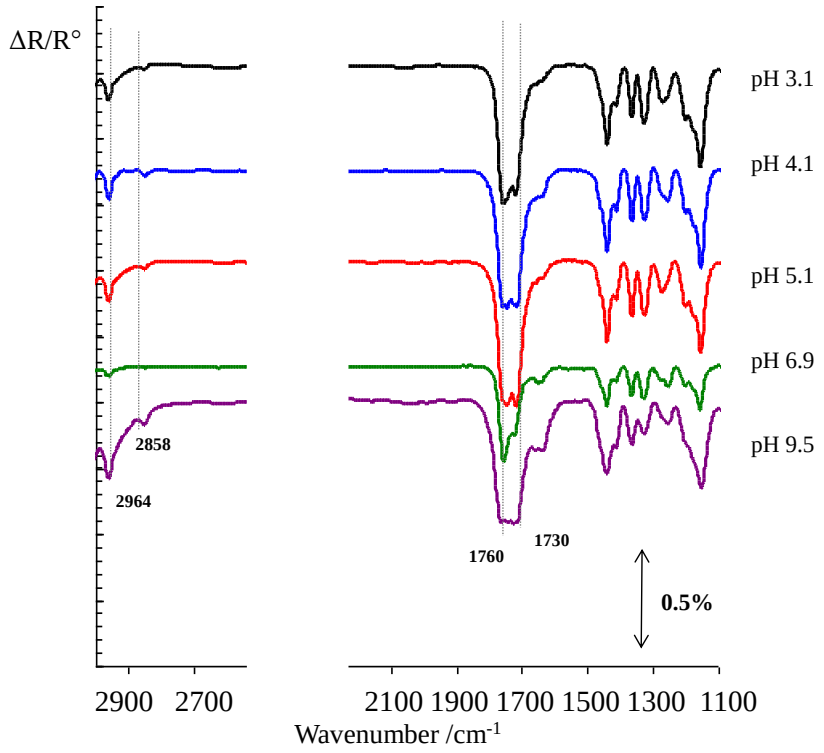

Fig. 4.8 RAIR spectra following immersion of *(S)*-Asp modified Ni{111} at 300 K with no water wash in an MAA:THF solution at 300 K as a function of pH.

4.3.1.4 ADSORPTION OF (S)-ASPARTIC ACID ON Ni{111} AS A FUNCTION OF MODIFICATION TEMPERATURE

Repeat experiments of the modification at 300 K were carried out at 350 K and at 373 K, at the optimum pH value for optimum enantioselectivity. These experiments were done in light of previous catalytic work by Izumi on various amino acids [1,7,8], as well as RAIRS studies by Jones and Baddeley on the closely related *(S)*-glutamic acid [12]. Izumi found that several amino acids showed a switch in enantioselectivity at increased modification temperature, as exhibited by *(S)*-Glu modified Ni catalyst. RAIRS work was useful in identifying the nature of the cause of the enantiomeric switch, as the study showed that the keto: enol ratio of the MAA present on the surface dropped with increasing temperatures. The diketo form was found to be the dominant tautomer interacting with *(S)*-Glu at low temperatures, whereas a switch to the enol form at temperatures above 350 K appeared to be the precursor for the *(S)*-enantiomeric product. It was suggested that, at low temperature, *(S)*-Glu behaved as a typical amino acid with an interaction between the

zwitterionic NH_3^+ functionality and the ketone group of the diketo form of MAA [12]. However, at greater temperatures, the *(S)*-Glu reacts more strongly with the NiO surface through the NH_2 group to form Ni glutamate and so is unable to bond to a diketo form of MAA, favouring the enol form (aliphatic COOH group hydrogen bonds to the ester C=O group of the MAA only).

In the case of *(S)*-Asp, this is the first known RAIRS study of its behaviour with modification temperature. From the work of Izumi and co-workers it was shown catalytically that, up to temperatures of 348 K, there was no evidence of a switch in enantioselectivity, but a decrease as temperature increased (Figure 4.1a) [8].

Figure 4.9 shows the RAIR spectra for the differences in the *(S)*-Asp modified Ni{111} surface with modification temperature change. The modification was carried out with an *(S)*-Asp solution altered to pH 5 by the addition of 1 M NaOH as this was found in catalytic studies to be the optimum pH for enantioselectivity, and the previous pH change RAIRS studies in Section 4.3.1.2. reinforces this as a potentially interesting region to study. A change in temperature from 300 K to 373 K results in a new peak emerging at 1736 cm^{-1} (assigned as a ν_s(C=O) symmetric stretch), an enhancement of the broad peak at 1421 cm^{-1} ($\nu_s(COO^-)$ of the γ- and α-carboxylate groups), and the continued appearance of the 1645 cm^{-1} peak ($\delta_{as}(NH_3^+)$). Briefly, the RAIRS spectra taken on the modified samples show a change in peak intensities from 300 K through to 373 K. At 300 K the most prominent peak is at 1645 cm^{-1} which has previously been assigned as a mixture of $\delta(NH_2)$ and $\delta_{as}(NH_3^+)$ contributions. As temperature increases the peaks become more asymmetric with a shoulder appearing at 1546 cm^{-1}, corresponding to $\delta(NH_2)$ coupled with ν(C=O) [14], or $\nu(COO^-Na^+)$ [32]. The presence of NH_2 is likely to be caused by the coordination of the lone electron pair on the NH_2 functionality to the Ni^{2+} ions (due to the NiO on the surface of the single crystal), or the formation of nickel aspartate complexes. This coordination has previously been observed for the Ni(II) aspartate salt by FTIR

and DFT work carried out by Cabral *et al.* [14]. Alternatively, found previously by Peica *et al.* [32] in IR studies of monosodium glutamate, a weak peak in the 1600 – 1555 cm^{-1} region may also be assigned to $\nu(COO^-Na^+)$. In the current study, the more asymmetric shape of the peaks at 1600 cm^{-1} could suggest the presence of a COO^-Na^+ stretch. This may suggest the greater presence of the sodium aspartate salt (formed due to NaOH added to alter pH value), with NH_2 binding to the Ni^{2+} surface.

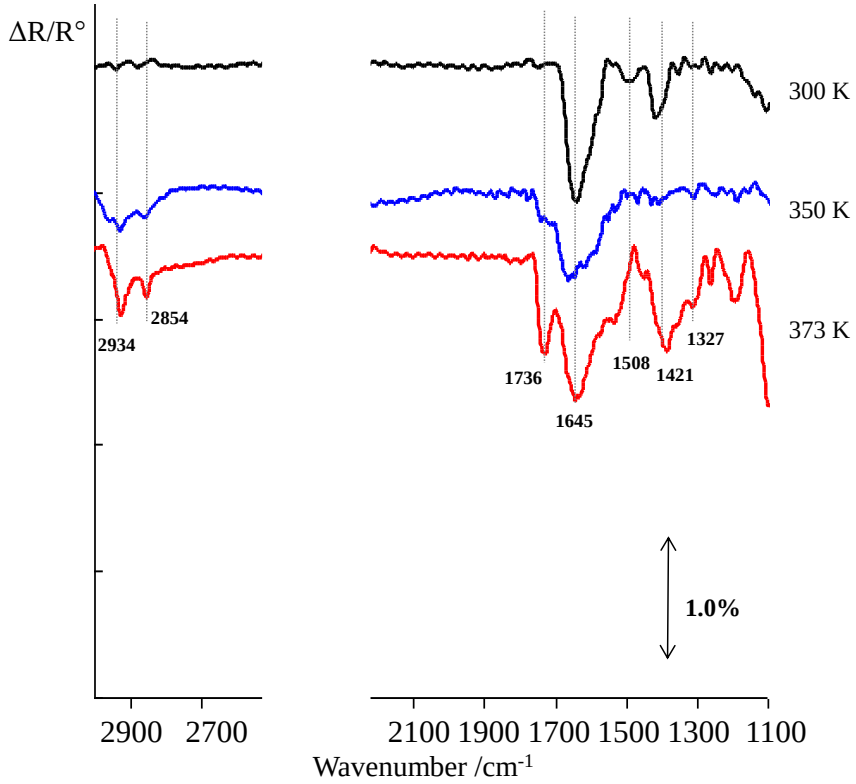

Fig. 4.9 RAIR spectra following *(S)*-Asp modified Ni{111} at pH 5 as a function of modification temperature.

After the post-modification water wash (Figure 4.10), a similar trend of a decrease of the peak intensities as observed at 300 K is noted, with the intermediate pH value close to that of the catalytic optimum showing very little detectable by RAIRS. The peak intensities drop by at least a factor of fifteen, reinforcing the idea that very low or no coverage of aspartic acid remains on the surface at elevated temperatures.

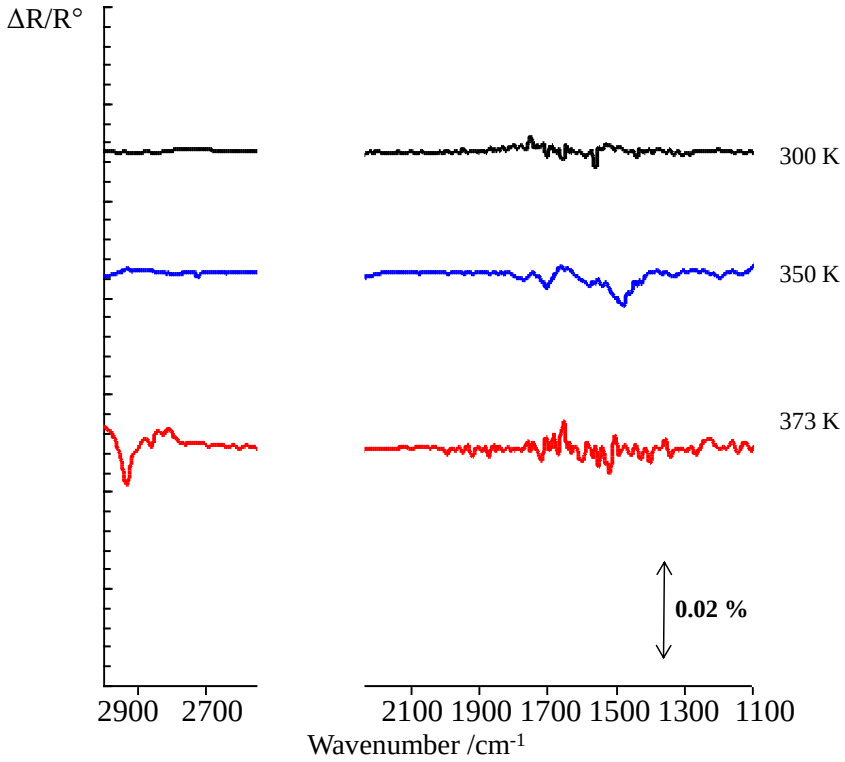

Fig. 4.10 RAIR spectra following post modification water wash of *(S)*-Asp modified Ni{111} at pH 5 as a function of modification temperature.

Figure 4.11 shows the RAIR spectra after MAA adsorption onto the modified Ni{111} surface as a function of modification temperature at pH 5. At lower modification temperatures, peaks at 2960, 2854, 1760 and 1730 cm^{-1} are dominant, as well as a number of peaks in the 1500 -1250 cm^{-1} region. At 373 K, a change in the spectrum occurs, with new peaks emerging at 1643 and 1251 cm^{-1}. The diketo form appears prominent at the lower temperatures, until the more intense 1645 and 1251 cm^{-1} peaks at 373 K suggest the presence of the enol tautomer.

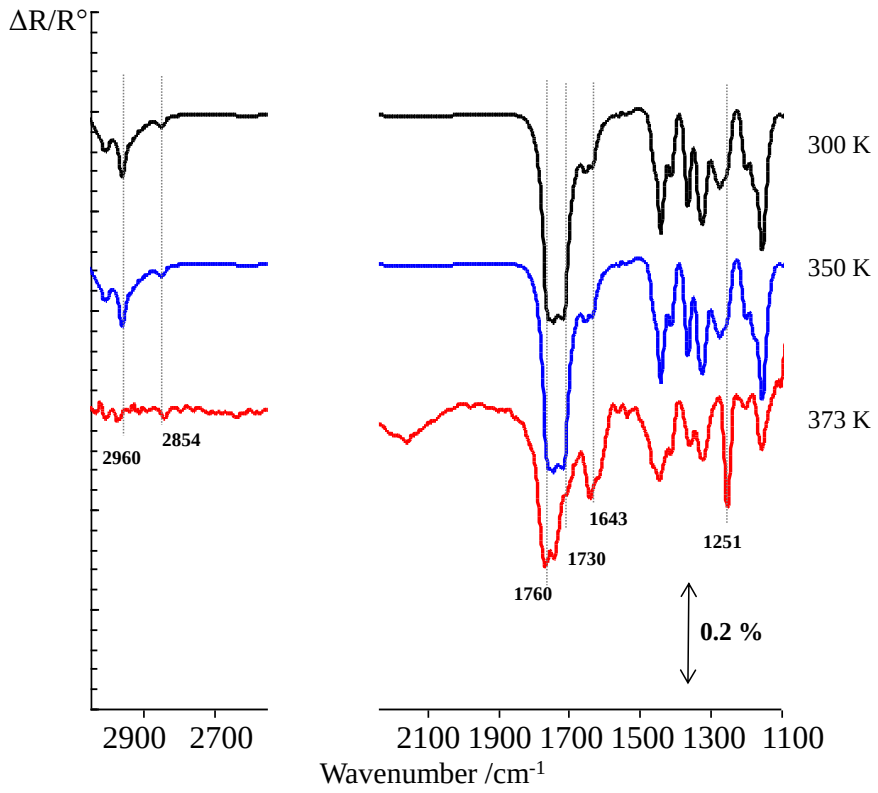

Fig. 4.11 RAIR spectra of Ni{111} modified with *(S)*-Asp at pH 5 in a 1:1 MAA:THF solution at 300 K, as a function of modification temperature.

At modification temperatures of 373 K, there is a clear indication that MAA adsorbs in its enol form. As this would be assumed to produce the *(S)*-MHB enantiomer (as noted in previous findings [10]), the control of the tautomeric form of MAA on the Ni{111} surface appears to be directly related to the optimisation of enantioselectivity of the catalytic reaction. The clear enantiomeric switch of the MHB product has previously been explained by the enol form of MAA being the precursor to *(S)*-MHB (dominating at high modification temperatures), and the diketo form being the precursor to *(R)*-MHB (dominating at the lower temperatures). The hydrogenation study of *(S)*-aspartic acid modified Ni{111} by Izumi *et al.* [8] at various modification pH and temperature values did not show an enantioselectivity switch (see Figure 4.1a); however the experiments were only carried out in the 273 – 348 K range. Our results, executed at higher modification temperatures, enables us to predict that *(S)*-Asp modified Ni{111} might be expected to exhibit a similar switch in enantioselectivity with increasing modification temperatures, as observed for the Ni/glutamate system [1,11].

4.3.2 LIQUID-SOLID INTERFACE XPS

4.3.2.1 CLEAN Ni POLYCRYSTALLINE FOIL XPS ANALYSIS

The full XP spectrum of the clean Ni foil is shown in Figure 4.12. Ni $2p_{3/2}$ and Ni $2p_{1/2}$ at 853 eV and 872 eV respectively, as well as the Ni LMM Auger peak at 641 eV, and Ni 3s and Ni 3p at 112 eV and 66 eV are present on the surface. A large O 1s peak at 532 eV is also present, with the O 2s at 24 eV. A small Na KLL Auger peak is present at 499 eV. The N 1s peak is apparent at 399 eV, and two small peaks at 199 eV and 99 eV are assigned as the Cl 2p and Si 2p signals respectively.

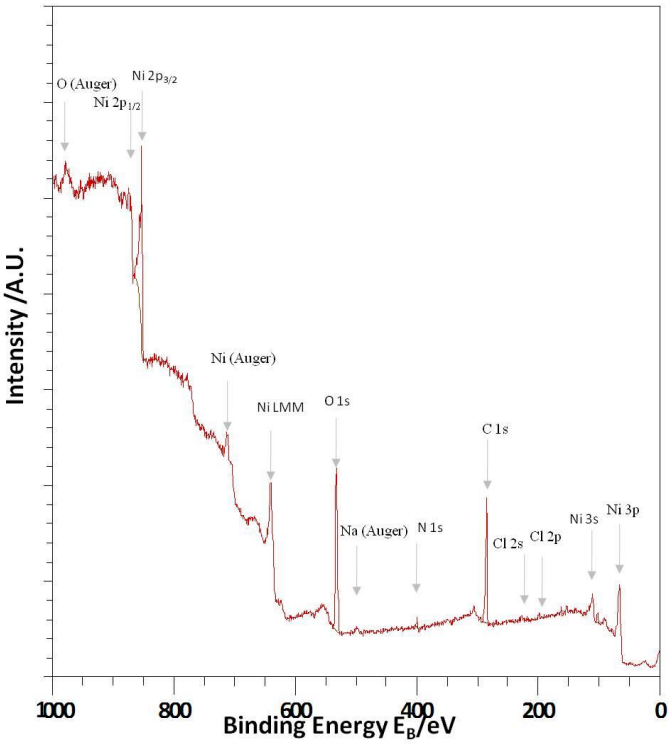

Fig. 4.12 Survey scan of Ni polycrystalline foil after cleaning procedure.

Individual component scans for Ni $2p_{3/2}$, O 1s, N 1s and C 1s of the clean Ni are shown in Figure 4.13. The compositions were calculated by fitting theoretical Gaussian-Lorentzian peaks using the iterative Shirley technique. The Ni $2p_{3/2}$ XP spectrum shows deconvoluted peaks at 852.4 eV (Ni^0), 853.9 eV (NiO), 854.9 eV and 855.9 eV ($Ni(OH)_2$), 856.9 eV and 858.1 eV (not assigned but characteristic of the native oxide [33]). The O 1s XP spectrum shows a spectral fit of four peaks at 529.2 eV (NiO), 530.9 eV ($Ni(OH)_2$), 532.3 eV (H_2O) and 533.7 eV. The N 1s

spectrum shows one peak at 399.6 eV (surface N), and the C 1s XP spectrum contains five deconvoluted peaks at 284.5 eV (graphitic carbon), 286 eV (C-OH), 287.4 eV (C=O or COO^-), 288.3 eV (C=O or COO^-) and 289.2 eV (COOR) [34]. The positions of the peaks verify typical XP spectra for a Ni surface which is covered in an oxide layer. The shape of the Ni 2p envelope, as well as the presence of a substantial O 1s peak, reveals the presence of the native oxide on the Ni foil [33]. Since the sample was exposed to air whilst transferring from the furnace to the UHV apparatus, there are large quantities of adsorbed carbon and oxygen present on the surface. Small quantities of Cl and N can be attributed to airborne contaminants from the transfer process, and Na can be attributed to the lubricants used in the rolling process of the foil [31]. It is noted that no special effort is made to exclude air before and during the modification of the Ni foil, as is the case for the real Ni catalysts used industrially. Also, the XPS data for *(S)*-aspartic acid at modification pH 11.8 was recorded on a separate occasion and so intensity values for a second piece of "clean" Ni foil are used where appropriate.

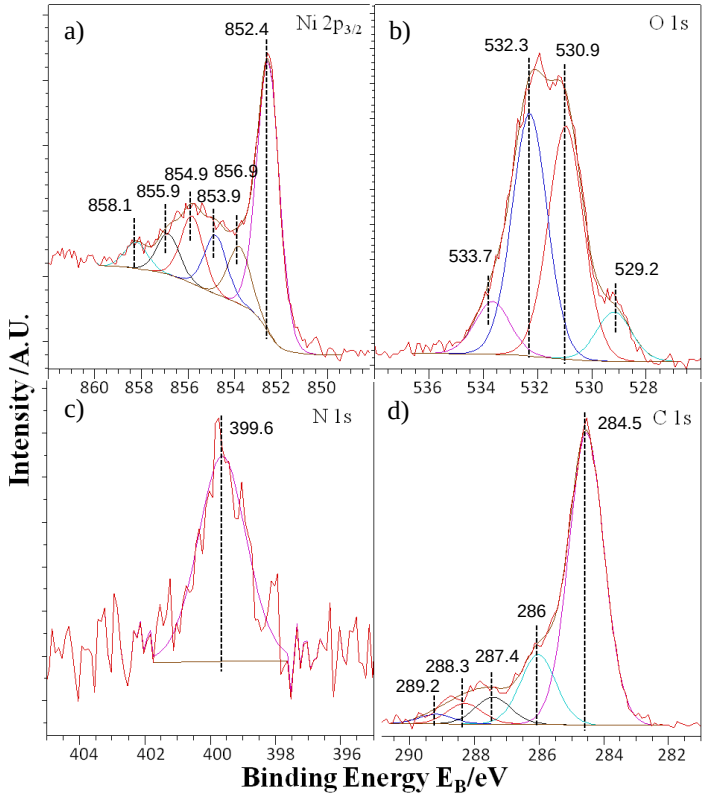

Fig. 4.13 Component scans of Ni polycrystalline foil treated in $H_2SO_{4\,(aq)}$ and annealed in 5% H_2/Ar: a) Ni $2p_{3/2}$, b) O 1s, c) N 1s and d) C 1s.

4.3.2.2 ADSORPTION OF (S)-ASPARTIC ACID ON Ni{111} AS A FUNCTION OF MODIFICATION pH AT 300 K

To investigate the coverage and chemical nature of the modifier layers on the Ni foil at different pH ranges, samples were modified with *(S)*-Asp at pH values of 2.4, 5.3 and 11.8 and individual scans were separately recorded of the Ni 2p, O 1s, N 1s and C 1s regions.

4.3.2.2.1 NICKEL 2p XP SPECTRA: ESTIMATION OF THE SURFACE COVERAGE OF ASPARTATE ON Ni FOIL

The following Figure 4.14 shows the individual XP scans for the Ni 2p region offset to show the "clean" Ni foil, modified Ni foil, washed Ni foil and foil after MAA adsorption clearly for each pH value. Overall, the component scans show significant perturbations which occur with changes to the environment of the Ni foil.

The attenuation of the Ni^0 peak at 852.4 eV due to adsorption of aspartic acid is important in calculating the thicknesses of the *(S)*-Asp overlayer in the modified samples, and the thicknesses of organic film remaining after the water wash, assuming that the overlayer has a uniform thickness [35]. In these two instances, any attenuation of the Ni^0 peak intensity from the original Ni^0 peak intensity of the clean sample is attributed entirely to the presence of *(S)*-aspartic acid. For the case of MAA adsorbed onto the modified and washed Ni surfaces, the Ni 2p signal is additionally attenuated by the MAA adsorbate and so any overlayer calculations will give a value representing a mixture of aspartate and MAA, and therefore is not as useful quantitatively.

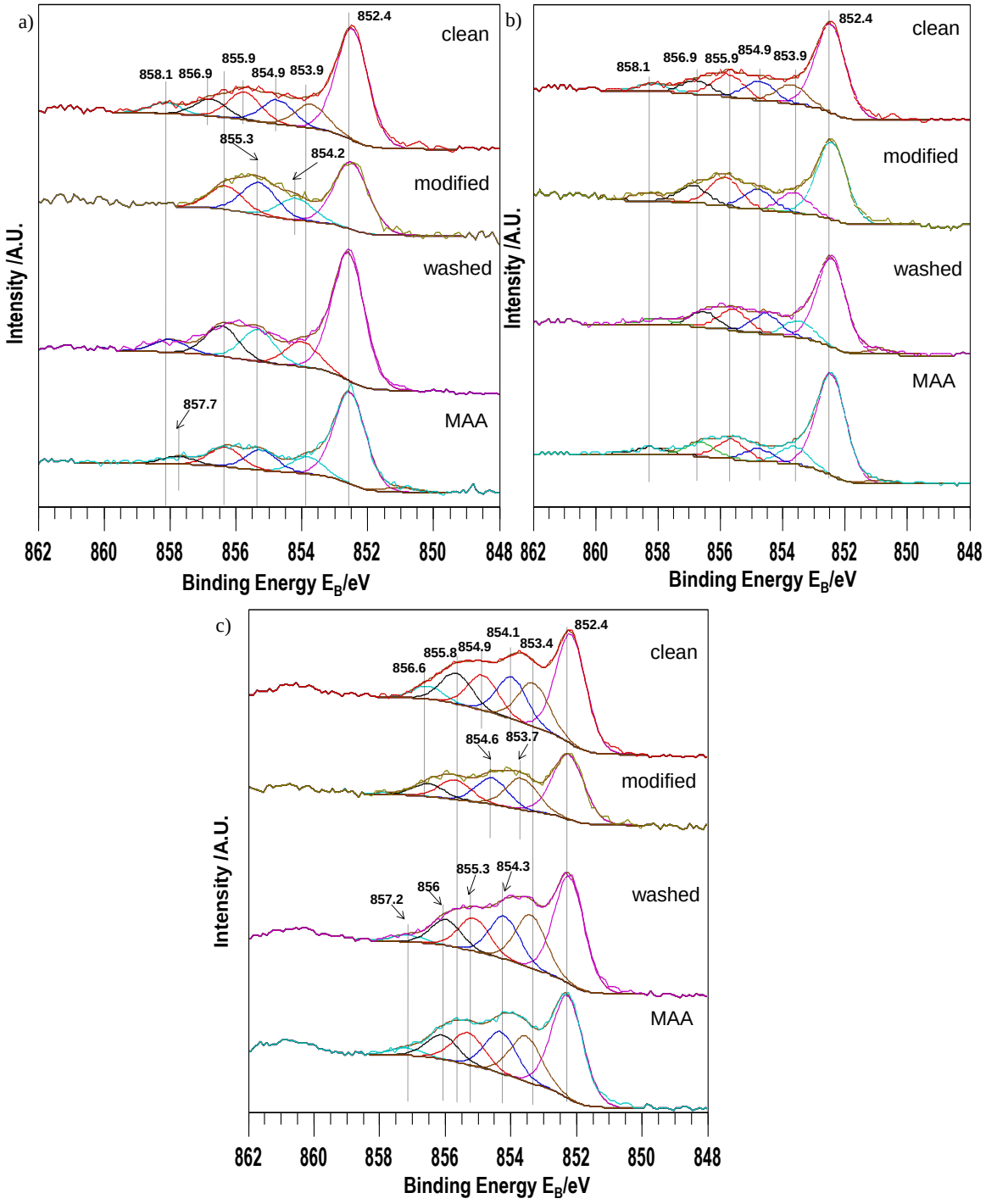

Fig. 4.14 Ni 2p XP region, for modification of Ni with *(S)*-Asp at a) pH 2.4, b) 5.3 and c) 11.8. Herein, in each figure, the spectra should be read, from top, as clean polycrystalline Ni foil, modified Ni foil, post modification water wash and interaction of MAA with modified Ni. Spectra are shown with reference to "clean" Ni foil treated in $H_2SO_{4\,(aq)}$ and annealed in 5% H_2/Ar as previously. Spectra are offset for clarity.

Table 4.3 shows the calculated thicknesses of the aspartic acid layer for each pH value using Equation 4.1 [36], where θ is the angle of collection at the XPS analyser with respect to the sample normal, and *I* is the area of the observed substrate (*I)* and clean substrate (*I_0)* Ni 2p peaks. In order to elucidate coverages, starting with preliminary calculations developed by Tanuma, Powell and Penn [37], the inelastic mean free path (λ) of Ni $2p_{3/2}$ photoelectrons through an organic film of density of 1.66 gcm^3 (the density of *(S)*-aspartic acid) is calculated as 2.01 nm, and the depths and volumes of the overlayer are calculated, assuming a 1 cm^2 area for each Ni foil.

$$d = -\lambda \cos\theta (\ln \frac{I}{I_0}) \qquad \textbf{Equation 4.1}$$

The main source of error in the calculations will originate from the assumption that Equation 4.1 is accurate for the system (i.e. that the aspartate thin film is of uniform thickness).

	pH 2.4	Water wash	MAA	pH 5.3	Water wash	MAA	pH 11.0	Water wash	MAA
d /nm	1.44	0.44	0.87	0.93	0.18	0.19	1.56	0.22	0.31
V /10^{-8} cm^3	14	4.4	8.7	9.3	1.8	1.9	16	2.2	3.1

Table 4.3 Overlayer thicknesses (d) and volumes (V) for *(S)*-aspartic acid modified Ni foil.

4.3.2.2.2 OXYGEN 1s XP SPECTRA

Figure 4.15 shows the O 1s XP spectra at the different pH values. Although positions and intensities appear similar, there are small increases and decreases which can be linked to the different environments of the surface following modification. It can be broadly observed that the NiO (529.5 eV [33]) and $Ni(OH)_2$ (531.2 ± 0.3 eV [38,]) peaks are strongly attenuated by the addition of *(S)*-aspartic acid to the Ni surface at all pH values, therefore suggesting an influence on the chemistry of the surface due to the overlayer. After washing with water, the intensity of the O 1s peaks return to a value closer to that of the clean foil, suggesting a removal of a percentage of the aspartate overlayer. It can be noted that the second clean Ni foil which was used in the pH 11 experiments appears to have a different O

1s envelope, with a greater intensity of the NiO peak at 529.5 eV. This is most probably due to slight nuances in the cleaning procedure, as well as likely changes in the atmosphere and environment as the experiments are carried out *ex-situ* and on different days.

The component at 532.5 ± 0.5 eV is assigned as either the C=O or C-OH groups (531 eV and 533.5 eV respectively from the XPS work of Kozlowski & Sherwood on carbon-fibre surfaces [40]), or may also refer to H_2O (532.6 eV [41]) which is certain to be present on the surface due to the aqueous chemistry involved in the preparation of the modified samples. Unfortunately it is not possible to distinguish the relative amount of each O 1s environment in the single deconvoluted peak, and thus it is assumed that the peak represents both surface water and the presence of the aspartate molecules. The higher binding energy component at 533.5 ± 0.2 eV is likely to represent the COO^- groups of aspartate. As the pH value is increased, the COOH groups are deprotonated to carboxylate groups and thus the intensities of the peaks at 532.5 ± 0.5 eV (representing C=O and C-OH) decrease, whilst the peak at ~533.5 eV increases. In general, the broadness and complexity of the O 1s peak indicates a strong interaction between the C=O and C-OH groups with the Ni surface [39], as well as the presence of the two different oxygen atoms in the carboxylic acid unit (as opposed to the presence of a more identical environment for the oxygens i.e. within two carboxylate COO^- groups) [42].

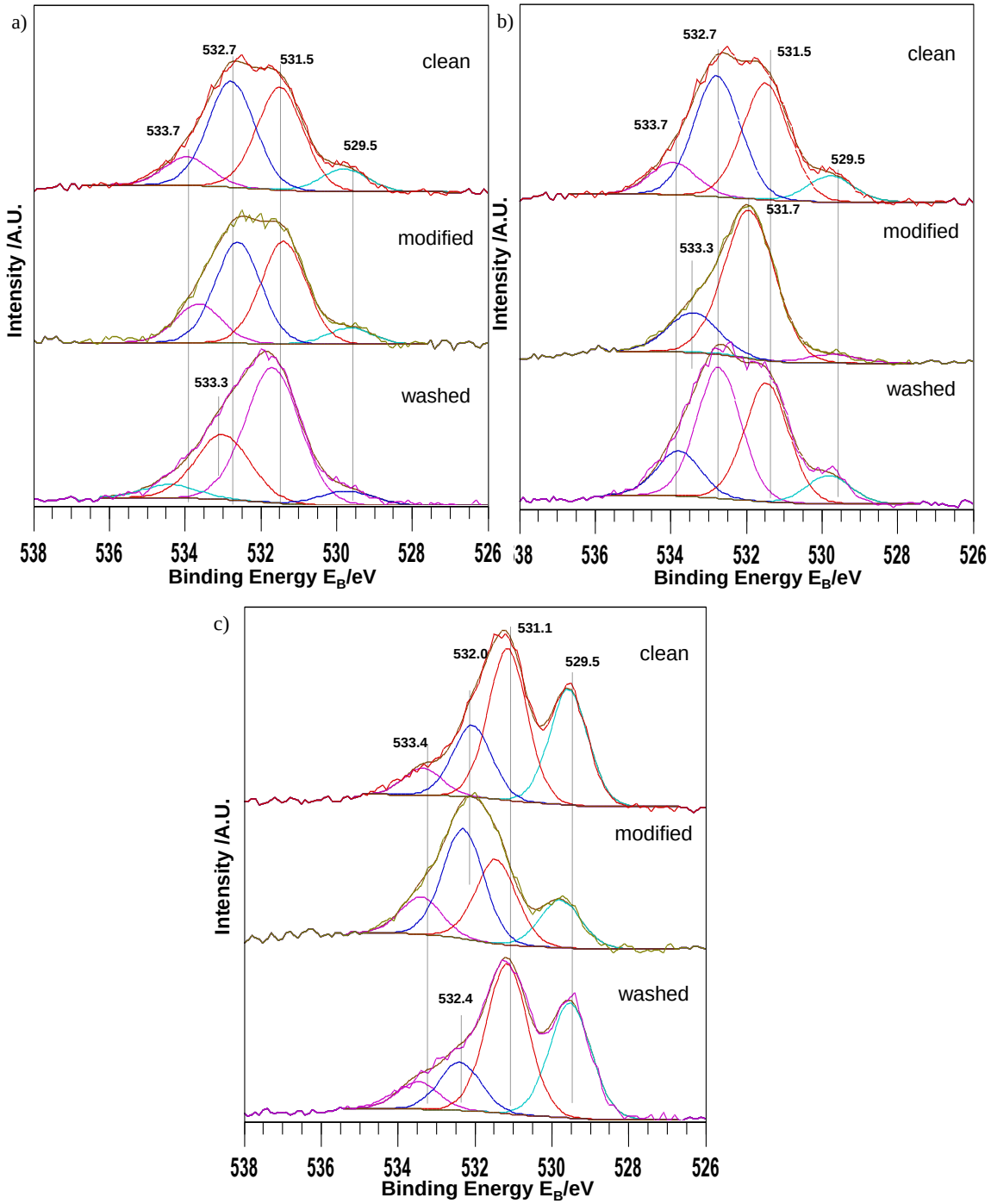

Fig. 4.15 O 1s XP region, for modification of Ni with *(S)*-Asp at a) pH 2.4, b) 5.3 and c) 11.8. Spectra are shown with reference to "clean" Ni foil treated in $H_2SO_{4\,(aq)}$ and annealed in 5% H_2/Ar as previously. Spectra are offset for clarity.

4.3.2.2.3 NITROGEN 1s XP SPECTRA: QUANTITATIVE CALCULATIONS OF *(S)*-ASPARTIC ACID COVERAGE ON Ni FOIL

Figure 4.16 shows the N 1s XP spectra accrued in the experiment at varying pH values. The peak at 399.6 eV, which is present in the unmodified Ni foil, is assigned to a nitrogen-based impurity, possibly from traces of ammonia in the atmosphere, which is characteristic of the foils being prepared outwith the UHV chamber [33]. Despite the acid treatment and hydrogen pre-treatment to reduce the amount of oxide formed on the Ni surface, the fact that the transportation of the foils and the modification are carried out under ambient conditions leads to a nitrogen-based impurity being present on all foils. Although spectra were collected, the N 1s XP spectra for the adsorption of MAA onto the modified and washed surfaces are not shown as any fluctuations in the N 1s signal no longer gives information exclusively on the aspartate surface coverage, but rather may also be attenuated by the co-adsorption of MAA.

Figure 4.16a shows the N 1s XP spectra after modification at pH 2.4. The 399.6 eV peak becomes sharper and more intense after modification by *(S)*-Asp which suggests that this peak corresponds to the coordination of the aspartic acid to the Ni surface [39]. This is lower in value by 1.3 eV than the binding energy of aspartic acid in its zwitterionic form (400.9 eV) and much closer to that of a nickel amine complex (approximately 399.4 ± 0.1eV [43]) and so confirms that the amino acid is coordinated to the Ni surface through the amino group [39]. Indeed, previous IR studies found that, on chelate formation, bands due to the NH_2 group appear instead of the NH_3^+ [44]. After the water wash, the peak at 399.6 eV shifts to a lower binding energy of 398.8 eV, suggesting a more nitride-like species [39].

Following modification at pH 5.3 (Figure 4.16b), as well as the intense 399.6 eV peak indicating the NH_2 group bound to the Ni surface, a sizeable contribution is observed at 401.1 eV. This peak has previously been assigned to the presence of a protonated amine group, or surface oxidised N [43]. The 399.4 eV peak indicates, as

previously, the NH_2 group bound to the Ni surface. After the water wash, the N 1s spectrum is similar in peak position and overall intensity to the clean Ni foil. Finally, following modification at pH 11.8 (Figure 4.16c) a peak is observed at 399.4 eV corresponding to the $–NH_2$ group of aspartic acid [43], as well as a peak at 401.3 eV. After the water wash, the N 1s spectrum shows a decrease in intensity with the overall N 1s spectrum resembling that of the modified surface.

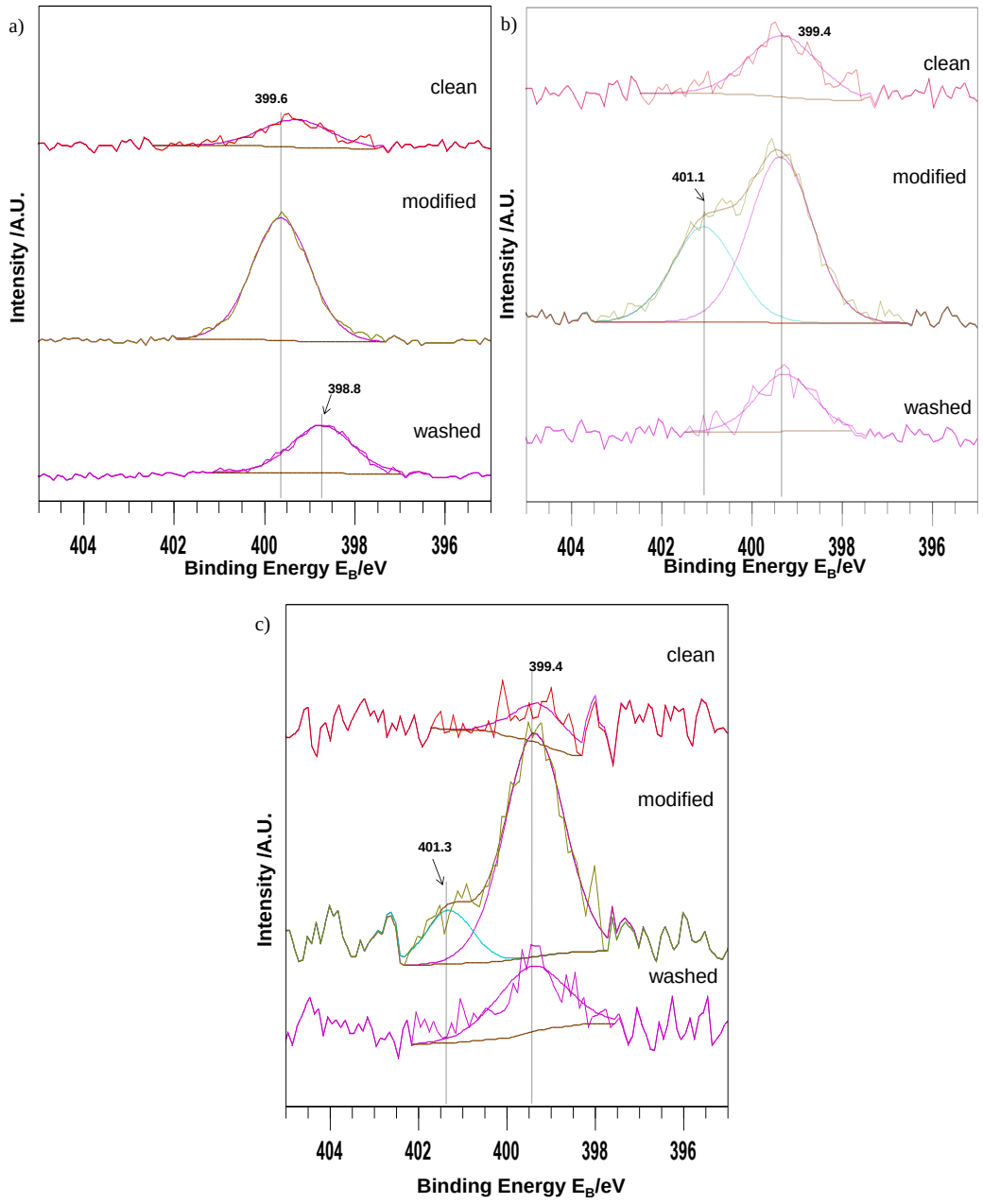

Fig. 4.16 N 1s XP region, for modification of Ni with *(S)*-Asp at a) pH 2.4, b) 5.3 and c) 11.8. Spectra are shown with reference to "clean" Ni foil treated in $H_2SO_{4\,(aq)}$ and annealed in 5% H_2/Ar as previously. Spectra are offset for clarity.

Whilst the analysis of the N 1s peak in a qualitative manner is useful in that it allows assignment of different nitrogen-containing species, further calculations can be carried out to quantitatively measure the concentration of aspartate on the surface. From the volume of the overlayer of *(S)*-aspartic acid calculated from the Ni 2p attenuation (Table 4.3), the surface coverage of nitrogen, and thus aspartic acid, on the foil can be worked out. This quantitative procedure can be carried out due to the relative simplicity of the N 1s signal, and the fact that the N 1s signal at 399.6 eV on the unmodified surface can be assigned to a nitrogen-containing impurity present on all the foils before modification, the origin of which has been discussed previously. It is possible to subtract this background impurity level from the N 1s signal to allow a reliable estimation of the number of N atoms on both the modified and washed surfaces, which can then be related to the number of aspartate species present (due to one N atom being present in every aspartate molecule). Table 4.4 shows the number of N atoms (and thus the number of aspartic acid molecules) on Ni foil with area dimensions 1 cm^2 and the aspartate film thicknesses as calculated in Table 4.3. Taking into account the density of Ni atoms in the most thermodynamically favourable {111} plane is 1.86×10^{15} atoms cm^{-2}, the surface coverage of each species in monolayers (ML) is shown in the final row of Table 4.4. Due to the pH 11.8 experiments being carried out on a separate occasion, N 1s intensity values for a second "clean" Ni foil are used in necessary calculations and noted in Table 4.4. It is estimated that the errors in the coverage measurement are approximately ±10% of the absolute coverage.

	Ni foil (for pH 2.4 & 5.3)	pH 2.4	Water wash	pH 5.3	Water wash	Ni foil (for pH 11.8)	pH 11.8	Water wash
d /nm	-	1.44	0.44	0.93	0.18	-	1.56	0.22
V / $\times 10^{-8}$ cm^3	-	14	4.4	9.3	1.8	-	16	2.2
$I_{N\ 1s}$	1727	10380	6316	8074	1770	332	2766	951
N /$\times 10^{15}$ atoms	0.132	1.1	0.33	0.7	0.135	0.05	1.2	0.15
N coverage / ML	0.07	0.59	0.18	0.38	0.07	0.02	0.65	0.08

Table 4.4 Absolute number of N atoms for Ni foil surfaces modified by aspartic acid at different pH values and after post-modification wash.

Monitoring the ML coverage of aspartic acid after the modification at each pH value, it is found that the level of N-based impurity on the Ni foil before modification (0.07

ML) is of the same magnitude of nitrogen present on the post modification wash sample at pH 5.3, whereas identical water washes following modification with aspartic acid at higher and lower pH values show residual modifier on the surface. This verifies in absolute terms that, at intermediate pH values of *(S)*-Asp (such as pH 5.3 as used in the XPS experiments), a water wash is effective in removing all measurable traces of aspartic acid from the Ni surface.

After subtraction of the N-based impurity coverage from the modified surface and water-washed surface ML values, coverage of aspartate is shown to range from 0.3 – 0.6 ML, with 0.3 ML present under conditions of maximum enantioselectivity at pH 5.3. After the post-modification water wash, the residual modifier coverage ranges from 0 – 0.1 ML, again with the lowest levels measured under conditions of maximum enantioselectivity. This is shown in graphical form in Figure 4.17.

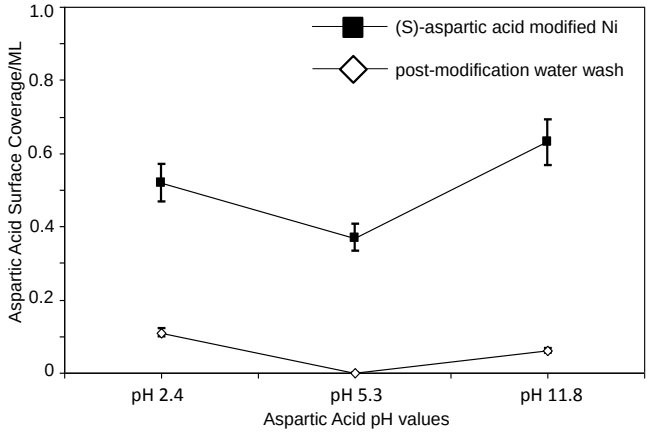

Fig. 4.17 Aspartic acid coverage versus pH values before and after post-modification water washing.

4.3.2.2.4 CARBON 1s XP SPECTRA

The C 1s spectra are shown in Figure 4.18, with the majority of the carbon-containing species assigned to the peak at 284.5 eV, representing carbonaceous contamination [34]. From the remaining carbon surface peaks, much can be deduced about the chemical environment of the aspartate overlayer, as shifts of the C 1s levels are predominantly influenced by nearest neighbour atoms. As the C-OH and C=O peaks change in intensity between the unmodified, modified and washed surfaces,

the peak can be used to judge the amount of modifier remaining on the surface after the water wash relative to the clean surface (Table 4.5). In the first instance, the C 1s XP spectrum of the unmodified Ni foil matches that observed on the native nickel oxide [33]. The peak at 285.8 eV represents C-OH or C-OR environments, whilst the peaks at 287.7 eV and 287.3 eV correspond to COOH or COOR. The highest binding energy peak at 288.8 eV is assigned to a CO_3 species.

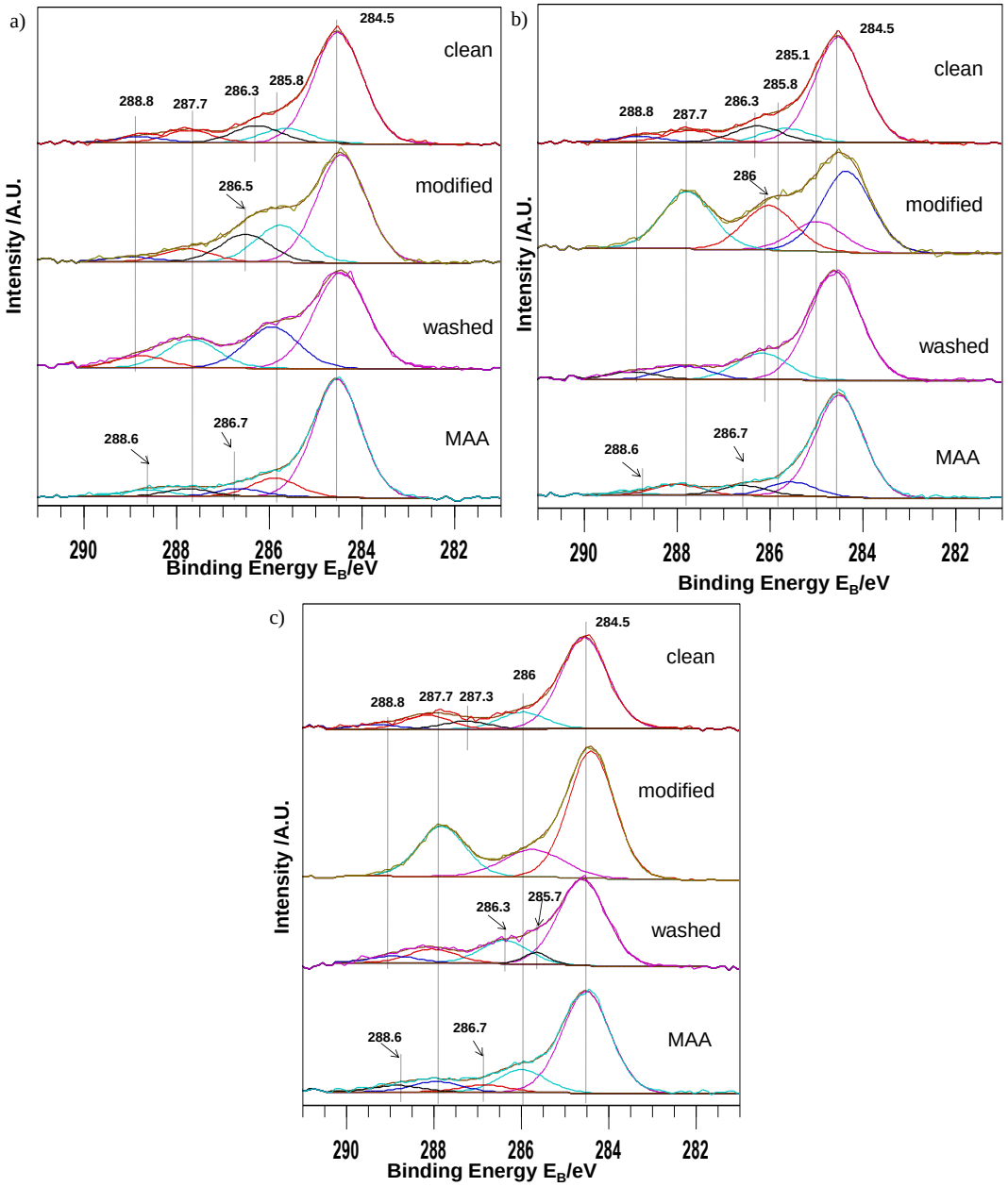

Fig. 4.18 C 1s XP region, for modification of Ni with *(S)*-Asp at a) pH 2.4, b) 5.3 and c) 11.8. Spectra are shown with reference to "clean" Ni foil treated in $H_2SO_{4\,(aq)}$ and annealed in 5% H_2/Ar as previously. Spectra are offset for clarity.

In the C 1s XP spectrum in Figure 4.18a (Ni modified with *(S)*-Asp at pH 2.4), the modifier XP spectrum shows an increase in the intensities of the peaks at 285.8 eV and 287.7 eV which are assigned to C-OH and C=O groups respectively [45]. After a post modification wash, the same peaks appear at similar intensities to the modified surface. If, as hypothesised, the two signals are from the aspartic acid modifier, they suggest that the amino acid is in its zwitterionic form at pH 2.4.

In the C 1s XP spectra in Figure 4.18b at modification pH 5.3, there are several noticeable changes which confirm that the aspartic acid adsorbs in the anionic form. The peak at 285.8 eV is present only at levels comparable to the unmodified Ni surface, and so it is suggested that no hydroxyl groups within the aspartic acid molecules are present on the surface. An increase of the peak intensity at 287.7 eV for the modified surface indicates a carbon in a C=O functionality present in aspartic acid. Both of these observations, alongside the N 1s results, confirm that aspartic acid is in its anionic form at this pH value. After the water rinse, there is considerable removal of the aspartate modifier, with the C 1s XP spectrum appearing very similar to that of clean Ni (with similar proportions of carbon present (see Table 4.5)).

In Figure 4.18c, with modification of Ni by *(S)*-Asp occurring at pH 11.8, the carbon atoms are in the same environment as at pH 5.3, with the only structural change being the deprotonation of the NH_3^+ group. This is apparent in the XP spectra for the modified surface, which shows no large increase in the C-OH C 1s peak (suggesting that there is no carboxylic acid group present), and an increase in the peak intensity for the C=O group. There is a substantial decrease in the intensity after the water wash, suggesting only small, but measurable, amounts of aspartate remaining on the surface.

	Ni foil	pH 2.4	Water wash	MAA	pH 5.3	Water wash	MAA	Ni foil	pH 11.8	Water wash	MAA
I_{C-OH}	2630	3263	4082	1646	2403	2744	1528	1494	1771	1554	2247
I_{O-CH3}	-	-	-	420	-	-	699	-	-	-	1249
$I_{C=O}$	1017	3000	2341	-	3463	1089	-	1903	1950	1490	-
$I_{C=O\ ester}$	-	-	-	809	-	-	1350	-	-	-	1340
Ratio O-CH_3: C=O ester				**1:1.93**			**1:1.93**				**1:1.07**

Table 4.5 Intensity of C 1s signal for Ni foil surfaces modified by aspartic acid at different pH values and after post-modification wash, and MAA adsorption.

As shown in Figure 4.19, MAA may exist in its diketo form at low pH values due to its role as a proton acceptor for the protonated forms of *(S)*-Asp, and in its proton donor enol form for more basic values of modifier. A strong indication of the presence of the diketo tautomer of MAA is a C 1s peak intensity ratio of 1:2 of the 286.7 eV (O-CH_3) and 288.6 eV ($C=O_{ester}$) peaks, and similarly a 1:1 ratio of the two peaks would represent the enol form. It would be difficult to use the C 1s XP peak intensities for the C-OH group (blue circle) as a reliable estimation of the presence of the enol form of MAA as the group is present on the bare Ni surface, as well as at low pH values of aspartic acid modifier (when the protonated form of *(S)*-Asp is present). However, it can be used in a qualitative fashion by examining any increases to the signal to reinforce the quantitative analysis of the O-CH_3 and O-C=O groups shown in Table 4.5.

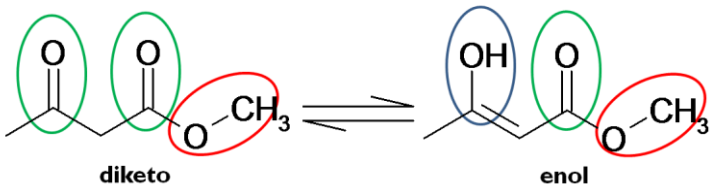

Fig. 4.19 Different carbon environments in the two tautomeric forms of MAA. Green circled C=O groups give a C 1s peak at 288.6 eV, red circled O-CH_3 groups represented by a C 1s peak of 286.7 eV, and blue circled C-OH group gives a C 1s XP peak at 285.8 eV.

From the C 1s XP spectrum in Figure 4.18a, when MAA is adsorbed onto the washed and modified surface at pH 2.4, the C-OH peak at 285.8 eV is at a lower intensity compared to the modified and unmodified surface, thus suggesting that the MAA does not contain a hydroxyl group, and therefore not in its enol form. Evidence of the MAA molecules being present in their diketo form transpires from an intensity

ratio of the O-CH_3 and C=O signals (at 286.7 and 288.6 eV respectively) of 1:2 (see Table 4.5).

With MAA adsorbed onto the *(S)*-Asp modified surface at pH 5.3 (Figure 4.18b), a similar situation to that at pH 2.4 occurs. The C-OH signal is attenuated by either the surface or the remaining modifier by the MAA adsorbate to give a low intensity, which suggests the likelihood that the enol tautomer is not present. The methoxy and ester group signals are measured in a 1:2 ratio and so confirm that the MAA molecules remain predominantly in their diketo form on the surface.

Adsorbed MAA onto the Ni surface modified with *(S)*-Asp at pH 11.8 (Figure 4.18c) gives an increase of the C-OH signal at 285.8 eV, suggesting the molecule contains this functional group. Furthermore, the ratio of the methoxy (286.7 eV) and ester group (288.6 eV) signals is now approximately 1:1 (see Table 4.5). Both of these features indicate the presence of the enol form of MAA on the substrate surface after modification and wash, consistent with RAIRS findings in Section 4.3.1.3.

4.4 IMPLICATIONS FOR ENANTIOSELECTIVE CATALYSIS AND CONCLUSIONS

RAIRS and XPS experiments in Section 4.3 have shown conclusively that the nature of the aspartic acid species as a function of modification pH follows a similar speciation pathway as observed in solution (Figure 4.2). At a low pH (above the first pK_a value of the molecule), aspartic acid adopts a zwitterionic state on the metal surface. With an increase in pH, aspartic acid becomes progressively deprotonated. The extent of protonation of aspartic acid was also shown to influence the subsequent adsorption of MAA. With increasing pH of the aspartic acid modifier, the diketo form of MAA favoured at low pH gives way to an increasing contribution of the enol form, illustrated by the appearance of RAIRS peaks as well as the change in the intensity ratios of the different C 1s XP environments of the C=O and OCH_3 groups.

This change in the majority form of MAA present on the modified surface is explained by the fact that the diketo form of MAA, with two carbonyl groups, can act as a proton acceptor by forming hydrogen bonds with the protonated aspartic acid molecules whereas, at higher pH, the enol form is preferable as it allows hydrogen bonding between itself and the deprotonated aspartic acid by acting as a hydrogen bond donor.

In terms of the different outcomes of the post-modification wash on the modified surface, it was found from RAIRS data that a dramatic effect occurred depending on the modification pH employed. Of catalytic significance is the fact that, under conditions where the catalyst operates most enantioselectively, the amount of adsorbed aspartate is found to be below the detection levels of the RAIRS technique (Section 4.3.1.2). Quantitative analysis by XPS has shown that, in absolute terms, at intermediate pH values of *(S)*-aspartic acid where enantioselectivity is known to be at its optimum, the levels of aspartate remaining on the surface after the water wash are essentially undetectable by XPS.

Furthermore, modification at pH values either side of the optimum lead to an increase in the surface concentration of aspartate, which catalytically results in a poorer enantioselective catalyst. In contrast, tartaric acid modified Ni at optimum enantioselectivity of pH 5 results in coverage of ~20% of a complete monolayer [46]. Jones and Baddeley showed by STM [47] that a similar tartrate coverage of ~20% was unable to form ordered domains on the surface when present on its own, however after MAA adsorption the MAA molecules rearranged nearby tartrate species and influenced local ordering of the *(R,R)*-TA on the surface, forming a co-crystalline phase. It was postulated that intermolecular H-bonding with several modifiers led to the stabilisation of one enantiotopic face of the MAA molecules on the modified Ni surface, therefore promoting enantioselective hydrogenation. Another modifier studied in depth, *(S)*-Glu, has proven to be a more successful modifier than aspartic acid in the hydrogenation reaction [1]. Glutamic acid has a

very similar structure to aspartic acid, having one additional methylene unit in the aliphatic chain leading from the chiral centre to the terminal carboxylic acid, and so it is interesting that a difference in enantioselectivity occurs. It is possible that the slightly greater flexibility of the larger *(S)*-Glu molecule allows a greater optimisation of the docking interaction with methylacetoacetate. Indeed, glutamic acid has recently been shown to form 2D assemblies with methylacetoacetate on Ni{111} [48].

Considering the present case, any possible mechanism requires consideration of the washing of aspartate covered Ni surfaces to pinpoint the origin of the enantioselectivity. Washing will remove excess aspartic acid and is also likely to result in the displacement of nickel aspartate into aqueous solution. The corrosion of nickel from metal particles by a chiral adsorbate is likely to result in the formation of chiral defects on the metal surface. It has been shown that the growth of chiral copper oxides by electrodeposition occurs in the presence of chiral molecules (tartrates) [49]. It is reasonable to believe that the leaching of metal from a particle would leave behind a chiral surface arrangement of metal atoms. Reaction of methylacetoacetate at these defects could occur enantioselectively and could account for the enantiomeric excess observed following modification at pH 5. The results discussed in Section 4.3.1.2. suggested two possible mechanisms which could be equally applicable from the results of the RAIRS experiment; either chiral amplification due to a small, residual amount of modifier remaining on step edges, or the chiral rearrangement of metal surface atoms due to leaching of metal by the modifier molecules. Fortunately, it is believed that the XPS results can distinguish between the two possible mechanisms in the Ni/aspartate system.

If it is rightly understood that aspartate molecules remain present at extremely low coverages after the water wash, it can be assumed they preferentially decorate the step sites of the Ni surface in a similar fashion. Typical intermolecular spacing for aspartate molecules is 0.6 nm, and if the surface is thought to be covered by parallel

steps separated by ~ 3 nm, the "unit cell" area of the low coverage aspartate molecules would be ~ 1.8 nm^2 (see Figure 4.20). This would result in a surface density of 5.6×10^{13} aspartate molecules cm^{-2}, and the coverage of Ni atoms on the {111} plane would be 1.85×10^{15} atoms cm^{-2}. Hence, the surface coverage of aspartate would be in the 0.03 ML range. This is expected to be the lower limit of coverage as it is unlikely the step density would be lower than this estimated value, either on a polycrystalline Ni foil or the facets of a Ni particle used in catalysis.

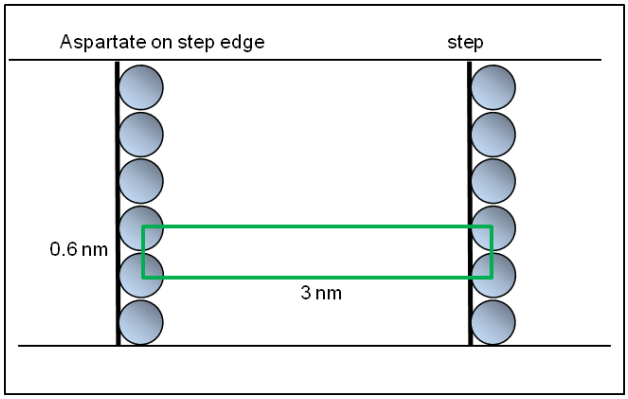

Fig. 4.20 Schematic diagram of estimated aspartate molecule unit cell on a stepped Ni{111} surface at low aspartate coverage.

From the estimation of the surface coverage from N 1s measurements in Table 4.4, it is implied that the coverage of aspartate after washing the catalyst surface prepared by modification at pH 5 is considerably lower than this value. This suggests, although some contribution due to the presence of modifiers adsorbed at step sites cannot be entirely ruled out, they are unlikely to contribute to the enantioselectivity in the Ni/aspartate system. The greater likelihood is that chiral defects produced by adsorbate-induced corrosion or by the adsorption of chiral modifiers at defect sites substantially contribute to the enantioselectivity of the Ni/aspartate system.

In terms of the possibility of chiral amplification occurring in the system it is necessary to consider the methyl acetoacetate (MAA) coverage. The MAA reactant molecule has similar dimensions to aspartic acid and tartaric acid, and the saturation coverage on the Ni surface has previously been found by Keane and Webb [46] to be in the likely range of 0.25 ML (relative to a saturated monolayer). In the present

study it can be assumed that, from the density of etched steps in terms of original aspartate coverage, 0.03 ML of MAA could decorate the step defects at any particular time. If the step defects catalysed the reaction enantioselectively while the remainder of MAA molecules on the terraces were hydrogenated racemically at the same rate, at any instant 0.22 ML of MAA would be racemically hydrogenated (0.03 ML subtracted from 0.25 ML). In numerical terms, as *(S)*-aspartic acid modified Ni gives an enantiomeric excess of *(R)*-MHB product over *(S)*-MHB, 0.03 ML of *(R)*-MHB at the enantioselective step sites can be added to 0.11 ML of *(R)*-MHB on the terraces, compared to the 0.11 ML of *(S)*-MHB formed only on the terrace, to give an e.e. value of $100 \times [0.14 - 0.11]/[0.14 + 0.11] = 12\%$ (see Equation 1.1). This is actually very similar in magnitude to the optimum enantioselectivity found by Izumi in the Ni/aspartate catalysis of MAA hydrogenation (8.2 % [1]). This suggests that the influence of the chiral defects are local in nature and not amplified out into the terraces, as otherwise a much greater enantiomeric excess would be observed. This implies that chiral amplification does not play a significant role in the Ni/aspartate system.

4.5 REFERENCES

[1] Y. Izumi, *Advanced Catalysis,* **32** (1983) 215.
[2] A. Tai & T. Harada, *Tailored Metal Catalysts,* Y. Isawawa (Ed.), D Reidel, (1986) 265.
[3] H.U. Blaser, *Tetrahedron: Asymmetry,* **2** (1991) 843
[4] C.J. Baddeley, *Topics in Catalysis,* **25** (2003) 17.
[5] A. Baiker, *Catalysis Today,* **100** (2005) 159.
[6] T. Mallat, E. Orglmeister & A. Baiker, *Chemical Review,* **107** (2007) 4863.
[7] Y. Izumi, M. Imaida, H. Fukawa & S. Akabori, *Bulletin of the Chemical Society of Japan,* **36** (1963) 21.
[8] Y. Izumi, M. Imaida, H. Fukuwa, S. Akabori, *Bulletin of the Chemical Society of Japan* **42** (1963) 2373.
[9] A.D. Roddick-Lanzilotta & A.J. McQuillan, *Journal of Colloid and Interface Science* **227** (2000) 48.
[10] T.E. Jones & C.J. Baddeley, *Langmuir,* **22** (2006) 148.
[11] T.E. Jones, A.E. Rekatas & C.J. Baddeley, *Journal of Physical Chemistry C,* **111** (2007) 5500.
[12] T.E. Jones & C.J. Baddeley, *Journal of Physical Chemistry C,* **111** (2007) 17558.
[13] V. Humblot, C.Methivier & C-M. Pradier, *Langmuir*, 22 (2006) 3089.
[14] O.V. Cabral, C.A Téllez S., T. Giannerini & J. Felcman, *Spectrochimica Acta A,* **61** (2005) 337.
[15] J.L. Castro, M.A. Montanez, J.C. Otero & J.I. Marcos, *Journal of Molecular Structure,* **349** (1995) 113.
[16] J.F. Pearson & M.A. Slifkin, *Spectrochimica Acta A,* **28** (1972) 2403.
[17] M.A. Keane & G. Webb, *Journal of the Chemical Society: Chemical Communications,* (1991) 1619.
[18] M. Bowker, S. Poulston, R.A. Bennett & P. Stone, *Journal of Physics-Condensed Matter,* **10** (1998) 7713
[19] Q. Chen, C.C. Perry, B.G. Frederick, P.W. Murray, S. Haq & N.V. Richardson, *Surface Science,* **446** (2000) 63
[20] Q. Chen, D.J. Frankel & N.V. Richardson, *Langmuir,* **17** (2001) 8276.
[21] H. Wang, X.Y. Zhao, R.G. Zhao & W.S. Yang, *Chinese Physics Letters,* **18** (2001) 445.
[22] X.Y. Zhao, *Journal of the American Chemical Society,* **122** (2000) 12584.
[23] C.F. McFadden, P.S. Cremer & A.J. Gellman, *Langmuir,* **12** (1996) 2483.
[24] J.D. Horvath & A.J. Gellman, *Journal of the American Chemical Society,* **123** (2001) 7953.
[25] A. Ahmadi, G. Attard, J. Feliu & A. Rodes, *Langmuir,* **15** (1999) 2420
[26] D.S. Sholl, A. Asthagiri & T.D. Power, *Journal of Physical Chemistry B,* **105** (2001) 4771
[27] D.J. Jenkins, A.M.S. Alabdulrahman, G.A. Attard, K.G. Griffin, P. Johnston & P.B. Wells, *Journal of Catalysis,* **234** (2005) 230
[28] A.J. Gellman, J.D. Horvath & M.T. Buelow, *Journal of Molecular Catalysis A-Chemical*, **167** (2001) 3.
[29] M. Parschau, T. Kampen & K.H. Ernst, *Chemical Physics Letters,* **407** (2005) 433

[30] M. Parschau, S. Romer & K.H. Ernst, *Journal of the American Chemical Society,* **126** (2004)15398
[31] N. V. Belova, H. Oberhammer & G.V. Girichev, *Journal of Physical Chemistry A,* **108** (2004) 3593.
[32] N. Peica, C. Lehene, C. Leopold, S. Schlucker & W. Kiefer, *Spectrochimica Acta Part A,* **66** (2007) 604.
[33] B.V. Crist, *Handbook of Monochromatic XPS spectra: The Elements and Native Oxides* **J Wiley & Sons Inc, Chichester, UK, 2000.**
[34] N.M.D. Brown, J.A. Hewitt & B.J. Meenan, *Surface and Interface Analysis,* **18** (1992) 187.
[35] D.J. Davis, G. Kyriakou, R.B. Grant, M.S. Tikhov & R.M. Lambert, *Journal of Physical Chemistry C,* **111** (2007) 1491.
[36] T.A. Carlson, *Surface and Interface Analysis,* **4** (1982) 125.
[37] S.Tanuma, C.J. Powell & D.R. Penn, *Surface and Interface Analysis,* **21** (1993) 165.
[38] D. Brigg & M.P. Seah, *Practical Surface Analysis: Auger and X-Ray Photoelectron Spectroscopy,* **J Wiley & Sons Inc, Chichester, UK, 1990.**
[39] Y. Inoue, K. Okabe & I. Yasumori, *Bulletin of the Chemical Society of Japan,* **54** (1981) 613.
[40] C. Kozlowski & P.M.A. Sherwood, *Journal of the Chemical Society: Faraday Transactions I,* **81** (1985) 2745.
[41] A.S. Lim & A. Atrens, *Applied Physics A,* **51** (1990) 411.
[42] M. Wühn, J. Weckesser & Ch. Wöll, *Langmuir,* **17** (2001) 7605.
[43] B.C. Beard & P. Spellane, *Chemistry of Materials,* **9** (1997) 1949.
[44] A. Hatta, Y. Moriya & W. Suetaka, *Bulletin of the Chemical Society of Japan***, 48** (1975) 3441.
[45] U. Gelius, P.F. Hedén, J. Hedman, B.J. Lindberg, R. Manne, R. Nordberg, C. Nordling & K.Siegbahn, *Physica Scripta,* **2** (1970) 70
[46] M.A. Keane & G. Webb, *Journal of Catalysis,* **136** (1992) 1
[47] T. E. Jones & C. J. Baddeley. *Surface Science*, **519** (2002) 237.
[48] A.G. Trant & C.J. Baddeley, *Journal of Physical Chemistry C,* **115** (2011) 1025.
[49] J.A. Switzer, H.M. Kothari, P. Poizot, S. Nakanishi & E.W. Bohannan, *Nature,* **425** (2003) 490.

Chapter 5

Characterisation Studies of Ni{111} modified with (S)-lysine in UHV and liquid-solid interface conditions

5.1 INTRODUCTION

The study of simple amino acids adsorbed onto relevant metal surfaces is of particular importance in the wider work investigating suitable chiral modifiers over a nickel catalyst. Chapter 4 shows *(S)*-aspartic acid (a poor modifier) behaving rather differently on Ni under optimum enantioselective conditions compared to *(R,R)*-tartaric acid and *(S)*-glutamic acid. Chapter 3 results were successful in showing the packing of *(S)*-aspartic acid on the surface by STM under UHV conditions on a single crystal substrate. RAIRS and TPD determined the orientation and stability of the adsorbate. Similar studies of the closely related lysine molecule on the Ni surface will allow comparisons to be made with *(S)*-aspartic acid between the similarities in structure and respective enantioselectivities.

5.1.1. CHARACTERISATION STUDIES OF (S)-LYSINE ON COPPER SUBSTRATES

(S)-lysine, alongside *(S)*-histidine and *(S)*-arginine, is one of the three naturally occurring basic amino acids and is the only amino acid with a side chain terminated by a basic amino group at the ε-position. At room temperature and atmospheric pressure, lysine is a white crystalline solid and in its zwitterionic form. Similar to other amino acids, the form of *(S)*-lysine in aqueous solution varies from divalent cationic, to monovalent cationic, to zwitterionic, and finally to anionic with increasing pH. Therefore, four molecular ion lysinate species can exist, depending

on solution pH. Figure 5.1 shows the speciation diagram for *(S)*-lysine, with pK_a values of 2.2, 9.1 and 10.7 [1].

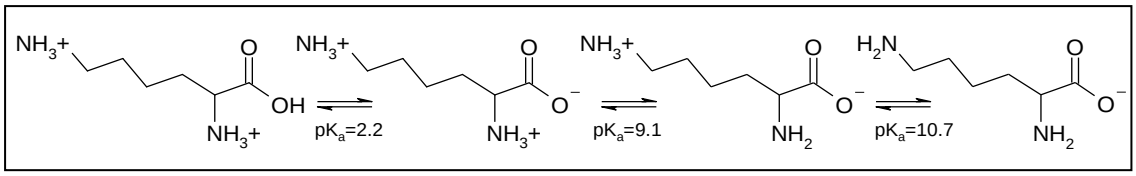

Fig. 5.1 Speciation of *(S)*-lysine

(S)-lysine has been a popular amino acid in terms of a subject of investigations by various surface science groups, in comparison with the lesser studied *(S)*-aspartic acid. The additional distal NH_2 functional group on the side chain has the potential for intermolecular hydrogen bonding, as well as creating a new bond to a metal substrate, and so offers great scope in differences in behaviour compared to smaller amino acids. Initial studies by Zhao made the discovery that *(S)*-lysine influences the chiral restructuring of steps when adsorbed on Cu{001} [2,3]. Further studies by Humblot and co-workers examined *(S)*-lysine adsorption on Cu{110} by STM, LEED and RAIRS under UHV conditions [4], as well as comparing UHV-RAIRS with liquid phase PM-RAIRS [5]. Most recently, Held and co-workers carried out XPS and NEXAFS studies to challenge the adsorption state and geometry of lysine on Cu{110} first suggested by Humblot *et al.* [6].

Under UHV conditions on Cu{001}, lysine was shown by STM to bind in its anionic form on the surface, to form two different superstructures, both with intermolecular hydrogen bonding between lysine molecules and both NH_2 groups bound to the Cu surface [2]. Adsorption of *(S)*-lysine under similar conditions onto Cu{110} resulted in the zwitterionic form present at low coverages, with a reorientation at higher coverages [4,5,7]. Although STM models appeared to corroborate with the images collected, it was wrongly stated that zwitterionic lysine would form a bond to the Cu{110} surface through the α-NH_3^+ group as well as the carboxylate oxygen atoms. In fact, the amine function in the ε-position is more basic than the α-amine and thus it is this group which is protonated in the zwitterionic species (Figure 5.1). It would be unfavourable for an NH_3^+ group to bond to a metal substrate and therefore, in the

studies by Humblot and co-workers, it is more feasible that the carboxylate group and the *neutral* α-amine group bind to the Cu{110} surface. Four different types of ordered adlayers were found on the surface, depending on coverage and annealing temperature. In the studies by Held and co-workers, XPS and NEXAFS were used to find the adsorption geometry of lysine on Cu{110} and concluded that a bonding mode through both amino nitrogen atoms and the carboxylate oxygen atoms was formed, at odds to the 3-point geometry of the complex proposed by Humblot *et al* [6].

The chiral faceting observed by Zhao and co-workers offered a strong example of the significance of amino acids and their possible role in enantioselective catalysis [3]. The lysine studies by Zhao on Cu{001} followed on from previous investigations of facets induced by glycine [8] and alanine [9], and showed that steps were facetted to the <310> directions, bunching to form {3 1 17} facets (Figure 5.2). Only four kinds of {3 1 17} facets out of a possible eight were observed, corresponding to the *R*-facets, suggesting adsorbate-induced surface chirality.

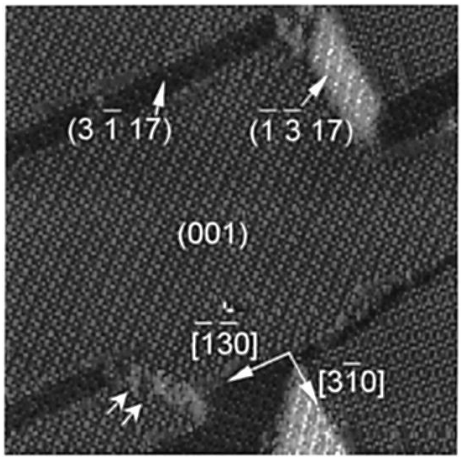

Fig. 5.2: STM image of chiral faceting on a Cu{001} surface with *(S)*-lysine adsorbed, annealed to 430 K for 20 minutes. {3 1 17} facets can be observed formed by bunching of the <310> steps. From [3].

TPD experiments were recently undertaken in the group of Gellman to ascertain the differences in adsorption energetics of *(R)*- and *(S)*-lysine on the chiral Cu{3 1 17} and achiral Cu{100} surfaces [10]. It was found that desorption energies of both enantiomers were greater on chiral surfaces than on achiral surfaces. Ultimately the *(S)*-lysine adsorption on Cu{3 1 17}^{R} was energetically favoured, consistent with previous STM studies [3].

5.1.2. CATALYTIC SIGNIFICANCE OF LYSINE IN THE Ni-CATALYSED β-KETOESTER HYDROGENATION REACTION

Lysine is an important amino acid in its role in cell adhesion and biomolecular recognition [11], and hence studies into its adhesion to metal surfaces aid in determining its active structure in these functions. Admittedly, there is a stronger motivation in this chapter to attempt to justify the use of lysine as a chiral modifier, and so this research focuses on the interaction of lysine on the catalytically relevant Ni substrate. To date, the only related work using *(S)*-lysine in the aforementioned catalytic system was part of a larger study carried out by Izumi *et al.*, in which a number of amino and hydroxy acids were systematically tested to quantify their value in terms of enantioselective activity in the Ni-catalysed hydrogenation of MAA (see Section 1.6.2.) [12]. The hydrochloride of *(S)*-lysine was tested, of which the results of the effect of modification temperature variation on enantioselectivity are shown in Table 5.1. Izumi and co-workers [13] proposed that the use of the hydrochloride salt of lysine as a modifier in the MAA hydrogenation causes a depression of the hydrogenation activity of the catalyst at higher modification temperatures, suggesting chlorine may act as a site blocker.

Modifying reagent	Modifying temperature /°C	e.e. (%)
(S)-lysine (HCl)	0	6.3
(S)-lysine (HCl)	40	6.2

Table 5.1 Correlation between enantioselectivity of the *(S)*-Lys.HCl modifier on RNi catalyst as a function of modification temperature (modifying conditions: isoelectric point, reaction conditions: MAA (neat), 60°C, atmospheric pressure). From [13].

5.1.3. AIM OF RESEARCH

The research in this chapter aims to characterise the adsorption of *(S)*-lysine on a Ni{111} surface under both UHV and liquid-solid interface conditions in order to study the packing and orientation of the modifier as well as considering the interactions at the liquid-solid interface, which is advantageous from a catalytic

perspective. As previously discussed, the more catalytically relevant Ni{111} surface is used, as well as polycrystalline Ni foil in the XPS studies.

In Part I of this chapter, UHV techniques including thermal desorption, vibrational spectroscopy and scanning tunnelling microscopy are employed to characterise *(S)*-lysine on the Ni{111} surface.

In Part II, RAIRS and XPS techniques are used to study the adsorption of *(S)*-lysine on Ni from aqueous solution and thus analyse any changes in bonding and orientation due to changes in modification pH and temperature. This approach affords a more realistic model of the importance of modification pH and temperature on binding habits of amino acids with metal surfaces, and aids progress in the characterisation of the amino acids under more applicable conditions for catalysis.

5.2 EXPERIMENTAL

5.2.1 UHV EXPERIMENTAL CONDITIONS

STM and RAIRS experiments were carried out in Chamber 1, as described in Section 2.8. The Ni{111} sample was prepared by argon ion bombardment (2 kV) and annealed to 893 K. *(S)*-lysine (Sigma Aldrich ≥98.0 %) was heated to ~410 K, and sublimed onto the substrate held at 300 K. Once RAIRS data were collected, the sample was transferred under UHV conditions to the STM chamber where data were taken in constant current mode using an electrochemically etched W tip. All STM images were recorded at 300 K. Subsequent imaging for MAA coverage was carried out by exposing the surface to MAA, purified by repeated freeze-pump-thaw cycles, dosed directly into the STM chamber from the RAIRS chamber by the opening of a succession of gate valves to achieve the desired vapour pressure. STM images were processed using WSxM software [14].

5.2.2 LIQUID-SOLID INTERFACE EXPERIMENTAL CONDITIONS

Briefly, as the liquid phase experimental details have already been given previously in Section 4.2.1, the Ni{111} was immersed in a 10 mM aqueous lysine solution diluted to concentration using Millipore water (18.2 MΩ), for 900 s under constant agitation. The pH was altered accordingly by addition of 1 M NaOH or concentrated HCl, whilst the temperature of the modification was controlled by use of a hot plate. The experimental pH values selected for this study were chosen to be lower or higher than each of the pK_a values of lysine in order to control the chemical form of the dominant species in solution (see Figure 5.1). After modification, a RAIR spectrum (256 scans, 4 cm^{-1} resolution) was recorded and ratioed against a background spectrum of the unmodified surface. Additionally, the rovibrational bands associated with small changes in gas-phase water levels in the beam path were subtracted from the spectra. The modified surface was then rinsed for several seconds in a flow of Millipore water (18.2 MΩ) and another RAIR spectrum was taken. The sample was subsequently immersed under constant agitation at 300 K in a 50:50 mixture of MAA (Fluka ≥99%) in tetrahydrofuran (THF) for 900 s and a further RAIR spectrum obtained. For XPS experiments, A VG Sigma Probe spectrometer using Al Kα radiation (angle between surface normal and analyser direction of 53°) with a 400 μm diameter spot (100 W) was used for the analysis. All the measurements reported were carried out at room temperature. The cleaned Ni polycrystalline foil substrates were treated as for the liquid phase RAIRS experiments in aqueous solutions of *(S)*-lysine as a function of pH. A clean Ni foil sample was used as a control experiment. Prior to loading into UHV chamber, the samples were dried under a light $N_{2\,(g)}$ flow.

5.3 RESULTS AND DISCUSSION

PART I – UHV CONDITIONS

5.3.1 UHV RAIRS

5.3.1.1 ADSORPTION OF *(S)*-LYSINE AS A FUNCTION OF COVERAGE ON Ni{111} AT 300 K

RAIRS data, shown in Figure 5.3, were obtained for the increasing coverage of *(S)*-Lys on the Ni{111} surface at 300 K. The RAIR spectra of amino acids adsorbed

onto metal surfaces are notoriously complex due to the possibility of several molecular confirmations bonding to the surface, and thus previous infrared studies on lysine are used to aid interpretation of the observed bands [1,4,15,16].

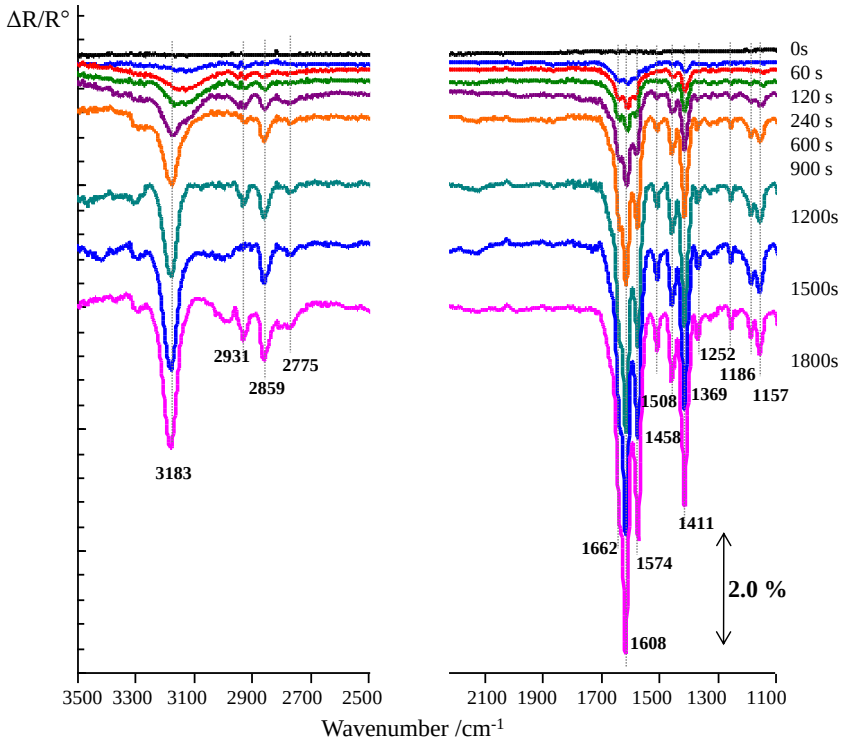

Fig. 5.3 UHV RAIRS of increasing coverage of *(S)*-lysine on Ni{111} at a single crystal temperature of 300 K.

At the onset of adsorption of *(S)*-lysine, the spectrum is dominated by bands in the 3300 – 2850 cm^{-1} region. The 3183 cm^{-1} peak corresponds to the N-H stretch, whilst the peaks at 2931 and 2859 cm^{-1} represent the asymmetric and symmetric stretches respectively of the CH_2 group. The 2775 cm^{-1} peak is likely to be the overtone peak of 1369 cm^{-1} (symmetric CH bend) [17]. Four distinguishable bands in the lower 2000 – 1000 cm^{-1} region of the spectrum are present at 1662, 1608, 1460 and 1415 cm^{-1}. A summary of the assignments are shown in Table 5.2. The peaks at 1608 and 1662 cm^{-1} are attributed to deformation modes of the NH_2 and NH_3^+ groups respectively. The less intense peak at 1460 cm^{-1} is attributed to the deformation mode of the alkyl chain CH_2 groups. The peak at 1415 cm^{-1} can be assigned as the symmetric stretch of the deprotonated carboxylic acid moiety, ν_s (COO^-). It is therefore possible to propose, from the analyses, that lysine is in its zwitterionic form on the Ni{111} surface at low coverages, due to the presence of NH_3^+, NH_2 and

COO^- groups, and the lack of vibrational modes associated with the carboxylic acid moiety.

The intense bands at higher coverages strongly imply the presence of multilayers of lysine on the Ni{111} surface. As well as the peaks present at low coverages remaining, new infrared features are observed as the coverage of *(S)*-lysine is increased. A relatively intense doublet of peaks at 1186 and 1157 cm^{-1} are attributed to the NH_2 wag. A small peak which emerges at 1252 cm^{-1} is assigned as a combination of ν(C-O) + δ(O-H) vibrations of the intact COOH group. CH_2 group IR active modes are represented by several peaks in the ~1300 cm^{-1} region. Peaks attributed previously to a symmetric stretch of the COO^- group and NH_2 and NH_3^+ group deformations remain present at high coverages, whilst two new peaks at 1508 and 1574 cm^{-1} are assigned to the symmetric deformation of the NH_3^+ group and asymmetric COO^- stretch respectively. It would appear that the zwitterionic form of lysine is present in the multilayers, with some evidence of neutral or anionic lysine species co-adsorbing.

Ni{111}/*(S)*-Lys 300 K /wavenumbers in cm^{-1}		**Assignment**
Low coverage	**High coverage**	
3183	3183	ν (N-H)
2960	2931	ν_{as} (CH_2)
2858	2859	ν_s (CH_2)
1662	1662	δ_{as} (NH_3^+)
1608	1608	δ (NH_2)
-	1574	ν_{as} (COO^-)
-	1508	δ_s (NH_3^+)
1460	1458	δ (CH_2)
1415	1411	ν_s (COO^-)
-	1369	CH_2 symmetric bend
1335, 1313	1340, 1311	CH_2 wag
-	1252	ν(C-O) + δ(O-H)
1151	1186, 1157	NH_2 wag

Table 5.2 Assignments of UHV RAIRS bands of *(S)*-lysine on Ni{111} at 300 K adsorption temperature.

The presence of the zwitterionic species at low coverages is similar to the observation made in the studies of *(S)*-Lys on Cu{110} by Humblot and co-workers

[5]. This is opposed to the study by Zhao and co-workers on Cu{001} [2] which suggested lysine is adsorbed on the surface in its anionic form. By comparing lysine adsorption behaviour at a Cu{001} surface with only that of glycine and alanine, the Zhao study does not give any further evidence as to why the functionalised side chain of lysine would prefer to remain in its neutral form. The presence of the zwitterionic form is more viable, however, as discussed in Section 5.1.1., the previous studies wrongly suggested a zwitterion structure of $NH_2(CH_2)_4CH(NH_3^+)COO^-$. The side chain amino group of lysine is known to be the more basic and nucleophilic, due to the electron withdrawing group next to the *α*-amino group [18], therefore the *ε*-amino group remains protonated while the *α*-amino group is deprotonated, resulting in the $(NH_3)^+(CH_2)_4CHNH_2COO^-$ structure. Furthermore, logically, it is highly unlikely for an NH_3^+ group to bond to a metal substrate unless an electrostatic interaction with a charged metal surface is present. On Cu single crystals, as used in the groups of Humblot [4,5] and Held [6], although it is entirely reasonable for the lysine to adopt different bonding conformations depending on the nature of the metal [19], it is argued that the NH_3^+ group of lysine would only take part in intermolecular zwitterion hydrogen bonding and not in bonding to the Cu substrate, as postulated in the research.

In the present case, the presence of and intensities of the zwitterionic-related IR peaks offer some idea into how lysine binds to the Ni{111} surface. The equal intensities of the two $\nu(CH_2)$ bands at 2960 and 2858 cm^{-1} at low coverages suggests that the side chain carbon backbone is tilted with respect to the Ni surface, as neither the symmetric nor asymmetric CH_2 stretch is more intense than the other to suggest a perpendicular or parallel orientation to the surface [21, 22]. The presence of the asymmetric NH_3^+ deformation band, combined with the lack of symmetric band, suggests that the *ε*-amino group is likely to lie almost parallel to the Ni surface (although not bonding to the surface). The presence of a relatively intense $\delta(NH_2)$ peak implies that the *α*-amino group will bind to the Ni surface (supported by previous work by Hatta *et al.* [20]). The lack of NH_2 scissor mode at 1050 cm^{-1} and presence of NH_2 wag suggests an orientation with the lone electron pair of nitrogen

interacting with the surface [23] as illustrated in Figure 5.4a. The antisymmetric carboxylate stretch at ~1570 cm^{-1} is not present, with only a symmetric stretch at 1415 cm^{-1}. This would suggest that both oxygen atoms of the carboxylate group are bound at an equal distance from the Ni{111} surface, thus attenuating the ν_{as} (COO^-) vibration significantly. A possible model for the low coverage of *(S)*-Lys on the Ni{111} based on the RAIRS data is shown in Figure 5.4a.

At the higher coverage phase, it can be presumed from changes in peak intensities and addition of new peaks that the geometry of the rest of the molecule with respect to the surface has changed compared with at low coverages. The emergence of the antisymmetric carboxylate stretch at 1574 cm^{-1}, which is of very similar intensity to the symmetric stretch at 1411 cm^{-1}, suggests that the oxygen atoms are now not at equal distance to the surface and are likely to be bonded through only one of the oxygens. The continued presence of a strong band at 1608 cm^{-1} verifies that the molecule is bonded to the surface through the NH_2 group. From the presence of a more intense symmetric CH_2 stretch in comparison with the asymmetric stretch, it is reasonable to assume that, as coverage increases, lysine reorientates itself to bind via one carboxylate oxygen as well as the α-NH_2 group which allows stacking on the surface in such a way that it maximises the more limited space available. Furthermore, the presence of a weak peak representing the COOH group suggests that a small fraction of neutral lysinate species is co-adsorbed with the zwitterionic form. This has previously been observed for multilayers of amino acids on metals [24, 25].

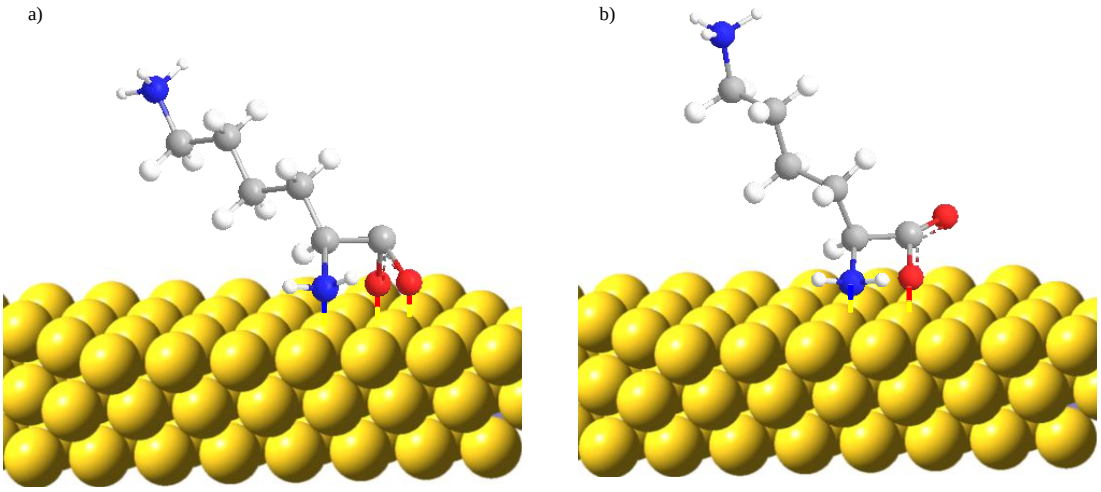

Fig. 5.4 Schematic models of possible molecular orientation of *(S)*-Lys on Ni{111} at a) low coverage and b) high coverage, based exclusively on RAIRS data.

A model of the lysine bonding at higher coverage is proposed in Figure 5.4b. It should be noted that both models in Figure 5.4 are approximate as they are exclusively based on the RAIRS results and it would be difficult to deduce exact orientations from such a complex spectrum, especially as there is a strong possibility that multiple orientations may exist. In summary, it is postulated that lysine binds extremely well to Ni{111}, and may possibly grow on the surface in the form of 3D islands, before the formation of multilayers at higher coverages.

5.3.1.2 ADSORPTION OF MAA ONTO A LOW COVERAGE OF (S)-LYSINE ON Ni{111} AT A SUBSTRATE TEMPERATURE OF 300 K

Adsorption of 5 L MAA on low (60 s) coverage *(S)*-Lys modified Ni{111} at 300 K has been studied by UHV-RAIRS and the spectra are shown in Figure 5.5. The MAA single beam spectra are ratioed against the spectra of the modified surface, which allows identification of the bands corresponding to MAA only. The amount of *(S)*-Lys adsorbed on the surface is comparable with the 60 s coverage in Figure 5.3 and so is in its zwitterionic form. Exposing the surface to 5 L of MAA yields new absorption bands at 2925 cm^{-1}, assigned as $\nu_s(CH_3)$, 1785 cm^{-1} with a shoulder at 1747 cm^{-1} ($\nu(CO)^{3\text{-fold bridge}}$ and $\nu(C=O)$ respectively), 1573 cm^{-1}, attributed to the O=C–C–C=O structure, 1457 and 1440 cm^{-1} ($\delta_{as}(CH_3)$), 1361 cm^{-1} ($\delta_s(CH_3)$) and finally 1329 cm^{-1} which is assigned as the CH_2 twist [26]. The bands present are

similar to those found in a previous study by Jones and Baddeley for MAA adsorbed onto a low coverage *(S)*-glutamic acid-modified Ni{111} surface [27], as well as MAA on clean Ni{111}, and suggest that, under such low coverage conditions, the MAA adsorbs as a mixture of diketo and enol tautomers, predominantly on the unmodified terrace sites, with little or no discernible interaction with the modifier.

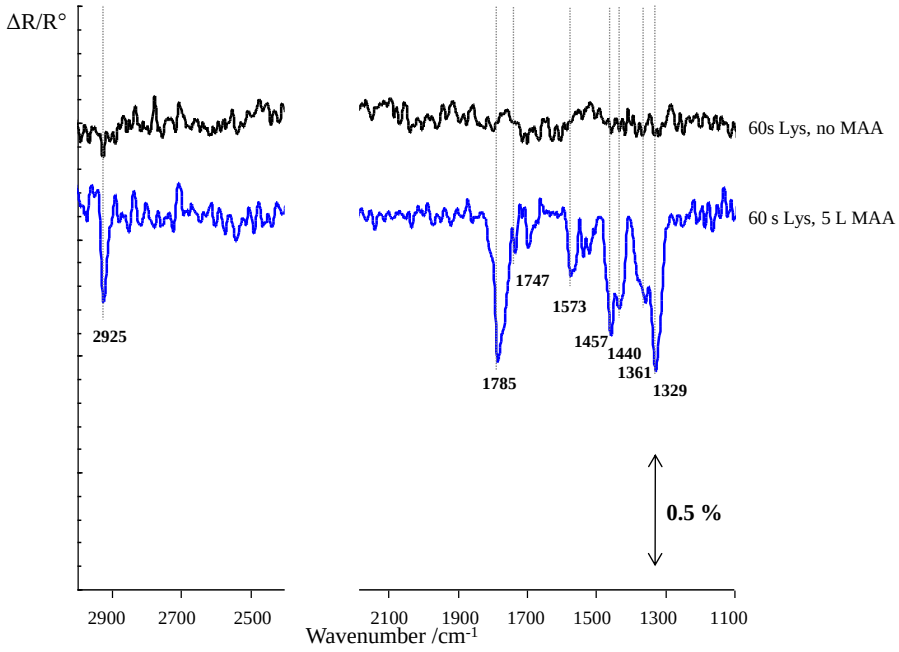

Fig. 5.5 RAIRS spectra following the exposure of MAA on *(S)*-Lys modified Ni{111} with a modifier coverage of 60 s at 300 K.

5.3.2. UHV TPD

5.3.2.1 TPD STUDIES OF INCREASING *(S)*-LYSINE COVERAGE ON Ni{111} AT A SUBSTRATE TEMPERATURE OF 300 K

TPD spectra for the adsorption of *(S)*-Lys in Ni{111} as a function of coverage at a single crystal temperature of 300 K are presented in Figures 5.6a-f. Spectra were recorded for *m/z* values of 2 (H_2), 16 (O), 17 (NH_3), 27 (HCN), 28 (CO or N-containing fragments) and 44 (CO_2), after a preliminary mass spectroscopy experiment showed these masses to increase in partial pressure when the surface was exposed to lysine. In each of the spectra, a low temperature desorption peak is frequently observed at approximately 325 – 330 K. As this peak is irreproducible in

shape and position, it is assigned as an artefact created by desorption of the species from the sample mounting.

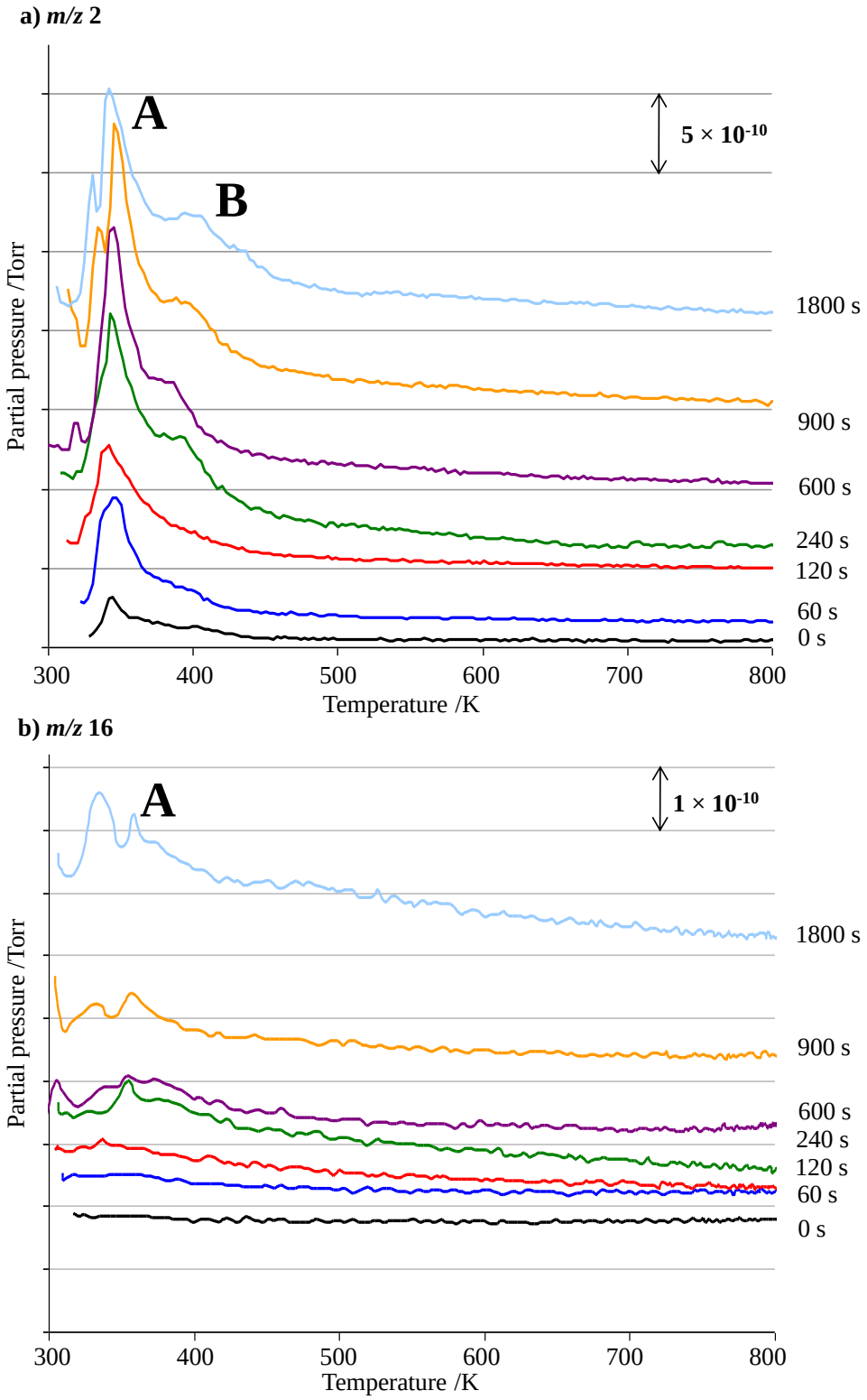

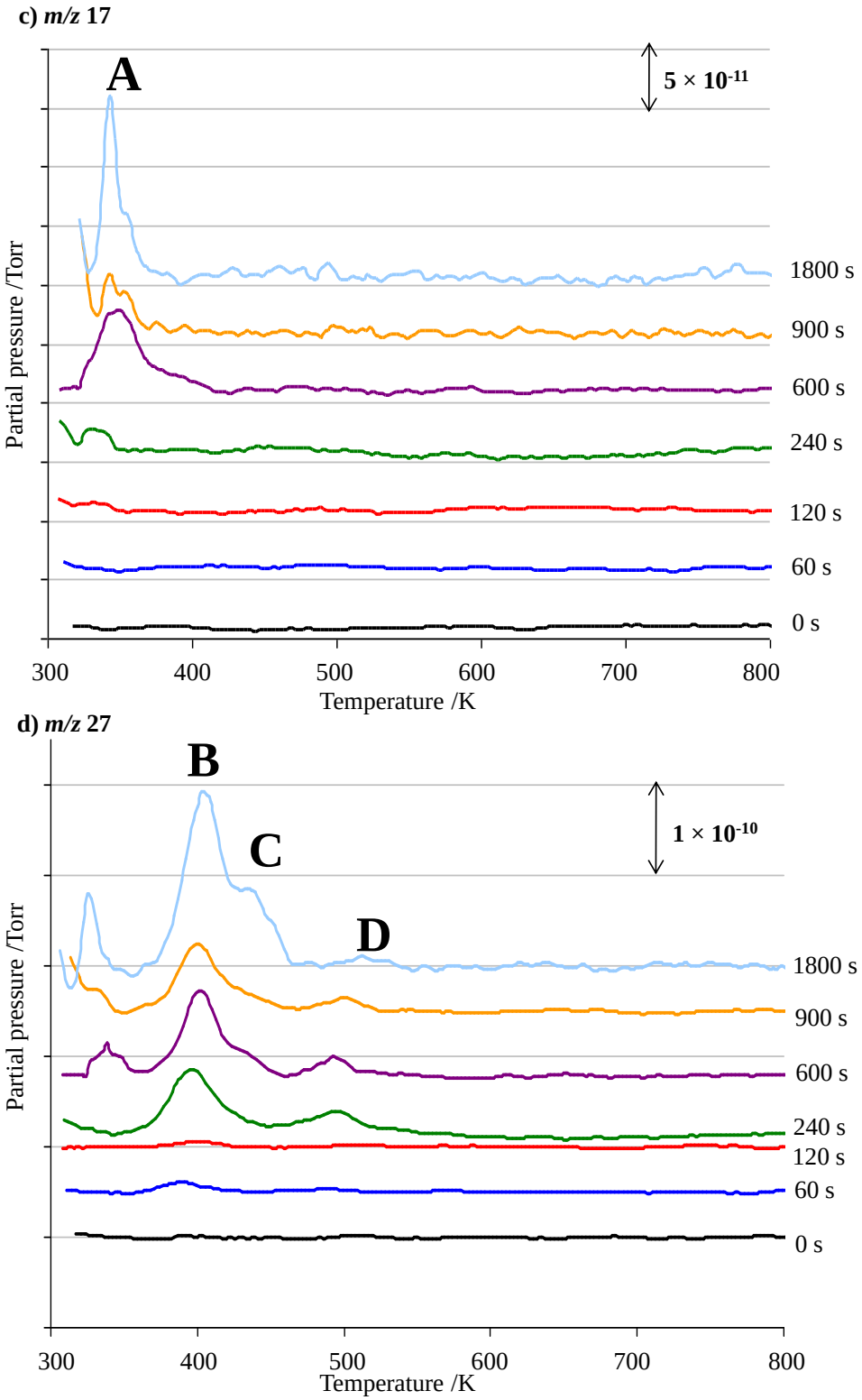
c) m/z 17
A
5 × 10-11
Partial pressure /Torr
1800 s
900 s
600 s
240 s
120 s
60 s
0 s
300
400
500
600
700
800
Temperature /K
d) m/z 27
B
C
D
1 × 10-10
Partial pressure /Torr
1800 s
900 s
600 s
240 s
120 s
60 s
0 s
300
400
500
600
700
800
Temperature /K

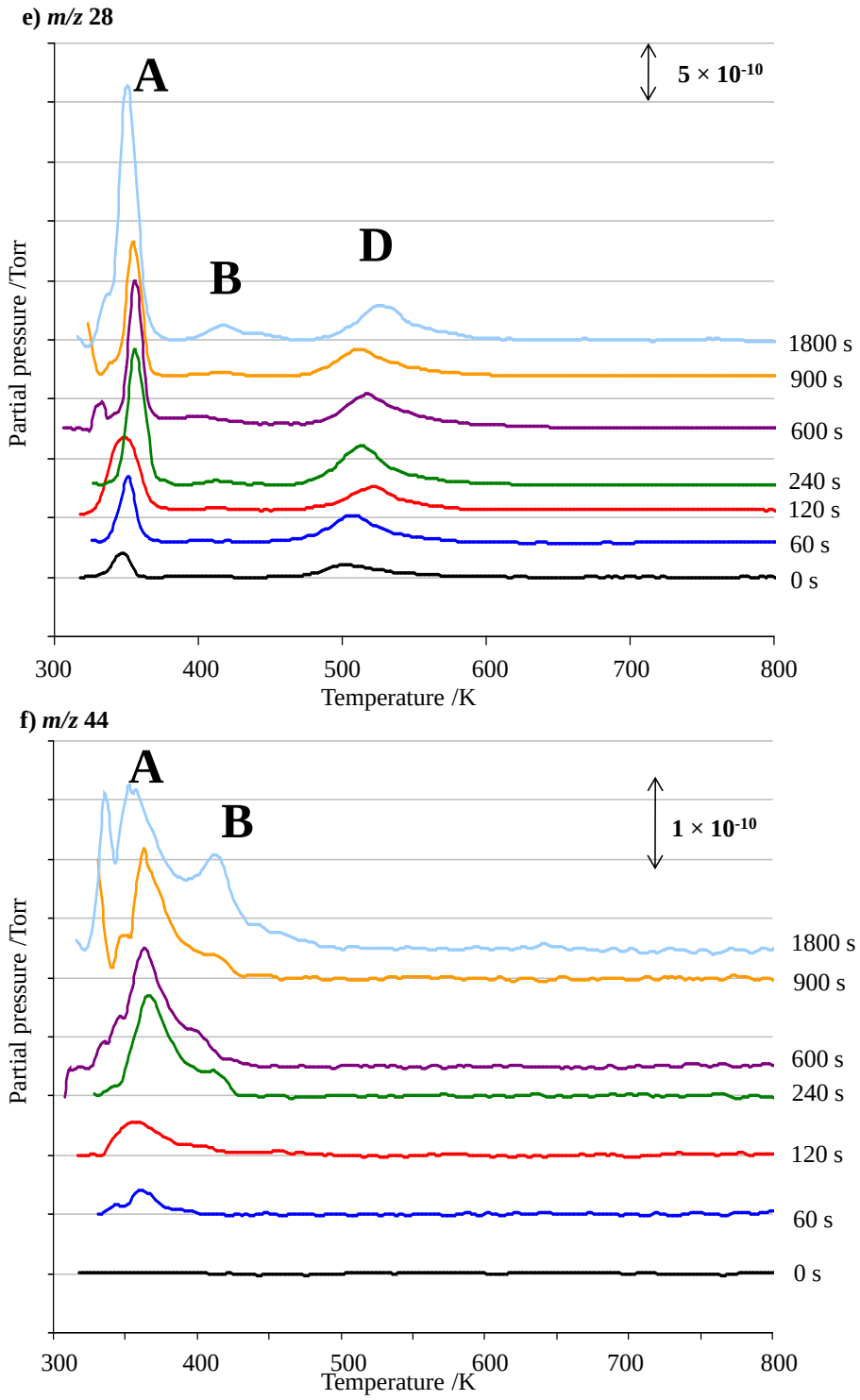

Fig. 5.6 UHV TPD spectra following *(S)*-lysine adsorption on Ni{111} at 300 K with increasing coverages, monitoring *m/z* values of: a) 2 (H_2); b) 16 (O);c) 17 (NH_3); d) 27 (HCN); e) 28 (CO, H_2CN or N_2); and f) 44 (CO_2).

	H_2	O	NH_3	HCN	*m/z* 28	CO_2
artefact peak	~330 K	~335 K	-	~325 K	~333 K	335 K
A	345 K	358 K	344 K	-	355 K	355 K
B	400 K	-	-	406 K	421 K	413 K
C	-	-	-	436 K	-	-
D	-	-	-	500 K	500 K	-

Table 5.3 TPD desorption peaks for *(S)*-lysine on Ni{111} at 300 K adsorption temperature.

Several peaks at different T_d values suggest different adsorption geometries on the surface (Table 5.3). The H_2 TPD spectra shown in Figure 5.6a initially has an asymmetric peak centred around 345 K which grows in intensity as coverage of lysine is increased (labelled **A**). This peak is also present in all remaining spectra. Its position, at a slightly higher temperature than that for atomic hydrogen (330 K [28]), strongly suggests that desorption follows zero-order kinetics, a direct consequence of the dissociation of the adsorbed lysine molecules, rate-limited by the lysine dissociation. In the present case, the sharp leading edge of peak A at all coverages, as well as the rapid drop when all molecules have desorbed, also suggests zero-order kinetics (see Section 2.6.1). There have been several studies carried out which indicate that this peak is likely to be due to multilayer desorption of the species [10, 29]. The TPD study by Gellman and co-workers of lysine adsorbed on Cu{100} suggested that a desorption peak at 360 K indicated multilayer desorption or 3D cluster desorption as it did not saturate with increasing exposure to lysine [10]. This is identical to the behaviour of the 345 K peak in the present study, and the closeness in temperature is reasonable as the desorption characteristics of a multilayer depend less on the substrate material and more on the physisorption behaviour between lysine molecules. The presence of NH_3 suggests cleavage of the basic side chain C-N bond [24].

Peak **B** at ~400 K, which is most intense in the HCN TPD spectra and also present in the H_2, *m/z* 28 and CO_2 spectra, is assigned as the desorption of the monolayer of adsorbate on the Ni{111} surface, which are bound somewhat more strongly than the multilayers. The presence of *m/z* 27 verifies that, at these coverages, all molecules that are directly bound to the Ni surface decompose prior to desorption, as *m/z* 27 is

not a typical lysine fragment. Decomposition products of *m/z* value 27 have previously been observed in the reaction of glycine on the surface of Pt{111} [30] and Pd{111} [24] and are thought to be HCN fragments from decomposition of the lysine, based on the RAIRS results that lysine adsorbs in its zwitterionic form on the surface. The difference with the present study compared to that of lysine on Cu{100} [10] is that lysine does not desorb as an intact molecule. However, many other amino acid desorption studies on metal surfaces also show thermal decomposition of the molecule on the surface [24, 25]. Furthermore, in studies of glycine on polycrystalline Ni, it was found that no desorption of intact glycine molecules occurred from the first monolayer, which was attributed to the reactivity of the substrate [31]. The observation that peak **B** increases in intensity is explained by assessing the likely mechanism of growth on the surface. As for many amino acids on metals [10, 32], it is feasible that lysine grows as 3D islands before saturation of the first layer and thus, during TPD experiments, the monolayer coverage increases as desorption of the multilayer at 345 K allows reorganisation of the lysine molecules on the surface. The presence of a peak which scales in each of the HCN, *m/z* 28 and CO_2 TPD spectra at ~400 K suggests that the *m/z* 28 fragment is a mixture of CO and nitrogen-containing species H_2CN ($H\text{-}C{\equiv}N^{+}H$) and N_2 [30]. The small shoulder (peak **C**) in the HCN spectra at the highest lysine coverage, which can also be seen in the CO spectra could be attributed to the change in orientation of the lysine molecules, which has been evidenced in the RAIRS studies in 5.3.1.1, with the change resulting in a slightly stronger bound species present at the Ni steps, as the lysine adsorbate can interact with more Ni atoms at the step than on a flat terrace. Finally, the peak at ~500 K (peak **D**) in the *m/z* 27 and 28 TPD spectra are likely due to an H_2CN fragment which further decomposes to HCN. The previous study of glycine on Pt{111} reported the observation of a similar peak [30].

In summary, the intact molecules which desorb can be assumed to originate from the multilayer or 3D clusters, whereas fragment peaks are assigned to decomposition products from the chemisorbed monolayer. Figure 5.7 illustrates the possible decomposition pathway for lysine on the Ni{111} surface. It is suggested that the

lysine undergoes cleavage of both the C-N bond on the basic side chain as well as C-C bond scission adjacent to the carboxylate group. Partial desorption as CO_2 and dissociation to CO occurs for the carboxy fragment and NH_3 desorption for the amine fragment, whilst dissociation of the remaining central fragment to H_2CN^+ as well as HCN occurs.

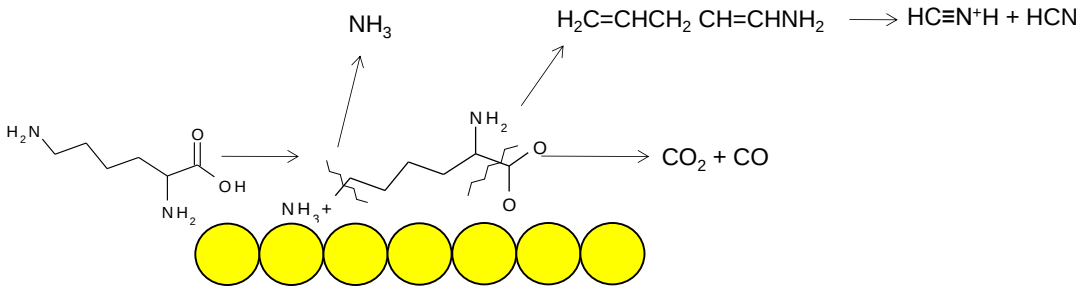

Fig. 5.7 Likely decomposition pathways for lysine on Ni{111}.

5.3.2.2 TPD STUDIES OF INCREASING *(S)*-LYSINE COVERAGE ON Ni{111} AT A SUBSTRATE TEMPERATURE OF 373 K

The TPD spectra for the dosing of *(S)*-lysine on Ni{111} at a substrate temperature of 373 K are illustrated in Figure 5.8a-i, with peaks labelled in Table 5.4. It can be observed that none of the spectra show an artefact peak as in experiments in Section 5.3.2.1.

	H_2	**O**	**NH_3**	**H_2O**	**HCN**	**CO**	**CO_2**	**m/z 55**	**m/z 81**
A	355 K	359 K	360 K	-	-	358 K	365 K	-	-
B	392 K	-	-	-	404 K	395 K	393 K	410 K	-
C	480 K	472-493 K	469-493 K	477-490 K	463-490 K	466 – 496 K	466-490 K	469-493 K	493 K
D	-	498-547 K	500-543 K	546 K	546 K	506-549 K	500-543 K	494-549 K	-

Table 5.4 TPD desorption peaks for *(S)*-lysine on Ni{111} at 373 K adsorption temperature.

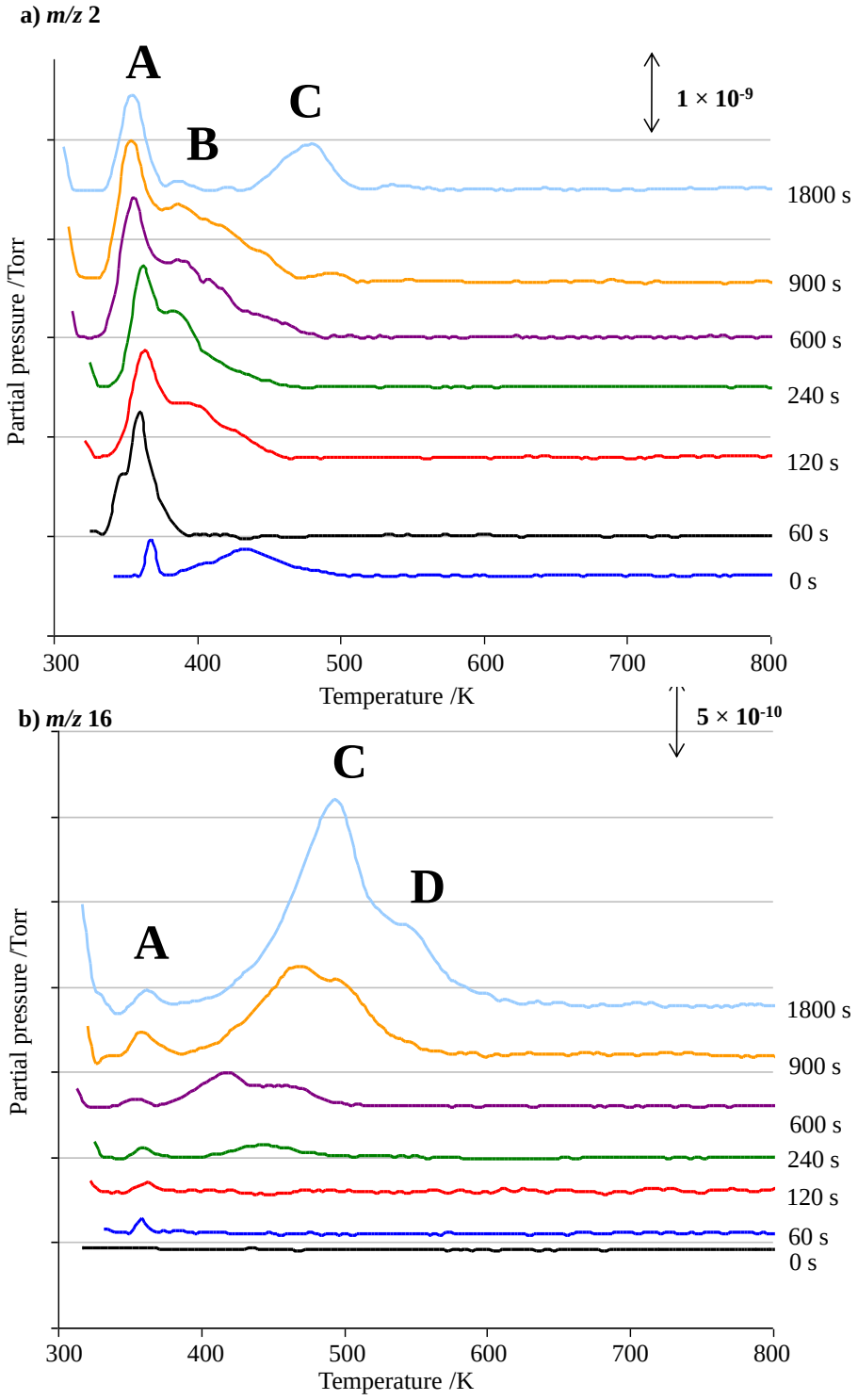
a) m/z 2
A
B
C
1 × 10-9
1800 s
900 s
600 s
240 s
120 s
60 s
0 s
Partial pressure /Torr
300
400
500
600
700
800
Temperature /K
b) m/z 16
C
D
A
5 × 10-10
1800 s
900 s
600 s
240 s
120 s
60 s
0 s
Partial pressure /Torr
300
400
500
600
700
800
Temperature /K

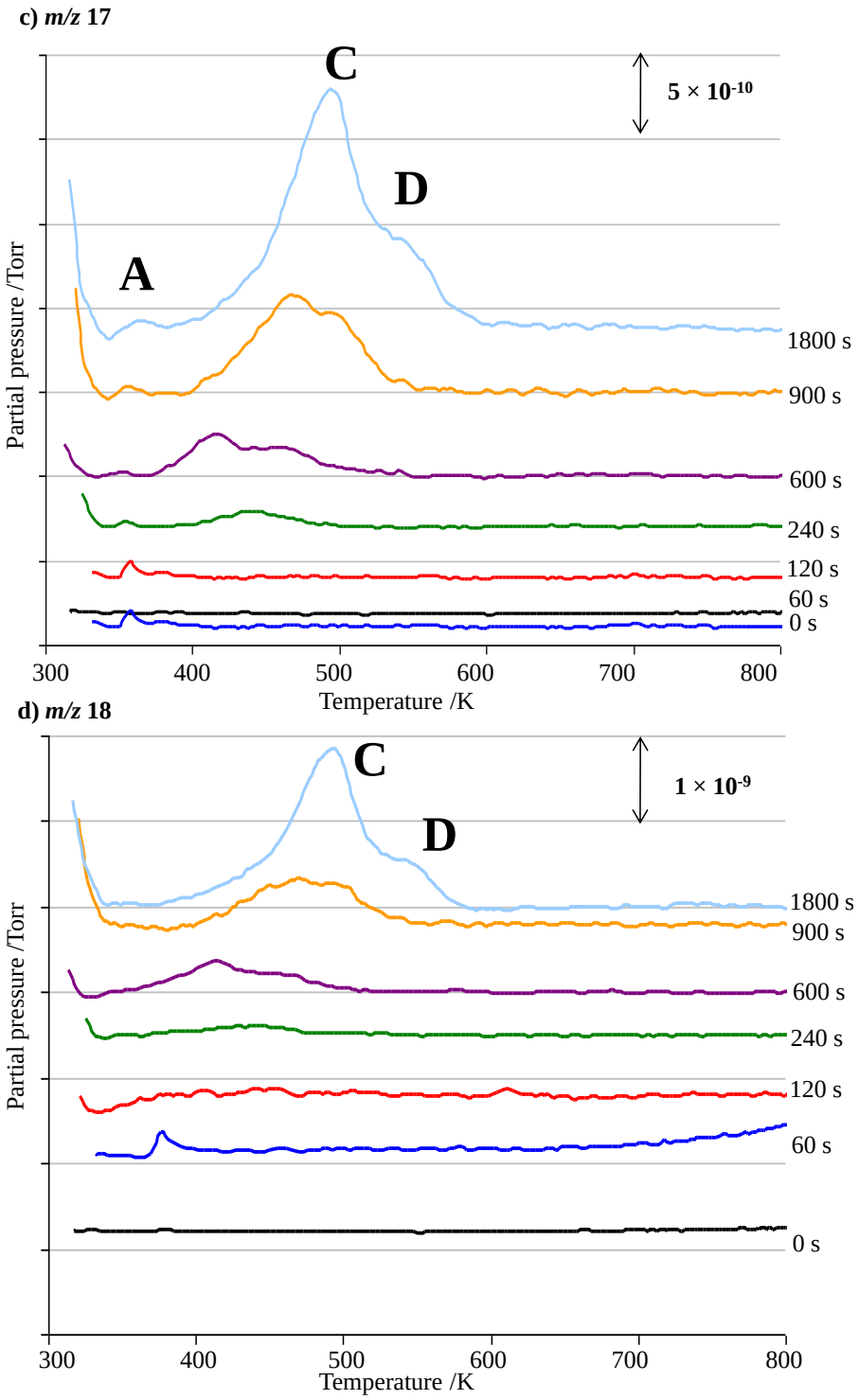
c) m/z 17
C
5 × 10-10
D
A
1800 s
900 s
600 s
240 s
120 s
60 s
0 s
Partial pressure /Torr
300
400
500
600
700
800
Temperature /K
d) m/z 18
C
1 × 10-9
D
1800 s
900 s
600 s
240 s
120 s
60 s
0 s
Partial pressure /Torr
300
400
500
600
700
800
Temperature /K

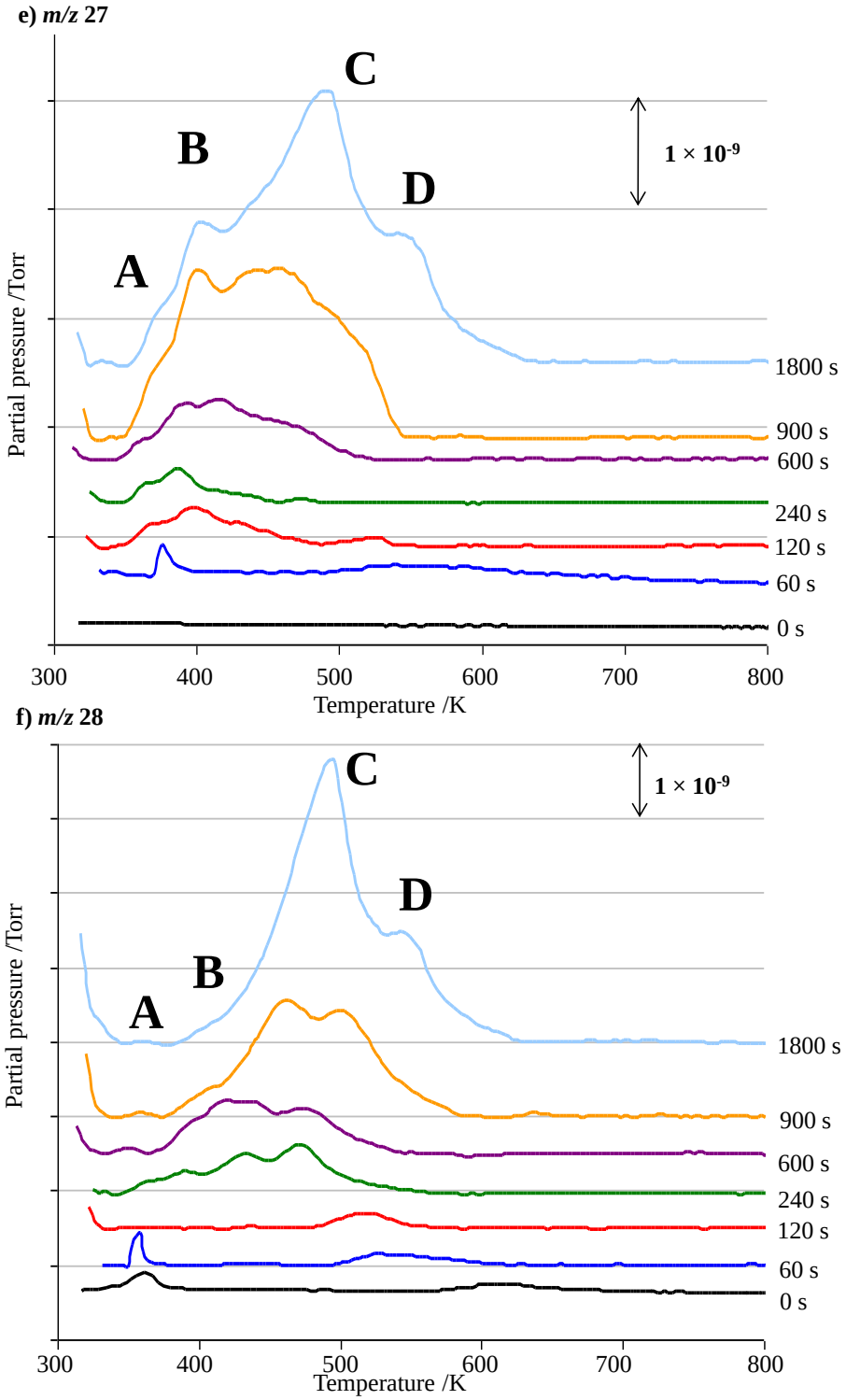
e) m/z 27
C
B
D
A
1 × 10-9
Partial pressure /Torr
1800 s
900 s
600 s
240 s
120 s
60 s
0 s
300
400
500
600
700
800
Temperature /K
f) m/z 28
C
D
B
A
1 × 10-9
Partial pressure /Torr
1800 s
900 s
600 s
240 s
120 s
60 s
0 s
300
400
500
600
700
800
Temperature /K

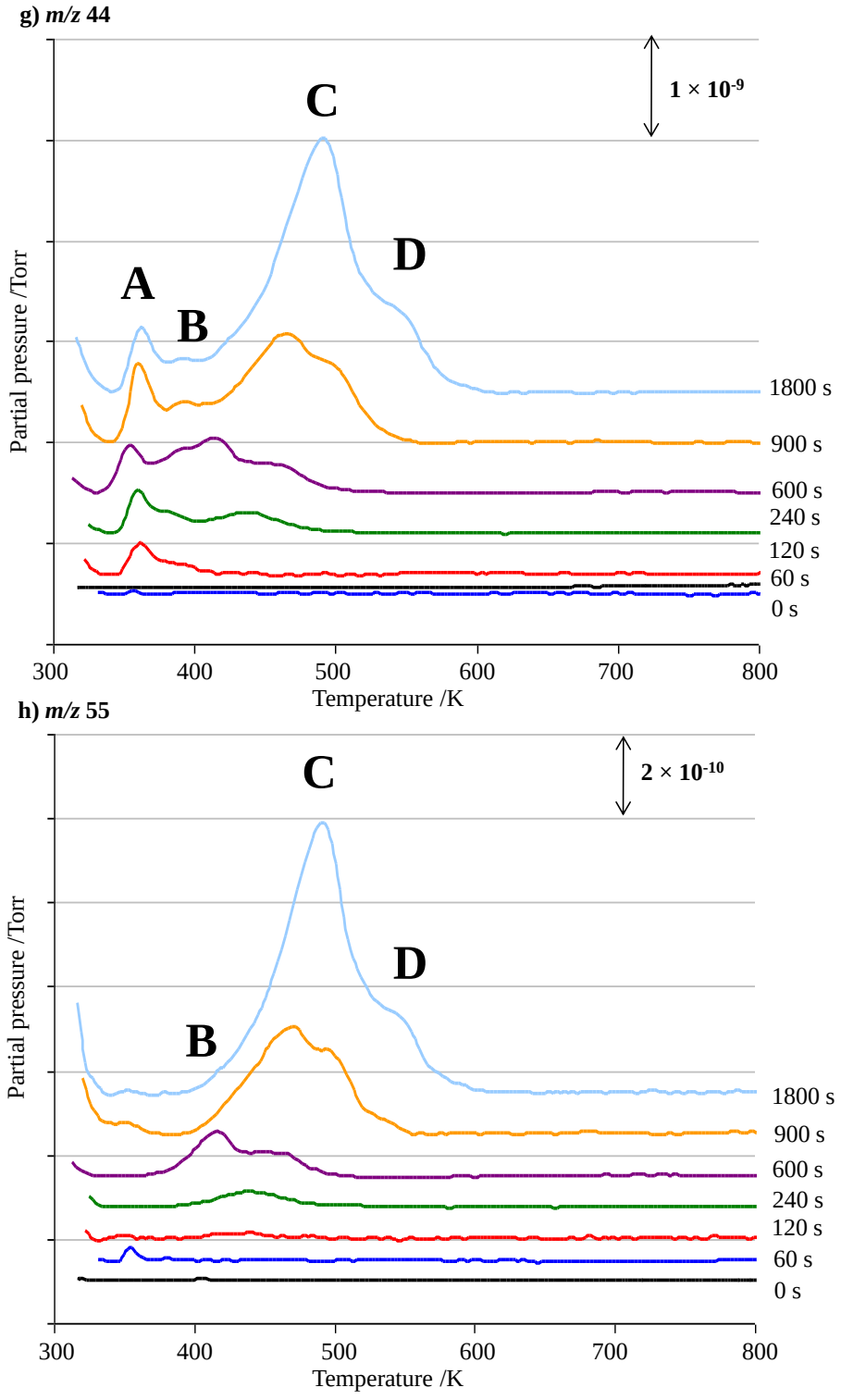
g) m/z 44
C
1 × 10-9
D
A
B
Partial pressure /Torr
1800 s
900 s
600 s
240 s
120 s
60 s
0 s
300
400
500
600
700
800
Temperature /K
h) m/z 55
C
2 × 10-10
D
B
Partial pressure /Torr
1800 s
900 s
600 s
240 s
120 s
60 s
0 s
300
400
500
600
700
800
Temperature /K

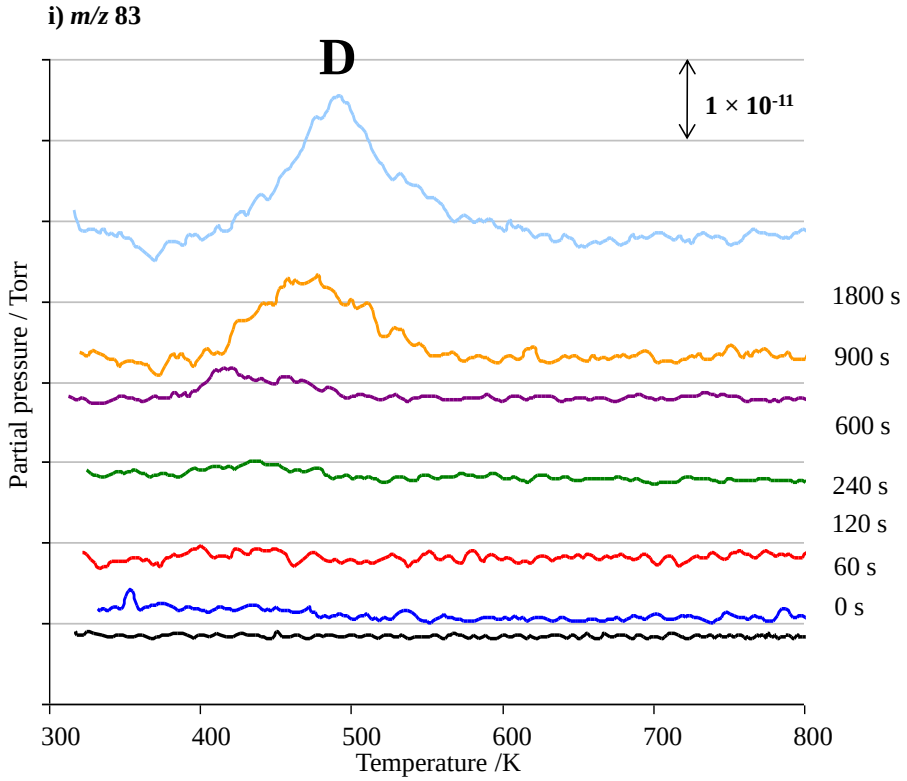

Fig. 5.8 UHV TPD spectra following *(S)*-lysine adsorption on Ni{111} at 373 K with increasing coverages, monitoring *m/z* values of a) 2 (H_2); b) 16 (O);c) 17 (NH_3); d) 18 (H_2O); e) 27 (HCN); f) 28 (CO, H_2CN or N_2); g) 44 (CO_2); h) *m/z* 55; and i) *m/z* 83.

Examining the TPD spectra, it is noted that the multilayer desorption peak **A**, present at 355 -365 K in the H_2, O, NH_3, CO and CO_2 spectra, occurs ~10 K higher than the equivalent feature following exposure at 300 K. This implies that the lysinate species adsorbed on the surface is slightly more stable on the substrate held at 373 K during dosing compared with 300 K. Peak **B**, which is present in the H_2, HCN, CO, CO_2 and *m/z* 55 TPD spectra, occurs at approximately 400 K, suggesting that lysine fragments desorb following decomposition on the surface, as for the experiments at a substrate temperature of 300 K. However, peaks **C** and **D** follow a different desorption pattern to the TPD at 300 K. Examining the desorption envelope of each *m/z* value shows that the TPD spectra for O, NH_3 and H_2O follow the same shape, as do *m/z* 28, CO_2 and *m/z* 55. The desorption peaks **C** and **D** are at higher temperatures (460-550 K region) and so, after consideration of a previous study by Idriss and co-workers of glycine on TiO_2{011} [29], it is feasible that lysine molecules polymerise by condensation. The condensation of amino acids into

peptides has been shown to occur at approximately 450 K [29]; in the present case a lysine polymer may form at a lower temperature due to a catalysed condensation reaction on the Ni surface, and desorb into fractions as well as partially decomposing by 550 K. The mass value at *m/z* 55 could have a possible structure of –CH-CO-N= or –CO-N=CH-, and *m/z* 83 could represent NH=CH-CO-N=CH-, another polymer fragment. The presence of coincident peaks for O, NH_3, H_2O, HCN, *m/z* 28 and CO_2 only serve to support the evidence for the presence of a polymer on the surface. H_2O would be likely to desorb due to the condensation reaction, and the remaining species as decomposition products from the polymer. The basic side chain is likely to decompose into HCN and H_2CN species. In this instance it would be difficult to accurately assign *m/z* 28 to one species as it is more likely to consist of CO as well as H_2CN fragments. A diagram for the possible formation of the lysinate polymer is shown in Figure 5.9.

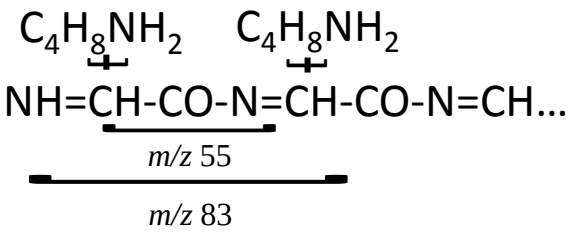

Fig. 5.9 Likely decomposition for lysinate polymer formed on Ni{111}.

5.3.3. UHV STM

The morphology of *(S)*-lysine on a Ni{111} surface at varying coverages at room temperature was imaged using STM. As was the case for the *(S)*-aspartic acid/Ni{111} system, we chose not to use LEED in our experiments due to its role in causing substantial beam damage to the lysinate overlayer on the Ni{111} surface. As lysine has been found to create ordered structures on Cu{001} and Cu{110} surfaces, lysine deposition onto the Ni{111} surface was carried out for the different coverages characterised in the RAIRS experiments in Section 5.3.1.1., in the hope that, despite the rapid accumulation of multilayers on the surface as shown by the TPD results, it may be possible to observe ordered overlayers on the substrate surface.

5.3.3.1 LOW COVERAGE STM OF *(S)*-LYSINE ON Ni{111} AT A SUBSTRATE TEMPERATURE OF 300 K

STM images of a clean Ni{111} surface and low coverage (10 s) of *(S)*-Lys on Ni{111} are shown in Figures 5.10a and b. With an extremely low coverage of lysine, clusters of disordered lysine are imaged on the Ni{111} surface (Figure 5.10b i) and ii)). Figure 5.10b i) shows that the adsorbate binds along step edges or on terraces at room temperature. On closer inspection, each individual protrusion represents a lysine molecule with a length of approximately 8.9 Å (measured from centre-to-centre distance in Figure 5.10b iii)). The apparent STM height of the molecules (~0.85 Å) suggests the formation of single molecule-layer islands. A closer inspection shows that more isolated species appear to decorate the step edges while clusters of lysine are more dominant on the terrace. The lateral interactions between molecules do not seem to be strong enough to stabilise any possible long-range ordering.

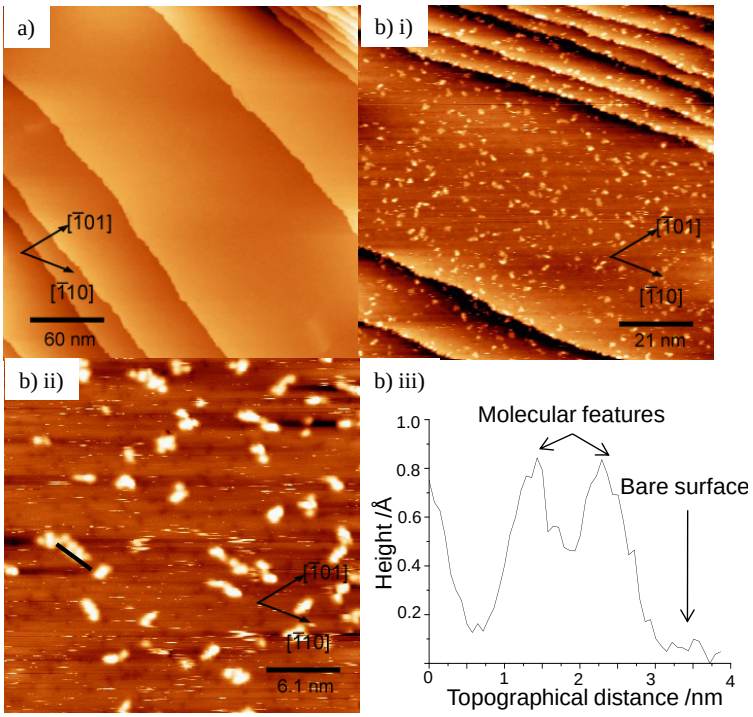

Fig. 5.10 a) STM image of clean Ni{111} i) 300 × 300 nm^2, 0.5 V, 1 nA; and b) 10 s *(S)*-lysine coverage i) 105 × 105 nm^2, -0.6 V, 0.6 nA; ii) 30.5 × 30.5 nm^2, -0.6 V, 0.6 nA; and iii) height profile from b)ii).

From analysis of the STM images in Figure 5.10, as well as the results from the TPD data of Section 5.3.2.1., a possible model for the growth of lysine on Ni{111} can be proposed. Volmer-Weber, or 3D island growth mode appears to occur on the surface, with atoms more strongly bound to each other than the substrate [33]. Figure 5.11 represents a model of the growth.

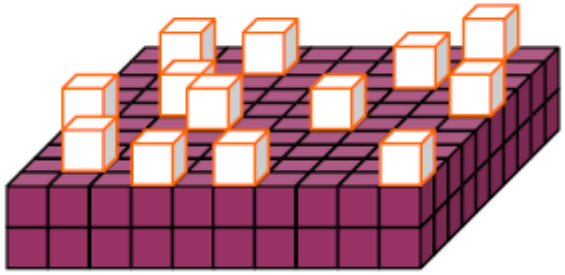

Fig. 5.11 Volmer-Weber growth mode. Adapted from [31].

5.3.3.2 MAA ADSORPTION ON LOW COVERAGE *(S)*-LYS ON Ni{111} AT A SUBSTRATE TEMPERATURE OF 300 K

Figure 5.12 a-c shows the Ni{111} surface after exposure of 5 L MAA (saturation coverage [26] with a low, submonolayer coverage of lysine. The STM image in Figure 5.12a indicates a significant contrast reversal, most likely caused by molecular motion under the STM tip [34 – 36]. This has most frequently been recorded previously for molecules which are only loosely attached to the metal substrate [36]. Molecules such as those are normally, due to their high mobility, undetectable by STM. If they become trapped under the STM tip their mobility can be diminished, which in turn gives rise to reverse contrast STM images [36]. A lower tip resistance can also aid in contrast reversal in STM as it causes a smaller tip-sample separation, and so traps the molecules under the tip more easily. The outcome, in the present case, is that the adsorbed lysine molecules appear as depressions in the substrate, and the mobile MAA molecules are imaged by the STM (Figure 5.12b and c). Unfortunately resolution of the unit cell could not be attained as the features are too poorly defined.

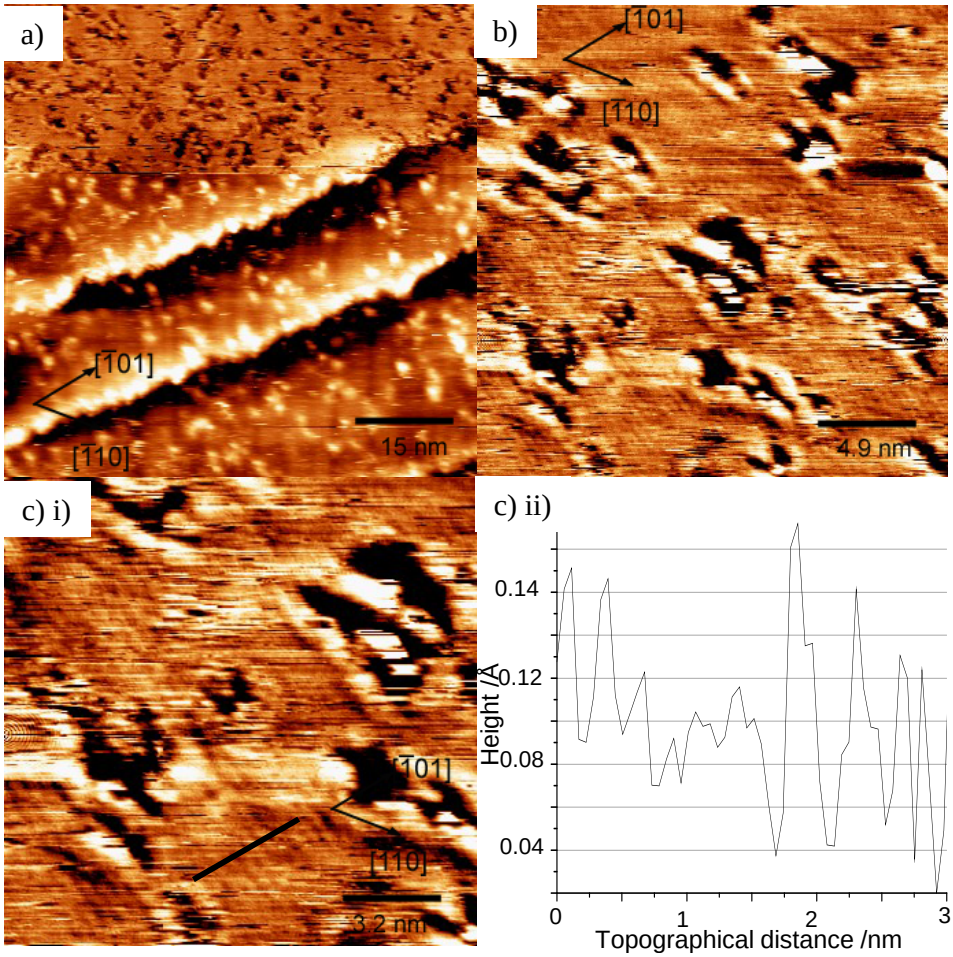

Fig. 5.12 STM images of a 1 L MAA dose on a low coverage of (S)-lysine on Ni{111} a) 75 × 75 nm^2, -1 V, 0.5 nA; b) 24.5 × 24.5 nm^2, -1 V, 1 nA c)i) 16 × 16 nm^2, -1 V, 1 nA and c) ii) line profile of c)i).

As illustrated in Figure 5.12b and c, chains of molecules running along the $[\bar{1}2\bar{1}]$ direction are present, with centre-to-centre distances of ~4.5 Å, and are assigned to MAA species as noted previously in STM studies by Trant *et al.* [37]. This suggests that the MAA molecules diffuse along a well-defined direction, and the distance between chains indicates that the MAA molecules adopt a configuration with the molecular plane perpendicular to the Ni surface, with no formation of 2D supramolecular assemblies with the *(S)*-lysine molecules. By examining the STM images further it is noted that, in spite of the lysine islands remaining on the surface, they are far more disordered than in Figure 5.10 and also smaller and more dispersed, suggesting that the incoming MAA molecules have disrupted the 3D islands. Comparing the STM data with the RAIRS spectra in Figure 5.5, it can be concluded

that the MAA molecules bond with their molecular plane perpendicular to the surface, predominantly on the terraces of the Ni{111} surface, and appear to have little interaction with the lysine modifier. This would suggest poor chiral recognition of the lysine molecules to influence the docking of methylacetoacetate.

5.3.3.3 HIGH COVERAGE STM OF *(S)*-LYSINE ON Ni{111} AT A SUBSTRATE TEMPERATURE OF 300 K

At high coverages of *(S)*-lysine on the Ni{111} surface, a saturated surface was imaged by STM (Figure 5.13a). No ordered structures have been observed at such a coverage. Although slight substrate step faceting can be observed at room temperature, the effects are much more apparent after annealing of the surface at 373 K, as shown in Figure 5.13b. Previous studies have shown that several amino acids have the capability to modify surface morphology, for example Gly, Ala and PheAla have all been shown to induce step faceting on Cu{001} [8,9,38]. Indeed, lysine showed chiral faceting on the Cu{001} surface, only after a gentle anneal to 430 K [2]. In the present case, we observe adlayer-induced step-faceting with steps reoriented into a saw-tooth arrangement lying at +15° to the <110> directions. Although the image does not show molecular resolution, at the very least it proves that lysine is adsorbed strongly enough to strongly alter the morphology of the Ni{111} substrate.

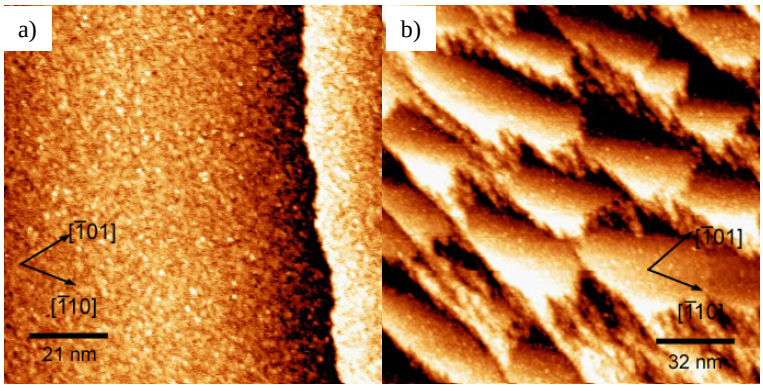

Fig. 5.13 a) STM image of a saturation coverage of (S)-lysine 105 × 105 nm^2, 0.24 V, 0.23 nA; and b) Saturation lysine coverage after annealing to 373 K 160 × 160 nm^2, 0.26 V, 0.43 nA.

STM images were not collected for MAA adsorbed onto the high coverage lysine surfaces as previous RAIRS results showed that MAA would not bind [27], indicating that the reactant molecules require an interaction with the substrate surface.

5.3.4.1. ADSORPTION OF *(S)*-LYSINE ON Ni{111} AS A FUNCTION OF MODIFICATION pH AT 300 K

Figure 5.14 shows the RAIR spectra of the *(S)*-lysine-modified Ni{111} single crystal at 300 K as a function of solution pH. Assignments are supported from research work by McQuillan and co-workers [1], and Pradier and co-workers [4,5]. Compared with IR data collected in solution, broadening of RAIRS peaks and possible wavenumber shifts are likely to occur due to the adsorbate interacting with the surface or due to intermolecular hydrogen bonding. Table 5.5 shows assignments of peaks at the four different pH values, chosen to represent differently charged species of *(S)*-lysine.

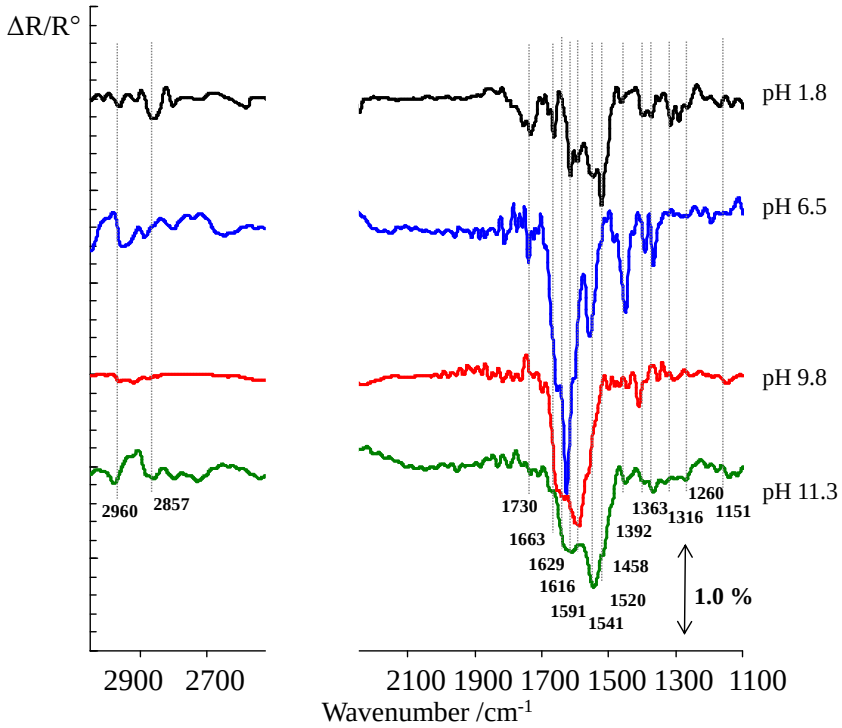

Fig. 5.14 RAIR spectra following adsorption of 10 mM *(S)*-lysine on Ni{111} at 300 K as a function of pH.

At pH 1.8, alongside absorption bands at 2960 and 2857 cm^{-1} which are present at all pH values and represent asymmetric and symmetric CH_2 stretches, strong absorption

bands are observed at 1730, 1663 and 1520 cm^{-1}. These bands can be attributed to the symmetric C=O stretch of the carboxylic acid group, and the asymmetric and symmetric deformation bands of the NH_3^+ groups respectively. The band at 1260 cm^{-1} represents the coupled C-O stretch and O-H bend, and thus the presence of these peaks confirms that the dicationic species of lysine is present on the Ni{111} surface at pH 1.8, as in Figure 5.1.

After modification of the surface with 10 mM *(S)*-lysine aqueous solution at pH 6.5, there is a change in the spectrum with a sharp band appearing at 1392 cm^{-1}, assigned to $\nu_s(COO^-)$, and an emergence of a sharper peak at 1556 cm^{-1}, representing the $\nu_{as}(COO^-)$. Vibrational peaks assigned to the NH_3^+ deformations remain present, and thus implies that the cationic species of lysine is present at pH 6.5. The dicationic species continues to exist in small fractions due to the continued presence of bands at 1739, 1654 and 1625 cm^{-1} which represent the carboxylic acid and protonated amino groups; nevertheless the cationic species appears dominant.

Treatment of the Ni{111} sample with *(S)*-lysine at pH 9.8 results in a broad IR active band from 1630 – 1520 cm^{-1}, including identifiable peaks at 1629 and 1591 cm^{-1}. These two peaks are assigned as $\delta_{as}(NH_3^+)$ and $\delta(NH_2)$ respectively. The broadness of the band is common due to the closeness in wavenumber of the two absorption bands, and frequently it is very difficult to observe both as separate peaks. In this study, good resolution of the IR bands has allowed identifiable peaks which are possible to assign. The presence of these peaks, alongside several remaining peaks, suggests that the lysine molecules are in their zwitterionic state, as observed in liquid phase studies [1].

Following modification with *(S)*-Lys aqueous solution at pH 11.25, a lack of peaks corresponding to $\delta(NH_3^+)$ confirm that lysine is in its anionic state, with both NH_3^+ groups deprotonated.

For all of the pH values studied, although the assumed form of lysine from solution work is mainly present, there are measurable fractions of species associated with lower pH values present in each case, suggesting that different lysine species are likely to coexist with each other on the surface. This observation is similar to that found in previous studies [5], where the best agreement to the form in solution occurred near to the isoelectric point of lysine where, almost exclusively, the zwitterionic form of lysine prevailed. It is suggested that the existence of intermolecular interactions between molecules in the first and second layers on the surface may result in the unexpected presence of peaks at certain pH values.

Ni{111}/*(S)*-Lys 300 K /wavenumbers in cm^{-1}				Assignment
pH 1.8	pH 6.5	pH 9	pH 11.3	
2960	2944	2960	2960	ν_{as} (CH_2)
2857	2883	-	2857	ν_s (CH_2)
1730	1739	-	-	ν_s (C=O)
1663, 1616	1654, 1625	1629	-	δ_{as} (NH_3^+)
-	-	1591	1611	δ (NH_2)
1541	1556	-	1543	ν_{as} (COO^-)
1520	-	-	-	δ_s (NH_3^+)
1458	1450	-	1447	δ (CH_2)
-	1392	1411	-	ν_s (COO^-)
1363	1363	1354	1366	CH symmetric bend
1316	-	-	1316	CH_2 wag
1260	-	-	-	ν(C-O) + δ(O-H)
-	-	1151	1151	NH_2 wag

Table 5.5 Assignments of RAIRS bands of *(S)*-lysine on Ni{111} at 300 K adsorption temperature as a function of pH.

5.3.4.2. ADSORPTION OF *(S)*-LYSINE ON Ni{111} AS A FUNCTION OF MODIFICATION pH AT 373 K

Figure 5.15 illustrates the adsorption of *(S)*-Lys onto the Ni{111} surface at a modification temperature of 373 K. The series of spectra are very similar to those at 300 K in terms of band intensities and peak positions. Peaks are present at pH 1.8 corresponding to the acidic COOH group as well as protonated NH_3^+ groups. At modification pH 6.5, peaks emerge corresponding to symmetric (1416 cm^{-1}) and

asymmetric (1599 cm^{-1}) $\nu(COO^-)$ bands, combined with deformation bands for NH_3^+, confirm that the lysine molecules are in their cationic form. Following modification at pH 9.8, lysine molecules are found to be in their zwitterionic state when adsorbed onto the Ni{111} surface, with a broadness of the absorption band centred at ~1640 cm^{-1}, which highlights the presence of NH_3^+ and NH_2 deformations. Finally, at modification pH 11.3 there is a decrease in the intensity of the NH_3^+ deformation bands which suggests that the anionic lysine species is predominantly present on the surface. However, as observed previously at the lower modification temperature, there are measurable amounts of other lysine species in each pH case suggesting that, after adsorption on the Ni{111} surface, the different lysine species can coexist with each other to an extent.

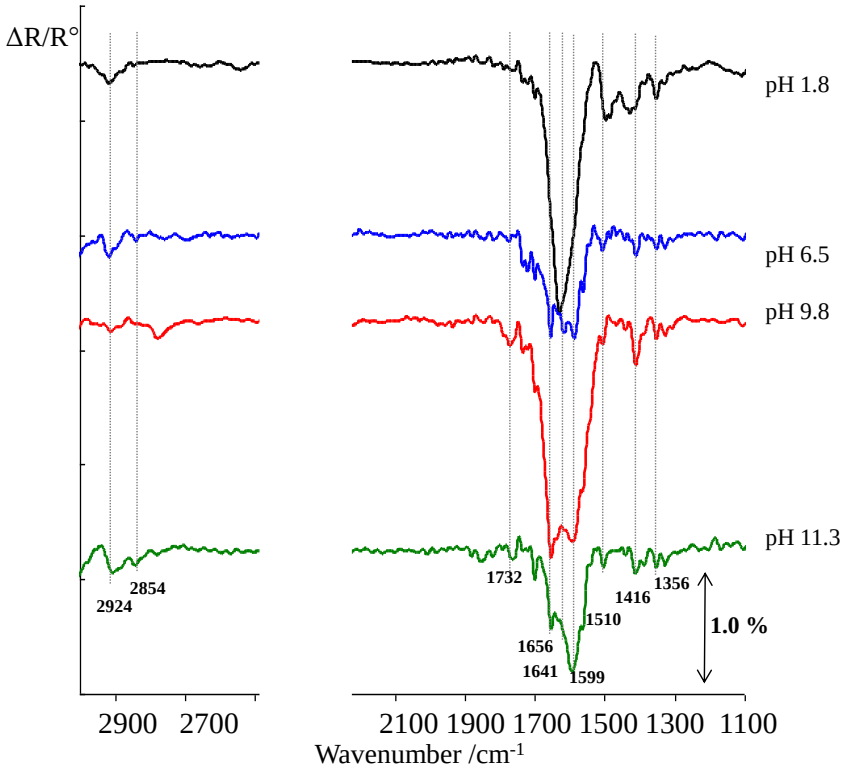

Fig. 5.15 RAIR spectra following adsorption of 10 mM *(S)*-lysine on Ni{111} at 373 K as a function of pH.

The increase of modification temperature from 300 K to 373 K does not appear to alter the effect of coexisting molecular species on the surface. Previously, it has been found in higher temperature glutamic acid studies that nickel glutamate salts are produced at low modification pH, and monosodium glutamate at higher pH values [31]. The present study shows this not to be the case for lysine, as the appearance of

NH_3^+ deformation bands at low pH values refute the idea that the N atoms may coordinate with Ni^{2+} ions. The increase in sodium ions as the solution pH is increased using aqueous NaOH is likely to influence the possibility of monosodium lysinate being produced at the higher pH values.

5.3.4.3 WATER WASH OF *(S)*-LYSINE MODIFIED Ni{111} AS A FUNCTION OF MODIFICATION pH AT 300 K AND 373 K

Figure 5.16a shows the RAIR spectra for the post-modification water wash of the Ni{111} surface after lysine modification at 300 K, whilst Figure 5.16b shows the RAIR spectra at 373 K modification temperature following a post-modification water wash.

In both modification temperature cases, the main lysine peaks reduce in intensity by approximately a factor of two to 0.5% which, when compared to the UHV RAIRS spectra in Figure 5.3 as well as the STM data in Section 5.3.3., suggests a coverage of approximately monolayer quantities of adsorbate over all pH values. This result is different to those found previously using *(R,R)*-tartaric acid as the modifier [40] and the *(S)*-aspartic acid studies in Section 4.3.1.2. For (*R,R)*-tartaric acid modified Ni{111}, a post modification rinsing step showed that the amount of modifier remaining on the surface depended on the modification pH, with lower modifier coverage at higher pH values. In Section 4.3.1.2., water wash of *(S)*-aspartic acid modified Ni{111} was shown to remove all detectable amino acid from the surface at intermediate pH values where enantioselectivity was greatest. Conversely, the current results show that the modification pH, and thus the dominant species of lysine on the surface, does not seem to affect its likelihood of remaining on the surface after the water wash.

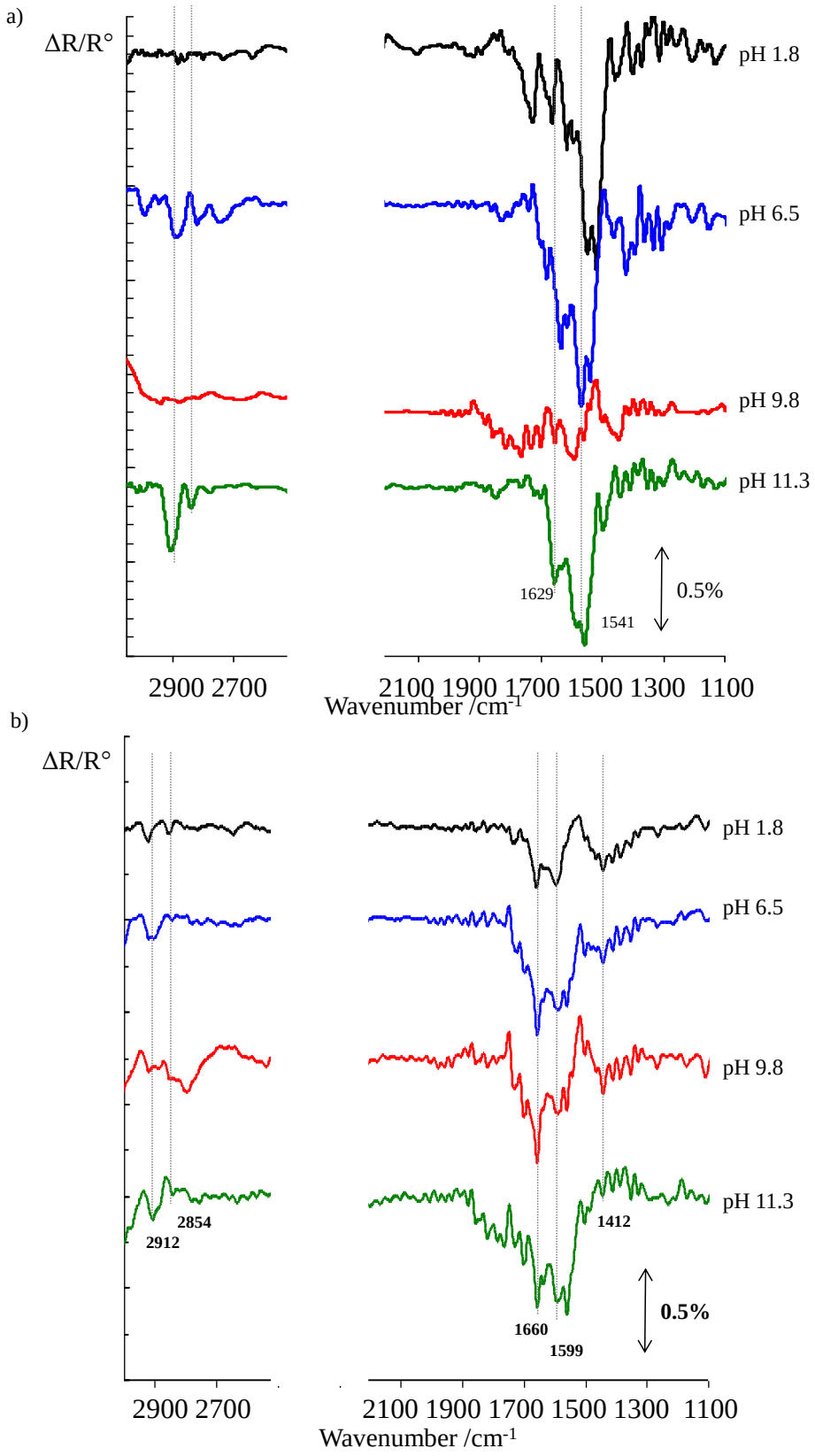

Fig. 5.16 RAIR spectra following a water wash of *(S)*-lysine modified Ni{111} at: a) 300 K, and b) 373 K, as a function of pH.

5.3.4.4. MAA ADSORPTION ON *(S)*-LYSINE-MODIFIED Ni{111} AS A FUNCTION OF MODIFICATION pH AT 300 K AND 373 K

Figure 5.17 shows the reactant MAA molecule existing in its two tautomeric forms, enol and diketo, with the OCH_3 group favouring the diketo and the CH_3 group favouring the enol form. IR matrix spectroscopy and DFT calculations have been carried out [33] to assign bands in the IR spectrum to the two different forms, the results of which have been previously shown in Table 3.2 in Section 3.3.2.2.

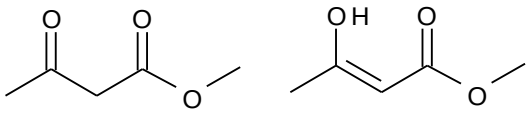

diketo form enol form

Fig. 5.17 Methylacetoacetate in its diketo and enol tautomeric forms

Figure 5.18a illustrates the RAIR spectra following adsorption of MAA onto the modified Ni{111} surface at 300 K modification temperature, whilst Figure 5.18b the MAA RAIR spectra at 373 K modification temperature.

In Figure 5.18a, at pH 1.8, the diketo form of MAA appears to be dominant on the modified and washed surface, with an intense peak at 1761 cm^{-1} ($\nu(C=O)_{keto}$), a shoulder at 1728 cm^{-1} ($\nu(C=O)_{keto}$) and a peak at 1440 cm^{-1} ($\delta(CH_2)_{keto}$) [41]. These three diketo peaks exist at similar intensities for all pH values, illustrating that the diketo form of MAA is present and, although there is a change of the lysine form from dicationic to anionic, there is no change to the modified surface to prefer the enol tautomer.

In Figure 5.18b, the diketo form of MAA is in excess at pH 1.8, with an intense peak at 1753 cm^{-1} and a shoulder at 1730 cm^{-1}. This form of MAA is present at all pH values, similar to the spectra recorded for lysine at 300 K (Figure 5.18a). However, at pH values of 9.8 and 11.3, the RAIRS data shows the presence of peaks at 1652 cm^{-1} ($\nu(C=O)_{enol} + \nu(C=C)_{enol}$) and 1253 cm^{-1} ($\nu(C\text{-}OH)_{enol}$), indicating the presence of the enol form [41].

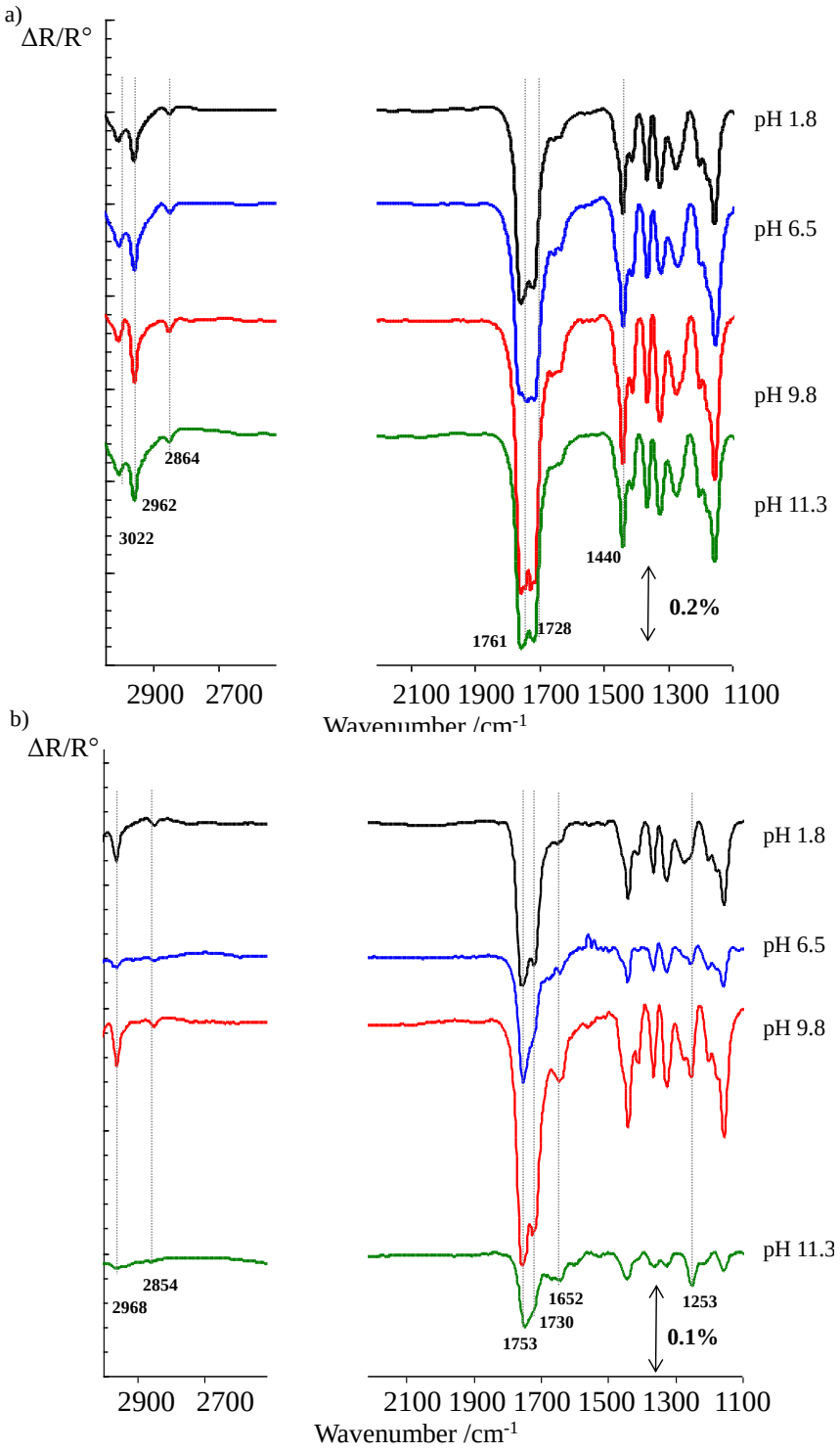

Fig. 5.18 RAIR spectra following immersion of *(S)*-lysine modified Ni{111} in an MAA:THF solution at 300 K as a function of pH (MAA spectra ratioed against the spectra recorded following the washing of the modified catalyst surface) a) modification temperature of 300 K and b) modification temperature of 373 K.

The MAA adsorption results in Figures 5.18 show that, with an increase of modification temperature, there is evidence that the presence of the enol form of MAA increases. This can be compared with results shown previously by Jones and Baddeley for *(S)*-glutamic acid in which the optimum modification procedure that produced the most enantioselective catalyst for the production of *(R)*-MHB adsorbed MAA primarily in its diketo form, and via its enol form for the production of *(S)*-MHB [39]. The clear enantiomeric switch in the MHB product was shown to depend on modification temperature, with the enol form dominant at higher temperatures, and the diketo MAA form at lower modification temperatures. For *(S)*-lysine, published catalytic work is limited to experiments carried out between the range of 273 – 313 K [13], and so it is of great interest that our RAIRS results, which were executed at greater modification temperatures, show a decrease in the diketo: enol ratio, predicting a possible switch from *(R)*- to *(S)*- MHB. This appears to illustrate a similarity between the behaviour of *(S)*-Glu on Ni{111} [39].

5.3.5 LIQUID-SOLID INTERFACE XPS STUDIES

5.3.5.1 ADSORPTION OF *(S)*-LYSINE ON Ni{111} AS A FUNCTION OF MODIFICATION pH AT 300 K

To investigate the coverage and the chemical nature of the modifier layer on the Ni foil, XPS measurements were performed on clean Ni, four samples of Ni foil modified with *(S)*-lysine at pH 1.2, 4.3, 10.2 and 12.4, four additional modified samples which were washed with distilled Millipore water, and finally four samples following MAA adsorption onto the *(S)*-lysine-modified Ni surface which had been subjected to the washing procedure. The full XP spectra for clean Ni{111}, recorded for components C 1s, N 1s, O 1s and Ni 2p, has been previously shown in Section 4.3.2.1. The results revealed the presence of a native oxide film on the unmodified Ni foil, as expected due to the preparation procedure when the sample was exposed to air while transferring from the furnace to the UHV apparatus. No special effort is

made to exclude air before and during the modification of working Ni catalysts [12], and thus the same level of attention is acceptable in the present experiments i.e. the foil surfaces are prepared outwith UHV conditions.

5.3.5.1.1 NICKEL 2p XP SPECTRA

A great deal of information can be garnered from the component scans on the changes to the environment of the Ni foil when modified and washed. Figure 5.19a-d shows the influence of modification pH on the Ni 2p XP spectra before and after modification, after washing with water and after exposure to MAA:THF solution.

The peak at 852.4 eV is attributed to the Ni^0 peak, whilst the peak at 854.0±0.4 eV represents NiO, 854.9 eV represents $Ni(OH)_2$, and 853.4 eV, 855.8±0.1 eV, 856.9 eV and 858.1 eV, although unassigned, are characteristic of the native nickel oxide [42]. Changes of intensities and positions of the Ni peak envelope are attributed to the chemical interaction between the *(S)*-lysine and MAA with the Ni surface. The attenuation of the Ni^0 peak is caused by the presence of the overlayer and Table 5.6 shows the estimated thicknesses *d*, in nm, of the lysine overlayer using the formula $d = -\lambda \cos\theta (\ln \frac{I}{I_0})$. The inelastic mean free path, λ, was calculated for an organic film of density of 1.12 gcm^3 (the density of *(S)*-lysine) [43] and the depths and volumes of the overlayer on each sample could be calculated, assuming a 1 cm^2 area for each Ni foil.

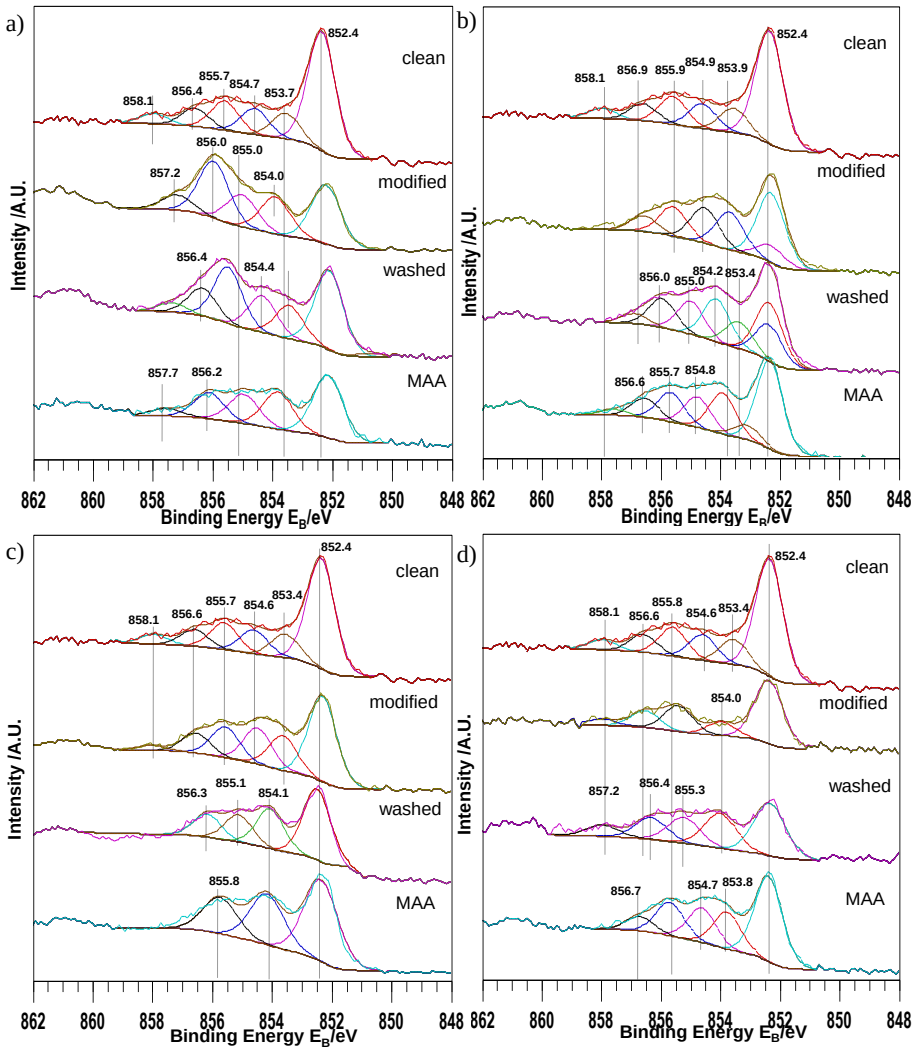

Fig. 5.19 Ni 2p XP spectra for modification of Ni with *(S)*-Lys at a) pH 1.2, b) 4.3, c) 10.2 and d) 12.4. Spectra are shown with reference to "clean" Ni foil treated in $H_2SO_{4\,(aq)}$ and annealed in 5% H_2/Ar. Spectra are offset for clarity.

	pH 1.2	water wash	MAA	pH 4.3	water wash	MAA	pH 10.2	water wash	MAA	pH 12.4	water wash	MAA
d /nm	2.42	2.0	2.63	2.25	1.69	1.75	2.04	1.83	1.86	3.4	3.2	2.31
V /10^{-8} cm^3	24.2	20.0	26.3	22.5	16.9	17.5	20.4	18.3	18.6	34	32	23.1

Table 5.6 Overlayer thickness (d) and volume (V) for *(S)*-lysine- modified Ni{111} foil.

The Ni 2p XP spectra show that, at all pH values, there is still a measurable amount of modifier present on the surface after the post-modification water wash, and thus confirms the RAIRS results in Section 5.3.4.3.

5.3.5.1.2 CARBON 1s XP SPECTRA

Figure 5.20a-d shows the C 1s XP spectra for the modified and washed Ni foil surfaces at each pH value. The most intense peak at 284.5 eV for each of the pH values is attributed to carbonaceous contamination. The peak at 285.8 eV represents C-OH or C-OR groups, the peaks in the region 287.3-287.7 eV represent the COOH or COOR groups, and the 288.9 eV peak is attributed to CO_3 species, and typical of the unmodified Ni surface [42]. The peaks at 286.7 eV ($O-CH_3$) and 288.6 eV (C=O ester) are related to the presence of MAA and their relative intensities can be used to confirm the tautomeric form of the pro-chiral molecule present.

For the modified and washed surfaces, it can be observed from the XPS data that a measurable amount of lysine remains on the surface at each pH. After adsorption of MAA, at pH 1.2, there is no increase in the C-OH peak compared with that on the modified surface, and the presence of the $O-CH_3$ and C=O peaks in a ratio of 1:2 suggests that the diketo form of MAA is present. At the remaining pH values, from pH 4.3 to 12.4, a similar situation occurs, with both peaks representing MAA existing in a 1:2 ratio and therefore agreeing with the previous RAIRS findings at 300 K modification temperature.

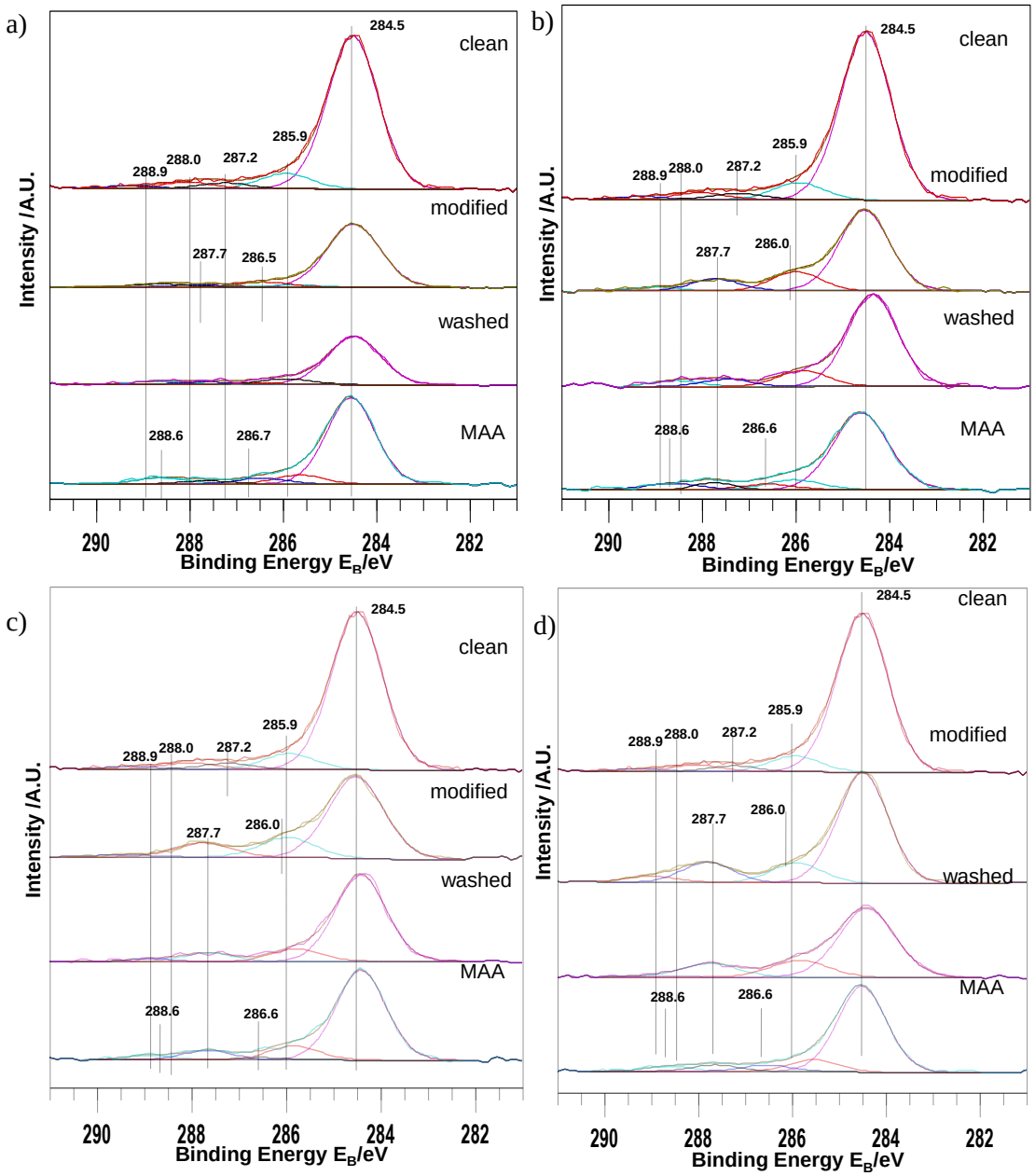

Fig. 5.20 C 1s XP spectra for modification of Ni with (S)-Lys at a) pH 1.2, b) 4.3, c) 10.2 and d) 12.4. Spectra are shown with reference to "clean" Ni foil treated in $H_2SO_{4\,(aq)}$ and annealed in 5% H_2/Ar. Spectra are offset for clarity.

	MAA C 1s signal at pH 1.2	MAAC 1s signal at pH 4.3	MAA C 1s signal at pH 10.2	MAA C 1s signal at pH 12.4
$I_{C\text{-}OH}$ (285.8 eV)	355.2	344.9	393.0	342.3
$I_{O\text{-}CH3}$ (286.7 eV)	182.9	192.4	55.3	189.1
$I_{C=O\ ester}$ (288.6 eV)	348.7	394.8	133.2	331.3
Ratio $O\text{-}CH_3$: $C=O_{ester}$	1:1.9	1:2.1	1:2.4	1:1.8

Table 5.8 Intensity of C 1s signal for Ni foil surfaces after modification, post-modification wash and MAA adsorption with respect to modification pH.

5.3.5.1.3 NITROGEN 1s XP SPECTRA

The N 1s region was originally monitored by XPS due to its sensitivity to the chemical state of the lysine molecules, as well as the relative simplicity of the spectra. It was thought that, similar to Section 4.3.2.2.3, a reliable estimation of the absolute concentration of lysine on the surface could be derived from peak intensity values. Unfortunately, due presumably to the mechanism of growth of lysine on the Ni surface, the N 1s spectra proved difficult to analyse. From the Ni 2p XP spectra results in Table 5.6, it is observed that lysinate layer thicknesses of ~2 nm (i.e. multilayers) remain even after washing of the surface. From the UHV-STM data in Section 5.3.2.1., it was established that stable 3D islands formed on the surface at sub-monolayer coverages. If these islands also form in the liquid-solid interface experiments, this would imply that the lysinate layer is stable enough to remain on the surface after washing and thus attenuate the N 1s signal to give XPS data which is not exclusively a measure of the surface nitrogen after washing (Figure 5.21). This addresses the ambiguity found for the 399.4 eV peak that the intensities alluded to seemingly less nitrogen species present after washing than on the clean surface.

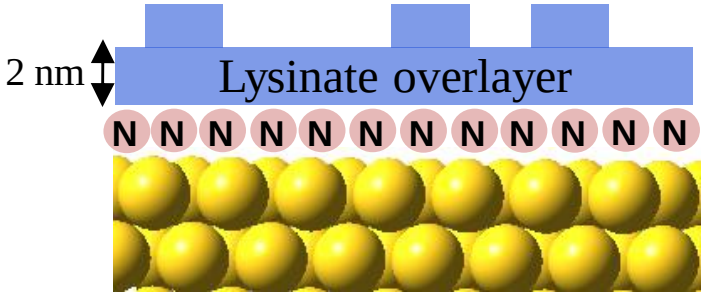

Fig. 5.21 Model of washed *(S)*-lysine-modified Ni surface showing surface nitrogen species. Attenuation of the N 1s XP peak for the surface nitrogen at 399.4 eV caused by the presence of the islands and overlayer of the adsorbate.

Chlorine 2p and 2s XP spectra were recorded but are not shown as the results do not attest to the possibility of chlorine acting as a site blocker on the modified surface. Although the presence of Cl is observed by XPS, the source of the signal is ambiguous as traces of chlorine can also be present in glassware.

5.4 IMPLICATIONS FOR ENANTIOSELECTIVE CATALYSIS AND CONCLUSIONS

As a potential modifier in the Ni catalysed MAA hydrogenation, lysine scores relatively well in catalytic studies. However, from the results found in this chapter, it is difficult to assign a mechanism to the modification of the surface and subsequent hydrogenation. The major conclusions drawn from the experimental data are that lysine binds to the Ni{111} surface with a high sticking probability, most likely growth in the form of 3D islands before the saturation of the monolayer, and exists in its expected form depending on solution pH, with some minor presence of other speciation forms. A water wash of the surface did not appear to remove the entire lysine adsorbate layer at any pH value, as opposed to aspartic acid in Chapter 3, but showed only a decrease in the signal for RAIRS and XPS, suggesting merely a removal of the multilayer lysine (its presence verified by TPD). In the UHV studies, MAA appeared to have no notable interaction with the modifier, prefer to adopt both tautomer forms on the surface, as previously observed for MAA on unmodified Ni{111}. Furthermore, at the liquid-solid interface, the diketo form of MAA appeared dominant on the surface at 300 K regardless of the pH of the lysine solution. This would suggest that the form of lysine present did not have an

influence over the preferred tautomeric form of MAA, due to non-interaction. The process of extensive faceting occurs, as shown in Section 5.3.3.3, but at saturation coverages of lysine, when MAA is shown not to bind and so, from these results, it would be unwise to suggest that chiral faceting provides the source of chiral recognition for the β-ketoester. In the absence of a recorded direct interaction between the modifier and the reactant, any chiral recognition present must originate from interactions mediated by the nickel metal substrate which do not require intermolecular H-bonding between modifier and reactant [44].

5.5 REFERENCES

[1] A.D. Roddick-Lanzilotta, P.A. Connor & A.J. McQuillan, *Langmuir,* **14** (1998) 6479
[2] X. Zhao, R.G. Zhao & W.S. Yang, *Langmuir,* **16** (2000) 9812
[3] X. Zhao, *Journal of the American Chemical Society,* **122** (2000) 12584.
[4] V. Humblot, C. Methivier, R. Raval & C-M. Pradier, *Surface Science,* **601** (2007) 4189
[5] V. Humblot, C. Methivier & C-M. Pradier, *Langmuir,* **22** (2006) 3089.
[6] T. Eralp, A. Shavorskiy & G. Held, *Surface Science,* **605** (2011) 468.
[7] F. Tielens, V. Humblot & C-M. Pradier, *Surface Science,* **602** (2008) 1032.
[8] X.Y. Zhao, R.G. Zhao, W.S. Yang & T. Sakurai, *Surface Science,* **424** (1999) L347
[9] X.Y. Zhao, R.G. Zhao & W.S. Yang, *Surface Science Letters,* **442** (1999) L995.
[10] W.Y. Cheong & A.J. Gellman, *Journal of Physical Chemistry C,* **115** (2011) 1031.
[11] S. Nakai & F. Yoneda, *Bioorganic & Medicinal Chemistry Letters,* **11** (2001) 1383
[12] Y. Izumi, *Advanced Catalysis,* **32** (1983) 215.
[13] Y. Izumi, M. Imaida, H. Fukawa & S. Akabori, *Bulletin of the Chemical Society Japan,* **36** (1963) 155
[14] I. Horcas, R. Fernández, J. M. Gómez-Rodríguez, J. Colchero, J. Gómez-Herrero & A. M. Baro, *Review of Scientific Instruments,***78**, (2007) 013705.
[15] X. Dou, Y.M. Jung, H. Yamamoto, S. Doi & Y. Ozaki, *Applied Spectroscopy,* **53** (1999) 133.
[16] S. Stewart & P.M. Fredericks, *Spectrochimica Acta Part A,* **55** (1999) 1641.
[17] D.H. Williams & I. Fleming, *Spectroscopic Methods in Organic Chemistry,* **3rd Ed,** McGraw-Hill Book Company (UK) Ltd, Ch. 2, 35-73
[18] J. Jones, *Amino Acid and Peptide Synthesis,* Oxford University Press, 2002, 42.
[19] A. Vallee, V. Humblot & C-M. Pradier, *Accounts of Chemical Research,* **43** (2010) 1297
[20] A. Hatta, Y. Moriya & W. Suëtaka, *Bulletin of the Chemical Society Japan,* **48** (1975) 3441.
[21] R. G. Nuzzo, L.H. Dubois & D. L. Allara, *Journal of the American Chemical Society,* **112** (1990) 558
[22] C.E.D. Chidsey & D.N. Loiacono, *Langmuir,* **6** (1990) 682
[23] J. Williams, S. Haq & R. Raval, *Surface Science,* **368** (1996) 303.
[24] F. Gao, Z. Li, Y. Wang, L. Burkholder & W.T. Tysoe, *Journal of Physical Chemistry C,* **111** (2007) 9981.
[25] F. Gao, Z. Li, Y. Wang, L. Burkholder & W.T. Tysoe, *Surface Science,* **601** (2007) 3276
[26] T.E. Jones & C.J. Baddeley, *Surface Science,* **519** (2002) 237.
[27] T.E. Jones & C.J. Baddeley, *Langmuir,* **22** (2006) 148.
[28] K. Christmann, O. Schober, G. Ertl & M. Neumann, *Journal of Chemical Physics,* **60**(1974) 4528
[29] J.N. Wilson, R.M. Dowler & H. Idriss, *Surface Science,* **605** (2011) 206
[30] P. Lofgren, A. Krozer, J. Lausmaa & B. Kasemo, *Surface Science,* **370** (1997) 277
[31] D. Holtkamp, M. Kempken, P. Kliisener & A. Benninghoven, *Journal of Vacuum Science & Technology A,* **5** (1987) 2912
[32] T. Eralp, A. Shavorskiy, Z.V. Zheleva, G. Held, N. Kalashnyk, Y.Ning & T.R. Linderoth, *Langmuir,* **26** (2010) 18841.

[33] E. Bauer, *Zeitschrift für Kristallographie*, **110** (1958) 372.
[34] M. Böhringer, W-D. Schneider, R. Berndt, K. Glöckler, M. Sokolowski & E. Umbach, *Physical Review B,* **57** (1998) 4081.
[35] M. Böhringer, K. Morgenstern, W-D. Schneider, R. Berndt, *Surface Science,* **457** (2000) 37.
[36] Q. Guo, J. Yin, R.E. Palmer, N. Bampos & J.K.M. Sanders, *Chemical Physics Letters,* **402** (2005) 121.
[37] A.G. Trant & C.J. Baddeley, *Langmuir*, **27** (2011), 1788.
[38] W. Hao, Z. Xue-Ying, Z. Ru-Guang & Y. Wei-Sheng, *Chinese Physics Letters,* **18** (2001) 445.
[39] T. E. Jones & C. J. Baddeley. *Journal of Physical Chemistry C,* **111** (2007) 5500.
[40] T.E. Jones & C.J. Baddeley, *Journal of Physical Chemistry C,* **111** (2007) 17558.
[41] N.V. Belova, H. Oberhammer & G.V. Girichev, *Journal of Physical Chemistry A,* **108** (2004) 3593
[42] B.V. Crist, Handbook of Monochromatic XPS spectra: The Elements and Native Oxides **J Wiley & Sons Inc, Chichester, UK, 2000**.
[43] S. Tanuma, C.J. Powell, D.R. Penn, *Surface and Interface Analysis,* **21** (1994) 165.
[44] S. Blankenburg & W.G. Schmidt, *Physical Review B,* **78** (2008) 233411.

Chapter 6

Characterisation Studies of (S)-lysine and (S)-aspartic acid on Au{111}

6.1 INTRODUCTION

The comparatively large study of amino acid behaviour on reactive metals in terms of their applicability as chiral modifiers in catalysis has been covered in detail in Chapters 3 to 5. Well-ordered amino acid layers on a variety of surfaces also have a great number of applications within the biomaterial and biosensor industries, not least because the molecules represent the most basic building blocks of a protein and so provide the means of developing a simple model of the interaction between a surface and a protein [1 – 7]. In Chapters 3 to 5, both *(S)*-Asp and *(S)*-Lys were tested in order to elucidate the mechanism of their operation as chiral modifiers in Ni-based catalysis. As a consequence of these investigations, both amino acids were also tested on Au, a metal often used in heterogeneous catalysis either on its own or to dilute the activity of other elements as well as alter the selectivity of reactions [8]. This was carried out primarily as a control experiment, following a similar unsuccessful attempt in previously published work to adsorb *(S)*-Glu on Au{111} [9], and prior to the investigation of amino acids adsorbed on a bimetallic Au{111}/Ni surface.

6.1.1. Au{111} SURFACE RECONSTRUCTION

The atomic scale structure of clean reconstructed Au{111} is well understood and reported on extensively [10 – 14]. It is the only fcc metal that shows a reconstruction of the close-packed {111} surface at room temperature. The top layer of atoms is laterally compressed along the $[1\bar{1}0]$ direction and the reconstruction pushes the gold

atoms sideways along the $[1\bar{1}1]$ direction towards hcp packing. At the boundary of hcp and fcc domains, atoms are squeezed out of position to fit 23 atoms into a length only large enough for 22 atoms in the bulk, causing a $22 \times \sqrt{3}$ reconstruction. This results in the formation of two ridges per unit cell. Discommensuration lines are formed in the transition regions between fcc and hcp sites 0.2 Å higher than the fcc sites, with transition from each domain taking place via bending of these lines by ±120°, hence the so-called herringbone reconstruction to offer stress relief to the surface (Figure 6.1). The reconstruction has been observed under UHV [10], air [13], and electrochemical [14] conditions. Due to the dominance of the herringbone reconstruction, any disruption to the order of the atomic arrangement will result in a change to the reconstruction. The herringbone form of Au{111} has been found to be stable up to 1250 K, however other non-equilibrium forms have also been discovered [15].

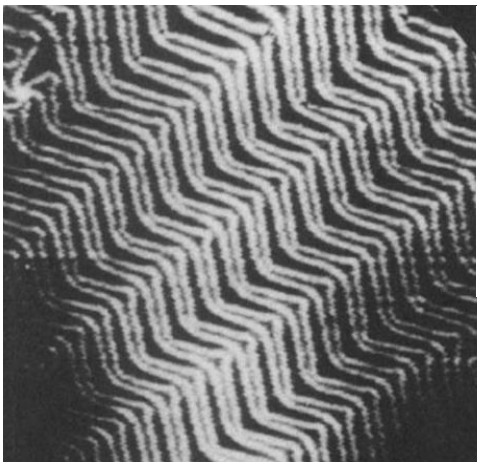

Fig. 6.1 STM image of reconstruction on a Au{111} surface from the first comprehensive STM study by Barth *et al.* Taken from [10].

6.1.2. Au{111} NANOFINGER FORMATION

The formation of nanofingers on a clean Au surface is a reported example of a non-equilibrium structure. Gold fingers several nanometres wide have been reproducibly formed by inducing a high localised electric field between the STM tip and the surface, with several studies by Palmer and co-workers carried out to elucidate direction of nanofingers and thermal stability [15-17]. It was verified that the images collected were not induced by scanning effects as the fingers did not align in the STM scan direction, but preferred to exclusively orientate themselves in one of three $< 1\bar{1}0 >$ directions, following the labelling of the herringbone. Initially, toothlike

structures which correlate with the reconstruction pattern were found to form (Figure 6.2 a) [15], before fingers developed aligned along a certain direction (Figure 6.2 b).

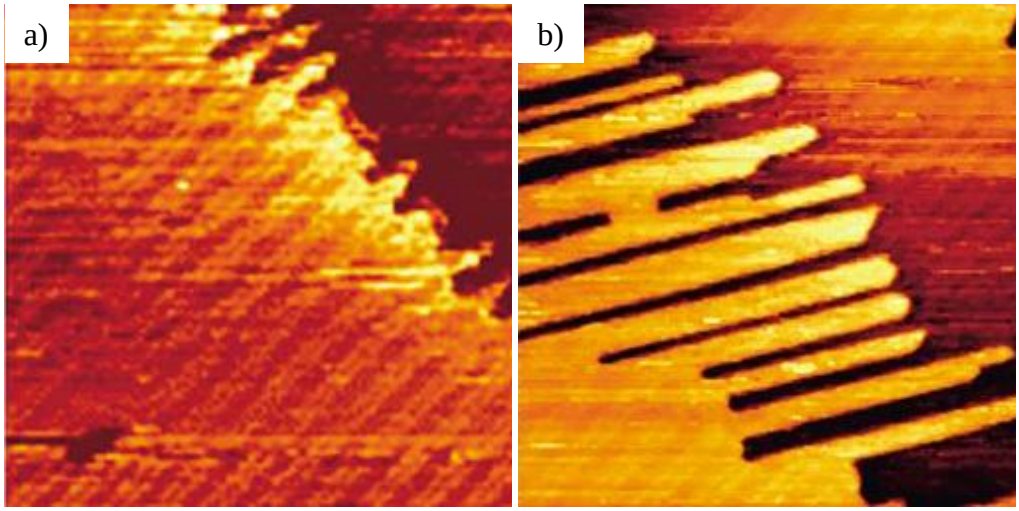

Fig. 6.2 STM images of the formation of nanofingers on a Au{111} surface: a) the sawtooth arrangement and b) the formation of nanofingers. From [15].

In the studies by Palmer [15-17], the initial formation of the fingers was solely due to extraction of atoms in the topmost surface layer from the Au step edges due to high field conditions between sample and tip. Subsequent atom attachment to the fingertips occurred at more typical tunnelling conditions.

6.1.3. AMINO ACID DEPOSITION ON GOLD

Previous work by Benninghoven and co-workers on secondary ion emission from amino acid overlayers on metals suggested only a physisorptive bond character exists between noble metals such as Au, and amino acids without a sulfur containing group, such as the *(S)*-glutamic acid study [9], due to a low desorption temperature [18]. Only sulfur-containing amino acids such as cysteine [19] and methionine [20] have previously been shown explicitly to strongly chemisorb to Au, via the formation of a Au-S bond, with evidence that both COOH and NH_2 groups also interact weakly with the surface (Figure 6.3).

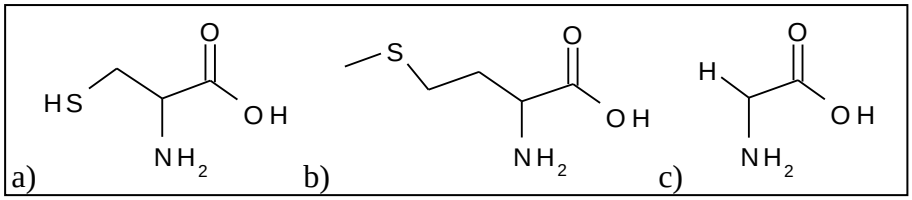

Fig. 6.3 a) cysteine, b) methionine and c) glycine.

Controversially, Yang and co-workers found that bonding of glycine on Au, an amino acid with no sulfur-containing functional group (Figure 6.3c), caused significant modification of the herringbone reconstruction, as well as the adsorbate glycine forming 2D gas phases, chain phases and solid phases on the Au surface at varying coverages, which suggested either a degree of chemisorptive behaviour (if the overlayers were commensurate with specific directions of the substrate [21]) or stabilising intermolecular interactions.

6.1.4. AIM OF RESEARCH

This chapter aims to investigate the deposition of *(S)*-aspartic acid and *(S)*-lysine on a Au{111} surface under UHV conditions. The use of the chemically inert Au substrate enables intermolecular interactions between lysine and aspartic acid molecules to be observed without too strong an influence from the substrate, as a more reactive metal could easily modify one or more of the functional groups [18].

We postulate that *(S)*-aspartic acid may interact differently to *(S)*-lysine on the Au{111} surface due to the effect of the variation in side chains. UHV techniques including RAIRS, high resolution electron energy loss spectroscopy (HREELS) and STM are employed to detect and characterise any species on the surface.

6.2 EXPERIMENTAL

6.2.1 UHV STM AND RAIRS EXPERIMENTAL CONDITIONS

Cleaning of the Au{111} single crystal is carried out in the preparation chamber of Chamber 1 (see Section 2.8) by cycles of argon ion bombardment (1.5 kV) and

annealing to 893 K until a characteristic herringbone LEED pattern is observed and STM indicated the presence of a clean surface exhibiting the ($\sqrt{3} \times 22$) herringbone reconstruction. The sample is then transferred to the RAIRS chamber and a background reference spectrum is taken of clean Au{111}, followed by sublimation of *(S)*-lysine (Sigma-Aldrich ≥98.0%) or *(S)*-aspartic acid (Fluka Biochemika 97%). Subsequent RAIRS spectra were recorded in real time to identify the formation of the required amino acid coverage, and represented as a ratio to the clean surface background spectrum. After completion of RAIRS the sample was transferred to the STM chamber where data were taken in constant current mode using an electrochemically etched W tip. All STM images were acquired at room temperature.

6.2.2. UHV HREELS EXPERIMENTAL CONDITIONS

Specular HREELS experiments were carried out in a second vacuum chamber (Chamber 3). The Au{111} sample was cleaned as previously with cycles of argon ion bombardment and annealing, and the cleanliness checked by LEED. Maximum likelihood-based resolution enhancement methods were used to recover the spectrum from broadening by the instrument, leading to an improved resolution of *ca.* 60 cm^{-1} [22].

6.2.3. DFT CALCULATION CONDITIONS

For the periodic DFT calculations carried out for the proposed lysine phase on Au{111}, the SIESTA program was utilised, employing the PBE functional. For the lysine molecule, a numerical split-valence PAO basis set with polarisation functions (SVP) and Troullier-Martins pseudopotentials were used. The Au{111} surface was modelled by two close-packed layers of gold atoms in the geometry of the optimised bulk, in a unit cell of 25 Å in the z-direction. For the lower Au layer, an SVP basis set was employed, whilst for the surface layer a diffuse basis function was added.

6.3 RESULTS AND DISCUSSION

6.3.1. ADSORPTION OF (S)-ASPARTIC ACID ONTO Au{111} AT 300 K

RAIRS experiments were carried out on *(S)*-aspartic acid modified Au{111} and it can be clearly observed that, after a 1280 s dose (similar to the *(S)*-aspartic acid coverage on the Ni{111} surface in Section 3.3.1.1.), no new features were noted, with only a slight miscancellation from the gas phase water bands (Figure 6.4a). This is contradictory to the Ni{111} RAIRS and STM results where a similar dose resulted in extensive adsorption on the metal surface. To verify the lack of *(S)*-Asp adsorption, several STM images were collected (one example shown in Figure 6.4b) and at no time did any of the scanned regions show amino acid adsorption, only the characteristic herringbone reconstruction. Due to the similarity in structure and side group to glutamic acid, it is expected that *(S)*-aspartic acid physisorbs to the Au{111} surface, with desorption below room temperature. These results offer conclusive evidence that *(S)*-Asp does not adsorb onto Au{111} under UHV conditions at room temperature.

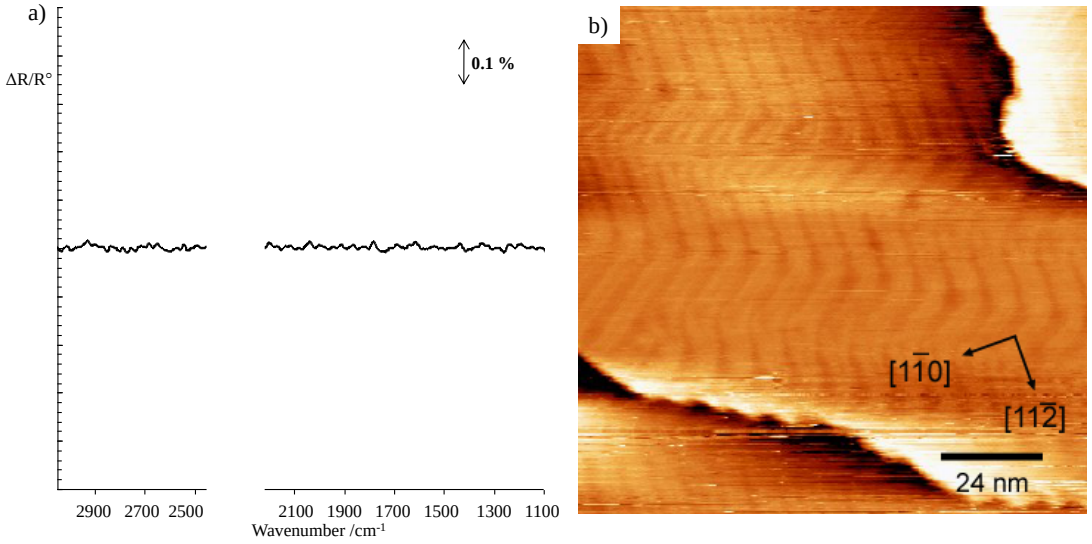

Fig. 6.4 RAIRS and STM data of a 1280 s coverage of *(S)*-aspartic acid adsorbed onto Au{111} at room temperature: a) RAIRS data showing no adsorption bands b) STM image 120 ×120 nm^2; -0.92 V, 0.9 nA.

6.3.2 ADSORPTION OF (S)-LYSINE ONTO Au{111} AS A FUNCTION OF COVERAGE AT 300 K BY UHV RAIRS AND HREELS

To test the possibility of *(S)*-Lys adsorbing on Au at 300 K, a preliminary RAIRS experiment of a saturated surface was carried out. Interesting results followed, with the appearance of several IR active bands associated with lysine adsorption, and so further RAIRS experiments were undertaken as a function of increasing *(S)*-lysine exposure. The HREELS technique was also used, firstly as it can be used as a match of peak assignments from the RAIRS data, and secondly as it allows recognition of peaks in the low frequency regime which is inaccessible in the RAIRS experiment. HREELS provides a means of identifying low wavenumber metal-adsorbate bonds, thus allowing greater conformation of the most likely orientation of the lysine molecule at low and high coverages. The Au{111} sample was exposed to *(S)*-Lys and the RAIRS and HREELS data as a function of increasing coverage at 300 K is shown in Figure 6.5, with peak assignments given in Table 6.1. HREELS data are shown in the bottom section of the graph, whilst RAIRS data are shown in the top section.

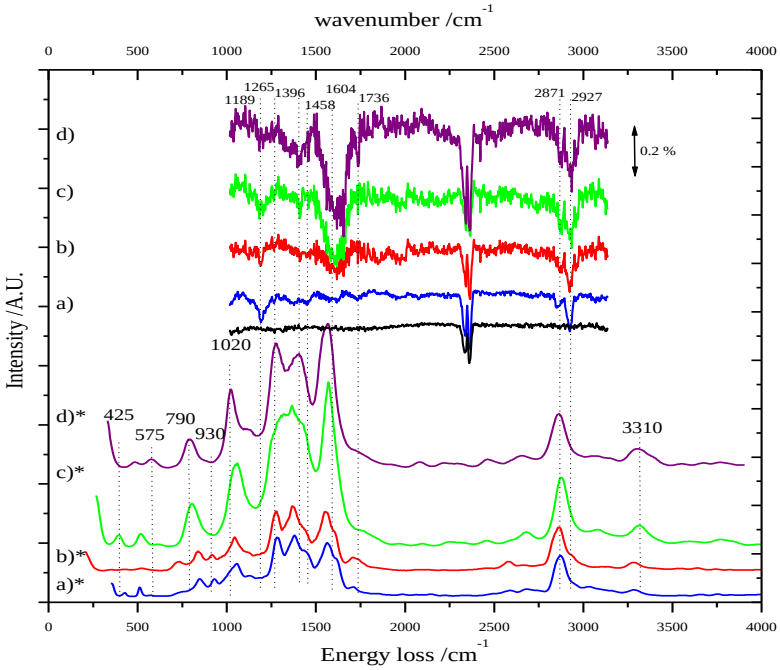

Fig. 6.5 RAIRS and HREELS data as a function of increasing *(S)*-Lys dose a) 90 s, b) 180 s, c) 600 s and d) 900 s on Au{111} at a sample temperature of 300 K.

Spectra labelled * are HREELS data.

For the RAIRS data, at lowest exposures, relatively intense bands were observed at 2927 and 2869 cm^{-1}, representing ν_{as} (CH_2) and ν_s (CH_2) respectively [23], accompanied by less intense bands at 1738, 1604, 1448, 1265 and 1189 cm^{-1}. The very weak 1738 cm^{-1} peak is assigned the ν_{acid} C=O stretch, whilst 1604 cm^{-1} suggests the presence of a $\delta(NH_2)$ deformation. $\delta(CH_2)$ is represented at 1448 cm^{-1}, and 1265 cm^{-1} is assigned as ν(C-O) + δ(O-H) [24]. Another noticeable peak at 1189 cm^{-1} is attributed to an NH_2 wag [25]. The lack of $\nu_s(COO^-)$, $\nu_{as}(COO^-)$, $\delta_s(NH_3^+)$ and $\delta_{as}(NH_3^+)$ IR peaks suggests that, at submonolayer coverage, lysine is in its neutral form on the Au{111} surface.

As coverage of *(S)*-Lys increases, more infrared active features are observed. The higher wavenumber peaks at 2927 and 2871 cm^{-1} continue to be present and reach a maximum intensity, whilst peaks in the lower 2000 – 1000 cm^{-1} region continue to grow, with some new additions. The broader peak at 1604 cm^{-1} is assigned to the $\delta(NH_2)$ deformation, with contributions from $\delta_{as}(NH_3^+)$ moieties shown by the small shoulder at 1656 cm^{-1} [26]. The peak at 1396 cm^{-1}, corresponding to ν_{sym} COO^-, becomes prominent, as well as the evolution of a more pronounced 1189 cm^{-1} peak. There is a continued presence of peaks assigned to the carboxylic acid at 1736 cm^{-1} (ν_{acid}(C=O)) and 1268 cm^{-1} (ν_{acid}(C-OH)), and a peak at 1458 cm^{-1} representing $\delta(CH_2)$. The RAIRS results suggest a measurable amount of the zwitterionic form of lysine at higher coverages. This is indicated by the appearance of the 1396 cm^{-1} $\nu_s(COO^-)$ band, and the small shoulder emerging on the broad 1604 cm^{-1} peak suggesting an NH_3^+ group. The $\nu_{as}(COO^-)$ stretch is absent which indicates, taking the surface selection rule into account, that both oxygen atoms are held equidistant from the surface [24]. The continued presence of acid peaks and the neutral amino peak infers coexistence of both neutral and zwitterionic forms of lysine present at high coverages on the Au{111} surface.

The contribution of the CH_2 groups in the alkyl chain is shown by the strength of the 2929 and 2871 cm^{-1} peaks. Previous studies of alkanethiolate monolayers on Au by

Chidsey and Loiacono [27] showed that peak intensities can be used as a guide to the tilt of the alkyl chain on the surface. The study suggested that weaker $\nu(CH_2)$ IR peak intensities indicate an alkyl chain geometry more parallel to the Au surface than those with stronger intensities, as the stretch modes would have less of a projection on the perpendicular IR electric field. In the present case, although we cannot compare the IR spectra of lysine to other lysine-related IR studies to establish tilt angles, the very existence of the bands at 2950-2850 cm^{-1} would suggest that the lysine molecules are tilted away from the Au surface. The presence of a small peak at 1124 cm^{-1} can be assigned to a ν(CN) stretch which may suggest some contribution from the neutral form of lysine where the distal NH_2 group is bonded directly to the surface, creating a bending of the whole molecule.

RAIRS /cm^{-1}		**HREELS /cm^{-1}**		
Low coverage	**High coverage**	**Low coverage**	**High coverage**	**Assignment**
-	-	3305	3310	ν (NH_2)
2927	2927	-	-	ν_{as} CH_2
2869	2871	2865	2868	ν_s CH_2
1738	1736	1715	-	ν_{acid} C=O
-	1656			δ_{as} NH_3^+
1604	1604	1554	1565	δ NH_2
1448	1458	-	-	δ CH_2
-	1396	-	1405	ν_{sym} COO^-
-	-	1368	-	ω (CH_2)
1265	1268	1280	1280	ν_{acid} C-OH
1189	1182	-	-	NH_2 twist
1120	1124	-	-	ν (CN)
-	-	1060	1020	ν (CN)
-	-	930	-	γ (OH)
-	-	840	-	ν (C=O)
-	-	730	790	NH_2 wag
-	-	-	575	ν (Au-N)
-	-	510	480	ν (Au- N)

Table 6.1 Vibrational assignments of adsorption RAIRS and HREELS bands (in cm^{-1}) of (S)-lysine adsorbed onto Au{111} at 300 K.

As the idea of (non S-containing) amino acids chemisorbing to gold is a relatively undiscovered phenomenon, an attempt to establish which functional group of lysine binds to the Au{111} surface was carried out by examining the HREELS data. First, the peaks within the RAIRS region can be verified from the HREELS results. The peak at 3305 cm^{-1}, and at 3310 cm^{-1} at high coverages, corresponds to the ν (NH_2) vibrations. Its broadness suggests the existence of intermolecular N-H…O hydrogen

bonding [20]. The peak at 1554 cm^{-1} (1565 cm^{-1} at higher coverages) is also assigned to the NH_2 group and corresponds to δ (NH_2). The peak at ~2865 cm^{-1}, as found for the RAIRS experiment, represents the asymmetric (CH_2) stretch, and the 1368 cm^{-1} peak at low coverage is assigned as the wagging mode of the alkyl chain ω (CH_2) [25]. The 1715 cm^{-1} peak, which is only present at low coverages in the EELS spectra, corresponds to ν_{acid} (C=O), and, coupled with the 1280 cm^{-1} peak (1273 cm^{-1} at higher coverages) suggests the presence of a carboxylic acid group [24].

Progressing to the lower wavenumber peaks observed only in the HREELS experiments, the 1060 cm^{-1} peak, which shifts to 1020 cm^{-1} at higher coverages, is assigned as ν(CN). The peak at 930 cm^{-1} at low coverages can be labelled as γ (OH) [28]. This feature is present only at low coverages, and with relatively weak intensity, and implies that a carboxyl group is present but not interacting directly with the surface. As the peak is not present at higher coverages, this suggests another form of lysine exists, with a possible deprotonated carboxylate group in place of the acid group (identified by the peak at 1404 cm^{-1} at high coverages, ν_{sym} (COO^-)). The peak at 840 cm^{-1} corresponds to ν (C=O) [28] at low coverages, further establishing the presence of a carboxylic acid group (peak is not present at higher coverages). The peak at 790 cm^{-1} at high (900 s) coverages is assigned as an NH_2 wag and its relatively large intensity suggests that the amine group is close to or interacting with the surface, and at a perpendicular orientation. At lower coverages this peak appears shifted to 730 cm^{-1} [28].

The peaks at 510 and 390 cm^{-1} for low coverages, and 575 and 480 cm^{-1} for higher coverages, are difficult to assign as, at these low energies, vibrational modes tend to involve motion of the majority of the molecule rather than the atoms in just one bond. Raval and co-workers previously found, in far-IR studies of chemisorbed methionine on Cu, a peak assigned to ν (Cu-N) at 481 cm^{-1} [29]. If it is assumed that gold-adsorbate bonds are similar in energy to copper-adsorbate, then the peaks

observed in the present HREELS data can be assigned as ν (Au-N) and so suggest a chemisorption bond between the lysine and the substrate.

In summary, at low coverages it would appear lysine molecules are adsorbed in their neutral form, with a fully protonated carboxylic acid group and two neutral NH_2 amino groups. In terms of bonding to the Au surface, the neutral NH_2 groups are reasoned to be the most probable anchoring site, with binding through the lone electron pairs. This is shown by the HREELS data, which suggests, by the presence of the ν (Au-N) stretches, that the lysine molecules are chemisorbed to the Au surface through the N atom of one or both of the amino groups, creating a chemisorptive Au-N bond. It has been suggested that Au is unable to displace hydrogen from an unprotected carboxylic acid [18, 30]. However, it is more likely that, although *(S)*-lysine leaves the solid doser as a zwitterion, the molecules will favour adopting their lowest energy conformation on the surface, and so H-transfer from the NH_3^+ group to the COO^- group is possible, unlike the ability of Au to deprotonate a thiol group [31], and in contrast to the typical bonding found for carboxylic and amino acids on other metal surfaces (strongly chemisorptive bonds consisting of binding through the amine group(s) and binding through the two oxygen atoms of the COO^- group(s) [32]). In studies of methionine on Au a similar situation was found, with RAIRS showing the presence of methionine in its zwitterionic form in the multilayer regime (with the charged NH_3^+ and COO^- groups involved in intermolecular bonding), and either the neutral or cationic species present at low coverages [20]. From the present low coverage data the RAIRS peaks are resolved sufficiently to distinguish between the δ (NH_2) and δ_{as} (NH_3^+) deformations, and the presence of the NH_2 twist, which is more intense at lower coverages, suggest the neutral species is dominant at low coverages. At higher coverages, as in the methionine study, it has been established that a mixture of neutral and zwitterionic forms of lysine are present on the Au{111} surface.

6.3.3 HREELS STUDIES OF (S)-LYSINE MODIFIED Au{111} AS A FUNCTION OF TEMPERATURE

An HREELS study was carried out following a 900 s exposure of *(S)*-Lys on the Au{111} surface at 300 K as a function of annealing temperature to establish the stability of the adsorbate on the surface. It is expected that *(S)*-Lys will interact less strongly with Au{111} than with Ni{111} due to the weaker magnitude of the bond with the substrate. The HREELS spectra were recorded after annealing the surface to 333 K, 353 K and 373 K and compared with the HREELS spectrum at room temperature (Figure 6.6).

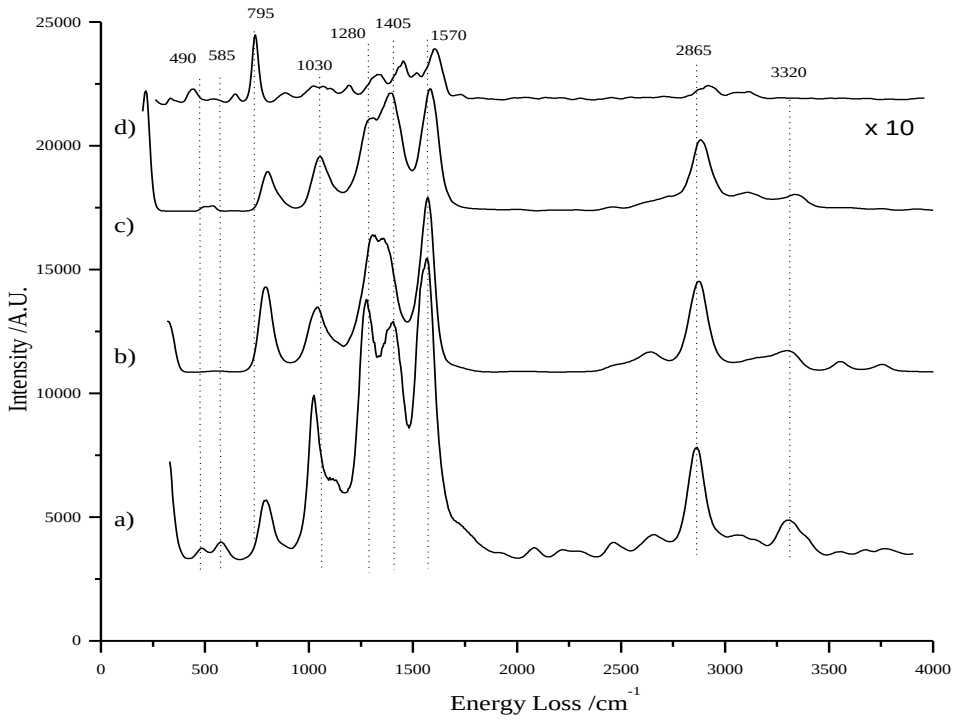

Fig. 6.6 HREELS data as a function of increasing annealing temperature of a 900 s dose of *(S)*-Lys on a Au{111} surface a) 298 K, b) 333 K, c) 353 K and d) 373 K.

The peaks, when compared with assignments in Table 6.1 [32-35], show the presence of a mixture of neutral and zwitterionic lysine species as expected in multilayers (1405 cm^{-1} corresponds to $\nu_{sym}(COO^-)$ and 1280 cm^{-1} is the ν_{acid}(C-OH) peak [34]). At 373 K, the EELS spectrum, which is plotted at ten times its original magnitude, shows only a small residual quantity of *(S)*-lysine on the surface, thus it can be

assumed a slightly higher annealing temperature would result in complete removal of the lysine from the Au{111} surface.

6.3.4 STM STUDIES OF A LOW COVERAGE OF (S)*-LYSINE ON Au{111}*

In an attempt to elucidate a definitive structure of lysine bound to the gold surface, a low (30 s) coverage of lysine was deposited onto a clean Au{111} substrate, initially held at room temperature, and STM image of this surface are shown in Figure 6.7. At the early stages of adsorption, a high diffusion rate of the molecule on the Au surface rendered the species invisible to STM, with the adsorbed lysine forming a 2D gas on the terraces. It is well known for atoms and molecules to have a high surface diffusion on a {111} surface to enable them to reach their minimum free energy state [36]. In the present case, a subsequent change in the appearance of the surface occurred after several hours, with domains of ordered lysine structures, and the results are shown in Figure 6.7, under conditions of good resolution.

The raised ridges of the herringbone surface reconstruction can be seen through the molecular array in Figure 6.7a, and the molecules appear to be oriented according to the underlying Au. If the molecular arrays are always observed with equivalent orientations with respect to the directions of the substrate, this may suggest that either a reasonably strong surface-molecule interaction occurs or, as witnessed in a recent investigation of methionine on Au{111}, there is a lack of a functional group with a strong affinity to the Au substrate [37]. Studies of thiolates on Au{111} [38] and cysteine on Au{110} [39], in which the sulfur atoms create a strong covalent bond between the molecules and the Au surface, show a removal of gold atoms and rearrangement of remaining atoms, resulting in the removal of the reconstruction of the Au{111} surface.

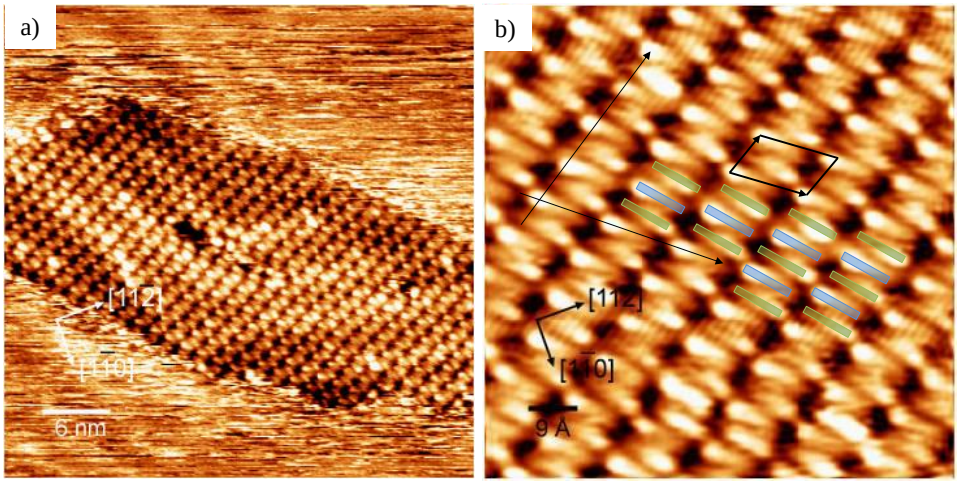

Fig. 6.7 STM images of a 30 s coverage of *(S)*-lysine on Au{111} at a sample temperature of 300 K a) 30 × 30 nm^2, -0.9 V, 0.6 nA b) 8 × 8 nm^2, -0.9 V, 0.6 nA.

In Figure 6.7b, it has been calculated that the structure is made up of a series of alternating head-to-tail lysine chains in the $[01\bar{1}]$ direction. A unit cell with lattice constants of 8.7 x 13.3 $Å^2$ is shown, where the longer side is oriented in the $[\bar{5}14]$ direction. A schematic diagram is overlaid on the STM image in Figure 6.7b showing the molecular packing of the lysine molecules. Given the dimensions, each lysine molecule is typically observed as a bright protrusion "head" with a fainter "tail". The "head-to-head" distance is measured as 11.2 Å. The longer length, in addition to the 8.14 Å length of a lysine molecule (from aliphatic NH_2 group to COOH group), suggests a stabilising H-bond between the molecules in the $[\bar{5}14]$ direction. The intermolecular distance between two adjacent "heads" is measured as 2.6 – 3.2 Å, consistent with a zwitterionic hydrogen-bonding distance [40]. It has previously been found that gold has a propensity for unfolding amino acid backbones to maximize the contact with the surface which, according to the STM measurements, occurs in the case of lysine [41], and so lysine is expected to be in its most favourable trans configuration, with adjacent molecules arranged to minimise any short-range steric repulsion [41].

On the basis of these observations, a proposed $\begin{pmatrix} 5 & -1 \\ 0 & 3 \end{pmatrix}$ phase on the gold surface was modelled by periodic DFT calculations (Figures 6.8a and b). Geometry optimisations were carried out starting from a variety of initial positions, with one or two lysine molecules in the unit cell. Both the neutral and zwitterionic forms of lysine were considered. The gold layer was kept frozen during all optimizations.

The most stable motif was found to be a dimer of two neutral lysine molecules, connected by a COOH-COOH bridge, which is formed by two O-H…O hydrogen bonds (adjacent bright protruding "heads" are consistent with H-bond lengths, as discussed above). The aliphatic NH_2 group is pinned on an atop gold atom site (as shown in the side profile of Figure 6.8b). Following previous DFT studies of amines on Au{111}, it was found that the largest binding energy occurred when the nitrogen atom of the amine group is positioned above a gold atom [43]. Sites with a high coordination number, such as bridge, fcc or hcp sites, are unfavourable, and the relatively weak adsorption of an amine group occurs only at an under-coordinated gold, such as an adatom site. As amines are strong bases, they are expected to act as two-electron donors (and not covalently bonded amides) and so bind by delocalization of the electron pair to the unsaturated surface gold atoms [44, 45]. In the model in Figure 6.8b it is suggested that the amino N atom does not bind to the substrate as it does not find a gold surface atom to preferentially bind to at an atop site. The fact that the ordered lysine structure appears to be commensurate with the surface implies that it is reasonable to assume the molecules are chemisorbed through the N atom to the Au surface which, although not influential enough to rearrange the Au reconstruction, is a significant metal-molecule interaction.

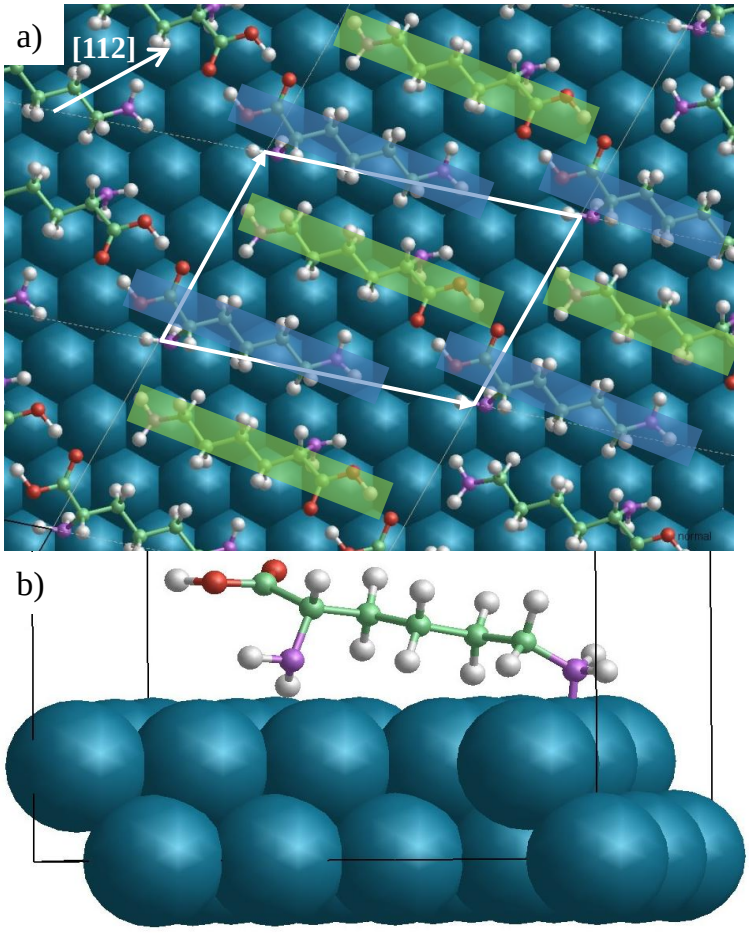

Fig. 6.8 STM images of low coverage *(S)*-lysine on Au{111} at a sample temperature of 300 K a) optimised Au{111} $\begin{pmatrix} 5 & -1 \\ 0 & 3 \end{pmatrix}$ *(S)*-lysine structure, with a defined unit cell of 8.7 x 13.3 Å^2, and b) a single lysine molecule from side view to show chemisorbed bond to Au{111} surface.

In summary, the STM results have shown that lysine molecules adsorb onto the Au{111} surface as an $\begin{pmatrix} 5 & -1 \\ 0 & 3 \end{pmatrix}$ ordered structure via its aliphatic amine group, leaving its carboxylic acid group intact. From the DFT calculations, it can be assumed that stabilisation for the ordered structure originates from the formation of intermolecular hydrogen bonds between the dimer carboxylic acid bridge and the aliphatic NH_2 groups, as well as the dimers favourably packing in the closest possible conformation to allow bonding of the aliphatic amine group to the gold substrate at an atop site.

6.3.5 STM STUDIES OF A HIGH COVERAGE OF (S)-LYSINE ON Au{111}

Exposing the Au{111} surface to a 1500 s dose of *(S)*-lysine at room temperature caused an unexpected effect on the surface. Figures 6.9a and b show initial faceted structures on the Au{111} surface. Figure 6.9a was collected using a high tunnelling current and relatively high voltage, whilst Figure 6.9b was collected under more typical conditions. It is assumed that image a) therefore visualises the coverage of lysine molecules, whilst in image b), the apparent step height is far more similar to the step height of Au{111} (measured as 2.3 ± 0.6 Å, compared to the Au step height of 2.35 Å). It was found in previous modelling studies using kinetic Monte Carlo simulations that, at 300 K, Au{111} steps will rearrange along two of the three close-packed directions to form a sawtooth pattern on step edges [46]. The STM image in Figure 6.9a shows a very similar pattern occurring at the onset of nanofinger growth, with significant sawtooth-like faceting of the Au step edges and lysine islands on the terraces. When the adatoms are attached to a close packed step they migrate to the edge but are trapped by any step defect, such as a kink. It is thought the trapping power of the kinks affects the growth and directionality of the fingers, and the reconstruction of the surface appears to also drive these factors.

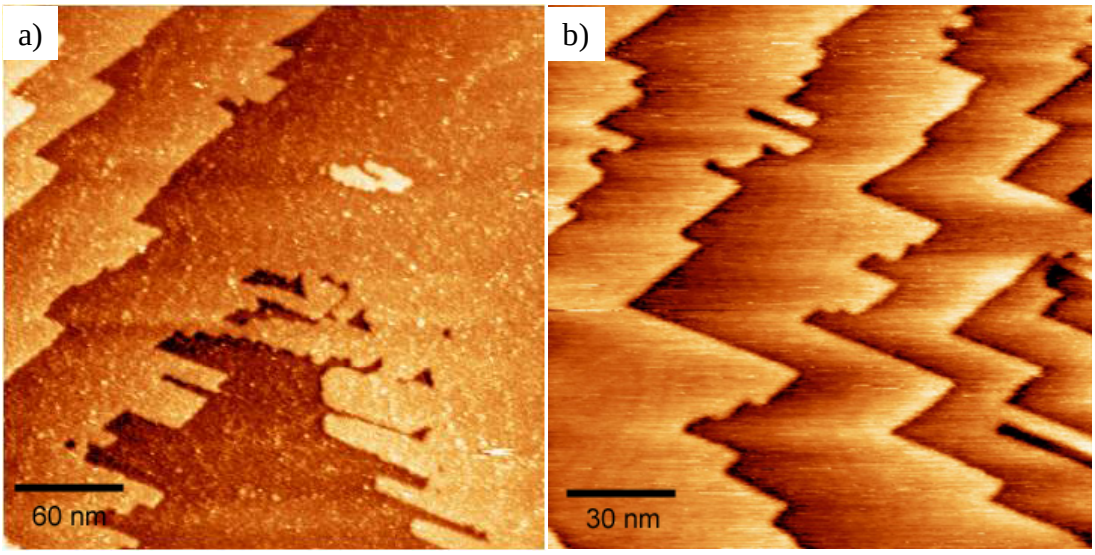

Fig. 6.9 STM images of a 1500 s dose of *(S)*-lysine on Au{111} at a sample temperature of 300 K a) 300 × 300 nm^2, 1.2 V, 2.1 nA and b) 150 × 150 nm^2, -0.4 V, 0.2 nA.

Figures 6.10 a-c show the changes to the modified Au surface after flash annealing to 350, 373 and 400 K respectively. STM images in Figures 6.10 a) and b) clearly identify the formation of Au nanofingers at relatively low tunnelling conditions. The nanofingers have an average width of 3-5 nm (typical finger widths have previously been found between 3 nm and 10 nm; with an average width of 4 nm [16]). Finger lengths seem to vary greatly in length, with the longest finger found to be 85 nm, and this trend has been observed in the previous studies by Palmer and co-workers, with the only limiting factor appearing to be the size of the terrace on which the nanofingers form [16].

It can be observed in Figure 6.10b that, initially, the fingers appear to correlate with the discommensuration line directions. However, with further annealing to promote the finger growth (Figures 6.10b i) and ii)), the direction of the nanofingers appears very well defined, with growth occurring exclusively in the non-close packed $[\overline{15}\,4]$ direction, without following the herringbone reconstruction.

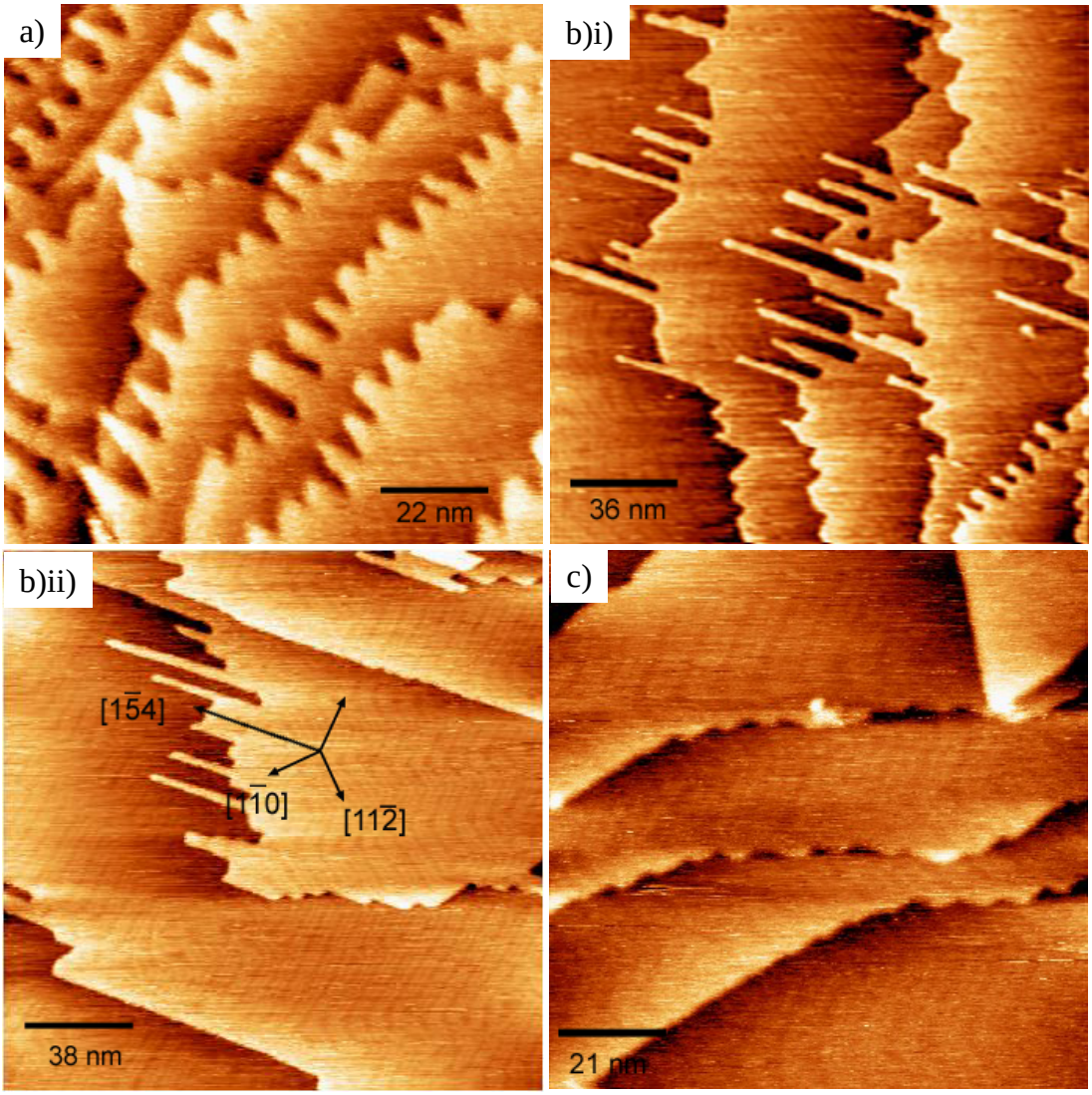

Fig. 6.10 STM images of a 1500 s dose of *(S)*-lysine on Au{111} at: a) a sample temperature of 350 K; 110 × 110 nm^2, -0.5 V, 0.6 nA; b) a sample temperature of 373 K i) 180 × 180 nm^2, -0.8 V, 1 nA ii) 190 × 190 nm^2, -0.51 V, 0.5 nA c) a sample temperature of 400 K; 105 × 105 nm^2, -0.34 V, 0.8 nA.

Finally, with a further anneal to 400 K (Figure 6.10c), the fingers become rounded as well as returning to follow the herringbone reconstruction direction, until they eventually disappear at temperatures just above 400 K, when the Au{111} surface is ultimately reinstated to a more typical appearance. In the work of Palmer, destruction of the nanofingers also occurred above 400 K; shown initially by roundedness at the edge of the fingers before a complete disappearance [15]. This STM result coincides with the HREELS results in Section 6.3.3., which showed only

a small, residual coverage of *(S)*-lysine. It should be noted that the recorded temperature of the surface in the STM instrument is measured by a thermocouple attached to the manipulator arm, and so a slightly lower temperature is recorded than the actual temperature of the single crystal surface, assumed to be lower by approximately 20 K. It can therefore be believed that, at the slightly higher annealing treatment used in the STM experiment, the likelihood is a removal of the amino acid from the surface, and the STM image in Figure 6.10c shows the return of the characteristic herringbone reconstruction of the clean Au{111} surface.

The tunnelling conditions employed by Palmer and co-workers were in stark contrast to the present work and found that, only by increasing the current from 0.1 nA to 30 nA (maintaining the bias at 1.5 V) would Au atom extraction from step edges occur, ultimately forming nanofingers. If the bias was reduced while maintaining a high current it was found nanofinger formation would cease to occur [15-17]. In these experiments, tunnelling conditions were not unusually high, with a voltage range of -1.0 V to -0.4 V and tunnelling current between 0.2 nA – 2.0 nA, which would suggest that the surface restructuring observed in Figures 6.9 and 6.10, is due to the interaction of the lysine molecules with the Au surface, causing displacement of Au atoms at step edges. Previous studies by Arima *et al.* on the zinc porphyrin-driven assembly of Au nanofingers found that the mobility of the gold adatoms on the Au{111} substrate was increased when a thiol was immobilised on the surface [47]. Initially, the strong adhesion of the S atom to the Au substrate weakened the surface Au atoms from underlying layers. Porphyrins were then added to the surface which resulted in an aggregation of Au atoms to form clusters, leading to nanosized fingers. Due to these two attractive forces acting to form Au nanofingers, it was shown that all that was needed was a weak electric field to trigger the mobility of the Au clusters and hence the high field conditions used in the work of Palmer and co-workers were not necessary. The present work in this chapter is likely to illustrate a similar phenomenon, with the bonding of the lysine NH_2 groups to the surface enough to weaken the adhesion between the Au atoms in the top layer and between the top and second layers.

The importance of the directions of the nanofingers and their correlation with the unit cell directions at lower coverages should not be overlooked. The longer side of the unit cell of the ordered structure at lower coverages (Figures 6.7 and 6.8) was found to orient in the $[\bar{5}14]$ direction, with a diagonal along the unit cell directed in the $[\bar{5}41]$ direction and, after careful inspection of many STM images of the nanofingers as those shown in Figure 6.10, it was found that the step-kinks, and ultimately the nanofingers, grow exclusively in the $<514>$ directions. These observations would suggest that the nanofingers consist of lysine molecules arranged in similar unit cells due to the equivalence in crystallographic directions.

Another conclusion from this work is that the measurements could suggest the presence of surface chirality. Figure 6.11a shows the stereographic projection along the {111} plane, whilst Figure 6.11b illustrates a schematic diagram of the Au{111} surface showing the unit cell of lysine shaded in green from the STM image and DFT calculations (Figures 6.7 and 6.8). The symmetry of the {111} surface of face-centred nickel is C_{3v} and therefore a total of six equivalent domains will exist. Focusing on the faceting and nanofinger growth direction, the formation of six $<514>$ directions would occur. There are two rotationally equivalent directions to the $[\bar{5}41]$ direction; $[1\bar{5}4]$ and $[41\bar{5}]$. About the $[\bar{1}2\bar{1}]$ azimuthal direction, there is a reflectionally equivalent direction to $[\bar{5}41]$, in the $[14\bar{5}]$ direction. This latter surface direction also has two rotationally equivalent directions; $[4\bar{5}1]$ and $[\bar{5}14]$. Similar to previous studies of <3 1 17> facets on Cu(100) surfaces [48,49], three rotationally equivalent directions are expected to have *R*-chirality, whilst the remaining three reflected about the $[\bar{1}2\bar{1}]$ azimuthal direction have *S*-chirality. In the present study, the formation of the unit cell, facets (and ultimately nanofingers) are only induced in the three $[1\bar{5}4]$, $[\bar{5}41]$ and $[41\bar{5}]$ rotationally equivalent directions (shaded blue in Figure 6.11a), and not in the $[\bar{5}14]$, $[14\bar{5}]$ and $[4\bar{5}1]$ directions (shaded red in Figure

6.11a). Thus, *(S)*-lysine imprints chirality onto the achiral Au{111} surface in the form of directed facets and nanofingers.

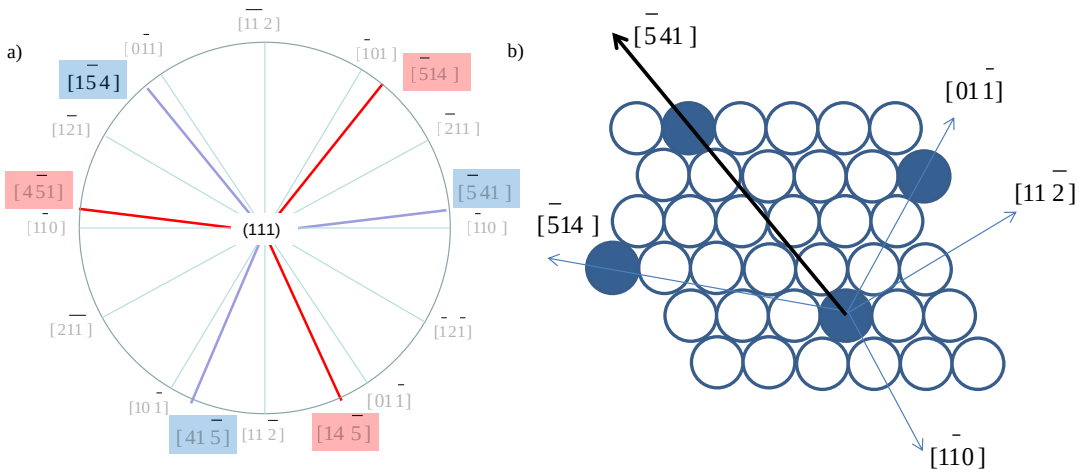

Fig. 6.11 a) Stereographic projection of the {111} plane, highlighting the $[\bar{5}14]$, $[4\bar{5}1]$ and $[14\,\bar{5}]$ (red) and $[1\bar{5}4]$, $[41\,\bar{5}]$ and $[\bar{5}41]$ (blue) directions, b) {111} surface showing the lysine unit cell in blue, the crystallographic directions of the cell, and the $[\bar{5}41]$ diagonal, i.e. the nanofinger direction.

Similar studies have been reported from several groups. It was reported by Schaaff and Whetten that Au clusters displayed chiral characteristics following adsorption of the chiral peptide glutathione [50]. Compared with the results in this section, it is reasonable to assume that the chiral facets were induced by the chiral peptide adsorbate on the surface of the Au clusters. In terms of *(S)*-lysine, several studies in the groups of Zhao and Gellman [48, 49] have shown a difference in adsorption energies of lysine on the Cu<3 1 17>^{R} and Cu<3 1 17>^{S} surfaces, and thus the observed enantiospecificity is suggested to derive specifically from the enantiospecific interaction of lysine with the chiral kinked steps.

6.4. CONCLUSIONS

In conclusion, the adsorption of *(S)*-aspartic acid and *(S)*-lysine onto Au{111} has resulted in several interesting investigations, depending on the amino acid and also the coverage of the molecule. The limited number of amino acids previously adsorbed onto Au has resulted only in physisorption, except methionine and cysteine which contain a sulfur atom and thus can chemisorb to the surface. In this chapter,

aspartic acid was shown not to stick to gold at room temperature, with evidence of its lack of binding shown by RAIRS and STM work.

In striking contrast, *(S)*-lysine was found to bind more strongly to the Au surface. At low coverages, RAIRS and HREELS has shown the presence of neutral lysine with a fully protonated carboxylic acid group and two NH_2 groups. Further STM work illustrated the likelihood that the lysine molecules form dimers connected by a COOH-COOH bridge, stabilised on the Au surface by the aliphatic NH_2 group chemisorbing at an atop Au site.

At higher coverages, RAIRS and HREELS suggested lysine was present as a mixture of its zwitterionic and neutral forms, with intermolecular O-H…O hydrogen bonding, as previously observed for methionine on Au{111} [20]. STM showed the formation of Au nanofingers on the surface following saturation coverage of lysine, which were formed at typical tunnelling conditions and were concluded to be caused by lysine weakening the surface Au atoms to ultimately drive the assembly of Au nanofingers.

In the case of faceting and nanofingers formation, the experiments within this chapter demonstrate that a chiral adsorbate can induce an achiral metal surface to develop chiral facets. Many high-index single-crystal surfaces of transition metals have been shown to portray chiral characteristics [51], and so chiral restructuring by an adsorbate demonstrates that the surface could presumably be used in enantioselective heterogeneous catalysis without the participation of tethered chiral reagents.

6.5 REFERENCES

[1] H.C. Freeman, *Inorganic Biochemistry,* **1**(1973) 121.
[2] A.F. Turner, *Sensors Actuators*, **17** (1989) 433.
[3] S. I. Stupp, P.V. Braun, *Science*, **277** (1997) 1242.
[4] B. Liedberg, C.Carlsson & I. Lundstrom, *Journal of Colloid and Interface Science,* **120** (1987) 64.
[5] A. Ihs, B.Lindberg, K. Uvdal, C. Tornkvist, P. Bodo & I. Lundstrom, *Journal of Colloid and Interface Science,* **140** (1990) 192.
[6] A.D. Roddick-Lanzilotta, P.A. Connor & A.J. McQuillan, *Langmuir,* **14** (1998) 6479.
[7] K. Imamura, Y. Kawasaki, T. Awadzu, T. Sakiyama & K. Nakanishi, *Journal of Colloid and Interface Science,* **267** (2003) 294.
[8] J. Schwank, *Gold Bulletin,* **18 (1)** (1985) 2.
[9] A. Trant, T.E. Jones & C.J. Baddeley, *Journal of Physical Chemistry C*, **111** (2007) 10534.
[10] J.V. Barth, H. Brune, G. Ertl & R.J. Behm, *Physical Review B,* **42,** (1990) 9307.
[11] S. Rousset, V. Repain, G. Baudot, Y. Garreau & J. Lecoeur, *Journal of Physics: Condensed Matter*, **15** (2003) S3363.
[12] A. Schiffrin, J. Reichert, W. Auwarter, G. Jahnz, Y. Pennec, A. Weber-Bargioni, V.S. Stepanyuk, L. Niebergall, P. Bruno & J.V. Barth, *Physical Review B,* **78** (2008) 035424.
[13] H-L. Zhang, H-L. Li & Z-F. Liu, *Microelectronic Engineering,* **63** (2002), 381.
[14] X. Gao, A. Hamelin & M.J. Weaver, *Journal of Chemical Physics*, **95** (1991) 6993.
[15] Q. Guo, F. Yin & R.E. Palmer, *Small*, **1** (2005) 76.
[16] F. Yin, R.E. Palmer & Q. Guo, *Surface Science,* **600** (2006) 1504
[17] F. Yin, R.E. Palmer & Q. Guo, *Physical Review B,* **73** (2006) 073405
[18] W. Lange, M. Jirikowsky & W. A. Benninghoven, *Surface Science,* **136** (1984) 419.
[19] O. Cavalleri, G. Gonella, S. Terreni, M. Vignolo, L. Floreano, A. Morgante, M. Canepa & R. Rolandi, *Physical Chemistry Chemical Physics*, **6** (2004), 4042.
[20] E. Cooper, F. Krebs. McD. Smith & R. Raval, *Journal of Electron Spectroscopy and Related Phenomena,* **64**(1993) 469.
[21] X. Zhao, H. Yan, R.G. Zhao & W.S. Yang, *Langmuir,* **18** (2002) 3910.
[22] B.G. Frederick, GL. Nyberg & N. V. Richardson, *Journal of Electron Spectroscopy and Related Phenomena*, **64-65**, (1993), 825.
[23] D.H. Williams & I. Fleming, *Spectroscopic Methods in Organic Chemistry,* **3rd Ed,** McGraw-Hill Book Company (UK) Ltd, Ch. 2 35-73.
[24] V. Humblot, C. Methivier & C-M. Pradier, *Langmuir,* **22** (2006) 3089.
[25] J.S. Suh & M. Moskivits, *Journal of the American Chemical Society*, **108** (1986) 4711.
[26] X. Dou, Y.M. Jung, H. Yamamoto, S. Doi & Y. Ozaki, *Applied Spectroscopy,* **53**(1999) 133.
[27] C.E.D. Chidsey & D.N. Loiacono, *Langmuir,* **6** (1990) 682.
[28] J.L. Castro, M.A. Montanez, J.C. Otero & J.J. Marcos, *Journal of Molecular Structure,* **349** (1995) 113.
[29] R. Raval, J. Williams, A.J. Roberts, T.S. Nunneye & M. Surman, *Development of Infrared Synchrotron Radiation and Applications to Materials Science,***20** (1997) 553.
[30] M. Weinhold, S. Soubatch, R. Temirov, M. Rohlfing, B. Jastorff, F.S. Tautz & C. Doose, *Journal of Physical Chemistry B,* **110**(2006) 23756.

[31] A. Vallee, V. Humblot, C. Methivier & C-M. Pradier, *Surface and Interface Analysis,* **40** (2008) 395.
[32] X. Zhao, H. Wang, R.G. Zhao & W.S. Yang, *Materials Science and Engineering C,* **16** (2001) 41.
[33] T. Mallat, E. Orglmeister & A. Baiker, *Chemical Review,* **107** (2007) 4863.
[34] X.Zhao, R.G. Zhao & W.S. Yang, *Langmuir,* **16** (2000) 9812.
[35] X. Zhao, H. Yan, X. Tu, R.G. Zhao & W.S. Yang, *Langmuir,* **19** (2003) 5542.
[36] S. Jensen, PhD Thesis *The Assembly of Molecular Networks at Surfaces:Towards Novel Enantioselective Heterogeneous Catalysts,* University of St Andrews, 2010.
[37] A. Naitabdi & V. Humblot, *Applied Physics Letters*, **97** (2010) 223112.
[38] A. Ulman, *Chemical Reviews,* **96** (1996) 1533.
[39] A. Kühnle, T.R. Linderoth, B. Hammer & F. Besenbacher, *Nature*, **415** (2002) 891.
[40] Q. Chen & N.V. Richardson, *Nature Materials,* **2** (2003) 324.
[41] M. Hoefling, F. Iori, S. Corni & K-E. Gottschalk, *Chem Phys Chem,* **11** (2010) 1763.
[42] G. Sridhar Prasad & M. Vijayan, *Acta Crystallographica,* **B47** (1991) 927.
[43] R.C. Hoft, M.J. Ford, A.M. McDonagh & M.B. Cortie, *Journal of Physical Chemistry C,* **111** (2007) 13886.
[44] L. Venkataraman, J.E. Klare, I.W. Tam, C. Nuckolls, M.S. Hybertsen & M.L. Steigerwald, *Nano Letters,* **6** (2006) 458.
[45] P.R. Selvakannan, S. Mandal, S. Phadtare, R. Pasricha & M. Sastry, *Langmuir,* **19**(2003) 3545.
[46] N. Toto, R. Ferrando, Q. Guo & R.L. Johnston, *Physical Review B,* **75** (2007) 195434.
[47] V. Arima, R. Blyth, F. Matino, L. Chiodo, F. Della Sala, J. Thompson, T. Regier, R. Del Sole, G. Mele, G. Vasapollo, R. Cingolani, & R. Rinaldi, *Small*, **4** (2008) 497.
[48] X.Zhao, *Journal of the American Chemical Society,* **122** (2000) 12584.
[49] W. Y. Cheong & A.J. Gellman, *Journal of Physical Chemistry C,* **115** (2011)1031.
[50] T.G. Schaaff & R.L. Whetten, *Journal of Physical Chemistry B*, **104** (2000), 2630.
[51] F.C. McFadden, P.S. Cremer & A.J. Gellman, *Langmuir,* **12** (1996) 2483.

Chapter 7

The adsorption of (S)-lysine and (S)-aspartic acid on Au {111}/Ni Bimetallic Surfaces

7.1 INTRODUCTION

The growth of transition metal nanoclusters on a second metal surface is a strategy which allows an attractive route to the formation of 2D metal-organic coordination networks, and thus creates an alternative opportunity to form a surface with controlled chirality. In Chapters 3-6, the two amino acids *(S)*-aspartic acid and *(S)*-lysine were adsorbed on Ni{111} and Au{111} surfaces. In Chapters 3-5, it was shown that the distribution of *(S)*-Asp and *(S)*-Lys on the Ni{111} surface appeared to be dominated by strong substrate-adsorbate bonds due to the reactivity of the nickel, as well as the capture of Ni adatoms. In Chapter 6 it was shown that only *(S)*-Lys could adsorb on Au{111} at room temperature as the bond strength between *(S)*-Asp and Au was presumably too weak. By alloying Ni with a Au{111} surface to form a bimetallic overlayer, and subsequent adsorption of the two amino acids, the possibility that chiral metal-organic coordination networks may form on the surface is increased. Section 1.7 describes the reasoning behind the attractiveness of bimetallic catalysts, whereas the following introductory section discusses the particular development of Ni clusters on a Au{111} surface.

7.1.1. Au/Ni BIMETALLIC CATALYSTS

As described in Section 6.1.1., clean Au{111} shows a hexagonal surface which reconstructs at room temperature into the (22 × √3) structure. At the elbows of the reconstruction, when the bridge site orientation of the gold atoms remains the same around the elbow, the discommensuration line is "pinched" whereas, when the orientation is changed by 120°, the elbow is "bulged" [1]. When metal atoms, such as iron [2], cobalt [3] or nickel [4,5], are deposited on the Au{111} surface they tend

to preferentially nucleate at these elbow sites (Figure 7.1). In terms of Ni deposition, it was determined that, at first, mobile Ni adatoms displace gold atoms via a place exchange process. Following this, the substituent nickel atoms act as nucleation sites for further incoming nickel atoms [5,6].

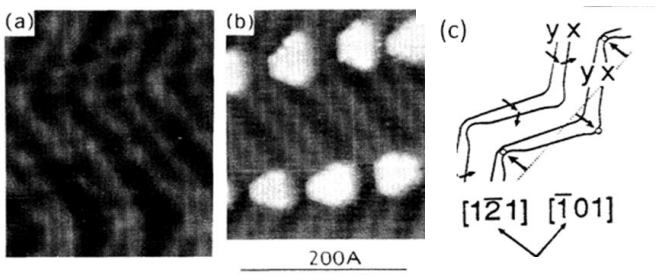

Fig. 7.1 STM images of a) clean reconstructed Au{111}, b) nucleation of 0.14 ML Ni islands and c) herringbone reconstruction and nucleation sites sketch showing bulged elbows. Taken from [4].

Alloying Au with a second element to form a bimetallic catalyst has been shown in previous studies to outperform either catalyst separately, especially in the synthesis of vinyl acetate from acetic acid and ethylene [7]. The potential in the use of Ni on Au as an enantioselective bimetallic catalyst has been shown in recent UHV studies of *(S)*-Glu on Au{111}/Ni [8,9]. In the Ni-catalysed hydrogenation of the *β*-ketoester MAA, it was found that modifying the Ni catalyst by adsorption of the modifier from the solution would create a surface which could enantioselectively hydrogenate prochiral MAA [8]. However, any unmodified Ni sites on the surface were found to compete with the enantioselective reaction by catalysing the racemic reaction. By alloying Ni with Au and modifying with *(S)*-Glu, Baddeley and co-workers were able to successfully create chiral metal-organic frameworks, firstly on the Ni clusters and then spilling over onto Au regions [8]. The MEIS studies in Ref. [9] tentatively proposed that adsorbate-induced surface segregation of Ni-rich regions (a common occurrence driven by the difference in the binding energies between the two metal atoms giving rise to a change in surface tension [10]) occurs, leaving Ni clusters on the Au/Ni surface wholly enantioselective in character, resulting in a catalyst more enantioselective than the pure Ni catalyst. The typical rate of the *(S)*-Glu induced etching of the Ni was also determined to have decreased, prolonging the lifetime of the catalyst.

7.1.2. METAL-ORGANIC FRAMEWORKS

Metal-organic frameworks have been formed by co-deposition of organic and metal species, such as in the studies by Barth and co-workers of the corrosive oxidation of Fe [11] and Co [12] clusters by coadsorption of terephthalic acid. In the present case of *(S)*-aspartic acid on the Au{111}/Ni surface, the two carboxylic acid groups are in a similar position as those in terephthalic acid and so could suggest possible network formation. Other dicarboxylic acids shown to create metal-organic frameworks by this procedure are *(S)*-glutamic acid on Ni clusters [8] as discussed in Section 7.1.1., and stilbenedicarboxylic acid leaching Mn atoms from Mn clusters [13]. Molecules containing other functional groups have also been reported to form metal-organic frameworks, notably chain and ladder structures reported by Mendez *et al*. from Fe clusters after the coadsorption of perylene tetracarboxylic dianhydride (PTCDA) [14], and by Jensen *et al.* from Ni clusters after coadsorption of perylene tetracarboxylic diimide (PTCDI) [15].

7.1.3. AIM OF RESEARCH

The catalytic objective of the research in this chapter is to initially quench the reactivity of any unmodified Ni sites which may compete unfavourably with the enantioselective modified regions by alloying with Au. A cluster size for Ni will be chosen which is large enough not to be etched away completely after adsorption of the chiral modifier.

Following adsorption of the modifiers *(S)*-aspartic acid or *(S)*-lysine onto the Au{111}/Ni bimetallic surface, UHV TPD, RAIRS and STM will be used with an aim to identify the orientation and thermal stability of the modifier adlayer, as well as its morphology. It is the intention to focus on the extent of any possible etching by the amino acids and, in light of the previous *(S)*-Glu/Au{111}/Ni work [16], to investigate the potential of *(S)*-Asp and *(S)*-Lys ability to form chiral metal-organic-framework structures.

7.2 EXPERIMENTAL

7.2.1 UHV STM AND RAIRS EXPERIMENTAL CONDITIONS

Cleaning of the Au{111} single crystal is carried out in Chamber 1 by cycles of argon ion bombardment (1.5 kV) and annealing to 873 K until the diffuse herringbone LEED pattern is observed. Ni was evaporated onto the Au{111} surface by means of a resistively heated W filament around which Ni wire (Advent Research Materials) had been wound. The deposition rate of Ni was calibrated via STM, monitoring the size of the Ni clusters, with 0.5 ML ultimately used. A background RAIR spectrum is taken of the clean Au{111}/Ni, followed by sublimation of *(S)*-Lys (Sigma Aldrich ≥98.0 %), heated to ~403 K, onto the substrate (held at 300 K). The sample was then transferred to the STM chamber where images are acquired in constant current mode using an electrochemically etched W tip.

7.2.2 UHV TPD EXPERIMENTAL CONDITIONS

TPD experiments are carried out in Chamber 2. The Ni was deposited onto the Au{111} surface by means of a heated tungsten filament. The growth of the 848 eV nickel Auger peak and the attenuation of the Au peak (69 eV) enabled an estimation of the nickel coverage. After the Au{111}/Ni sample was prepared and cooled to a suitable temperature, it was positioned in close proximity to the quadrupole mass spectrometer within the main chamber, and a temperature ramp applied, heating through the wires used to mount the sample onto the manipulator. In the preliminary TPD experiments, all masses in the range 0–150 amu were monitored to note which peaks increased as a function of sample temperature. This would allow establishment of whether molecular desorption occurs on the substrate or if the molecule dissociates before desorption.

7.3 RESULTS AND DISCUSSION

7.3.1 DEPOSITION OF Ni CLUSTERS ONTO Au{111}

Initially, Ni was deposited onto Au{111} held at 300 K as a function of coverage. It was observed, as previously, that Ni growth began by nucleating into 2D islands at the elbows of the herringbone reconstruction [4]. Figure 7.3a shows the STM image of 0.1 ML Ni deposited onto the Au{111} surface, where the Ni clusters are approximately 3 nm in diameter (indicated in the profile). Figure 7.3b illustrates the STM image for 0.5 ML Ni on the clean Au{111} surface, with islands approximately 7 nm in diameter.

As will be discussed in the following sections, the adsorption of both *(S)*-Asp and *(S)*-Lys on 0.1 ML Ni on Au{111} resulted in the disappearance of Ni islands (observed by STM). Following the growth of 0.5 ML Ni on Au{111}, the Ni clusters are still visible after adsorption of the modifier, and hence it was decided that RAIRS and TPD experiments would be carried out on this size of Ni clusters.

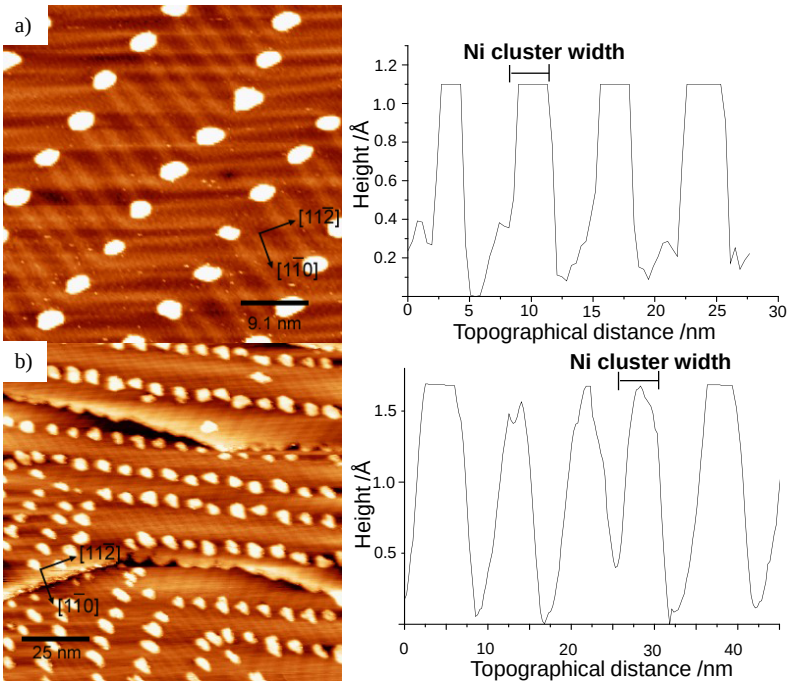

Fig. 7.3 STM images of a) 0.1 ML Ni on Au{111} at 300 K 155 × 155 nm^2, 1 V, 0.5 nA; height profile shown; and b) 0.5 ML Ni on Au{111} 125 × 125 nm^2, 0.75 V, 1.2 nA; height profile shown.

7.3.2. DEPOSITION OF (S)*-ASPARTIC ACID ON Au{111}/Ni SURFACES*

7.3.2.1. RAIRS STUDIES OF THE ADSORPTION OF (S)-ASPARTIC ACID AS A FUNCTION OF COVERAGE ON Au{111}/Ni AT 300 K

As Section 6.3.1 shows, *(S)*-Asp does not adsorb onto Au{111} at room temperature. Exposure of the 0.5 ML Ni on Au{111} surface at 300 K to an increasing coverage of *(S)*-aspartic acid (exposures in keeping with the equivalent experiments carried out on Ni{111}) results in the RAIRS data as shown in Figure 7.4. Table 7.1 gives a summary of the peak positions and assignments. It can be observed that only a weak RAIRS signal is present, with intensities of the strongest 1732 cm^{-1} band measuring approximately 0.1 %. Compared to the strongest band intensity of ~0.2 % in the case of *(S)*-Asp on Ni{111} (Section 3.3.1.1.), the loss in intensity can be explained by the fact that the adsorption of *(S)*-Asp will be proportional to the amount of Ni on the surface, with *(S)*-Asp bonding mainly to the Ni clusters, and a small peripheral effect likely at the interface between Ni and Au at the edge of islands as coverage increases.

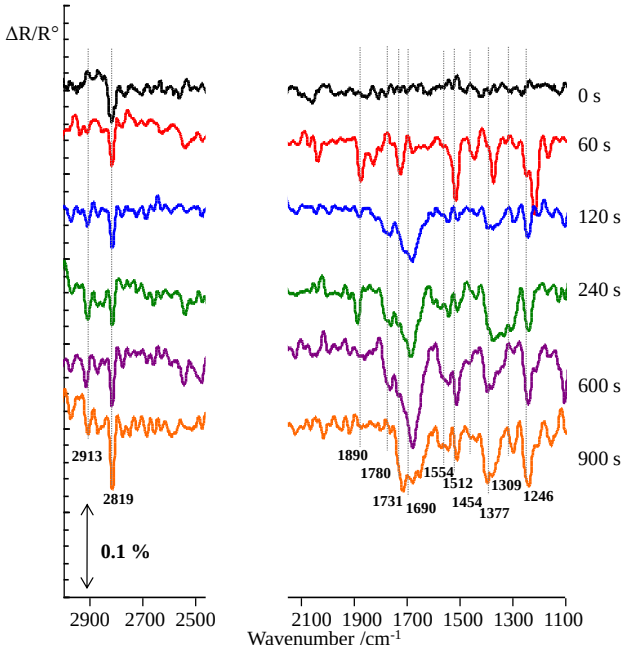

Fig. 7.4 UHV RAIRS of increasing coverage of *(S)*-aspartic acid on Au{111}/Ni at 300 K adsorption temperature.

At all coverages, two peaks at 2913 and 2819 cm^{-1} are present, representing asymmetric and symmetric CH_2 stretches respectively. At low coverages, the RAIR

spectrum is dominated by peaks in the low wavenumber region at 1890, 1780, 1731, 1512, 1377 and 1246 cm^{-1}. The peak at 1890 cm^{-1} is likely to be associated with CO adsorption at a Ni bridge site [17], and is ultimately displaced at higher coverages of *(S)*-Asp, which agrees with previous studies of *(R,R)*-TA on Ni{111} [18]. The peak at 1780 cm^{-1} can be assigned to the ν_s(C=O) of the imide group in a polysuccinimide species present at low coverages (see Section 3.3.1.1.), and the asymmetric stretch at 1731 cm^{-1} [19]. The lower wavenumber peaks at 1512 (δ_s (NH_3^+)), 1377 (ν_s (COO^-) α-carboxylate), 1309 ($\delta(CH_2)$ + ν(CC) + ν(CN)) and 1246 cm^{-1} (ν(C-O)+ δ(O-H)) are indicative of a small presence of the more typical zwitterionic aspartate species. The succinimide bands saturate after ~ 60 s, followed by the growth of bands which are characteristic of the presence of the zwitterionic species of aspartic acid (namely NH_3^+ deformations and the α-carboxylate stretch as well as those associated with carboxylic acid). There is some indication at the highest coverages, due to the presence of the $\delta(NH_2)$ at 1554 cm^{-1}, that the anionic lysine form is present.

300 K /wavenumbers in cm^{-1}		Assignment
Low coverage	High coverage	
2913	2913	ν_{as} (CH_2)
2819	2819	ν_s (CH_2)
1890	-	bridge site CO
1780	-	ν_s (C=O) imide
1731	-	ν_{as} (C=O) imide
1690	1690	ν(C=O) γ-carboxylic acid
-	1554	$\delta(NH_2)$
1512	1512	δ_s (NH_3^+)
1377	1377	ν_s (COO^-) α-carboxylate
1309	1309	$\delta(CH_2)$ + ν(CC) + ν(CN)
1246	1246	ν(C-O)+ δ(O-H)

Table 7.1 Assignments of UHV RAIRS bands of *(S)*-aspartic acid on Au{111}/Ni at 300 K adsorption temperature.

From the RAIRS data the dramatic change in the spectra after 60 s exposure suggests that, initially, the Ni clusters become populated with the PSI polymers (polysuccinimide formation catalysed by the nickel cluster edges), binding from the centre of the Ni islands outwards, until they are displaced by more compact zwitterionic and anionic aspartate species at higher coverages. It is believed that the succinimide formation is actually more facile on the Ni clusters than Ni{111}. Ni grows pseudomorphically on Au in the clusters, therefore expanding by 15.7 % (lattice constant for Au 288.4 pm compared to Ni 249.2 pm). At the elbows of the

Au herringbone there is thought to be a few % of contraction in the Au lattice spacing; even so Ni will still be expanded compared to the Ni{111} surface. In effect, this would create a less densely packed surface of Ni atoms for the polymerisation to take place. Also, the presence of the catalytically active Ni cluster edges will act as nucleation points for the polymerisation.

7.3.2.2. TPD STUDIES OF INCREASING (S)-ASPARTIC ACID COVERAGE ON Au{111}/Ni AT A TEMPERATURE OF 300 K

Figure 7.5 a-c shows the TPD data for the adsorption of *(S)*-aspartic acid on 0.5 ML Ni on Au{111}. On this surface, the primary desorption products occurred at *m/z* values of 2 (H_2), 28 (CO) and 44 (CO_2). Table 7.2 summarises the labelled desorption peaks present.

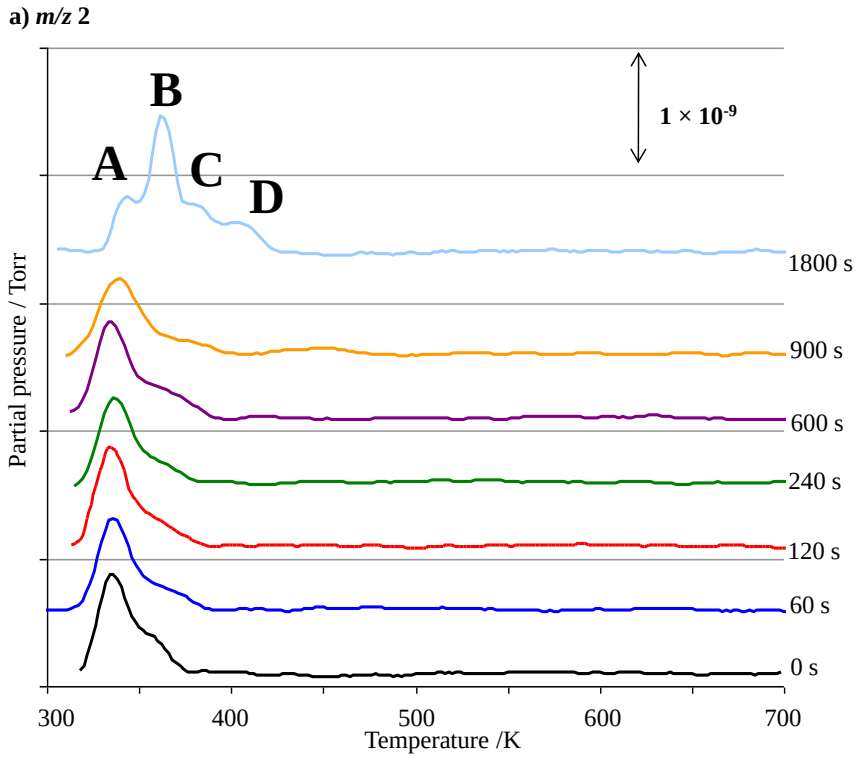

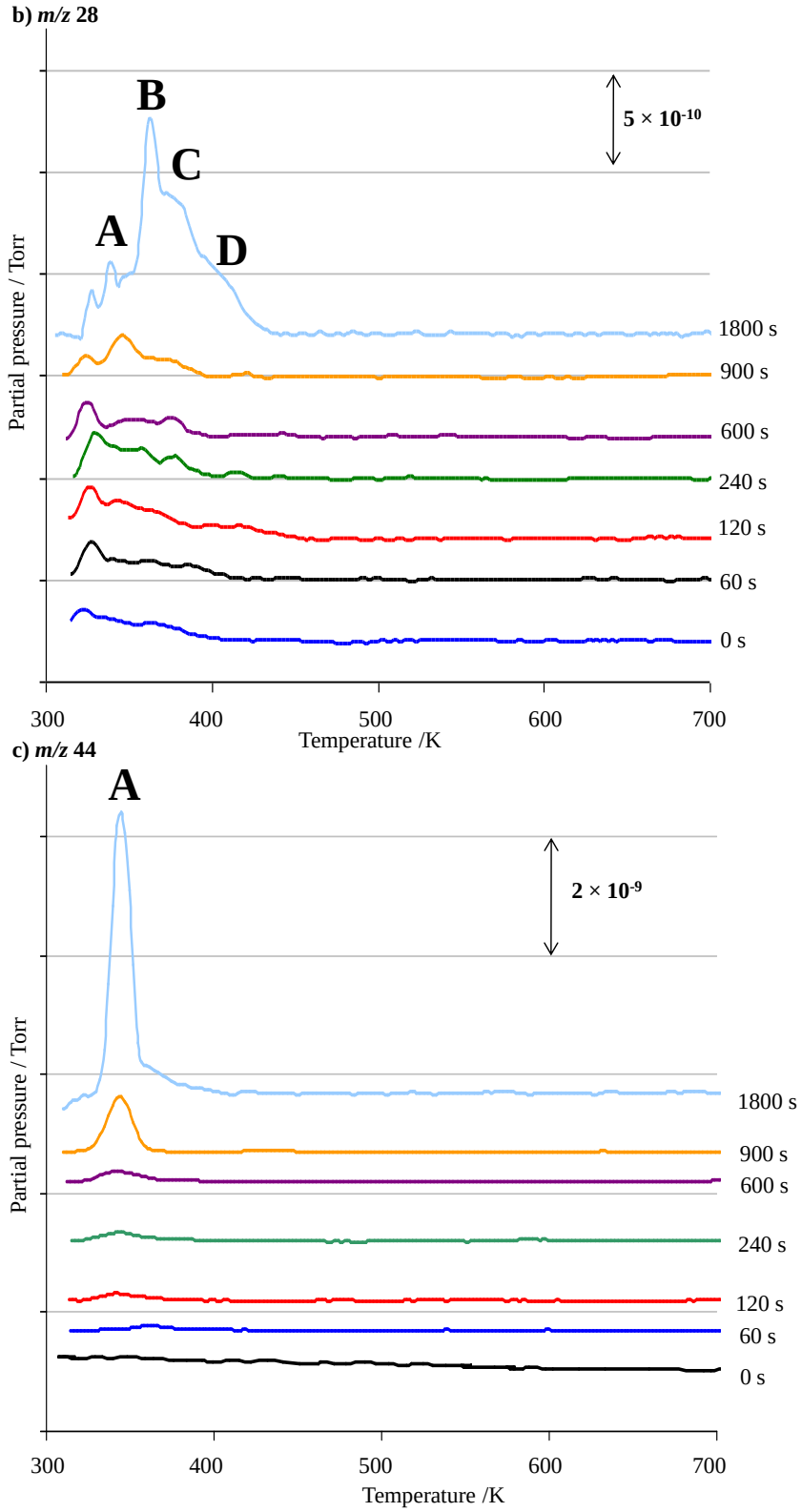

Fig 7.5 UHV TPD spectra following *(S)*-aspartic acid adsorption on 0.5 ML Ni on Au{111} at 300 K with increasing coverages monitoring masses a) 2 (H_2); b) 28 (CO) and c) 44 (CO_2).

The peak at ~330 K in the CO TPD spectrum is most likely to be an artefact due to desorption from the sample mounting. In each spectrum, desorption of H_2, CO and CO_2 shows a peak with a T_{max} of ~340 K (labelled **A**). A second peak (peak **B**) at ~360 K appears in the H_2 and CO TPD spectra, as well as a third and fourth peak at higher *(S)*-aspartic acid coverages at ~380 K (**C**) (also present in CO_2 spectra) and ~410 K (**D**). Peak **A** is assigned to the dissociation of the adsorbed molecules. The lack of desorption peak in the CO_2 spectra until 120 s points to the exclusive presence of polysuccinimide at low coverages.

As peak **A** is found in the CO_2 TPD spectra at 120 s and above, which is expected to infer the presence of the amino acid on the surface, it is likely that, as the Ni islands become more populated, less defect sites are present for the polymerisation of the aspartic acid to polysuccinimide and so aspartate molecules begin to bind to the Ni clusters. At the higher coverages, the presence of other fragment peaks **B**, **C** and **D** at higher desorption temperatures suggest decomposition products from the aspartate molecules on the surface.

	H_2	**CO**	**CO_2**
artefact peak	-	~328 K	-
A	336 K	342 K	342 K
B	362 K	364 K	-
C	381 K	380 K	-
D	409 K	407 K	-

Table 7.2 TPD desorption peaks for *(S)*-aspartic acid on 0.5 ML Ni on Au{111} at 300 K adsorption temperature.

7.3.2.3. HIGH COVERAGE STM OF *(S)*-ASPARTIC ACID AND MAA ON Au{111}/Ni AT A SUBSTRATE TEMPERATURE OF 300 K

7.3.2.3.1. 0.1 ML Ni on Au{111}

At a Ni coverage of 0.1 ML, the Ni clusters have average diameters of 3 nm. The STM images shown in Figure 7.6b and c show the behaviour of a sufficiently large coverage (900 s) of *(S)*-aspartic acid on the Au{111}/0.1 ML Ni surface, compared to the surface before aspartic acid dosing in Figure 7.6a. It can be observed that

nickel atoms in the cluster have been entirely etched away by the presence of the aspartic acid. Only the presence of faceting is observed in the STM images in Figure 7.6b and c. The regular sawtooth arrangement of the step edges indicates an adsorbate-induced faceting. There is thought to be a strong correlation between the periodicity direction of an adsorbed adlayer and the facet directions; unfortunately however no molecularly resolved STM images were recorded for the present system. Gentle annealing of the surface did not establish any new structure on the surface, contradictory to the network of interconnecting molecular chains found for *(S)*-glutamic acid on Au{111}/Ni [8]. The disappearance of the clusters suggest that nickel (II) aspartate or nickel (II) succinimidato complexes are formed which are mainly too mobile to image by STM, with only some indication of brighter features at the step edges which may represent the nickel complexes.

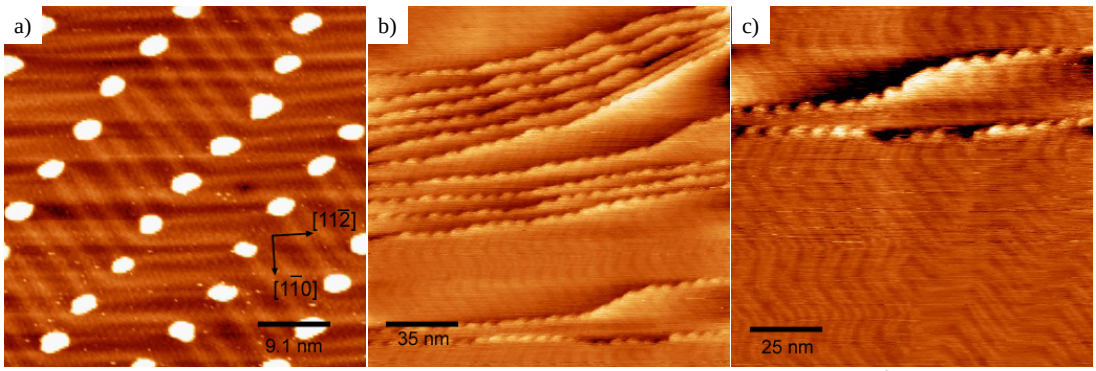

Fig.7.6 STM image of a) 0.1 ML Ni on Au{111} at 300 K 45.5 × 45.5 nm^2, 1 V, 0.5 nA; b) 900 s dose *(S)*-Asp on surface at 300 K 175 × 175 nm^2, -0.5 V, 1 nA and c) 900 s dose *(S)*-Asp on surface at 300 K 125 × 125 nm^2, 0.5 V, 1 nA.

7.3.2.3.2 0.5 ML Ni ON Au{111}

7.3.2.3.2.1 (S)-aspartic acid adsorption at 300 K

Figure 7.7 shows the behaviour of a 900 s coverage of *(S)*-aspartic acid on a 0.5 ML Ni/Au{111} surface. It is observed that extensive corrosion of Ni clusters occurs, presumably due to adsorbate-induced etching. Initially, a diffuse 2D gas-phase of molecules was present (Figure 7.7a). With time, molecular features appeared to nucleate on clusters (Figures 7.7b-f). In the first instance, features are observed to apparently dock on only one side of the Ni clusters (Figure 7.7b and indicated by an arrow in Figure 7.7c), showing a "footprint" structure. Over an order of hours, the

molecular features are observed on top of the Ni clusters (Figure 7.7e) in a disordered array, and also appear to "spillover" onto the Au{111} surface (Figures 7.7d and f).

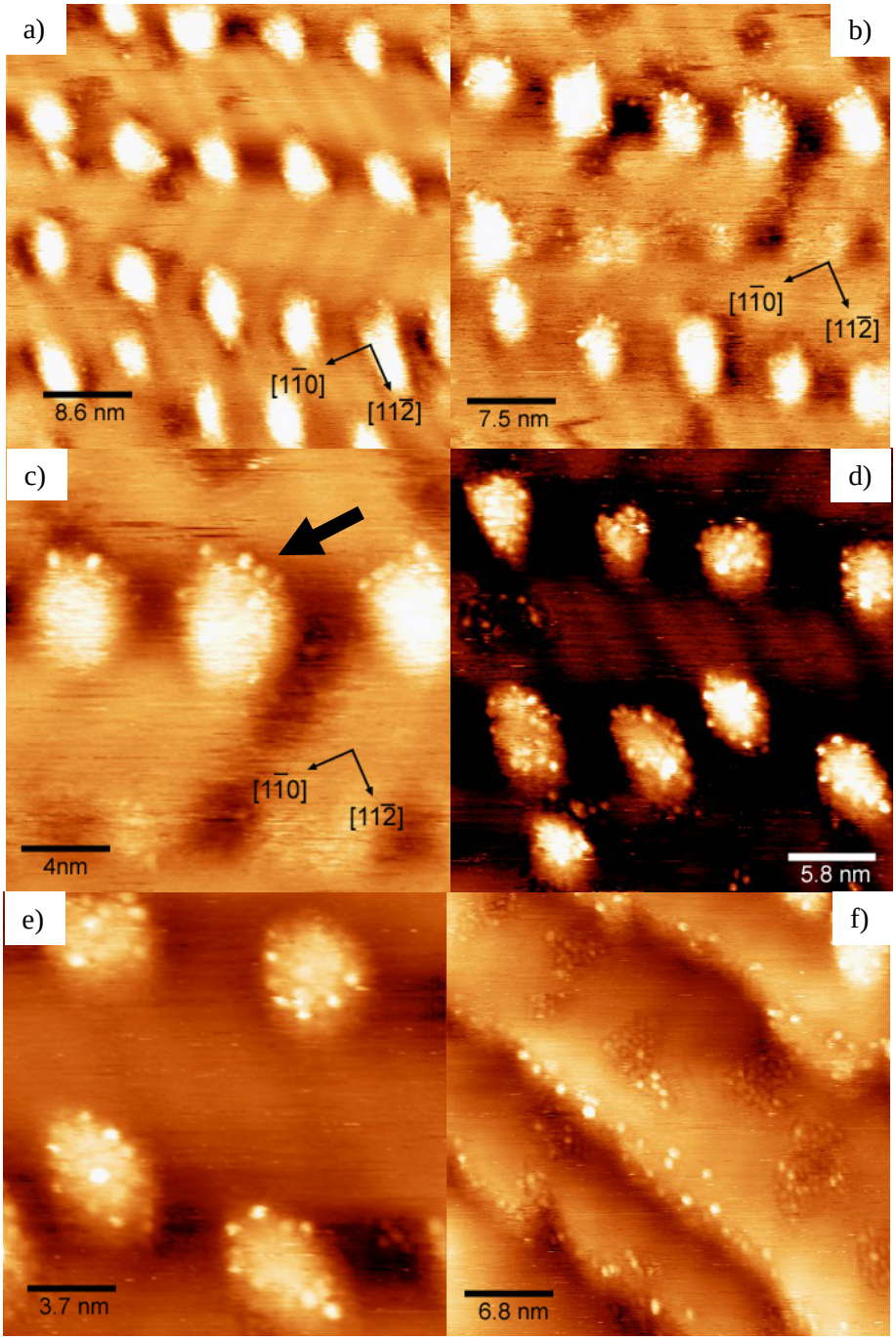

Fig. 7.7 STM images following exposure of 0.5 ML of nickel on Au{111} to (S)-aspartic acid at 300 K a) gas-phase molecules 43 × 43 nm^2, -0.8 V, 0.4 nA; b) "footprint" structure 37.5 × 37.5 nm^2, -0.8 V, 0.4 nA; c) "footprint" structure 20 × 20 nm^2, -0.8 V, 0.4 nA; d) molecular features on Ni clusters 44 × 44 nm^2, -0.8 V, 0.4 nA; e) 18.5 × 18.5 nm^2, -0.8 V, 0.4 nA; and f) 19 × 19 nm^2, -0.8 V, 0.4 nA.

Examining Figures 7.7d and e, the individual molecular features on top of the Ni islands measure ~6 Å in width, in accordance with the dimensions of the succinimide molecules observed on the Ni{111} surface (Chapter 3). Although tetramers are not observed as such on the imaged areas, definite oligomer structures are present, and thus suggest that polycondensation of aspartic acid occurs on the rough edges and defects of the nickel clusters to form polysuccinimide, in accordance with the RAIRS data in Section 7.3.2.1.

As aspartic acid did not bond to Au at room temperature (Section 6.3.1), and due to extensive corrosion of the Ni islands, it can be concluded that the bunch of features in Figure 7.7f must contain the corroded Ni, most likely in the form of Ni^{2+} ions formed via oxidation of nickel. It is probable that, due to the d^8 electron configuration of Ni^{2+} complexes, a square planar geometry is adopted with the carbonyl imide groups and the imide N of the succinimide molecules stabilised by ionic interactions (Figure 7.8b). Modest evidence of Ni presence is shown in the isolated zoom capture image in Figure 7.8a. In this figure, it is thought that a Ni ion appears between the two larger features, creating a metal-organic framework.

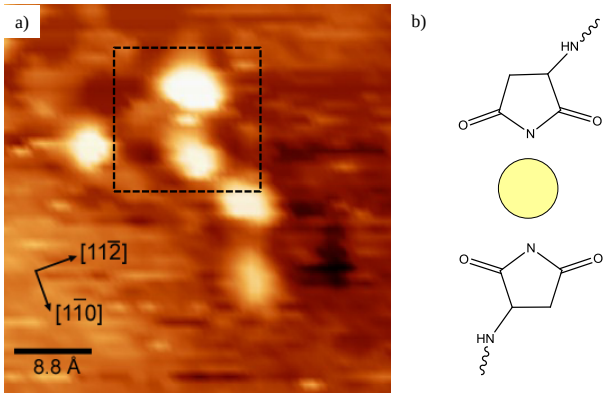

Fig. 7.8 Zoomed-in STM topographical image showing atomic scale features (Ni^{2+} ions) between polysuccinimide molecules.

The most intriguing aspect of the STM study is that no long-range ordered structures appear on the surface. The inability of aspartic acid to bind to the Au surface signifies that the Ni islands, and in turn Ni ions, must play an important part in the presence of molecules on the Au{111} surface. The presence of polysuccinimide

and corresponding succinimidato Ni complexes limit the chance of widespread order [20].

7.3.2.3.2.2 MAA adsorption onto (S)-aspartic acid-modified Au/Ni at 300 K

The adsorption of 5 L MAA onto the *(S)*-Asp modified 0.5 ML Ni/Au{111} surface is illustrated in the topographical STM images shown in Figures 7.9a-e. MAA on Au{111} and submonolayer Ni on Au{111} has been recently studied by Baddeley and co-workers [21,16], where it was shown not to adsorb to Au, and no ordered arrangements were detected on Ni{111} nor Au{111}/Ni. It can be observed in Figures 7.9a-e that, after *(S)*-aspartic acid modification of the Au{111}/Ni surface, widespread ordered domains of methylacetoacetate are detected.

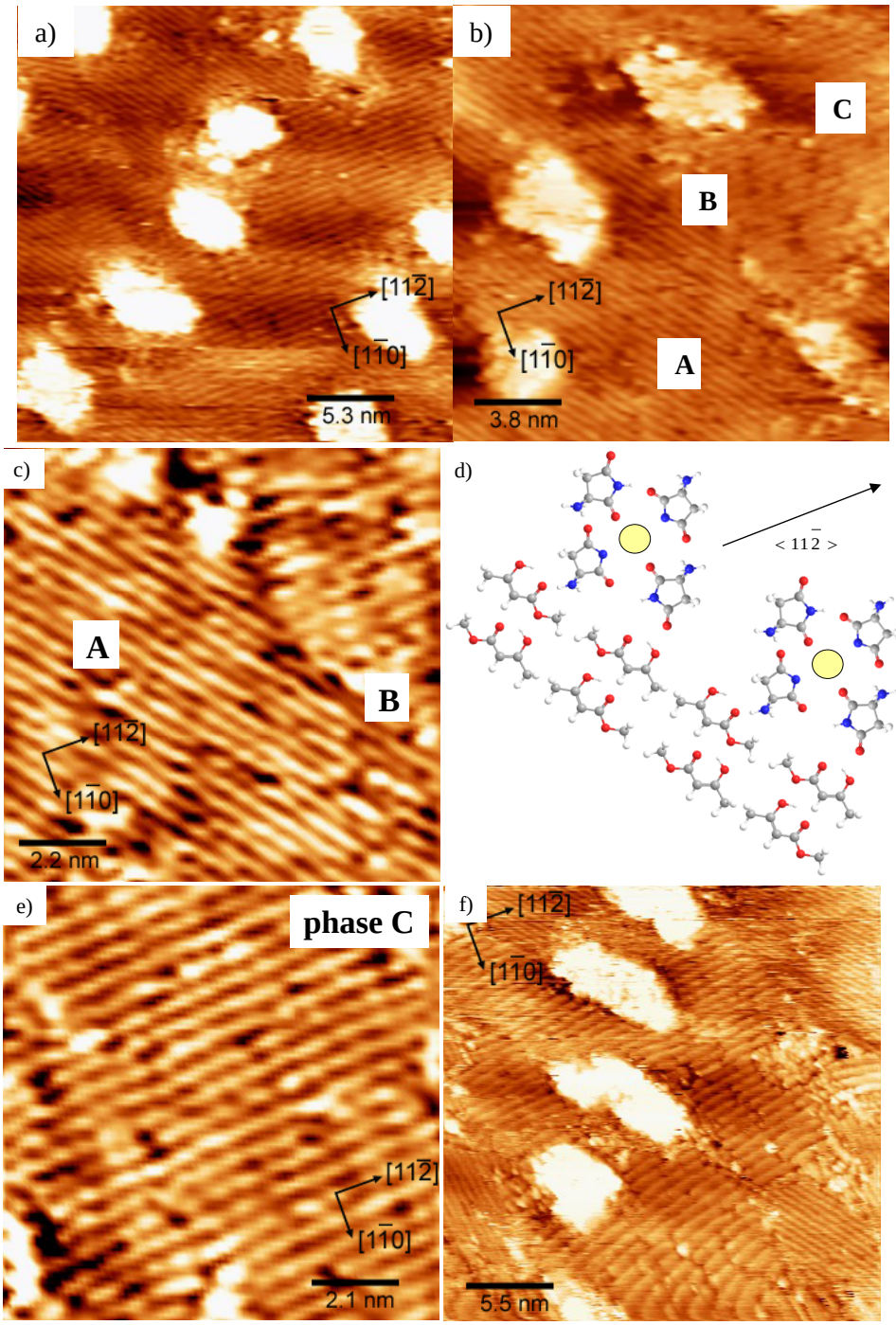

Fig. 7.9 STM images following exposure of 0.5 ML of nickel on Au{111} to *(S)*-aspartic acid and 5 L MAA at 300 K a) 26.5 × 26.5 nm^2, -1.1 V, 1.2 nA; b) presence of two phases A and C, and phase boundary B 19 × 19 nm^2, -1.1 V, 1.2 nA; c) 11 × 11 nm^2, -1.1 V, 1.2 nA; d) schematic model of the proposed model between MAA and succinimidato nickel complex; e) 10.5 × 10.5 nm^2, -1.1 V, 1.2 nA; f) change in proportion of phases over time 27.5 × 27.5 nm^2, -1.1 V, 1.2 nA.

At the onset of MAA adsorption, chains of MAA are observed between Ni clusters, predominantly aligned along the $[11\bar{2}]$ crystallographic direction. Small areas on the surface show adsorption along the $[\bar{2}11]$ direction, 120° to the $[11\bar{2}]$ direction. The likely explanation of the orientation of the chains is that the growth follows the soliton boundaries of the Au herringbone reconstruction. The change in direction of MAA chains occurs at phase boundaries. In Figure 7.9b, conditions of good resolution have been achieved and thus it is possible to identify a number of phases, and measure dimensions of individual features. Phase A, the most commonly observed phase, shows features ~6.2 Å in length and parallel rows of chains separated by ~4.7 Å, which can be assigned to MAA species (Figure 7.9c). At the phase boundary (B), some disordered features are defined and suggest the presence of another species. It is thought that the change in direction is initiated by the existence of the clusters of molecules, as observed in Figure 7.7f. At the phase boundary B, brighter features are perceived to be Ni, with some evidence of features which may be assigned to succinimide molecules (diameters of approximately 6 Å). It is proposed that an interaction occurs between an MAA chain and a row of tetramer rings of succinimidato Ni complexes, growing in one crystallographic direction until the chain collides with a cluster of succinimidato nickel complexes and is forced to change its direction by 120°. The schematic model of the proposed interaction between MAA and the succinimidato nickel complex, shown in Figure 7.9d, indicates that the tetramer rings interact with the adsorbed MAA with no preference for one of the two enantiomers. The key factor underpinning the lack of chiral recognition is the H-bonding with the N-H group acting as an H-bond donor (bonding to the ester functional group) and C=O functionality acting as an H-bond acceptor (interacting with the enol O-H group) of the succinimide oligomers: to achieve optimum H-bonding the MAA molecules have to align in an alternate fashion along each chain, extending into the adjacent rows to maintain H-bonding.

Phase C is not as tightly packed as phase A, the distances between chains measure approximately 6 Å (Figure 7.9e), suggesting that the molecules may be in a more planar orientation on the surface. Over a period of hours (Figure 7.9f), the

proportion of both phases A and C change, suggesting their stability is predominantly controlled by the coverage of MAA.

After exposure to MAA, the STM images show sufficient evidence of its adsorption between clusters. However, the formation of any ordered 2-D supramolecular assemblies with aspartic acid, or polysuccinimide, has not been conclusively observed.

7.3.3. DEPOSITION OF (S)*-LYSINE ON Au{111}/Ni SURFACES*

7.3.3.1. RAIRS STUDIES OF THE ADSORPTION OF *(S)*-LYSINE AS A FUNCTION OF COVERAGE ON Au{111}/Ni AT 300 K

Figure 7.10 illustrates the RAIRS spectra for the adsorption of *(S)*-lysine on 0.5 ML Ni on Au{111} at 300 K, with peak assignments shown in Table 7.3. Studies by Humblot *et al.* and Stewart and Fredericks are used to assign the majority of the peaks [22-25]. The highest wavenumber peaks at 2933 and 2871 cm^{-1} are assigned to the asymmetric and symmetric CH_2 stretches respectively, whereas the 1469 cm^{-1} band is related to the CH_2 scissor mode. The peaks at 1643 cm^{-1} and 1616 cm^{-1} represent asymmetric NH_3^+ and NH_2 deformations. At low coverages the $\delta_s(NH_3^+)$ band at ~1508 cm^{-1} is absent whereas the presence of the asymmetric deformation suggests that the C-N bond is almost parallel to the surface. The bands at 1578 and 1414 cm^{-1} are the asymmetric and symmetric $\nu(COO^-)$ respectively. Collectively, the peaks point to the zwitterionic form of lysine being present, with the presence of both NH_3^+ and NH_2 groups as well as the COO^- group.

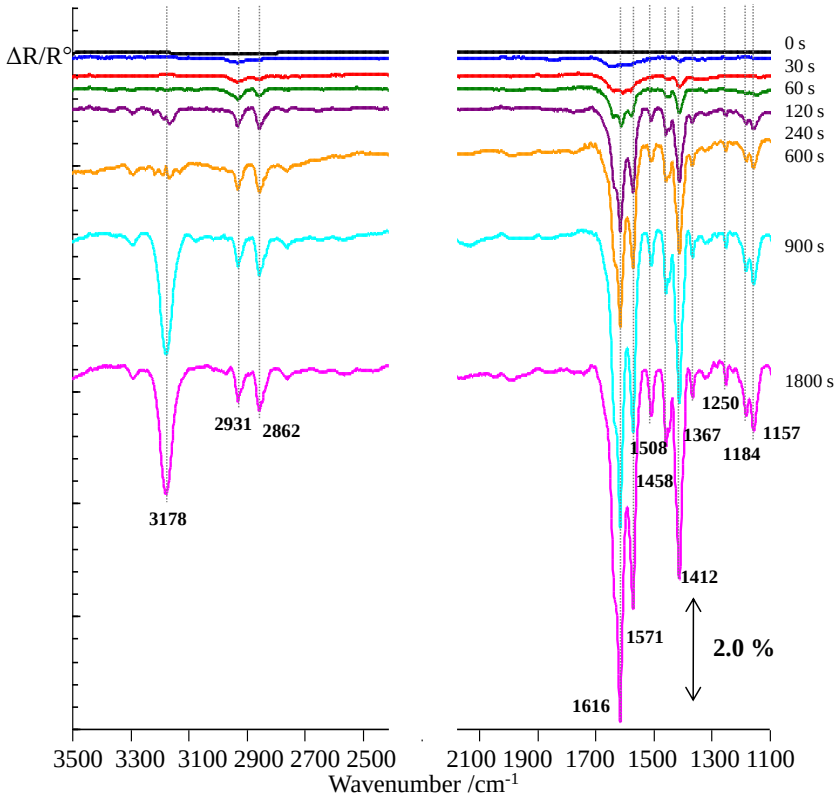

Fig. 7.10 UHV RAIRS of increasing coverage of *(S)*-lysine on Au{111}/Ni at a single crystal temperature of 300 K.

As the exposure of *(S)*-lysine to the surface is increased, the completion of the monolayer and formation of multilayers is noted. This is observed at ~600 s by several changes in the spectrum: an increase in intensity of the spectral bands, and a new band at 3178 cm^{-1} appearing. This band is assigned to the N-H stretch and is common for the NH_3^+ group of amino acids, with its broadness related to intermolecular hydrogen bonding [26]. Peaks representing the zwitterionic form of lysine remain present, as well as newly observed infrared features. NH_2 wagging modes of the amine group are proposed as the doublet bands at 1184 and 1157 cm^{-1}. The presence of the $\delta_s(NH_3^+)$ band at 1508 cm^{-1} and disappearance of the $\delta_{as}(NH_3^+)$ band suggests a change in geometry of the lysine molecules at higher coverages, with the C-N bond no longer parallel to the Au{111}/Ni surface. The peak at 1250 cm^{-1} suggests that a small fraction of lysine molecules with their carboxylic acid group intact are present, presumably neutral lysine species.

300 K /wavenumbers in cm^{-1}		Assignment
Low coverage	High coverage	
-	3178	ν (N-H)
2933	2931	ν_{as} (CH_2)
2871	2862	ν_s (CH_2)
1643	-	δ_{as} (NH_3^+)
1616	1616	δ (NH_2)
1578	1571	ν_{as} (COO^-)
-	1508	δ_s (NH_3^+)
1469	1458	δ $(CH_2)_{scissor}$
1414	1412	ν_s (COO^-)
1363	1367	CH symmetric bend
1338	1336	CH_2 wag
-	1250	$\nu(C\text{-}O)_{acid} + \delta(O\text{-}H)_{acid}$
-	1184,1157	NH_2 wag

Table 7.3 Assignments of UHV RAIRS bands of *(S)*-lysine on 0.5 ML Ni on Au{111} at 300 K adsorption temperature.

Lysine adsorption on the bimetallic Au{111}/Ni surface exhibits very similar behaviour to that observed on the Ni{111} surface (Section 5.3.1.1.), albeit changes occur at slightly different exposure times but this may be explained by a change in flux if the substrate happens to be at a different distance from the lysine doser. At low coverages, the presence of only the symmetric carboxylate stretch at 1414 cm^{-1} in the RAIRS spectra suggests that both oxygen atoms are bonded to the surface. At multilayer coverages (600 s and greater) the symmetric and asymmetric carboxylate stretches are present which suggest the carboxylate group is tilted with respect to the surface with only one oxygen atom bonded. At initial low coverages the asymmetric CH_2 stretch at ~2930 cm^{-1} is more intense than the symmetric (suggesting that the side chain carbon backbone is close to parallel on the substrate). After 600 s, the symmetric stretch appears more intense. Both of these observations suggest that the zwitterionic lysine molecules initially bond to the surface through both oxygen atoms of the carboxylate group with the side chain parallel to the surface (the appearance of only the asymmetric NH_3^+ deformation reinforces this). After completion of the monolayer, the lysine adsorbates reorient to a more upright geometry in the multilayer.

a) b)

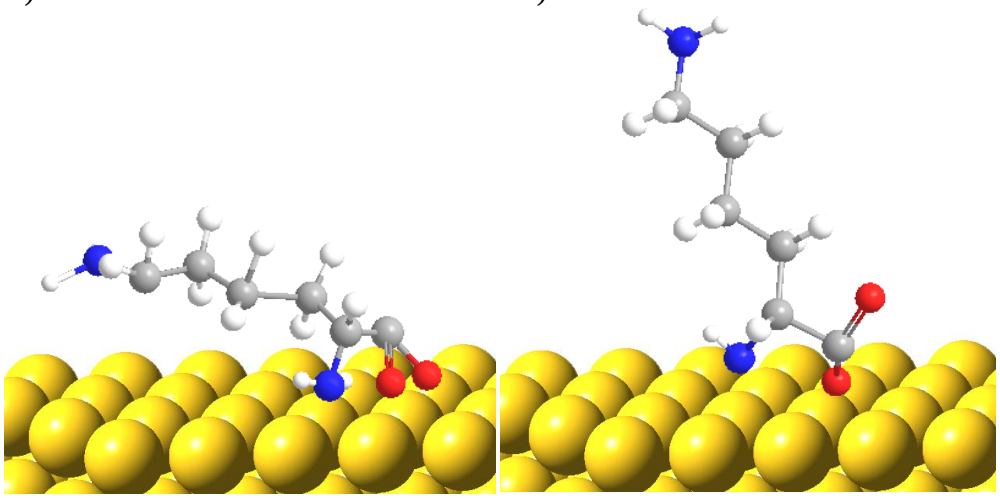

Fig. 7.11 Model of *(S)*-lysine on Au{111}/Ni at a) monolayer coverages and b) multilayer coverages.

7.3.3.2. TPD STUDIES OF INCREASING *(S)*-LYSINE COVERAGE ON Au{111}/Ni AT 300 K

Figures 7.12 a-f illustrate the TPD data for the adsorption of *(S)*-lysine on 0.5 ML Ni on Au{111}. TPD experiments at *m/z* values of 2 (H_2), 17 (NH_3), 27 (HCN), 28 (CO), 30 and 44 (CO_2) were recorded after an initial mass spectrum was recorded during dosing to identify the fragmentation pattern of lysine. The *m/z* value of 30 was not previously seen in Chapter 5 for lysine desorption but it was noted as a major fragment in studies by Cheong and Gellman [27]. It is likely to be composed of a nitrogen-containing fragment, most likely $H_2C{=}^{+}NH_2$ as previously observed for glycine [28], and represents intact lysine.

a) ***m/z 2***

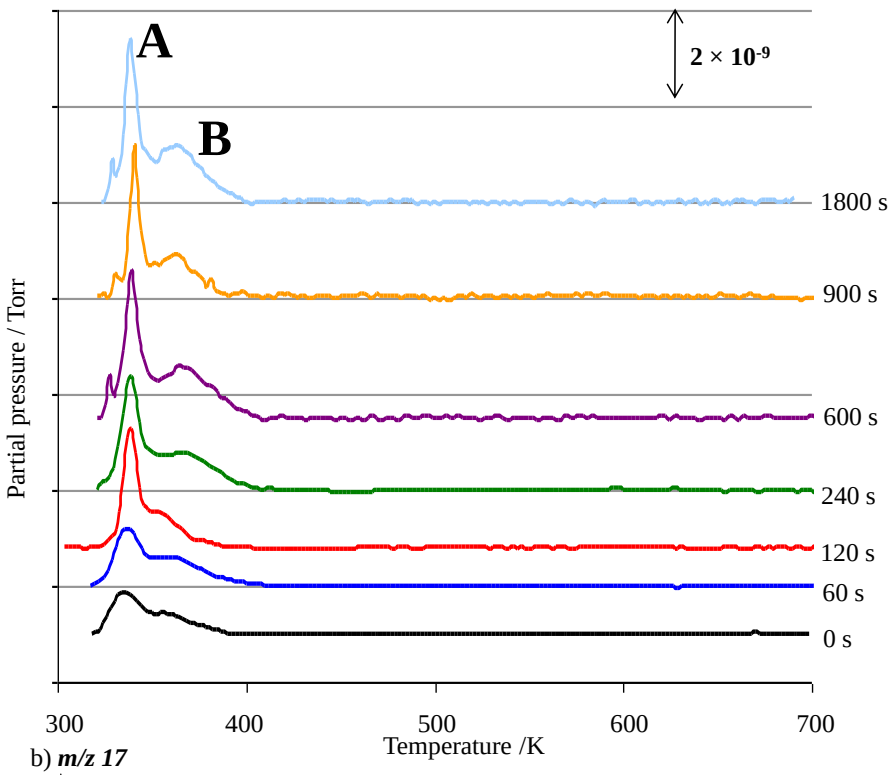
A
B
2 × 10-9
1800 s
900 s
600 s
240 s
120 s
60 s
0 s
Partial pressure / Torr
300
400
500
600
700
Temperature /K

b) ***m/z 17***

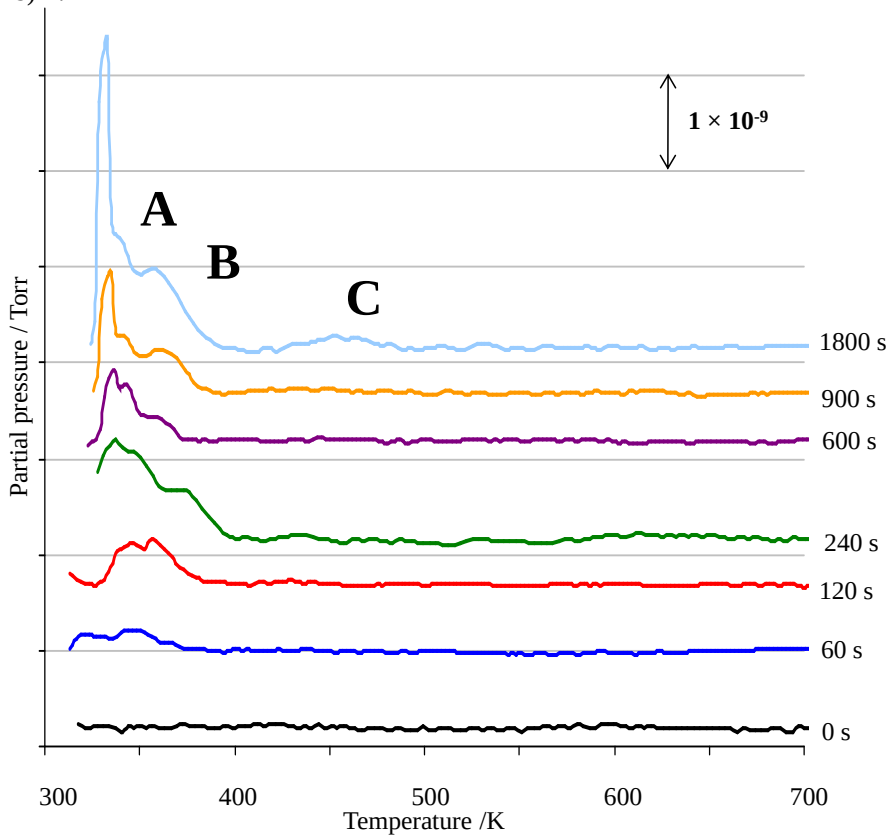
A
B
C
1 × 10-9
1800 s
900 s
600 s
240 s
120 s
60 s
0 s
Partial pressure / Torr
300
400
500
600
700
Temperature /K

c) ***m/z 27***

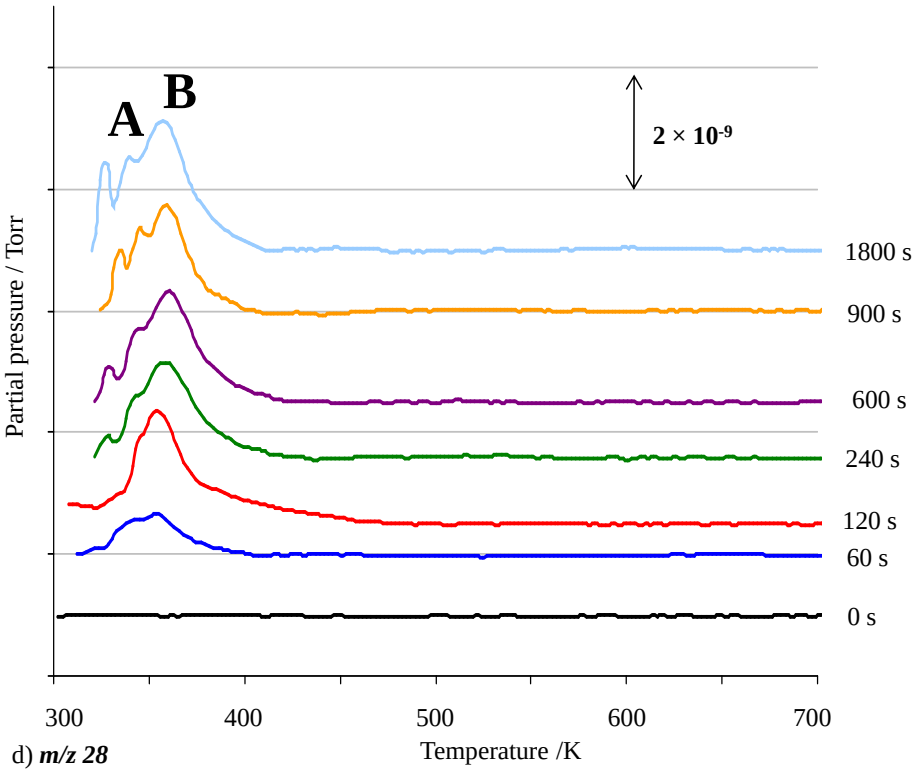
A
B
2 × 10-9
Partial pressure / Torr
1800 s
900 s
600 s
240 s
120 s
60 s
0 s
300
400
500
600
700
Temperature /K

d) ***m/z 28***

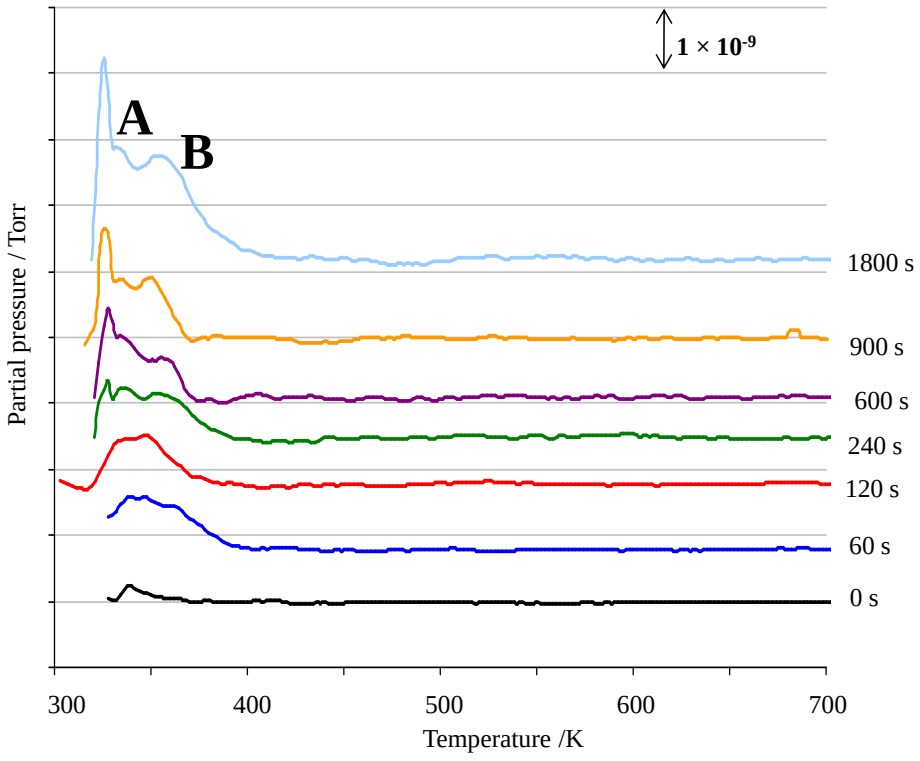
1 × 10-9
A
B
Partial pressure / Torr
1800 s
900 s
600 s
240 s
120 s
60 s
0 s
300
400
500
600
700
Temperature /K

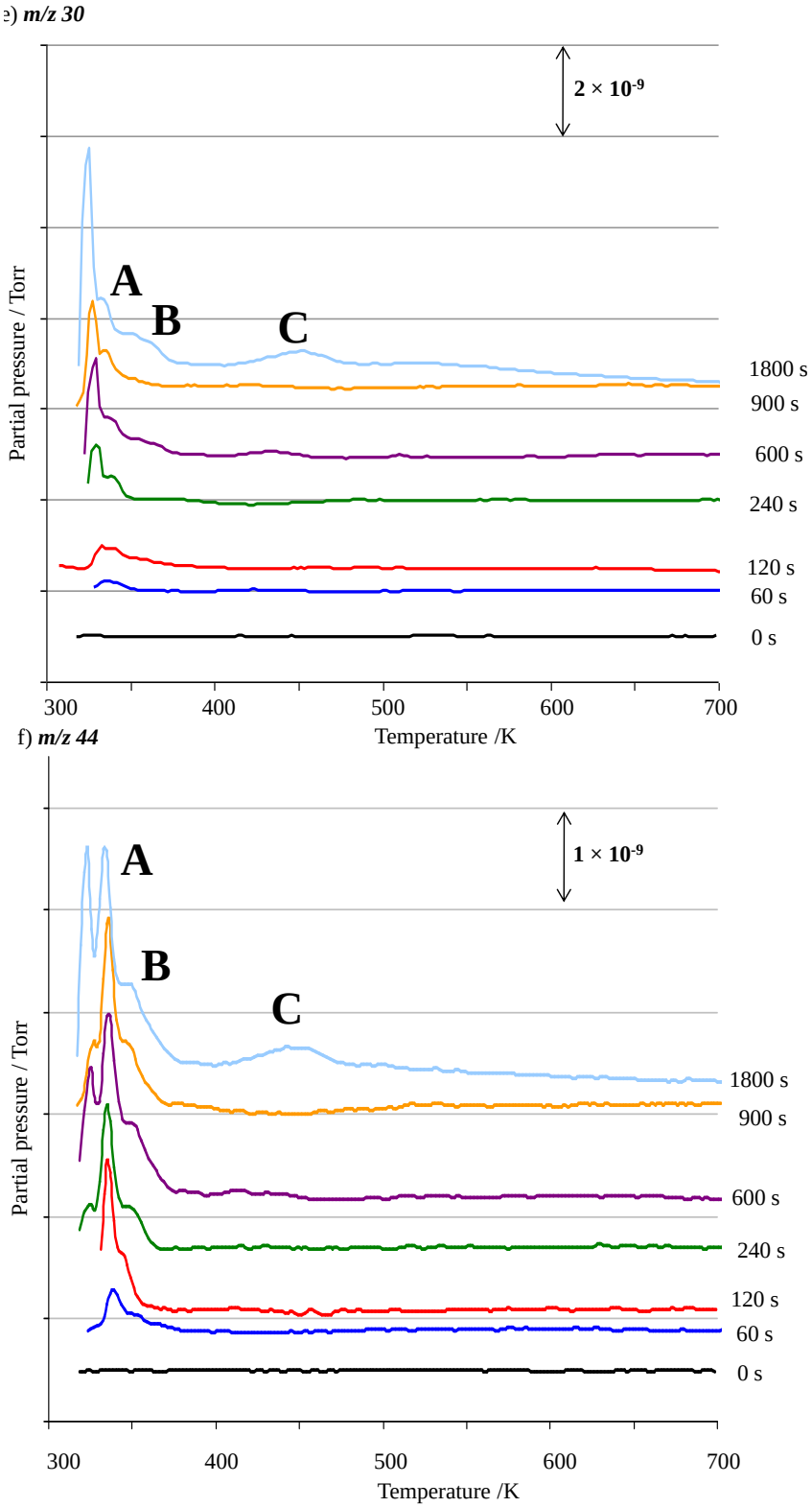

Fig.7.12 UHV TPD spectra following *(S)*-lysine adsorption on 0.5 ML Ni on Au{111} at 300 K with increasing coverages, monitoring *m/z* values of a) 2 (H_2); b) 17 (NH_3); c) 27 (HCN); d) 28 (CO, H_2CN or N_2); e) 30; and f) 44 (CO_2).

	H_2	NH_3	HCN	CO	$H_2C=^+NH_2$	CO_2
A	328 K + 338 K	332 K + 341 K	324 K + 342 K	325 K + 337K	325 K + 334 K	323 K + 334 K
B	367 K	362 K	360 K	359 K	360 K	355 K
C	-	456 K	-	-	453 K	447 K

Table 7.4 TPD desorption peaks for *(S)*-lysine on Au{111}/Ni at 300 K adsorption temperature.

In several of the spectra, a small sharp desorption peak at the onset of the experiment is assigned as an artefact peak caused by desorption of the lysine species from the sample mounting. The peaks labelled **A** at approximately 330 K and 340 K (table 7.4) are present in each of the TPD spectra, suggesting a multilayer desorption of the species. The presence of multilayers of lysine is consistent with the RAIRS analysis in Section 7.3.3.1.). The lower 330 K peak becomes sharper after 120 – 240 s exposure times which may indicate multilayer desorption from the Au{111} surface in between the Ni islands, where the desorption energy of the lysine molecule is likely to be weaker. The 330 K peak is most intense in the H_2, NH_3, $H_2C=^+NH_2$, CO and CO_2 spectra which are all fragments of the intact lysine molecule and so suggests intact lysine desorbs at this temperature. At the slightly higher 340 K peak, HCN desorption is also present which verifies that decomposition of lysine must occur before desorption at this temperature, as HCN is not a common lysine fragment. This may be attributed to a direct molecule-metal interaction, as it has been previously found that the reactivity of the substrate has a strong influence on whether the desorption of amino acids occurs intact [29].

Peak **B** at ~360 K is indicative of a lysine monolayer as the peak saturated in intensity after an exposure time of approximately 240 s. The peak is present in all spectra and so indicates that it arises from desorption of the decomposed lysine species on the surface. Finally, peak **C**, present in the NH_3, $H_2C=^+NH_2$ and CO_2 TPD spectra at ~450 K, suggests a further decomposition of fragments.

In summary, the TPD data has suggested that the pathway of desorption of the lysine molecules on the 0.5 ML Ni on Au{111} proceeds as follows. There is a more or less coincident desorption of multilayer lysine and desorption of the lysine monolayer from Au regions. The more strongly bound monolayer of lysine decomposes and desorbs at a higher temperature, with further decomposition of fragments at even greater temperatures. Compared with Section 5.3.2.3., there is no evidence of polymerisation of the lysine on the surface. Also, compared with previous *(S)*-glutamic acid studies in Au{111}/Ni [9], no indication has emerged of the formation of a related pyrolysate structure. The presence of either structure would increase the stability of lysine on the bimetallic surface.

7.3.3.3. HIGH COVERAGE STM OF *(S)*-LYSINE ON Au{111}/Ni

7.3.3.3.1. 0.1 ML Ni ON Au{111}

Figure 7.13a – c shows the adsorption of a saturation (1800 s) coverage of *(S)*-lysine onto 0.1 ML Ni/Au{111} at room temperature. It is observed that, in a similar fashion to the lysine adsorption on Au{111} in Chapter 6, major faceting occurs on the surface. The Ni islands appear to have been fully leached from the Au{111}, and the likelihood is that the Ni atoms are present in lysinate complexes but it was not possible to image such species at 300 K, presumably due to the high diffusion rate [30]. Indeed, in Figure 7.13a, step heights measure ~3.0 ± 0.2 Å on average, whilst Figure 7.13b measures step heights closer to that of clean Au{111} (2.3 ± 0.6 Å). It may be that, in Figure 7.13a, the lysine nickel complexes contribute to the greater step heights (one monolayer of lysine has a typical apparent height in STM of 0.5 Å).

Step edges, which were randomly oriented on the unmodified Au{111}/Ni surface, reorient due to faceting into regularly directed steps and kinks. In Figures 7.13a and b, due to the imaging of the herringbone reconstruction, the long steps can be confidently assigned to align +40° to the $[11\,\bar{2}]$ direction, i.e. in the $[\bar{5}\bar{1}4]$ direction. Identical step orientations were previously observed on Au{111} in Section 6.3.5. and so strongly suggests that lysine has a large enough etching ability to modify the

Au{111}/0.1 ML Ni surface in a similar fashion. Figure 7.13c shows a topographical STM image from one of several small areas on the substrate surface where extensive faceting produced a seemingly regular sawtooth rearrangement of steps. On closer inspection, the saw tooth directions resolutely follow the same as those in Figures 7.13a and b. Adsorbate-induced faceting has been observed in numerous cases [30 – 34], with a strong correlation between the crystallographic directions of the substrate and the facet induced by the adsorbate. Although molecularly resolved STM images were unfortunately not obtained in this experiment, the triangular nature of the facets is very striking, and the presence of long and short step edges strongly suggests a pronounced chirality in the facets. As STM is a localised technique, further work would have to be done to determine the statistical distribution of the handedness of such facets across an entire modified surface.

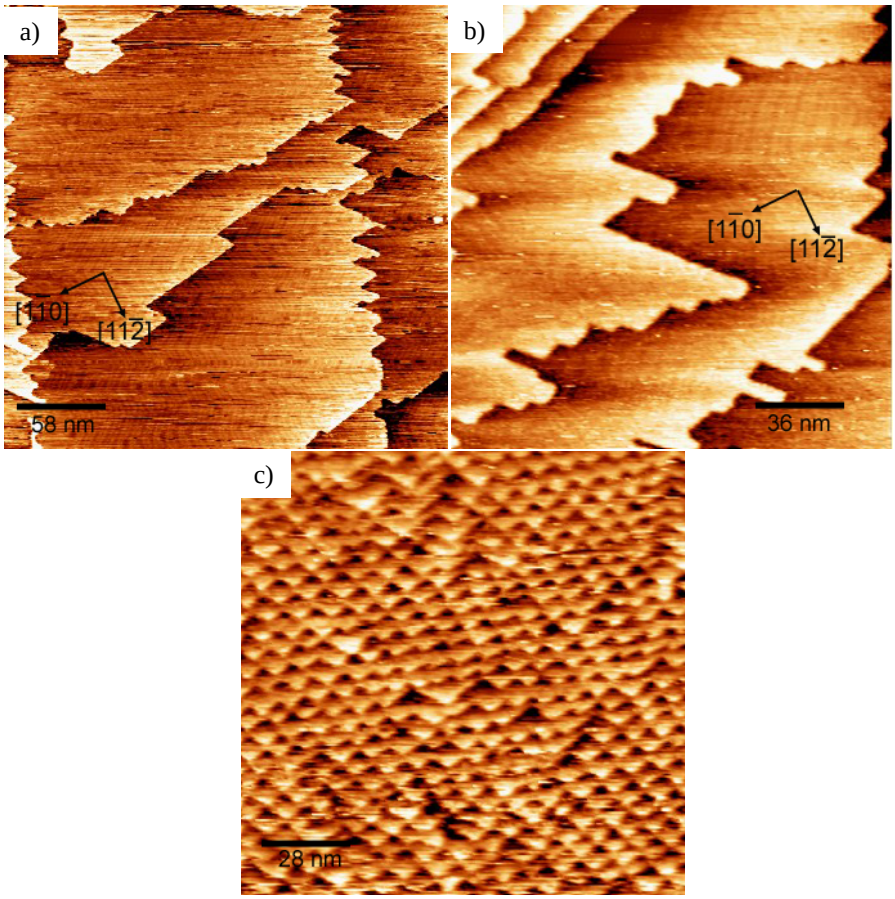

Fig. 7.13 STM images following exposure of 0.1 ML of nickel on Au{111} to *(S)*-lysine at 300 K a)290 × 290 nm^2, -1 V, 1 nA; b)180 × 180 nm^2, 1 V, 1 nA; and c) 140 × 140 nm^2, 1 V, 1 nA.

After flash annealing the surface to 373 K, the formation of nanofingers [35] over a timescale of ~16 minutes was recorded by STM and shown in Figures 7.14a – d. Initially, it can be observed that the substrate steps becomes progressively more faceted, with islands "dislodged" from the main steps (circled in Figure 7.14c), and the growth of several nanofingers occurs, in the $[1\bar{5}4]$ direction (annotated in Figure 7.14a). The nanofingers are approximately 5 nm wide, and 3.5 – 4 Å in height.

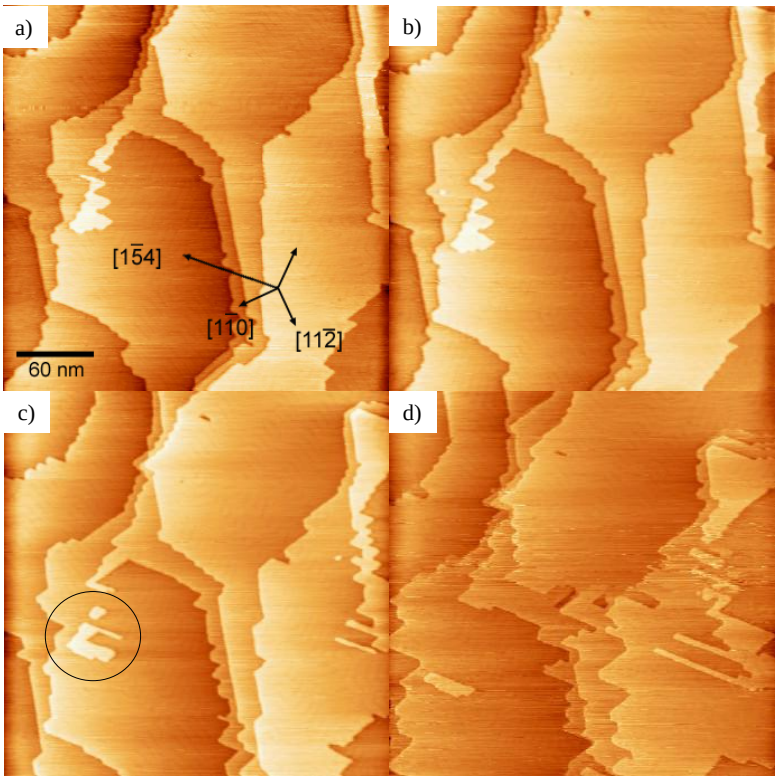

Fig. 7.14 STM images following exposure of 0.1 ML of nickel on Au{111} to *(S)*-lysine annealed to 373 K 300 × 300 nm^2, -1 V, 1 nA; a) 0 min b) 4 min c) 8 min d) 12 min.

In the present experiments, it is expected that lysine, or nickel lysinate complexes, have aided in displacing Au atoms at step edges, as observed for the breakaway of the island in Figure 7.14c. The propensity of lysine to etch Ni has been previously observed in an infrared study of lysine adsorbed onto several transition metal cation-substituted montmorillonites, including Ni [36]. It was found that the montmorillonites adsorbed significantly greater amounts of lysine than any other α-amino acids, and it was suggested that chelation with the transition metal occurred. A chelated complex of zwitterionic lysine attached to a Ni adatom may be readily formed on the Au{111}/Ni surface (Figure 7.15). Although the Au-lysine interaction

is relatively weak compared to the Ni-lysine interaction, the Au atom mobility in the presence of these complexes is large enough to reorder the Au atoms to form nanofingers.

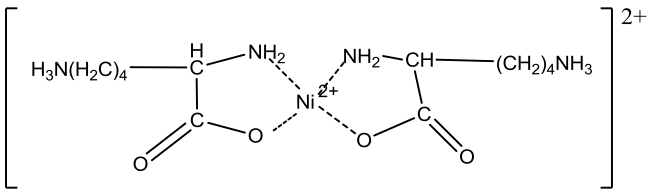

Fig. 7.15 Configuration of Ni chelate complex with zwitterionic lysine. From [36].

7.3.3.3.2. 0.5 ML Ni ON Au{111}

After adsorption of a 30 s coverage of lysine onto the 0.5 ML Ni on Au{111} surface, the initial observation is the change in size of the large Ni clusters. The islands become uneven around the edges, eventually becoming rounded as the particles diffuse away from them. Figure 7.16 shows a visual comparison, using STM, of the clusters before and after adsorption. Although the edges of the islands are somewhat poorly resolved, an estimate can be made of the number of peripheral Ni atoms removed following lysine adsorption, by assuming Ni islands adopt a hexagonal shape as observed previously [6].

If the average diameter of Ni islands before lysine adsorption is 7 nm (i.e. 28 Ni atoms), the number of Ni atoms within the island will add up to approximately 600 (Figure 7.16c). After lysine adsorption, Ni islands have less uniform sizing, with some much smaller than others. However, an average can be taken from the STM image shown in Figure 7.16b. Although there is obvious adsorption on top of the Ni islands which may disrupt the island shape, taking the diameter of some of the smaller islands as a reasonable measure for the effect of corrosion, 5 nm (or ~300 Ni atoms) is calculated. It is therefore clear that, for only a small decrease in Ni island size, a substantial change in the number of Ni atoms occurs. This calculation may prove important in terms of the origin of the etched Ni atoms.

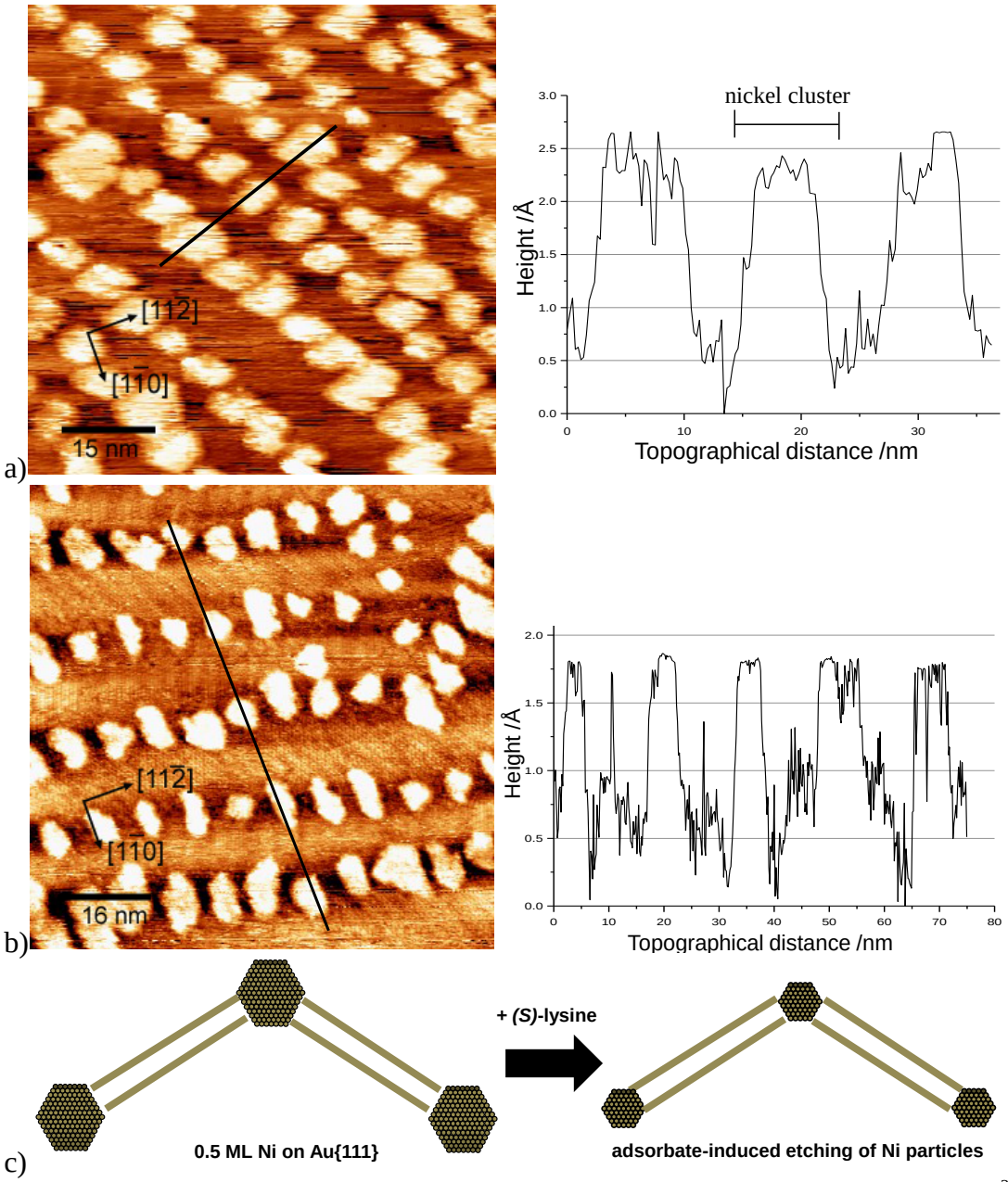

Fig. 7.16 STM images illustrating a) 0.5 ML Ni on Au{111} before adsorption 75 × 75 nm^2, -1 V, 0.5 nA and b) after adsorption of *(S)*-lysine 80 × 80 nm^2, 0.9 V, 1.2 nA.

At room temperature, lysine undergoes widespread adsorption onto both the Ni islands and the Au{111} substrate. The molecules appear to align according to the underlying herringbone reconstruction, with the presence of soliton boundaries imaged as brighter strips under the molecular features (Figure 7.17a). Disordered arrangements on top of the Ni islands, as seen in Figures 7.16b and 7.17a, suggest the possibility of Ni complexes formed by interaction of etched Ni particles with the lysine molecules. It should be noted that the height difference between the Ni islands

and the modified Au makes it difficult to image features on clusters at the same time as those on the Au terraces.

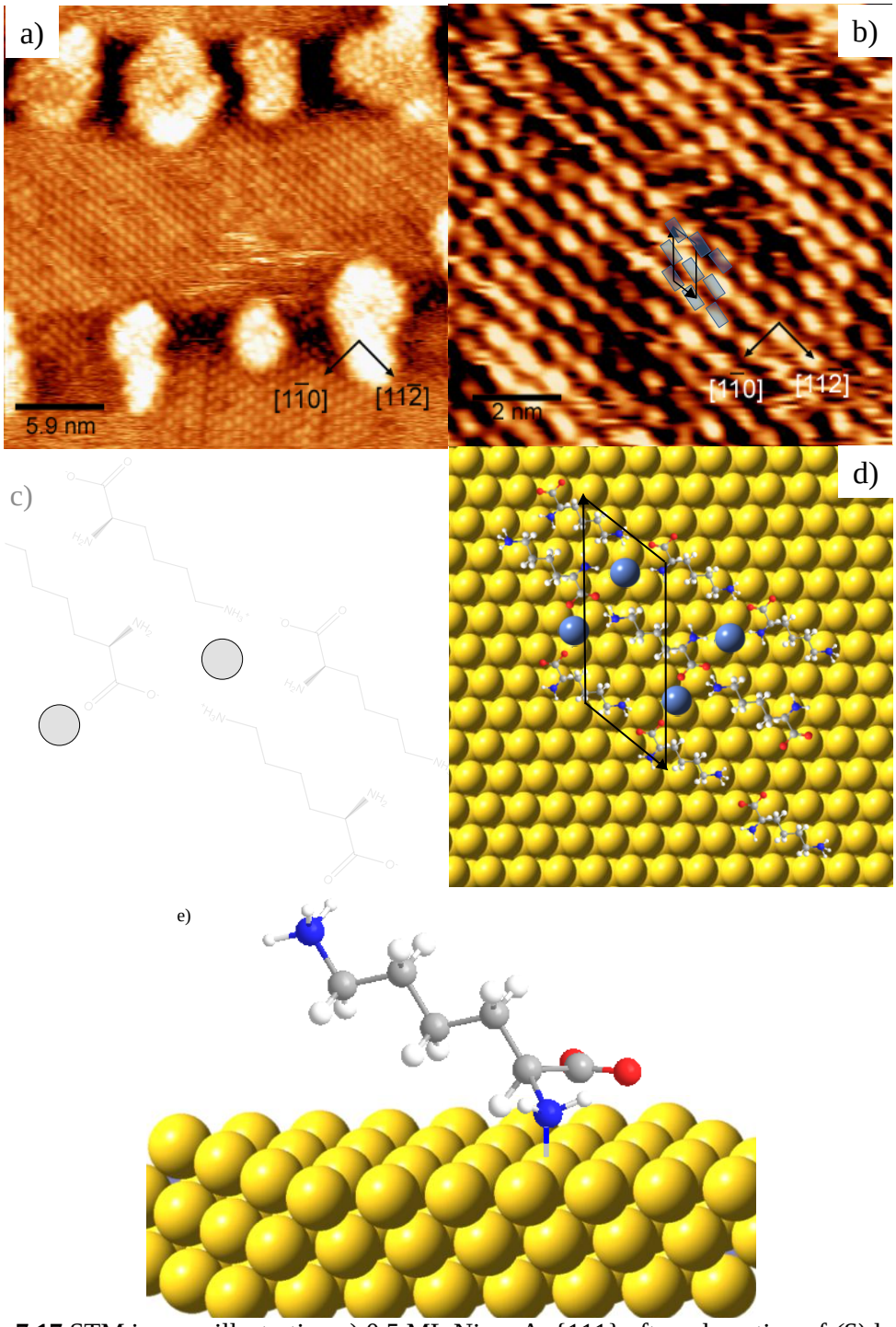

Fig. 7.17 STM images illustrating a) 0.5 ML Ni on Au{111} after adsorption of *(S)*-lysine 29.5 × 29.5 nm^2, -1 V, 0.5 nA; b) 10 × 10 nm^2, 0.9 V, 1.2 nA; c) simplistic possible bonding model incorporating Ni adatoms; d) a model of the framework on the Au terrace; and e) side view of lysine on Au terrace.

It is interesting that extensive ordering of the lysine molecules occurs in between the islands, on the Au{111} surface. The high coverage phase of lysine, as suggested by the RAIRS data, is mainly in its zwitterionic form, with the presence of some neutral species, on the 0.5 ML Ni/Au{111} surface. The most likely scenario for adsorption of lysine onto the surface is, at low coverage, the zwitterionic lysine bonds to the Ni islands, first in the geometry shown in Figure 7.11a, and then, with increasing coverage, in a more upright position. As multilayers of lysine, or nickel lysinate complex begin to build up on the islands, it "spills over" onto the Au{111} terraces.

A possible metal-organic framework model for the ordered structure in Figure 7.17b is shown in Figure 7.17c with the lysine in its zwitterionic form, with each bright feature in the STM images representing one lysine molecule (length 8.14 Å). A unit cell with lattice constants of 8.2 × 14.5 $Å^2$ is shown in Figure 7.17b, where the shorter side is oriented along the $[11\bar{2}]$ direction and the internal angle between the vectors measures 130°. It is important to emphasise that, even though the unit cell may seem similar to that in Section 6.3.4., the packing of the lysine molecules is different with the present case showing the molecules stacked, all at the same angle, compared to lysine on Au{111} where the "heads" and "tails" of adjacent molecules are shifted out of plane to one another. Furthermore, the dimensions of the unit cell are inconsistent with those of *(S)*-Lys on Au{111} (Section 6.3.4.). The present model therefore postulates that Ni is included in the superstructure. Firstly, this would be a reasonable account for the fate of atoms etched from the 2D Ni clusters. Secondly, Ni would stabilise the long-range ordered overlayer by the formation of metal-ligand bonds and counteract the steric repulsion which would occur between opposing COO^-–COO^- and NH_3^+–NH_3^+ pairs, and thirdly the strong indication from the RAIRS that zwitterionic lysine is present at comparable coverages could only occur if Ni was present on the terraces. Unfortunately, the resolution of the STM images was not sufficient to image individual Ni atoms. The Ni is suggested to be present in its ionic Ni^{2+} form, and coordinate ionically to the carboxylate and protonated aliphatic amine units to form a "bridge" between the $[11\bar{2}]$ rows. In previous studies, ionically bonded chains have been observed either with each Ni^{2+}

ion bonded in a bidentate arrangement to aliphatic carboxylate units (for glutamic acid on Ni and Cu) [8, 12], or with the N and amino acid O atoms of different glutamate species interacting with the metal [8]. In the present case, the NH_2 group in the α-position may interact with the Au{111} surface, and so a bonding orientation similar to that shown in Figure 7.17e is likely. This therefore leaves the N atoms of the aliphatic NH_3^+ group and the carboxylate O atoms free to bind to the central Ni^{2+} ion, as shown in Figure 7.17c. It can be observed in the STM image in Figure 7.17b that each molecule is slightly twisted out of the unit cell direction, which would maximise the zwitterionic hydrogen-bonding of neighbouring molecules within rows between the NH_3^+ and COO^- groups. It has been assumed that the Ni-O and Ni-N distances are approximately 2 Å, in agreement with that found for nickel complexes [20].

A second bonding phase was imaged on the 0.5 ML Ni/Au surface with a unit cell measuring 15.8 × 18.7 $Å^2$. Figure 7.18a shows the presence of the bonding phase in different orientations, rotated by 120° and thus following the geometry of the underlying Au substrate. The top of the rhombus-like footprints are oriented in the $[\bar{1}10]$ direction (Figure 7.18b). The lysine molecules appear to be pairing together to create a repeat unit along the $[\bar{2}11]$ crystallographic axis. On the basis of the STM images and the unit cell measurement, a proposed model is illustrated in Figures 7.18c and d. The dimensions shown in Figure 7.18c are consistent with measurements previous reported for lysine on Cu{110} [23], and a similar model is shown. Paired chains of lysine are stabilised by hydrogen bonding between the carboxylate groups and amine groups. The spacing of 9 Å between the rhombus footprints in the $[\bar{2}11]$ direction is likely due to the lack of attractive interactions between the functional groups out with the rhombus structure. The preferential growth direction of the chains suggests that the domains possess chirality, similar to conclusions found in the lysine/Cu{110} work [23]. It is highly possible that the phase shown in Figure 7.18 is evidence of chiral recognition as footprints in one direction appear preferential over others at ±120° rotations on the surface. More

work would have to be carried out by STM to record the statistical distribution of each phase.

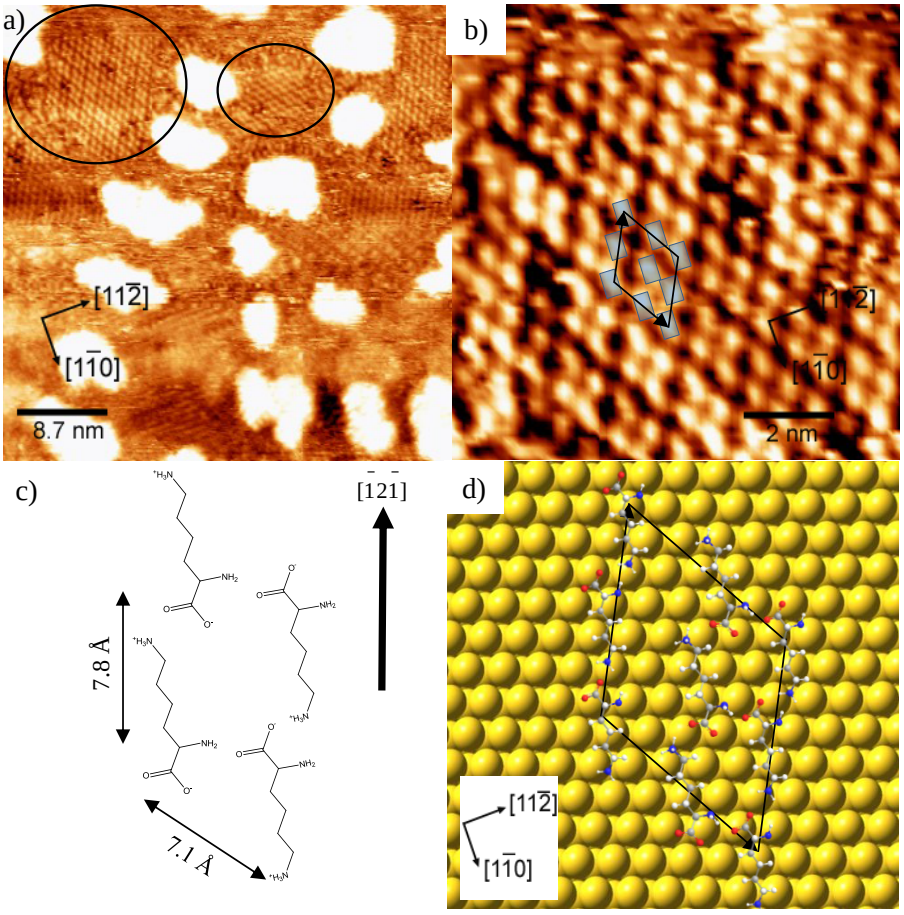

Fig. 7.18 STM images illustrating second phase of lysine on the 0.5 ML Ni/Au{111} surface a) 43.5 × 43.5 nm^2, 0.9 V, 2 nA; b)10 × 10 nm^2, 0.9 V, 2 nA; c) simplistic bonding model; and d) bonding framework of chiral phase on the Au surface.

After the modified surface was annealed to 350 K a new ordered structure appeared, as illustrated in Figure 7.19. Change to the modified surface domains sees darker areas in the network, as shown in the inset of Figure 7.19a. Examining the corresponding line profile, it can be determined that the depressions equate to the bare Au surface. A porous network is shown in Figure 7.19b, with a zoomed STM image shown in Figure 7.19c. The unit cell measures 14.2 × 12.9 Å^2, with an angle of 70° between unit cell vectors. Each bright feature measures ~5.3 Å, which is markedly smaller than a lysine unit.

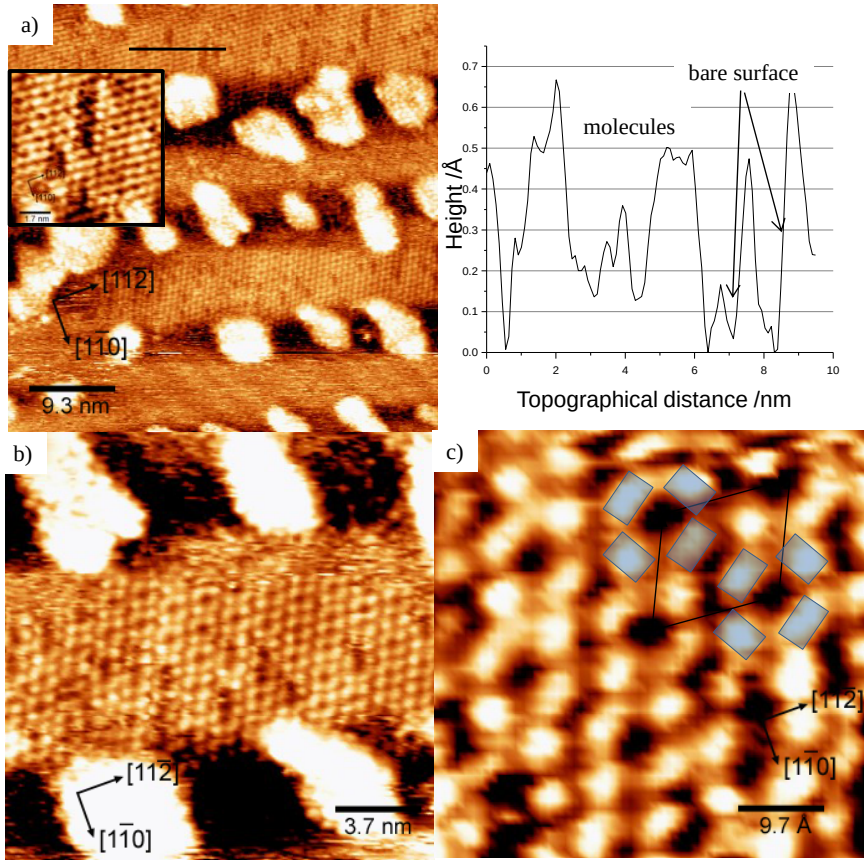

Fig. 7.19 STM images illustrating *(S)*-lysine modified 0.5 ML Ni/Au{111} surface annealed to 350 K a) 46.5 × 46.5 nm^2, 0.9 V, 2.2 nA; b)18.5 × 18.5 nm^2, 0.9 V, 2.2 nA; and c) zoomed image 4.9 × 4.9 nm^2, 0.9 V, 2.2 nA.

To attempt to elucidate what is occurring at the surface, it was necessary to examine the thermal chemistry literature of lysine. The thermal condensation of lysine has been found not to follow a typical peptide preparation pathway; instead the N-terminus is blocked by the formation of a cyclic lactam and acylated ε-NH_2 group [37,38]. It was found that, in an aqueous solution and at a temperature between 150 - 170°C, the formation of α-amino-ε-caprolactam was greatly favoured, with evolution of water [37] (Figure 7.20a). The stability of a 7-membered lactam ring is well known, especially as the nitrogen atom within the ring is able to provide an empty pi-orbital to allow aromatic stabilisation. It is possible that, with gentle heating to 350 K as carried out in the present experiment, the condensation of lysine species on top and at the edge of the Ni islands is catalysed by the metal, under UHV conditions, to form α-amino-ε-caprolactam. A model is proposed in Figures 7.20b and c, composed of an arrangement of four lactam molecules surrounding a central Ni

atom. An alternative, and equally feasible, model could consist of the 4 lactam structures without a central Ni atom.

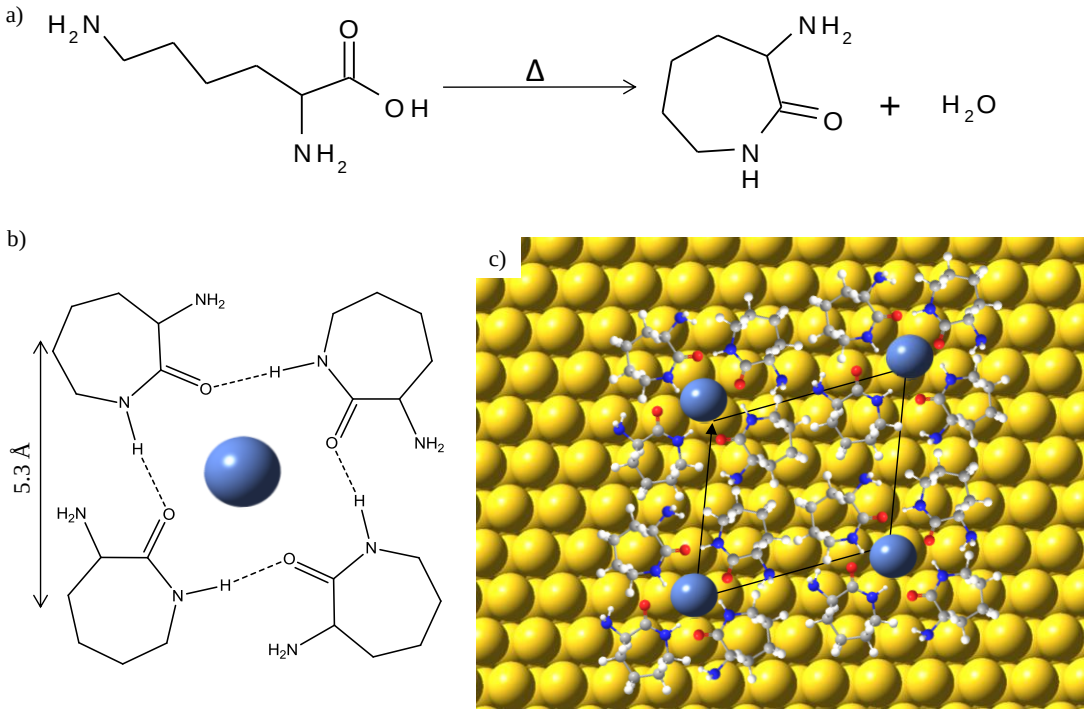

Fig.7.20 Model of *α*-amino-*ε*-caprolactam bonding framework.

Intermolecular interactions between N-H…O=C invoke the ordered structure observed in the STM images in Figure 7.19, with the defects thought to be created by Ni adatoms. This is a strange phenomenon in terms of previous images where the Ni features appear brighter than the molecular features. This idiosyncrasy has been witnessed previously [15] and it has been suggested that the Ni atoms may still be mobile when "trapped" within the structure, and so are imaged as dark features by the STM. Using the present set up, RAIRS cannot be measured at elevated temperatures, otherwise it could be possible to judge whether Ni is involved in a Ni(II) lactam complex due to a substantial downshift in the C=O stretch from free molecule to complexed ligand [39].

7.4 CONCLUSIONS

The adsorption of *(S)*-aspartic acid and *(S)*-lysine on Au/Ni has highlighted strong differences between their adsorption characteristics, despite their similarity in conformation. The importance of the nickel cluster size is not to be underestimated: Ni nanoparticles under ~ 3nm were found to completely disperse after modification

by both aspartic acid and lysine, resulting in the molecules interacting on the surface in a similar way to their adsorption characteristics on a clean Au{111} surface. With a greater Ni cluster size, both amino acids corroded the surface visibly.

In the case of *(S)*-Asp, it is postulated that Ni is "pulled out" onto the terraces to form complexes with the succinimide modifier. This resulted in long-range domains of MAA forming on the modified surface. In terms of enantioselective catalysis in the *(S)*-aspartic acid/0.5 ML Ni/Au system, it is clear that, although the docking interaction of MAA with the succinimidato nickel complexes extends several rows away from the primary site, there is a lack of chiral recognition in the system as the geometry caused by the H-bonding between the complex and MAA molecules forces MAA to adopt alternate enantioface adsorption to the surface along each row. This would therefore rule out *(S)*-aspartic acid as a potential modifier for a Au-based bimetallic catalyst used in the hydrogenation of *β*-ketoesters.

(S)-Lys has proved to have an extreme tendency for: a) etching Ni, and b) forming wide-range order on the bimetallic surface. Different phases were noted on the surface, with at least one domain showing chirality. As lysine has been shown in Chapter 6 to bind to Au, the adsorption geometry to Au/Ni is somewhat ambiguous. However, due to the difference in unit cell size, it is expected that Ni plays a part in the domains. Upon heating, a porous network is formed on the terraces. By analogy to the thermal chemistry of lysine, it was suggested that, due to the periodicity of the STM features being too small to represent lysine, condensation of the molecules had occurred to form α-amino-ε-caprolactam. As for the *(S)*-lysine/0.5 ML Ni/Au system as a potential enantioselective catalyst, the propensity for lysine to bind to the Au as well as Ni sites rules out the idea that Au may quench reactive racemic sites on the Ni. However, the adsorbate-induced etching is very promising due to the fact that widespread chiral facets are formed at the step edges, and thus could direct the hydrogenation reaction to proceed enantioselectively. This supports the conclusions found in Chapter 6.

7.5 REFERENCES

[1] J.V. Barth, H. Brune, G. Ertl & R.J. Behm, *Physical Review B,* **42** (1990) 9307.
[2] B. Voigtlander, G. Meyer & N.M. Amer, *Surface Science,* **255**, (1991) L529.
[3] B. Voigtlander, G. Meyer & N.M. Amer, *Physical Review B,* **44** (1991)10354.
[4] D.D. Chambliss, R.J. Wilson & S. Chiang, *Physical Review Letters,* **66** (1991) 1721.
[5] J.A. Meyer, I. D. Baikie, E. Kopatzki & R.J. Behm, *Surface Science,* **365** (1996) L647.
[6] W.G. Cullen & P.N. First, *Surface Science,* **420** (1999) 53.
[7] J. Schwank, *Gold Bulletin,* **18** (1985) 2.
[8] A.G. Trant, T.E. Jones & C.J. Baddeley, *Journal of Physical Chemistry C,* 111 (2007) 10534.
[9] A.G. Trant, T.E. Jones, T.C.Q. Noakes, P. Bailey & C.J. Baddeley, *Surface Science,* **604** (2010) 300.
[10] C.J. Baddeley, *The Chemical Physics of Solid Surfaces,* **10** (2002) 495.
[11] S. Clair, W. Pons, H. Brune, K. Kern & J.V. Barth, *Angewandte Chemie-International Edition,* **44** (2005) 7294.
[12] S. Clair, W. Pons, S. Fabris, S. Baroni, H. Brune, K. Kern & J.V. Barth, *Journal of Physical Chemistry B,* **110** (2006) 5627.
[13] Y.F. Zhang, N. Zhu & T. Komeda, *Journal of Physical Chemistry C,* **111** (2007) 16946.
[14] J. Mendez, R. Caillard, G. Otero, N. Nicoara & J.A. Martin-Gago, *Advanced Materials,* **18** (2006) 2048.
[15] S. Jensen & C.J. Baddeley, *Journal of Physical Chemistry C,* **112,** (2008) 15439.
[16] A.G. Trant & C.J. Baddeley, *Langmuir,* **27** (2011), 1788.
[17] K.S. Smirnov & G. Raseev, *Surface Science,* **384** (1997) L875.
[18] T.E. Jones, C.J. Baddeley, *Surface Science,* **513** (2002) 453.
[19] L. E. Niţă, A. P. Chiriac, C. M. Popescu, I. Neamţu & L. Alecu, *Journal of Optoelectronics & Advanced Materials,* **8(2)** (2006) 663.
[20] H. J. Cumming & D.Hall, *Acta Crystallographica,* **B32,** (1971) 1281.
[21] T.E. Jones & C.J. Baddeley, *Surface Science,* **519** (2002) 237.
[22] V. Humblot, C. Methivier & C-M. Pradier, *Langmuir,* **22** (2006) 3089.
[23] V. Humblot, C. Methivier, R. Raval & C-M. Pradier, *Surface Science,* **601** (2007) 4189
[24] F. Tielens, V. Humblot & C-M. Pradier, *Surface Science,* **602** (2008) 1032.
[25] S. Stewart & P.M. Fredericks, *Spectrochimica Acta Part A,* **55** (1999) 1641.
[26] D.H. Williams & I. Fleming, *Spectroscopic Methods in Organic Chemistry,* **3rd Ed,** McGraw-Hill Book Company (UK) Ltd, Ch. 2 35-73
[27] W. Y. Cheong & A.J. Gellman, *Journal of Physical Chemistry C,* **115** (2011)1031.
[28] G. Tzvetkov, M.G. Ramsey & F.P. Netzer, *Surface Science,* **526** (2003) 383.
[29] D. Holtkamp, M. Kempken, P. Kliisener & A. Benninghoven, *Journal of Vacuum Science & Technology A,* **5** (1987) 2912.
[30] T.E. Jones, C.J. Baddeley, A. Gerbi, L. Savio, M. Rocca & L. Vattuone, *Langmuir,* **21** (2005) 9468.
[31] J.V. Barth, J. Weckesser, N. Lin, A. Dmitriev & K. Kern, *Applied Physics A,* **76** (2003) 645.
[32] Q. Chen, C.C. Perry. B.G. Fredrick, P.W. Murray, S. Haq & N.V. Richardson, *Surface Science,* **446** (2000) 63.

[33] Q. Chen & N.V. Richardson, *Progress in Surface Science*, **73** (2003) 59.
[34] X.Y. Zhao, *Journal of the American Chemical Society*, **122** (2000) 12584.
[35] F. Yin, R.E. Palmer & Q. Guo, *Surface Science,* **600** (2006) 1504
[36] S.D. Jang & R.A. Condrate, *Clays and Clay Minerals*, **20** (1972) 79.
[37] K. Harada, *Bulletin of the Chemical Society of Japan*, **32** (1959) 1007.
[38] P. Melius & J. Y-P. Sheng, *Bioorganic Chemistry*, **4** (1975) 385.
[39] J.H Bright, R.S. Drago, D.M. Hart & S.K. Madan, *Inorganic Chemistry*, **4** (1965) 18.

Chapter 8

Project Conclusions and Outlook

Throughout the course of this PhD, which forms part of a larger research project into amino acid adsorption on metals, a number of interesting findings have been accomplished. This chapter is presented in two sections: first, an overview is given of the main conclusions presented in each result chapter. Second, a brief discussion outlining the outcome of this work in relation to possible future research is given.

8.1 CONCLUSIONS

Chapter 3 focused on the adsorption of *(S)*-Asp onto the Ni{111} surface under UHV conditions. Techniques used included RAIRS, STM, AES, LEED and TPD. RAIRS successfully established the form aspartic acid adopted on adsorption at the Ni surface, with the intriguing evidence for the succinimide polymer formed at low coverages via catalysis of the polycondensation reaction, presumably by step and kink defects on the Ni. STM showed the formation of tetramer species at step edges, stabilised by a Ni adatom in the centre of each tetramer ring. The formation of the ring structures is thought to explain the lack of extended molecular ordering on the surface. MAA was shown to bind in its enol form which was unusual compared to other studies, but was the favourable tautomer in terms of binding to a succinimide molecule as the proposed hydrogen bonding interaction between the MAA and oligomer stabilises the enol. MAA was found by STM to preferentially interact via hydrogen bonding to the tetramer rings at the functional groups nearest the step edge, substantiating previous evidence of the "active chiral site" model that the MAA-modifier interaction also involves attractive interactions with the substrate. The presence of tetramer structures were found to go some way in offering an explanation of the relatively low enantioselectivity. As MAA appears to bind in a 1:1 fashion with the modifier, the relatively small amount of modifier tetramer species on the surface indicates that only a small level of enantioselectivity could be achieved,

taking into account that the areas of "bare" Ni sites would catalyse the reaction racemically.

Chapter 4 described liquid phase RAIRS and XPS experiments carried out to bridge the gap between UHV work and catalytic work on the *(S)*-aspartic acid modified Ni catalyst system. Both techniques were used in such a way that the modified Ni surface could be analysed as a function of modification pH and temperature. Highlights from the results include the important discovery that, at conditions which gave the highest enantioselectivity for the hydrogenation of MAA in the heterogeneous catalytic reaction, the presence of aspartate on the surface was at levels undetectable by either RAIRS or XPS. Furthermore, XPS measurements allowed detailed calculations on the possibility of a small but finite amount of aspartate on the surface and concluded that the only plausible explanation for the measured enantioselectivity originated from chiral faceting on the modified Ni surface, which remained even once all measured traces of aspartate molecules were washed away.

Chapter 5 progressed onto the second of the two modifiers studied within this research project – *(S)*-lysine. UHV and liquid phase experiments including RAIRS, TPD, STM and XPS, were carried out in a similar fashion to *(S)*-Asp studies in Chapters Three and Four, for *(S)*-Lys on Ni{111}. Under UHV conditions, it was found that the zwitterionic form of lysine was present on the surface, with a change in geometry between low and high coverages to accommodate the molecules on the Ni{111}. Lysine was shown by STM to bind extremely well to the Ni{111} surface, and results suggested the modifier adopts a Volmer-Weber type growth, forming 3D island clusters on the Ni{111} surface. Adsorption of MAA as a mixture of both its tautomeric forms was shown to occur predominantly on terrace sites, not interacting with the modifier islands sufficiently enough to cause chiral recognition. At higher modification temperatures, TPD data suggested that a lysinate condensation polymer was present on the Ni{111} surface. In the liquid-solid interface RAIRS and XPS

experiments, changes to the lysine form adsorbed on the Ni surface were shown to occur depending on pH. A water wash appeared to remove only the multilayer lysine molecules, in contrast to the behaviour of aspartic acid, and MAA showed little evidence of interacting with the modifier following modification at 300 K. It was therefore postulated that the most likely explanation for the measurable e.e. values found for the system in previous catalytic studies was the presence of some chiral recognition of the MAA mediated by a docking interaction with the nickel metal substrate, and not influenced directly by the *(S)*-lysine-containing clusters.

Chapter 6 discusses the adsorption of both *(S)*-Asp and *(S)*-Lys on Au{111}. *(S)*-lysine, with its two NH_2 groups, was found by a combination of RAIRS, EELS and STM to bind favourably to Au{111}, while *(S)*-aspartic acid was shown not to bind. Very little work had been previously carried out into amino acid adsorption on Au, with the exception of those amino acids containing thiol or thioether functionalities. An interesting discovery from the *(S)*-Lys/Au{111} system was the chiral restructuring of the surface into the formation of Au nanofingers, formed due to the attractive interaction of lysine with the gold surface extracting gold atoms from the uppermost layer step edge, which would then migrate to form nanofingers. The highlight of this discovery was that surface chirality appeared present, with directed fingers and facets; only three out of the six {514} type facets on the Au{111} surface were observed, in the <514> directions. Clearly, this would have potential applications in enantioselective catalysis as enantiospecific facets and fingers could act as docking sites for chiral recognition of reactants. It is even possible that the chiral facets/fingers could retain their chirality once tethered modifier molecules are removed, and thus create a chiral metal surface more suitably robust under typical catalytic conditions.

Chapter 7 examines the potential use of bimetallic Au{111}/Ni catalysts in the hydrogenation of MAA, based on the hypothesis that Au could quench the reactivity of Ni towards racemic product production, and thus enhance enantioselectivity.

Ordered arrays of nickel islands were formed on the Au{111} surface following nucleation of the nickel atoms within the elbows of the herringbone reconstruction. In the *(S)*-Asp-Au{111}/Ni system, it was found by STM and RAIRS that *(S)*-Asp did not appear to bind in any long range order, instead adsorbing mainly in the proximity of the Ni clusters. The Ni atoms were found to be leached by *(S)*-Asp to produce metal-organic structures and, once MAA was adsorbed onto the modified surface, two domains of MAA between clusters were clearly observed and a docking interaction between MAA and the succinimidato Ni complexes was suggested. Due to the configuration of the molecules on the surface, a lack of chiral recognition of the reactant was apparent. In contrast, *(S)*-Lys showed long range order of possible Ni lysinate chelate complexes when adsorbed onto the Au{111}/Ni surface, with some chiral arrays formed on the surface at room temperature. The most prominent effect to the bimetallic surface was the widespread etching, caused by lysine adsorption, and highlighted the etching power of the amino acid, as observed in Chapter 6. Using a similar strategy to create ordered arrays of metal-organic frameworks, there is a strong possibility that a modified bimetallic Au/Ni catalyst could offer useful insight into the design of an enantioselective heterogeneous catalyst.

8.2 FUTURE WORK

The results of this body of research have instigated many potential avenues of investigation. Prior to this work, a number of studies of chiral modifiers on several metal substrates had been undertaken. This work however has presented detailed results on the adsorption of two potential chiral modifiers onto the catalytically active Ni metal; neither of which had been examined in such systematic detail before. A natural continuation of the work would be to carry out similar studies on a selection of amino acids, chosen based on their applicability as modifiers in the hydrogenation reaction of β-ketoesters. Indeed, RAIRS and XPS studies carried out by the author on the closely related alanine, phenylalanine and proline-modified Ni surfaces (not discussed) have shown relevance in the endeavour to verify proposed models and possible mechanisms in enantioselective heterogeneous catalysis. Care would need to be taken however to choose only those amino acids which have

potential to add to our knowledge of the catalytic system, and not just add to a "library" of data.

As this type of catalysis relies heavily on the adsorption of chiral modifiers from solution, it is increasingly thought that the more desirable method for examining catalytic systems in order to close the "pressure gap" between UHV studies and real catalysts in industry is to employ *in-situ* measurements, in particular vibrational spectroscopy and STM. The use of a liquid cell to carry out *in-situ* infrared spectroscopy would provide an insight into the bonding of the molecules at the catalyst surface during the catalytic reaction. The same technique could then be used during the hydrogenation of the modified and reacted surface by forcing a continuous flow of H_2 through the cell. A foray into the use of electrochemical STM would similarly allow more relevant *in-situ* measurements. Also, Ni could be electrochemically deposited onto Au and so the bimetallic system could be studied at the liquid phase.

If a docking interaction between the chiral modifiers or modified surface and prochiral reagents is observed and a system is thought to show large enough potential, as many techniques as are available and relevant should be utilised to give as rounded an analysis as possible. The results of this would ultimately decide whether a system was worthwhile enough to put through rigorous catalytic testing.